

**WestminsterResearch**

<http://www.westminster.ac.uk/westminsterresearch>

**Biosynthesis of Poly-3-Hydroxybutyrate and its Application in  
Controlled Drug Delivery  
Puthussery, H.**

This is an electronic version of a PhD thesis awarded by the University of Westminster.  
© Ms Hima Puthussery, 2019.

---

The WestminsterResearch online digital archive at the University of Westminster aims to make the research output of the University available to a wider audience. Copyright and Moral Rights remain with the authors and/or copyright owners.

---

Whilst further distribution of specific materials from within this archive is forbidden, you may freely distribute the URL of WestminsterResearch: (<http://westminsterresearch.wmin.ac.uk/>).

In case of abuse or copyright appearing without permission e-mail [repository@westminster.ac.uk](mailto:repository@westminster.ac.uk)

# **BIOSYNTHESIS OF POLY-3-HYDROXYBUTYRATE AND ITS APPLICATION IN CONTROLLED DRUG DELIVERY**

Hima Puthussery

A thesis submitted in partial fulfilment of the requirements of the University  
of Westminster for the degree of Doctor of Philosophy.

January 2019

## **AUTHOR'S DECLARATION**

---

I hereby declare that the present work was carried out in accordance with the Guidelines and Regulations of the University of Westminster. The work is original except where indicated by special reference in the text.

The submission as a whole or part is not substantially the same as any that I previously or am currently making, whether in published or unpublished form, for a degree, diploma or similar qualifications at any university or similar institution.

Until the outcome of the current application of the University of Westminster is known, the work will not be submitted for any such qualification at another University or similar institution.

Any views expressed in this work are those of the Author and in no way represent that of the University of Westminster.

Signed: Hima Puthussery

Date: 14-01-2019

## Acknowledgments

---

I would like to sincerely thank my supervisor Prof. Ipsita Roy for her expert advice and kindness, which was an invaluable contribution towards my research. Prof. Roy has been a pillar of support and constant source of encouragement throughout. I would also like to thank Prof. Tajalli Keshavarz for his words of encouragement throughout my stay in the University of Westminster. I would also like to thank Dr. Anatoly Markiv and Dr. Eugen Stulz for their guidance in my project.

I would like to wholeheartedly thank all my colleagues, especially Pooja, Barbara, Louise, Ranjana di, Moe and Tayebah for their unconditional support and guidance. I am particularly indebted to Pooja for all her help and guidance, especially with Rapamycin work. I am also grateful to Ranjana Di for her help in Tacrolimus work. I also wish to extend my warm gratitude to staff at university of Westminster and UCL; especially, Neville, Thakor, Harry, Steve, Nicky and Vanita.

I also thank Cavendish Scholarship committee, REBIOSTENT and Neurimp for financial support.

I am indebted to my family, especially my didis for believing in me and for all their sacrifice in my well-being. I also profusely thank Prasattan, for being amazingly kind. I could not have managed to be enjoying this opportunity, without their kindness. I thank my partner Chethan and his family, for joining in my journey and making it more enjoyable with their unconditional support. I also thank my friends Arjun, PASHAS and Nimisha.

This thesis is dedicated to Ms. Hannah Edwards, the amazing human being who was incredibly kind to me and restored my complete faith in humanity. Without her, this path would not have been possible for me and I aspire to be as kind as her, moving forward.

## Abstract

---

Controlled drug delivery has become a research focus in view of many of the drawbacks of conventional drug delivery including increased biodistribution and lack of target specificity, resulting side effects, and thus decreased patient compliance. Controlled delivery is the sustained administration of therapeutic agents, keeping dosage fluctuations within the therapeutic window. Controlled drug delivery relies on the design and modification of specialised drug delivery systems (DDS) for encapsulating and delivering therapeutic agents. Biodegradable polymers have been exploited extensively for this purpose, since post-administrative procedures for removal of these systems from the body is not a requisite, because their degradation can be catalysed by physiological enzymes and autocatalytic hydrolysis. Particulate DDS such as microspheres and nanospheres have gained prominence in this context, and the optimisation of these to cater to the type of target, therapeutic agent to be encapsulated and the mode of delivery is a growing need.

Polyhydroxyalkanoates (PHAs) are a class of natural polyesters that are receiving great attention in many biomedical applications such as tissue regeneration, synthesis of medical devices and drug delivery. Poly(3-hydroxybutyrate), P(3HB), is a short chain length variety of this polymer which has specifically been recognised for its potential to form DDS. In the first part of this study the solid-in-oil-in-water technique was used to optimise production of P(3HB) microspheres. The optimization process used a response surface methodology based on the Box Behnken design. The effect of process parameters such as polymer concentration, surfactant concentration and stirrer speed on microsphere size was analysed. The results of these optimisation experiments were used to tailor micro and

nanospheres of different size ranges and these were characterised for their size distribution, porosity, amount of surface residual surfactant and hydrophobicity.

The second part of this study focused on developing micro and nanospheres with encapsulated therapeutic agents relevant in cardiovascular diseases. Encapsulation of two antiproliferative drugs namely rapamycin and tacrolimus were studied in the context of their application in drug eluting stents. Rapamycin encapsulated P(3HB) and PLLA microspheres were compared for their physical properties and drug release kinetics and their release kinetics were found to be comparable. However, P(3HB) microspheres were more suitable for applications as their degradation products were found to be less acidic than that of PLLA microspheres. Tacrolimus encapsulated micro and nanospheres of P(3HB) were compared, to analyse drug encapsulation and release kinetics with respect to size of the spheres. Microspheres were found to have increased encapsulation efficiency, with a slower drug release rate, in comparison with nanospheres. Vascular Endothelial Growth Factor (VEGF), commonly used in the context of cardiovascular regeneration, was encapsulated within P(3HB) micro and nanospheres and were embedded in collagen scaffolds. The differences in release of VEGF from spheres embedded and not embedded in the collagen scaffold were quantified and it was established that embedding in the scaffolds reduced burst release.

In the next stage of this study, P(3HB) microspheres were developed as novel target specific photodynamic drug delivery systems, with potential anticancer therapy applications. Three derivatives of a commonly used photosensitiser, namely porphyrin, were encapsulated within P(3HB) microspheres. The reduction in cell viability of these with respect to drug loading was quantified. Encapsulation efficiency was found to increase with drug loading

and reduction in cell viability was found to be a direct reflection of this. These microspheres were made target specific by adsorbing an antibody 'Anti- HER-2', which specifically binds to HER2, a cancer marker overexpressed on breast cancer cells. The incorporation of the antibody was found to result in increased cytotoxicity of the formulations, for all three derivatives.

P(3HB) is a crystalline, hydrophobic polymer and degrades through surface erosion. There are applications that necessitate drug delivery systems that can retain moisture (especially in the context of wound healing) and a quicker release of drug moieties. Bearing this requirement in mind, a conjugate of P(3HB) with hyaluronic acid (HA) was synthesised by Contipro a.s. and the final part of this study examined the optimisation of microsphere synthesis using these conjugates. As this conjugate was amphiphilic, a water in oil emulsion, coupled with crosslinking was employed for the synthesis process. Microspheres of  $\sim 20 \mu\text{m}$  diameter were synthesised, and hydrophilic and hydrophobic drugs were encapsulated within them. The microspheres were found to be fast degrading, maintaining their structure up to a maximum of 11 days. The drug release kinetics from these showed an increased burst release compared to P(3HB) microspheres.

## TABLE OF CONTENTS

---

<b>CHAPTER 1. INTRODUCTION.....</b>	<b>1</b>
<b>1.0. CONTROLLED DRUG DELIVERY .....</b>	<b>2</b>
<b>1.1. MICRO AND NANOSPHERES .....</b>	<b>4</b>
1.1.1. Spray drying.....	5
1.1.2. Supercritical fluid technology .....	5
1.1.3. Solvent evaporation method.....	6
<b>1.2. EFFECT OF PROCESS PARAMETERS IN THE PREPARATION OF MICRO/ NANOSPHERES USING SOLVENT EVAPORATION TECHNIQUE .....</b>	<b>9</b>
1.2.1. Polymer.....	9
1.2.2. Surfactant.....	10
1.2.3. Agitation .....	11
<b>1.3. MECHANISMS OF DRUG RELEASE .....</b>	<b>12</b>
1.3.1. Dissolution followed by diffusion .....	12
1.3.2. Partitioning .....	13
1.3.3. Osmotic release.....	14
1.3.4. Swelling.....	14
1.3.5. Erosion .....	15

1.3.6. Targeting.....	16
<b>1.4. THEORY OF DRUG RELEASE .....</b>	<b>20</b>
1.4.1. Zero- order model.....	22
1.4.2. First- order model.....	23
1.4.3. Higuchi model.....	24
1.4.4. Hixson- Crowell model .....	25
1.4.5. Korsmeyer-Peppas model.....	26
<b>1.5. BIODEGRADABLE POLYMERS IN DRUG DELIVERY .....</b>	<b>28</b>
1.5.1. Synthetic Polymers.....	28
1.5.2. Natural polymers .....	29
<b>1.6. POLYHYDROXYALKANOATES (PHAS) .....</b>	<b>30</b>
1.6.1. P(3HB).....	35
1.6.2. P(3HB) Biosynthesis .....	35
1.6.3. Thermal and physical properties of P(3HB) .....	37
1.6.4. Biodegradability of P(3HB) .....	37
1.6.5. Biocompatibility of P(3HB) .....	38
1.6.6. Biomedical applications of P(3HB).....	40
<b>1.7. P(3HB) IN DRUG DELIVERY .....</b>	<b>41</b>
1.7.1. Addition of PHA binding proteins .....	44
1.7.2. Folate mediated targeting.....	45

1.7.3. Other surface functionalization strategies .....	46
1.8. AIMS AND OBJECTIVES .....	47
<b>CHAPTER 2. MATERIALS AND METHODS.....</b>	<b>49</b>
<b>2.1. MATERIALS.....</b>	<b>50</b>
2.1.1. Water .....	50
2.1.2. Chemicals and Reagents .....	50
2.1.3. Bacterial strains and cultures .....	50
2.1.4. Cell lines and maintenance.....	51
2.1.5. Plasmids .....	51
2.1.6. Porphyrins.....	51
2.1.7. Reagents used for the in vitro drug release and in vitro degradation studies.....	51
2.1.7.1. Phosphate buffered saline solution (PBS):.....	51
2.1.7.2. Simulated body fluid (SBF):.....	51
2.1.8. Buffers and Reagents .....	52
2.1.8.1. Buffers for SDS-PAGE: .....	52
2.1.8.2. Resolving gel buffer .....	52
2.1.8.3. Stacking gel buffer .....	52
2.1.8.4. 5X Reservoir Buffer.....	52
2.1.8.5. Coomassie brilliant blue stain (for staining SDS-PAGE gels).....	52
2.1.8.6. Destaining solution (for destaining SDS-PAGE).....	52
2.1.8.7. 5X TBE, pH 8.0, (g/L) .....	52
2.1.9. Media components.....	53
<b>2.2. EXPERIMENTAL METHODS:.....</b>	<b>53</b>
2.2.1. Production of P(3HB).....	53

<b>2.2.2. Optical density .....</b>	<b>54</b>
<b>2.2.3. Temperature, pH and dissolved oxygen tension (DOT) .....</b>	<b>54</b>
<b>2.2.4. Polymer extraction techniques.....</b>	<b>55</b>
2.2.4.1. Extraction of PHA by chloroform/ sodium hypochlorite dispersion .....	55
2.2.4.2. Soxhlet extraction method .....	56
<b>2.2.5. Characterization of the P(3HB) produced .....</b>	<b>56</b>
2.2.5.1. Fourier Transform Infrared Spectroscopy (FTIR).....	56
2.2.5.2. Nuclear Magnetic Resonance Spectroscopy (NMR).....	56
2.2.5.3. Molecular weight analysis.....	56
<b>2.2.6. Production of P(3HB) micro/nanospheres .....</b>	<b>57</b>
2.2.6.1. Solid-in-oil-in-water emulsion technique .....	57
2.2.6.2. Optimisation of microsphere production.....	58
<b>2.2.7. Preparation of Amphiphilic HA- P(3HB) microspheres.....</b>	<b>59</b>
2.2.7.1. Hydrolytic depolymerisation of P(3HB) and HA conjugation .....	59
2.2.7.2. Amphiphilic HA- P(3HB) microsphere preparation .....	59
<b>2.2.8. P(3HB) microsphere: physical characterization techniques</b>	
<b>60</b>	
2.2.8.1. Microstructural studies using Scanning Electron Microscopy (SEM) .....	60
2.2.8.2. Particle size analysis .....	61
2.2.8.3. Porosity .....	61
2.2.8.4. Determination of Residual PVA content .....	62
2.2.8.5. Determination of surface hydrophobicity.....	62
2.2.8.6. Protein adsorption studies.....	62
2.2.8.7. In vitro degradation.....	63
2.2.8.8. Water uptake and weight loss measurement .....	63
2.2.8.9. Swelling studies on HA-P(3HB) microspheres .....	64
2.2.8.10. Biocompatibility studies .....	65
I. Cell culture maintenance of HMEC-1.....	65
II. Sample sterilization .....	65
III. Cell seeding.....	65
<b>2.2.9. Drug quantification methods.....</b>	<b>66</b>
2.2.9.1. Determination of the drugs: encapsulation efficiency .....	66
i. High Performance Liquid Chromatography (HPLC) for Rapamycin .....	66

ii.	HPLC for Tacrolimus .....	66
iii.	Fluorescence spectrometry for Porphyrin quantification .....	67
iv.	UV-VIS spectrometry for Curcumin quantification.....	67
v.	UV-VIS spectrometry for Gentamycin quantification .....	67
vi.	UV-VIS spectrometry for Aspirin quantification.....	67
vii.	VEGF quantification using VEGF human ELISA kit .....	67
<b>2.2.10.</b>	<b>Drug release kinetics .....</b>	<b>68</b>
<b>2.2.11.</b>	<b>Application of drug release data on mathematical models</b>	<b>68</b>
<b>2.2.12.</b>	<b>Protein expression and purification .....</b>	<b>69</b>
<b>2.2.13.</b>	<b>Surface adsorption of anti-HER2 on porphyrin encapsulated microspheres .....</b>	<b>69</b>
<b>2.2.14.</b>	<b>Cell viability studies .....</b>	<b>70</b>
2.2.14.1.	Cell culture maintenance of SK-BR-3.....	70
2.2.14.2.	Metabolic activity assay .....	71
2.2.14.3.	Calculation of Inhibitory concentration (IC50) .....	71
<b>2.2.15.</b>	<b>Confocal imaging .....</b>	<b>71</b>
<b>2.2.16.</b>	<b>Determination of the Minimum Inhibitory Concentration (MIC) of HA-P(3HB) with encapsulated curcumin against Methicillin Resistant <i>Staphylococcus aureus</i>.....</b>	<b>72</b>
<b>2.2.17.</b>	<b>Determination of Minimum Bactericidal Concentration (MBC) of curcumin encapsulated HA-P(3HB) against Methicillin Resistant <i>Staphylococcus aureus</i>.....</b>	<b>72</b>
<b>2.2.18.</b>	<b>Statistical analysis .....</b>	<b>73</b>
<b>CHAPTER 3.....</b>	<b>.....</b>	<b>74</b>
<b>3.1. INTRODUCTION .....</b>	<b>.....</b>	<b>75</b>
<b>3.2. RESULTS .....</b>	<b>.....</b>	<b>78</b>

<b>Part I: Statistical optimisation of synthesis of P(3HB) microspheres</b>	<b>78</b>
3.2.1. Production of P(3HB) from <i>B. cereus</i> SPV	78
3.2.2. Characterisation of the polymer	80
3.2.2.1. FTIR analysis of P(3HB) produced using <i>B. cereus</i> SPV	80
3.2.2.2. Nuclear Magnetic Resonance	80
3.2.2.3. Molecular weight analysis	82
3.2.3. Optimisation of microsphere production	82
3.2.3.1. Pilot experiments	82
3.2.3.2. Design of experiments	84
3.2.4. Surface morphology and particle size analysis	85
3.2.5. Modelling of response surface	87
3.2.5.1. Mathematical modelling and effect of independent variables on the particle properties	89
3.2.5.2. Graphical representation of significant effect of independent variables	90
3.2.5.3. Validation of method	92
3.2.6. P(3HB) microsphere characterization	93
3.2.6.1. Porosity	93
3.2.4.1. Hydrophobicity and correlation between residual PVA and hydrophobicity	96
3.2.7. Optimisation of production parameters for microspheres and nanospheres of varying size ranges.	97
3.2.7.1. Surface morphology of nanospheres and microspheres under SEM	98
<b>Part II: Optimisation of nanospheres production from P(3HB) extracted using <i>B. subtilis</i> OK2.</b>	<b>103</b>
3.2.8. P(3HB) production using <i>B. subtilis</i> OK2	103
3.2.9. Characterisation of the polymer	104
3.2.9.1. FTIR analysis of P(3HB) produced using <i>B. subtilis</i> OK2	104
3.2.9.2. Nuclear Magnetic Resonance	105
3.2.9.3. Molecular weight analysis	107

3.2.10. Optimisation of nanospheres production using P(3HB) extracted from <i>B. subtilis</i> OK2 .....	107
3.2.10.1. Observation of surface morphology under SEM .....	108
<b>Part III: Comparison of nanospheres and microspheres prepared using P(3HB) extracted from <i>B. cereus</i> SPV and <i>B. subtilis</i> OK2 ....</b>	<b>110</b>
3.2.11. Characterisation .....	111
3.2.11.1. Particle size distribution .....	111
3.2.11.2. Porosity .....	113
3.2.11.3. Surface residual PVA.....	114
3.2.11.4. Hydrophobicity.....	114
<b>3.3. DISCUSSION .....</b>	<b>115</b>
3.3.1. Effect of process parameters on particle size and morphology.....	116
<b>CHAPTER 4.....</b>	<b>121</b>
4.1. INTRODUCTION.....	122
4.2. RESULTS.....	126
<b>Part I: Comparison of P(3HB) and PLLA microspheres in the encapsulation and controlled release of rapamycin .....</b>	<b>126</b>
4.2.1. Hydrolytic depolymerisation of P(3HB).....	126
4.2.2. Optimisation of the process of microsphere production using solid-in-oil-in-water emulsion technique.....	126
4.2.3. Characterisation of PLLA and P(3HB) microspheres.....	127
4.2.3.1. Surface morphology under SEM .....	127
4.2.3.2. Rapamycin encapsulation in P(3HB) and PLLA microspheres: Surface morphology under SEM .....	129
4.2.3.3. Particle size analysis .....	130
4.2.3.4. Porosity .....	132
4.2.3.5. Surface residual PVA .....	133

4.2.3.6.	Surface hydrophobicity .....	134
4.2.3.7.	Protein adsorption .....	135
4.2.3.8.	In vitro Degradation of P(3HB) and PLLA microspheres .....	136
I.	Water uptake and weight loss analysis.....	136
I.	pH changes.....	137
4.2.4.	<b>Rapamycin encapsulation and release kinetics.....</b>	<b>138</b>
4.2.4.1.	Encapsulation efficiency.....	138
4.2.4.2.	In vitro Release kinetics .....	140
<b>Part II: Comparison of P(3HB) nano and microspheres with encapsulated tacrolimus.....</b>		<b>142</b>
4.2.5.	<b>Production of micro/nanospheres with encapsulated tacrolimus using solid-in-oil-in-water emulsion technique .....</b>	<b>142</b>
4.2.6.	<b>Characterization of P(3HB) microspheres and nanospheres with encapsulated tacrolimus.....</b>	<b>143</b>
4.2.6.1.	Surface morphology analysis using SEM .....	143
4.2.6.2.	Particle size analysis .....	144
4.2.6.3.	Porosity .....	146
4.2.6.4.	Residual PVA.....	147
4.2.6.5.	Hydrophobicity .....	148
4.2.6.6.	Protein adsorption .....	149
4.2.6.7.	In vitro degradation.....	150
I.	Water uptake and weight loss .....	150
I.	pH changes.....	152
4.2.7.	<b>Tacrolimus encapsulation and release kinetics .....</b>	<b>152</b>
4.2.8.	<b>Release kinetics .....</b>	<b>153</b>
<b>Part III P(3HB) microspheres as VEGF delivery systems in Collagen scaffolds for Cardiac regeneration.....</b>		<b>156</b>
4.2.9.	<b>Process optimisation of spheres of different size ranges with encapsulated VEGF.....</b>	<b>156</b>
4.2.10.	<b>Surface morphology under SEM.....</b>	<b>157</b>

<b>4.2.11. Characterization of VEGF encapsulated particles chosen for incorporation in 3D-collagen scaffolds .....</b>	<b>158</b>
4.2.11.1. Particle size analysis .....	158
4.2.11.2. Porosity .....	159
4.2.11.3. Surface residual PVA.....	160
4.2.11.4. Hydrophobicity.....	161
4.2.11.5. Protein adsorption .....	162
4.2.11.6. In vitro degradation studies .....	163
I. Water uptake and weight loss .....	163
I. pH changes.....	164
<b>4.2.12. Incorporation of VEGF encapsulated microspheres and nanospheres in Collagen scaffolds .....</b>	<b>166</b>
4.2.12.1. Characterization.....	166
I. Surface morphology analysis under SEM .....	166
I. Swelling studies .....	167
<b>4.2.13. Encapsulation efficiency.....</b>	<b>168</b>
<b>4.2.14. Release kinetics .....</b>	<b>169</b>
<b>4.3. DISCUSSION .....</b>	<b>173</b>
<b>4.3.1. Comparison of rapamycin encapsulated P(3HB) and PLLA microspheres .....</b>	<b>173</b>
4.3.1.1. The effect of process parameters on characteristics of microspheres...173	
4.3.1.2. Encapsulation efficiency and drug release .....	176
<b>4.3.2. Comparison of tacrolimus encapsulated P(3HB) microspheres and nanospheres.....</b>	<b>178</b>
<b>4.3.3. P(3HB) microspheres as VEGF delivery systems in Collagen scaffolds for Cardiac regeneration .....</b>	<b>181</b>
<b>CHAPTER 5.....</b>	<b>185</b>
<b>5.1. INTRODUCTION.....</b>	<b>186</b>

<b>5.2. RESULTS.....</b>	<b>190</b>
<b>5.2.1. Encapsulation of Porphyrin derivatives.....</b>	<b>190</b>
<b>5.2.2. Characterization of porphyrin encapsulated microspheres</b>	<b>192</b>
5.2.2.1. Surface morphology and particle size analysis of Porphyrin encapsulated microspheres.....	192
5.2.2.2. Porosity.....	194
5.2.2.3. Residual PVA and hydrophobicity.....	196
4.2.2.1. Protein adsorption.....	197
<b>5.2.3. Encapsulation efficiency.....</b>	<b>198</b>
<b>5.2.4. Expression and purification of RFP linked Anti -HER2 antibody.....</b>	<b>199</b>
<b>5.2.5. Antibody adsorption on the microspheres.....</b>	<b>201</b>
<b>5.2.6. Cell viability studies.....</b>	<b>202</b>
<b>5.2.7. Confocal imaging.....</b>	<b>204</b>
<b>5.2.8. Calculation of IC50 for 10 wt% TPP encapsulated P(3HB) microspheres with and without anti-HER-2 conjugation.....</b>	<b>206</b>
<b>5.3. DISCUSSION.....</b>	<b>207</b>
<b>CHAPTER 6.....</b>	<b>211</b>
<b>6.1. INTRODUCTION.....</b>	<b>212</b>
<b>6.2. RESULTS.....</b>	<b>214</b>
<b>6.2.1. Optimisation of microsphere production.....</b>	<b>215</b>
<b>6.2.2. Analysis of surface morphology and particle size distribution.....</b>	<b>216</b>

6.2.3.	Characterisation of P(3HB)- HA microspheres .....	218
6.2.3.1.	FTIR.....	218
6.2.3.2.	Swelling studies at different pH.....	218
6.2.4.	Hydrophilic drug encapsulation.....	219
6.2.5.	Drug release kinetics .....	221
6.2.6.	Hydrophobic drug encapsulation.....	222
6.2.7.	Drug release kinetics .....	222
6.2.8.	Comparison of drug release profiles.....	223
6.2.9.	Antibacterial activity of Curcumin.....	224
6.2.9.1.	Growth inhibition .....	224
6.2.9.2.	Quantification of Minimum inhibitory concentration (MIC).....	225
6.3.	DISCUSSION .....	226
	CHAPTER 7.....	232
7.1.	CONCLUSIONS .....	233
	CHAPTER 8: FUTURE WORK.....	238
8.1.	FUTURE WORK .....	239
8.1.1.	Statistical optimisation of preparation of nanospheres using P(3HB) from different producer organisms .....	239
8.1.2.	Characterization of microspheres and nanospheres.....	239
8.1.3.	Cardiovascular drugs.....	239
8.1.4.	Photodynamic therapy.....	240
8.1.5.	P(3HB)- HA microspheres in wound healing.....	240
	REFERENCES: .....	241

## LIST OF FIGURES

<b>Figure 1.1:</b> A schematic representation of stages of commercialization of a new drug molecule .....	2
<b>Figure 1.2:</b> Schematic representation of preparation of microspheres to encapsulate hydrophobic drugs, using water-in-oil emulsion technique. ....	7
<b>Figure 1.3:</b> Schematic representation of preparation of microspheres to encapsulate hydrophilic drugs, using double emulsion technique. ....	8
<b>Figure 1.4:</b> strategies of CSC targeting .....	18
<b>Figure 1.5:</b> Graphical representation of drug release of zero- order release kinetics. ....	23
<b>Figure 1.6:</b> Graphical representation of drug release of first- order release kinetics	24
<b>Figure 1.7:</b> Graphical representation of drug release following Higuchi model.....	25
<b>Figure 1.8:</b> Graphical representation of drug release following Hixson- Crowell model.....	26
<b>Figure 1.9:</b> Graphical representation of drug release following Korsmeyer-Peppas model.....	27
<b>Figure 1.10:</b> General chemical structure of Polyhydroxyalkanoates .....	31
<b>Figure 1.11:</b> Biosynthetic pathway of P(3HB) in <i>C. necator</i> .....	36
<b>Figure 2.1:</b> Layers containing sodium hypochlorite with cell debris and chloroform with polymer .....	55
<b>Figure 3.1:</b> Schematic representation of polymeric particles prepared by a) single emulsion method and b) double emulsion method .....	76
<b>Figure 3.2:</b> Representation of experimental runs on a Box-Behnken design. ....	77
<b>Figure 3.3:</b> Temporal growth profile of <i>B. cereus</i> SPV for the production of P(3HB) in 5L bioreactors.....	79
<b>Figure 3.4:</b> FTIR spectra of P(3HB) produced using <i>B. cereus</i> SPV.....	80
<b>Figure 3.5:</b> a) Proton NMR and b) <sup>13</sup> C NMR spectra of P(3HB) produced using <i>B. cereus</i> SPV .....	81
<b>Figure 3.6.a:</b> SEM images of microspheres corresponding to experiments 1,3&4 ....	83
<b>Figure 3.6.b:</b> SEM images of microspheres corresponding to 7-10.....	83
<b>Figure 3.7:</b> SEM images of microspheres corresponding to experiments 1-15. ....	85
<b>Figure 3.8:</b> Average diameter of microspheres.....	86
<b>Figure 3.9:</b> Linear regression plot correlating the actual value and predicted value for mean particle diameter.....	90
<b>Figure 3.10.a:</b> response surface plots showing the effect of PVA concentration and polymer concentration on particle size.....	91
<b>Figure 3.10.b:</b> response surface plots showing the effect of PVA concentration and stirrer speed on particle size .....	91
<b>Figure 3.10.c:</b> 3- D response surface plots showing the effect of polymer concentration and stirrer speed on particle size. ....	92
<b>Figure 3.11:</b> a) SEM images of microspheres.....	92

<b>Figure 3.12:</b> a) Porosity of microspheres corresponding to experiment number 1-11 and 13 and 14 b) Comparison of effect of stirrer speed on porosity c) Comparison of effect of polymer concentration on porosity.....	94
<b>Figure 3.13:</b> Surface residual PVA of microspheres .....	95
<b>Figure 3.14:</b> Surface hydrophobicity microspheres.....	97
<b>Figure 3.15:</b> SEM images of nanospheres prepared under process conditions corresponding to <b>a)</b> experiment number 1, <b>b)</b> experiment number 2.....	99
<b>Figure 3.16:</b> SEM images of microspheres produced using process parameters corresponding to <b>a)</b> experiment number 4, <b>b)</b> experiment number 5.....	100
<b>Figure 3.17.a:</b> SEM image of microspheres prepared under process conditions corresponding to experiment number 7. ....	101
<b>Figure 3.17.b:</b> SEM image of microspheres corresponding to experiment number 9 .....	101
<b>Figure.3.18:</b> SEM images of a) Nanospheres prepared under conditions corresponding to experiment 3, microspheres prepared under conditions corresponding to experiment number b)6, c)8, and d)10.....	102
<b>Figure 3.19:</b> Temporal growth profile of <i>B. subtilis</i> OK2 for the production of P(3HB) in 5L bioreactors.....	103
<b>Figure 3.20:</b> FTIR analysis spectrum of P(3HB) produced from <i>B. subtilis</i> OK2 .....	105
<b>Figure 3.21:</b> <b>a)</b> Proton NMR and <b>b)</b> <sup>13</sup> C NMR of P(3HB) produced using <i>B. subtilis</i> OK2 .....	106
<b>Figure 3.22:</b> TEM images.....	108
<b>Figure 3.23:</b> SEM images of spheres prepared using process conditions corresponding to experiment number a)1, b) 2, c)3 and d)4. ....	109
<b>Figure 3.24:</b> SEM images of nanospheres prepared under process conditions corresponding to experiment number <b>a)</b> 5, <b>b)</b> 6, and <b>c)</b> 7.....	110
<b>Figure 3.25:</b> Size distribution charts of nanospheres and microspheres prepared from A) <i>B. subtilis</i> OK2 B-E) <i>B. cereus</i> SPV, corresponding to conditions in table 3.8.....	112
<b>Figure 3.26:</b> Porosity of nanospheres prepared using P(3HB) extracted from <i>B. subtilis</i> OK2 and nanospheres and microspheres prepared using <i>B. cereus</i> SPV, corresponding to conditions in table 3.8.....	113
<b>Figure 3.27:</b> Representation of percentage residual PVA on nanospheres prepared using P(3HB) extracted from <i>B. subtilis</i> OK2 and nanospheres and microspheres prepared using <i>B. cereus</i> SPV, corresponding to conditions in table 3.8.....	114
<b>Figure 3.28:</b> Comparison of hydrophobicity of nanospheres prepared using P(3HB) extracted from <i>B. subtilis</i> OK2 and nanospheres and microspheres prepared using <i>B. cereus</i> SPV, corresponding to conditions in table 3.8 .....	115
<b>Figure 4.1:</b> Mechanism of action of ‘Limus’ group of drugs .....	123
<b>Figure 4.2:</b> SEM images of a) microspheres produced using P(3HB) of Mw 9341 Da, b) magnified image of intermittent nanospheres c & d) microspheres produced using P(3HB) (98,268 Da) and PLLA (30-50 kDa). ....	128
<b>Figure 4.3:</b> a) P(3HB) microspheres with 5 wt% Rapamycin, b) P(3HB) microspheres with 10 wt% Rapamycin, c) PLLA microspheres with 5 wt% Rapamycin, d) PLLA) microspheres with 10 wt% Rapamycin.....	129
<b>Figure 4.4:</b> Size distribution analysis.....	131
<b>Figure 4.5:</b> Porosity measurements .....	132
<b>Figure 4.6:</b> Surface residual PVA measurements .....	133

<b>Figure 4.7:</b> Hydrophobicity expressed as a function of surface bound Rose Bengal dye.....	134
<b>Figure 4.8:</b> Protein adsorption .....	135
<b>Figure 4.9:</b> Water uptake and weight loss measurements .....	137
<b>Figure 4.10:</b> pH changes.....	138
<b>Figure 4.11:</b> Encapsulation efficiency .....	139
<b>Figure 4.12:</b> Rapamycin release profile.....	140
<b>Figure 4.13:</b> SEM images of a) unloaded P(3HB) nanospheres, b) unloaded P(3HB) microspheres.....	143
<b>Figure 4.14:</b> SEM images .....	144
<b>Figure 4.15:</b> Particle size distribution .....	145
<b>Figure 4.16:</b> Porosity measurements .....	146
<b>Figure 4.17:</b> Surface residual PVA.....	147
<b>Figure 4.18:</b> Hydrophobicity expressed as a function of surface bound Rose Bengal dye.....	148
<b>Figure 4.19:</b> Protein adsorption.....	149
<b>Figure 4.20:</b> Water uptake measurements and weight loss measurements .....	151
<b>Figure 4.21:</b> pH changes.....	152
<b>Figure 4.22:</b> Representation of percentage of Tacrolimus encapsulated .....	153
<b>Figure 4.23:</b> Tacrolimus release from P(3HB) nanospheres and microspheres with 1 wt%, 5 wt% and 10 wt% drug loading .....	154
<b>Figure 4.24 a-i:</b> SEM images of spheres corresponding to experiment number 1-9 in table 4.7.....	158
<b>Figure 4.25:</b> Particle size distribution of VEGF encapsulated a) nanospheres b) microspheres in the size range of 5-15 $\mu\text{m}$ and c) microspheres in the size range of 20-30 $\mu\text{m}$ .....	159
<b>Figure 4.26:</b> Porosity measurements .....	160
<b>Figure 4.27:</b> Surface residual PVA.....	161
<b>Figure 4.28:</b> Hydrophobicity expressed as a function of amount of Rose Bengal dye bound .....	162
<b>Figure 4.29:</b> Protein adsorption.....	163
<b>Figure 4.30:</b> Water uptake measurements and weight loss measurements .....	164
<b>Figure 4.31:</b> Comparison of pH changes.....	165
<b>Figure 4.32:</b> SEM images of collagen scaffolds embedded with a) nanospheres, b) microspheres of size range 5-15 $\mu\text{m}$ and c) microspheres of size range 20-30 $\mu\text{m}$ . .....	167
<b>Figure 4.33:</b> Comparison of swelling ratio of collagen scaffolds with particle embedded collagen scaffolds .....	167
<b>Figure 4.34:</b> Encapsulation efficiency of VEGF in nanospheres and microspheres before and after being embedded in collagen scaffolds .....	168
<b>Figure 4.35:</b> Comparison of VEGF release profile .....	170
<b>Figure 5.1:</b> Porphyrin derivatives.....	187
<b>Figure 5.2:</b> SEM images of Porphyrin encapsulated microspheres.....	190
<b>Figure 5.4:</b> Particle size distribution .....	194
<b>Figure 5.5:</b> Porosity of porphyrin encapsulated microspheres .....	195
<b>Figure 5.6.a):</b> Surface residual PVA of porphyrin encapsulated microspheres .....	196
<b>Figure 5.6.b):</b> Hydrophobicity represented as a function of the amount of Rose Bengal dye.....	197

<b>Figure 5.7:</b> Amount of protein adsorbed on the surface of porphyrin encapsulated microspheres.....	198
<b>Figure 5.8:</b> Encapsulation efficiencies of microspheres with increasing loadings of porphyrin derivatives.....	199
<b>Figure 5.9:</b> SDS-PAGE and Coomassie stained gel of anti-HER-2 antibody 4D5-8 with RFP, 4D5-8RFP12 .....	200
<b>Figure 5.10:</b> Amount of Anti- HER-2 adsorbed on P(3HB) microspheres encapsulated with 10 wt% drug loading of PP, HP and TPP.....	201
<b>Figure 5.11:</b> Percentage cell viability of SK-BR-3 .....	203
<b>Figure 5.12:</b> Confocal images of live/dead assay conducted on SK-BR-3.....	205
<b>Figure 5.13:</b> IC50 calculations for 10 wt% TPP encapsulated microspheres .....	206
<b>Figure 6.1:</b> P(3HB)-HA microspheres prepared under conditions corresponding to experiment number 8 .....	216
<b>Figure 6.2:</b> SEM images of P(3HB)-HA microspheres prepared under conditions corresponding to experiment number 10 .....	216
<b>Figure 6.3:</b> P(3HB)-HA microspheres a) not washed with isopropanol b) washed twice with isopropanol and c) washed 4 times with isopropanol .....	217
<b>Figure 6.4:</b> Particle size distribution of P(3HB)-HA microspheres .....	217
<b>Figure 6.5:</b> FTIR spectra of P(3HB)- HA microspheres .....	218
<b>Figure 6.6:</b> Swelling studies of P(3HB)-HA microspheres at different pH values.....	219
<b>Figure 6.7:</b> P(3HB)-HA microspheres encapsulated with a) Aspirin, b) Gentamycin	220
<b>Figure 6.8:</b> Drug release profile of a) Aspirin and b) Gentamycin encapsulated in P(3HB)- HA microspheres.....	221
<b>Figure 6.9:</b> P(3HB)- HA microspheres encapsulated with curcumin .....	222
<b>Figure 6.10:</b> Release profile of curcumin from P(3HB)-HA microspheres .....	223
<b>Figure 6.11:</b> MRSA inhibition of free and encapsulated curcumin .....	225

## LIST OF TABLES

<b>Table 1.1:</b> Correlation between release exponent 'n' and release mechanism in spherical DDS, following Korsmeyer-Peppas model (Carbinatto et al., 2014).....	27
<b>Table 1.2:</b> Thermal and mechanical properties of some PHAs (Valappil et al., 2006).....	33
<b>Table 1.3:</b> Biomedical applications of PHAs (Nigmatullin et al., 2015).....	34
<b>Table 2.1:</b> Drugs encapsulated and their wt.% with respect to polymer .....	58
<b>Table 2.2:</b> Optimization conditions for Amphiphilic microspheres .....	60
<b>Table 2.3:</b> Drug release models .....	68
<b>Table 3.1:</b> Conditions used for pilot experiments in making P(3HB) microspheres... ..	82
<b>Table 3.2:</b> Boundary conditions for microsphere optimization.....	84
<b>Table 3.3:</b> Design of experiments generated using MiniTab Express .....	84
<b>Table 3.4:</b> The observed and fitted value for particle diameter .....	88
<b>Table 3.5:</b> Analysis of variance for factors and factor interactions influencing particles size, performed using the JMP software. A: Polymer concentration, B: PVA concentration, and C: Stirrer speed.....	88
<b>Table 3.6:</b> Conditions for the optimization of micro and nanospheres of varying size ranges .....	98
<b>Table 3.7:</b> Process conditions for the preparation of nanospheres using P(3HB) extracted from <i>B. subtilis</i> OK2.....	107
<b>Table 3.8:</b> Coding for microspheres used in comparative study and their corresponding fabrication methods.....	111
<b>Table 3.9:</b> Table representing the mean particle size of nanospheres prepared using P(3HB) extracted from <i>B. subtilis</i> OK2 and nanospheres and microspheres prepared using polymer extracted from <i>B. cereus</i> SPV, corresponding to conditions in table 3.8. ....	112
<b>Table 4.1:</b> Molecular weight analysis of P(3HB) subjected to hydrolytic depolymerization.....	126
<b>Table 4.2:</b> Processing conditions for the optimization of PLLA and P(3HB) microspheres.....	127
<b>Table 4.3:</b> Size distribution analysis of P(3HB) and PLLA microspheres with and without encapsulated rapamycin. ....	132
<b>Table 4.4:</b> Summary of model fitting for Rapamycin release from P(3HB) and PLLA microspheres.....	141
<b>Table 4.5:</b> Processing conditions for the production of P(3HB) microspheres and nanospheres with encapsulated Tacrolimus.....	143
<b>Table 4.6:</b> Summary of model fitting for Rapamycin release from P(3HB) and PLLA microspheres.....	155
<b>Table 4.7:</b> Process parameters employed for the synthesis of VEGF encapsulated microspheres and nanospheres.....	157
<b>Table 4.8:</b> Summary of model fitting for VEGF release from free P(3HB) nanospheres and microspheres and P(3HB) nanospheres and microspheres embedded in collagen. ....	172

<b>Table 5.1:</b> Experimental design for optimization of porphyrin encapsulated microspheres production. ....	191
<b>Table 5.2:</b> Average particle diameter of porphyrin encapsulated microspheres (n=3, error= $\pm$ s.d). ....	193
<b>Table 6.1:</b> Optimization of microspheres using P(3HB)- HA conjugate.....	215
<b>Table 6.2:</b> Comparison of P(3HB)-HA microspheres encapsulated with Aspirin and Gentamycin. ....	220
<b>Table 6.3:</b> Summary of model fitting for drug release from free P(3HB)- HA microspheres.....	224

## Abbreviations

---

CSC	Cancer stem cells
DCW	Dry cell weight
DDS	Drug delivery system
EPR	Enhance permeability and retention
Eth D-III	Ethidium homodimer- III
FTIR	Fourier transform infrared spectroscopy
GPC	Gel permeation chromatography
GST	Glutaraldehyde saturated toluene
HP	Hematoporphyrin ether
HPLC	High performance liquid chromatography
IGF-1	Insulin-like growth factor
LPS	Lipopolysaccharide
Mab	Monoclonal antibody
MCL-PHA	Medium-chain length PHA
MIC	Minimum inhibitory concentration
MRSA	Methicillin resistant <i>Staphylococcus aureus</i>
P(3HB)	Poly(3-hydroxybutyrate)
PBS	Phosphate buffer saline
PCL	Polycaprolactone
PDLA	Poly(D-lactic acid)
PDR	Photodynamic reaction
PDT	Photodynamic therapy
PEG	Polyethylene glycol
PHA	Polyhydroxyalkanoate
PIT	Photoimmunotargeting
PLGA	Poly(L-lactic acid)
PP	Photoporphyrin IX
PVA	Polyvinyl alcohol
RESS	Rapid expansion of supercritical solutions

ROS	Reactive oxygen species
RPM	Revolutions per minute
SBF	Simulated body fluid
SCF	Supercritical fluid
SCL-PHA	Short-chain length
TPP	Tetraphenylporphyrin
VEGF	vascular endothelial growth factor
W/O/W	Water-in-oil-in-water

# Chapter 1.

# Introduction

## 1.0. Controlled drug delivery

The process of drug formulation and commercialization is lengthy and extremely costly (Vilos and Velasquez, 2012). Commercialization of a drug involves 3-5 years of preclinical development, 6-8 years of clinical trials and 2-3 years of market surveillance (**Figure 1.1**). Even after the lengthy process of the development of drug molecules, their successful commercialization is minimal (Vilos and Velasquez, 2012). Between 2007 to 2016, only 134 new drug molecules were approved worldwide of which, 30.6% was by the European Medicines Agency (EMA) (Zeukeng, Seoane-Vazquez and Bonnabry, 2018).

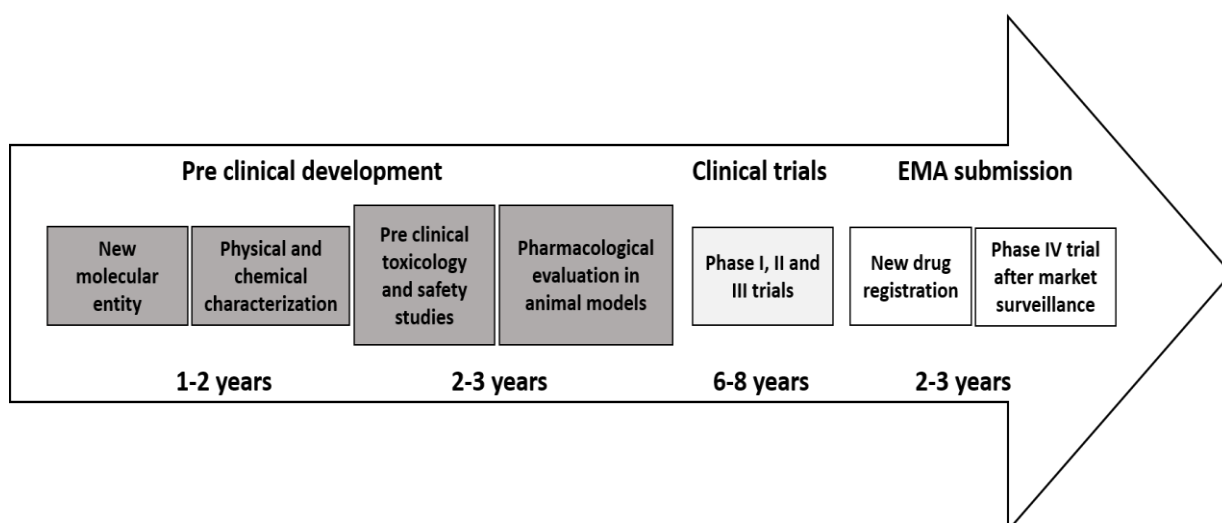


**Figure 1.1:** A schematic representation of stages of commercialization of a new drug molecule, as required by European Medicines Agency (EMA) (adapted from Vilos and Velasquez, 2012).

Apart from the time and economic constraints of the process of drug development, conventional therapeutics also suffers from its inability to often attain efficient disease management. This is because of the fact that conventional modes of delivery, often fail in maintaining minimally fluctuating therapeutic dosage of drug molecules for a prolonged period of time in the blood stream (Mansour *et al.*, 2010). The drawbacks of conventional

therapeutics that are administered in the forms of oral (tablets and capsules), and intravenous injections are several. These include limited solubility of drug molecules in the blood stream, short half-lives that result in diminished or no delivery to the site of action, interaction with other molecules in the biological milieu, and increased biodistribution (Cullis, 2014). The low solubility and short half-life of molecules frequently imposed the need to have repeated administration protocols, which result in fluctuations that reach toxic blood levels of the administered molecules. Poor solubility of drugs can also result in precipitation of drugs in aqueous environment, which can again be toxic. Biodistribution of cytotoxic drugs such as doxorubicin can also cause necrosis and tissue damage, in the case of 'free' drugs (Cullis, 2014). Also, lack of target specificity of conventional administration often results in suboptimal bioavailability of drugs at the target site (Rabinow *et al.*, 2004). All these impediments of conventional drug delivery necessitated the development for new therapeutic modes of applications for existing drug molecules.

Controlled drug delivery is the sustained release of therapeutic agents, with time or stimuli, allowing for the maintenance of drug concentrations in the biological milieu within the therapeutic window (Yun *et al.*, 2014). By using suitable drug delivery systems (DDS) such as lipid/ polymer particulates, implants, gastro-retentive and transdermal systems, the functionalities of 'free' therapeutic agents can be controlled and improved (Cullis 2014). These drug delivery systems can alter the pharmacokinetics and biodistribution in a desirable fashion and act as a reservoir for the agent being transported. Hence, the physicochemical properties and biocompatibility of the materials used as drug delivery systems are of huge significance. The desirable properties of these materials would include increased circulation time within the body in comparison with drug molecules of low half-life, low cytotoxicity, inertness to biological environment, and higher uptake at target sites

(Elzoghby *et al.*, 2012). Various natural and synthetic materials have historically been used to formulate drug delivery systems. Although petro-chemically derived polymers such as plastics have been extensively used in pharmaceuticals, their non-biodegradability required post implant procedures to eliminate these systems from the body. A well-designed DDS is identified as one that is capable of specific targeting, intracellular absorption, biocompatibility, along with responsive behaviour to physiological conditions. The most defined progress in modern drug delivery is the spatiotemporal release of therapeutics in both pulsatile dose delivery products and implanted reservoir systems, from polymeric drug delivery systems (Liechty *et al.*, 2010). Controlled drug delivery is a dynamic research field which traces its history of 60 years from the macro to micro and nano eras, referring to the size range of DDS formulation, with new entrants of DDSs being formulated constantly ( Elzoghby *et al.*, 2012).

### **1.1. Micro and Nanospheres**

The applications of biodegradable and biocompatible polymers in biomedical applications have accelerated, and drug delivery systems based on these materials have received increased attention. The most prominent of these are micro and nanospheres formulations. Microparticles are drug delivery systems that range between 1-1000  $\mu\text{m}$  in size and nanoparticles are those that range between 1-1000 nm in size. These particulate DDS have reduced the administration frequency of existing therapeutic formulations, especially of proteins and nucleic acids (Mansour *et al.*, 2010). The manipulability of these particulate DDS is significant and hence, these are increasingly employed in delivery of a multitude of drug molecules; both of hydrophobic and hydrophilic nature; and of varying molecular size ranges. Although different classes of drugs such as opioids, growth

hormones, contraceptives and antibiotics come under the purview of controlled drug delivery using polymeric particulate DDS, the advancement of these in anticancer drug delivery is so promising. The technique followed for the synthesis of polymeric particulate DDS depends primarily on the therapeutic drug being incorporated, polymer used, size range of the anticipated spheres (<250  $\mu\text{m}$ , ideal for parenteral administration) and reproducibility (Park, Ye and Park, 2005). The most common methods employed are spray drying, supercritical fluid technology and the solvent evaporation method.

### **1.1.1. Spray drying**

Spray drying involves spraying a solution or suspension of polymer and drug in a volatile organic solvent to a stream of heated air. The narrow tip of the nozzle used for spraying atomizes the solution/suspension droplets, and this process determines the size of the particles obtained. Atomization pressure, feed rate, airflow, inlet temperature, outlet temperature, and the size of nozzle orifice are the determinant variables for particle size range using this technique. Spray drying is a technique widely used in the food industry and pharmaceuticals and has several advantages such as good reproducibility, better control over particle size range and less dependency on organic solvents being used. Low process yield is one of the main disadvantages of this technique, since formation of large aggregates during the process can result in a lot of the material being lost ( Park, Ye and Park, 2005; Mansour *et al.*, 2010).

### **1.1.2. Supercritical fluid technology**

Substances are said to be at their supercritical fluid (SCF) state when they are exposed to pressure and temperature above their critical points. Supercritical fluid technology is said to be highly economical with low process operatives (maintenance of temperature and

pressure) (Thakkar *et al.*, 2009). At SCF state, substances exhibit the solvent properties of a liquid and flow properties of gas. CO<sub>2</sub> is a commonly used SCF solvent, due to its low critical temperature (T<sub>c</sub> = 31.1 °C) and pressure (P<sub>c</sub> = 73.8 bar).

There are two main techniques of generating particles using SCF technology. The first technique to generate particles using SCF technology is rapid depressurization of the SCF in which the polymer and drug are dissolved. This rapid depressurization is achieved by Rapid Expansion of Supercritical Solutions (RESS) through fine nozzles at supersonic speeds resulting in the supersaturation of the solute and its precipitation (Thakkar *et al.*, 2009). Polar high molecular weight molecules such as proteins are insoluble in supercritical CO<sub>2</sub> and in these instances, a suitable solvent in which the molecule is soluble is used, which is later impregnated with supercritical CO<sub>2</sub>, Producing a gas saturated solution (GSS). This will result in lowering of the solute concentration in the entire volume of the solution, and reduced viscosity. This solution is then subjected to rapid decompression, resulting in the precipitation of particles (Mansour *et al.*, 2010). Often salting out of particles is preferred using an antisolvent technology, wherein a poor solvent of the solute is rapidly added to the SCF, which results in the rapid precipitation of the solutes. The main disadvantage of this technique is the poor control over size and morphology as crystallization need not always result in spherical moieties (Thakkar *et al.*, 2009).

### **1.1.3. Solvent evaporation method**

Although polymeric micro/nanospheres are prepared by various techniques such as spray drying, solvent evaporation of emulsions, phase separation coacervation, spray congealing, solvent extraction, and Quassi emulsion solvent diffusion, solvent evaporation for emulsions is the most extensively researched technique and is followed throughout this

project (Nigmatullin *et al.*, 2015). Based on the type of the encapsulated drug, the nature of emulsions can vary; hydrophobic drugs can be better encapsulated in oil-in-water (o/w) emulsions and hydrophilic drugs in water-in-oil-in-water (w/o/w) emulsions. In the encapsulation of hydrophobic drugs, the drug and the polymer are dissolved and dispersed in an organic solvent (oil phase), which is then emulsified in an aqueous phase containing surfactants (water phase) as illustrated in **Figure 1.2**.

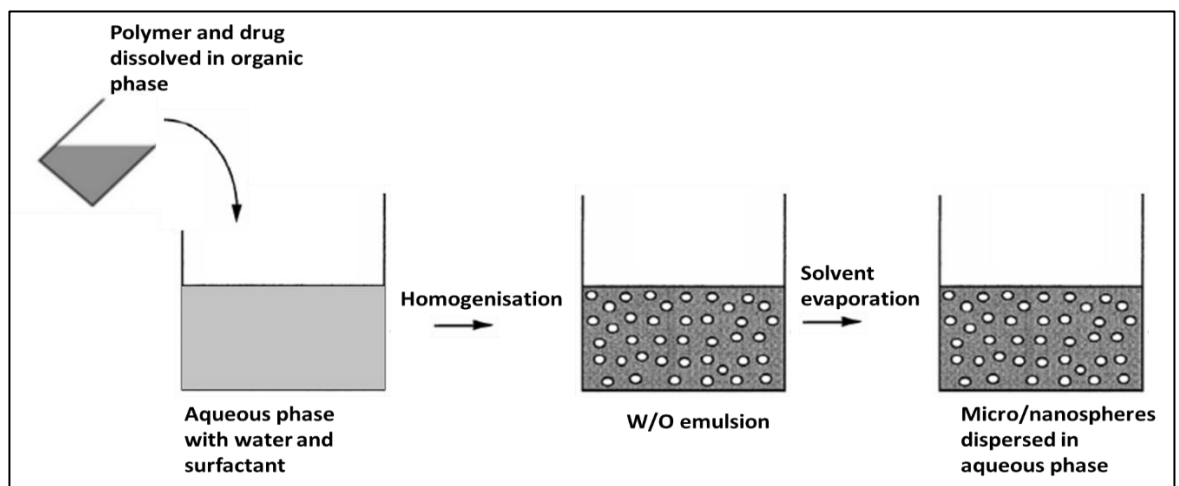


**Figure 1.2:** Schematic representation of preparation of microspheres to encapsulate hydrophobic drugs, using water-in-oil emulsion technique.

Emulsification can be achieved through different methods of agitation such as sonication, homogenisation, or mechanical/magnetic stirring, during which the oil phase is dispersed throughout the water phase. The agitation breaks down the emulsion droplets to smaller sizes, and this process can be optimised to get different size ranges.

As the organic solvent evaporates, the polymer shrinks around the core, assuming spherical geometry, due to the circular nature of agitation. Hydrophobicity of the drug enables the drug to agglomerate towards the shrinking polymer as opposed to hydrophilic drugs, which might tend to remain in the aqueous phase.

In the case of hydrophilic drug encapsulation, the drug is dissolved in a water phase and then dispersed in the organic phase as illustrated in **Figure 1.3**. This continuous phase is added to a water phase containing surfactants, to form an emulsion. During solvent evaporation, the polymer starts shrinking towards the core, also entrapping microdroplets of the emulsion which coalesce to form a honey comb structure with interconnecting water channels (Nigmatullin *et al.*, 2015).

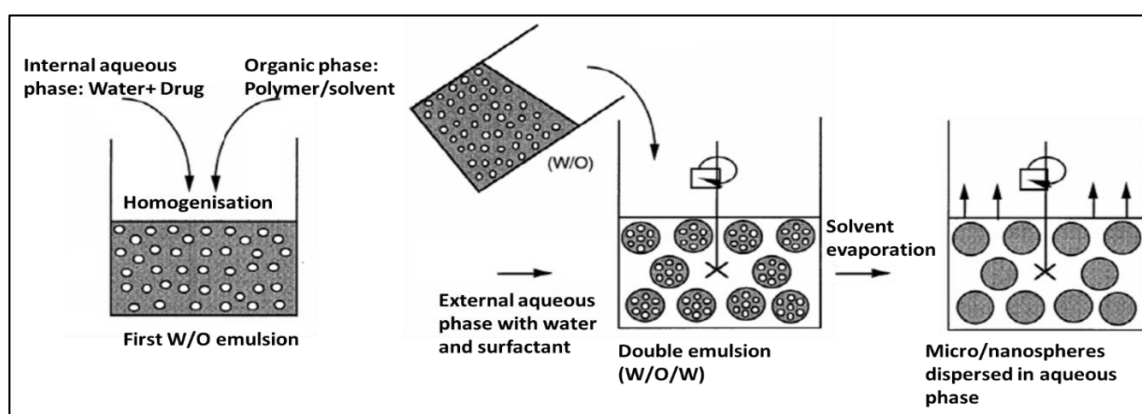


**Figure 1.3:** Schematic representation of preparation of microspheres to encapsulate hydrophilic drugs, using double emulsion technique.

The preparation of microspheres using solvent evaporation of emulsions considers a range of parameters such as material properties of the polymer, concentration of the polymer in the organic phase, chemical composition of organic phase, concentration of the surfactant in the water phase, rate of solvent evaporation which is governed by stirring speed and temperature (Nidhi *et al.*, 2016). Material properties of the polymer such as molecular weight, crystallinity and hydrophobicity have a pronounced effect on the process. Molecular weight and concentration of the polymer is directly correlated with the viscosity of the organic phase. Hence, an increase in these parameters is expected to increase the viscous forces against which the shear forces of agitation must act. An increased viscosity

would mean a reduced distribution of shear forces, hence resulting in the formation of larger emulsion droplets. Therefore, keeping all the other variables stable, an increase in polymer concentration or use of a polymer of higher molecular weight is expected to produce spheres of larger sizes (Srivastava *et al.*, 2016). Nature of the organic solvents used can also affect the process, since different solvents have different viscosity and miscibility with the aqueous phase and the rate of evaporation also can vary based on their surface tension.

## **1.2. Effect of process parameters in the preparation of micro/nanospheres using solvent evaporation technique**

### **1.2.1. Polymer**

The nature of the polymer, especially the molecular weight plays a significant role in determining the morphology and size of particles produced using solvent evaporation technique, and subsequent drug release. Mark-Houwink-Sakurada (MHS) equation states viscosity as a function of relative molecular weight of a polydispersed polymer ( $\eta = KM_w$ , where  $\eta$  is the viscosity, K is the MHS constant and  $M_w$  is the relative molecular weight) (Reis *et al.*, 2007). Molecular weight of a polymer depends on its origin, and in the case of biopolymers, is influenced by production variables such as the microorganisms used and their amino acid pool, nutrients supplied, aeration, and the length of fermentation process. Weight fraction of the polymer used (concentration) is yet another parameter that influences viscosity. Viscosity of the dispersed phase can influence the disentanglement of polymeric chains and hence the higher the viscosity, the greater is the amount of energy required for this process. Therefore, an increased viscosity can result in formation of larger

emulsion droplets which subsequently form larger spheres of increased wall thickness. A reduction in disentanglement due to increased viscosity would also result in closely packed matrices, which has a pronounced effect on the porosity of the microspheres formed (Subedi, Shrestha and Shakya, 2016).

Ahmed *et al.*, optimised a depot injectable atorvastatin biodegradable *in situ* gel using PLGA and PEG and the experimental design and analysis was carried out using a central composite design (Ahmed *et al.*, 2016). Concentration of PLGA and molecular weight of PEG were amongst the independent variables analysed and were found to have pronounced effects on the synthesis process and release profile of the drug. It was found that high molecular weight formulations of PEG (PEG 4000) were difficult to inject as opposed to the low molecular weight ones (PEG 400). The burst release after 2 hours was found to decrease from 30.79% to 17.24% when PEG4000 and PEG400 respectively, were used (Ahmed *et al.*, 2016).

Crystallinity of the polymer used is also known to influence drug release rate, since crystallinity can influence the rate of polymer degradation. Crystalline regions of a polymer are mechanically stronger than amorphous regions and less prone to hydrolytic degradation. Highly crystalline polymers with slower degradation rates are ideal for release of drugs that require a prolonged release kinetics (Akhtar *et al.*, 1992).

### **1.2.2. Surfactant**

Aggregation of the spheres formed is a major concern in any of the synthesis techniques employed to make micro/nanospheres. Surfactant such as PVA is used to circumvent this issue. Surfactants are amphiphilic moieties with a hydrophilic head and hydrophobic tail (Ansary *et al.*, 2014). The nature and concentration of surfactant used have been reported

to affect morphology of spheres produced and drug release kinetics. Surfactants being amphiphilic, can increase the wettability and thereby the degradation rate of the polymer, resulting in a faster release of the incorporated drug. Increasing the surfactant concentration results in the lowering of interfacial energy between emulsion droplets, which causes in the formation of smaller particles. Increase in surfactant concentration is also known to affect extent of drug entrapment as a high concentration of surfactant in the dispersed phase can result in the drug molecules having a higher affinity to the surfactants, as opposed to the polymer matrix. Further to this, high amount of surface residual surfactant can result in high amount of surface residing drug molecules, and this is likely to cause a burst release (Shrestha and Shakya, 2016).

### **1.2.3. Agitation**

Agitation or stirring in solvent evaporation technique is employed to ensure effective dispersion of the emulsion and reduction of emulsion droplet size. An agitation influences the extent to which the emulsion droplets are broken down, which subsequently translates to the size range of the spheres formed. Finer dispersions result in spheres of reduced porosity, and this can become a limiting factor in drug release. Therefore, increased agitation can be argued to bring about two antagonistic effects with respect to drug release; first one of which is smaller particle size- leading to increased surface area and therefore faster release, and the second is reduced porosity, which results in slower release. (Francis *et al.*, 2011; Caetano, Almeida and Gonçalves, 2016)

Francis *et al.*, in their study on Polyhydroxybutyrate microsphere with encapsulated gentamycin that illustrates the effect of stirrer speed on the size range of microspheres. When all the other parameters were maintained constant, and the stirrer speed was

increased from 300 rpm to 800 rpm, microspheres size was observed to decrease from 2  $\mu\text{m}$  to 1.58  $\mu\text{m}$  (Francis *et al.*, 2011).

### **1.3. Mechanisms of drug release**

Drug delivery systems are designed to attain optimal pharmacokinetic and pharmacodynamic profiles of a therapeutic agent in a temporally and spatially controlled manner. The design of these systems is heavily dependent on the polymer's biodegradability, biocompatibility, processability, and thermo-mechanical properties. Only polymers that are small enough (<50 kDa) to permeate through the renal globular membrane can be directly excreted from the body via renal excretion. This includes a very small window of non- biodegradable polymers and hence the need to consider other options. Controlled drug delivery systems cover a wide spectrum of structures or constructs, such as subcutaneous implants, compressed tablets for oral administration and micro-particulate carriers for subcutaneous and intravenous use. The type of drug delivery systems can influence the mechanism of drug release and hence pharmacokinetics, degradation profile and extent of entrapment. Mechanism of controlled release from these DDS varies depending on the type of polymer used, nature of encapsulated drug, and the physiological conditions they are exposed to. Different kinds of release mechanisms- dissolution followed by diffusion, partitioning, osmosis, swelling, erosion, and targeting- or one or more of their combinations usually affect drug release rate (Nigmatullin *et al.*, 2015).

#### **1.3.1. Dissolution followed by diffusion**

Dissolution is the transfer of a substance from its solid phase to the surrounding liquid medium. Solubility in a given medium is defined as the concentration of any substance at its saturation. Drug delivery systems controlled by dissolution involve phase erosion of the

polymer carrier or drug that is associated with fast or slow dissolution of the macromolecular chains. This method is adopted in two kinds of devices- monolithic and reservoir. In monolithic devices, the therapeutic agents are entrapped homogeneously within the polymer matrix, whereas in a reservoir device a protective coating of polymer encloses the therapeutic agent in a core. The release rate of therapeutic agents encapsulated in a reservoir can be modulated by controlling dissolution parameters of the polymer or the coating of polymers. The thickness of the coating in this case can affect the rate of release (Shen *et al.*, 2004). Polymer molecular weight, water, polymer and drug diffusion coefficients, equilibrium water concentration in the polymer, and water-polymer interaction are the parameters that control the mechanism and rate of drug release by dissolution, followed by diffusion (Narasimhan and Peppas, 1997). Diffusion and dissolution are interdependent as both are influenced by the concentration of the therapeutic agent in the surrounding medium.

### **1.3.2. Partitioning**

Partition coefficient, which is the relative affinity of a substance to two different materials or phases, can be exploited to manipulate drug release kinetics. Hydrophilicity and hydrophobicity of drug molecules greatly affect the design of delivery systems. Hydrophobic drugs have been known to encapsulate in DDS with a hydrophobic core and hydrophilic corona to increase their uptake into the blood stream (Lao, Venkatraman and Peppas, 2008). PLA micelles as an excipient of Paclitaxel are such an example where the hydrophobic drug is partitioned into the core and can be retained until their delivery to the site of action (Kim *et al.*, 2010).

### 1.3.3. Osmotic release

This type of delivery depends on the availability of a semipermeable membrane protecting the hydrophilic therapeutic agent, allowing a controlled amount of water to enter the core and dissolve the therapeutic agent. The flux of water to the core is determined by the chemical potential of water or water potential on either side of the polymer membrane (Omidian *et al.*, 2012). Here, the pores or delivery orifices of the membrane are designed in such a manner that they coincide with a certain release rate. Therefore, with the water influx, the drug molecules either dissolve in the water or are released through these pores. Hydroxy ethyl cellulose, carboxy methylcellulose, hydroxy propyl methylcellulose, high-molecular-weight poly(vinylpyrrolidone) are examples for the hydrophilic polymers and ethyl cellulose and wax materials are examples for the hydrophobic polymers used for this purpose. Sometime molecules known as osmogens are incorporated within the core, that would increase the osmotic pressure and expel the medicament faster. Sodium chloride, potassium chloride, and mannitol are such examples and various poorly soluble therapeutic agents are encapsulated as their salts to increase solubility. Another strategy is the use of wicking agents, which have the inherent ability to absorb water, on the polymeric membranes. Wicking agents form water channels between the outer and inner surfaces of the membrane. Colloidal silicon dioxide, PVP and Sodium lauryl sulphate are common examples of such agents that aid in forming such channels via physisorption of water (Keraliya *et al.*, 2012).

### 1.3.4. Swelling

Swelling occurs when the polymeric matrix or shell takes up water and increases in volume, a common phenomenon that precedes dissolution. However, swelling does not necessarily

lead to dissolution, especially in the case of hydrogels. Swelling is often by virtue of large polymer chains or by the introduction of crosslinks forming networks that trap water. In polymers that swell rapidly, diffusion of the drug is controlled by the swelling rate. Swelling is dependent on parameters such as temperature and pH and therefore alternating these physiological conditions can result in reverse swelling, hence it is possible to create a DDS with a controllable drug diffusion (Omidian *et al.*, 2012).

### **1.3.5. Erosion**

Erosion is a very significant and rate-determining phenomenon in controlled drug delivery, especially with hydrolytically labile polymers. There are two mechanisms of erosion, bulk and surface erosion, which dictate the directionality of degradation. In bulk erosion, water penetrates the entire matrix of the polymer and initiates hydrolysis and chain scissions, across the matrix. The initial chain scissions would accelerate water diffusion into the core of the matrix and thereby degrade the whole matrix in a rapid fashion. This phenomenon can also be autocatalytic when the erosion products are acidic, and the hydrolysis of the polymer is acid catalysed (Omidian *et al.*, 2012). In surface erosion, mass loss and degradation occur near the surface of the DDS, in a mechanism that is analogous to the peeling of an onion. This happens either due to slow penetration of water into the matrix where highly hydrophobic polymers are used. The water first hydrolyses the surface that it is in contact with, and this leads to the release of the therapeutic agent that is trapped in that layer. This process follows until the entire DDS has experienced mass loss, resulting in a progressive reduction in size of the DDS. Surface erosion brings about more linear changes in mechanical performance, drug release, and volume reduction, and hence is an attractive attribute in DDS. Both surface and bulk erosion follow the same molecular

phenomenon of hydrolytic scission in the presence of water but are differentiated by how quickly the waterfront can penetrate through the matrix (Lyu and Untereker 2009). A matrix undergoes surface erosion, if the degradation of the surface polymer is faster than the rate of water penetration into the entire matrix. It is the difference in thickness of the diffusion zones that dictate whether a sample would undergo surface or bulk erosion. For example, for a PLA sphere to undergo surface erosion the sample size needs to be more than 40mm in diameter, which is a size that is unsuitable for drug delivery applications (Lyu and Untereker 2009).

### **1.3.6. Targeting**

Targeting is a strategy to increase localization and therefore uptake of the therapeutic agents by designing DDS with materials that have an inherent affinity to the target site or incorporating adjuvants with affinity. Targeting is especially adopted in the case of micro and nano encapsulations, extensively in anti-cancer drug delivery. Cancer drugs are generally highly cytotoxic and can adversely affect non-cancerous tissues and hence the preference of targeting anti-cancer drug delivery. Several targeting methods are currently in use, as described in the section below.

#### ***1. Strategies for targeted anti- cancer therapy***

Cancer treatment necessitates the use of highly cytotoxic drugs, which can cause unacceptable side effects to normal tissues. Therefore, there is a preference for localization and delivery of the therapeutic agents precisely at the site of action as far as drug delivery of anticancer agents are concerned. Chemotherapy, which is the most common form of cancer intervention, has many drawbacks due to the low specificity and high toxicity of cancer drugs. Chemotherapeutic agents typically disrupt cell replication by inducing

apoptosis, and in most cases, this is not selective to cancer cells. Paclitaxel, doxorubicin, daunorubicin, cisplatin, and docetaxel are examples of some of the most commonly used anticancer drugs. These do not discriminate between cancer cells and healthy cells and highly proliferative tissues such as the hair, intestinal epithelial cells, and bone marrow become susceptible to their cytotoxic effect (Walker *et al.*, 2009).

Particulate DDS have the potential to decrease the side effects of anticancer agents, by improving target specificity and therapeutic efficacy (Walker *et al.*, 2009). These can be surface functionalised with cancer specific markers making them target specific. Encapsulating highly cytotoxic agents can reduce biodistribution, which ultimately translates to lower side effects and improved patient compliance. The design rationale of these systems increasingly depends on the tumour physiology, which is characterised by leaky vasculature, ill-defined lymphatic systems, and presence of growth factors such as Vascular Endothelial Growth Factors (VEGF) and several cancer specific markers. These physiological features render cancer tissues with Enhanced Permeability and Retention (EPR) of high molecular weight drug formulations, a phenomena DDS exploit.

Zhang *et al.*, illustrated the efficacy of PLGA microspheres encapsulated with the anticancer drug Temozolomide, in malignant glioma (Zhang *et al.*, 2010). According to this study, a dual therapeutic agent system consisting of Temozolomide encapsulated microspheres in combination with Vatalanib; an anti-angiogenic drug was found to be more effective in inducing cytotoxicity. In another study, having identified degradation products of PLGA as highly acidic and inflammatory, nanoscale Hydroxyapatite (nHA) was used as an adjuvant, to increase biocompatibility of the degradation products (Zhang *et al.*, 2012). This study compared two morphologies of DDS encapsulated with Temozolomide, the first one of

which was microspheres, and the second, rod shaped, for their ability for sustained drug release and cytotoxicity. The results showed that nHA addition had a significant effect in reducing burst control in both these structures.

Cancer stem cells (CSC) are considered as potent targets for cancer treatments as they are significant in initiation, propagation and regeneration of cancer (Li *et al.*, 2017). Cancer stem cell targeting is an accelerating area of research since the identification and characterization of cancer stem cells is rapidly advancing, providing a multitude of targeting strategies (Figure 1.4).

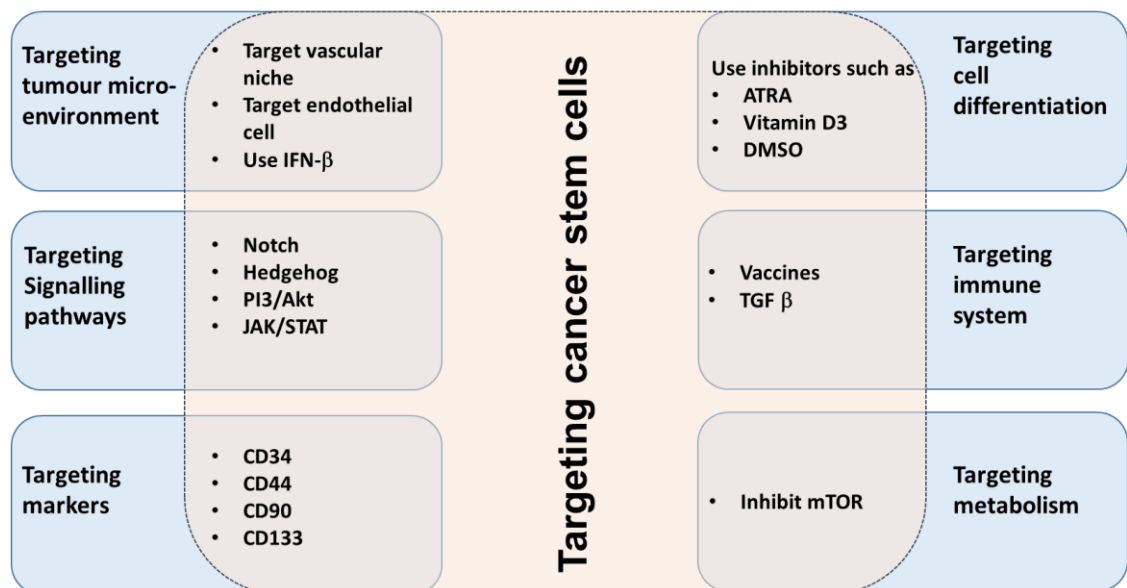


**Figure 1.4:** strategies of CSC targeting (reproduced from li *et al.*, 2017).

Li *et al.*, in their comprehensive review of cancer cell targeting mechanisms list six strategies for CSC targeting, as follows. A CSC niche supported by tumour microenvironment has an important role in multidrug resistance (MDR) and therefore, targeting elements such as vasculature and endothelial cells of this microenvironment and use of anti-inflammatory (IFN) drugs is the first strategy. A novel Rhodamine encapsulated integrin-targeted nanoparticle (ITNP) system was developed by Xie *et al.*, with the prospect

of targeted drug delivery and imaging of cancer angiogenesis. Integrin  $\alpha_v\beta_3$ , a cell surface receptor overexpressed in cancer angiogenesis, was targeted, using a lipid-based integrin antagonist. The INTPs exhibited increased uptake in comparison with control nanoparticles, when administered in C3H, mice bearing murine squamous cell carcinoma (Xie *et al.*, 2007). The second strategy is targeting signalling pathways involved in self-renewal (Notch), growth (Akt1 pathway) and apoptosis (Hedgehog). The other strategies include targeting markers such as CD33, CD44 and CD90, targeting cell differentiation, targeting immune system, and targeting metabolism. The targeting strategies that interfere with metabolism such as the limus family of drugs (everolimus, sirolimus and tacrolimus) that inhibit mammalian target of rapamycin (mTOR) are exclusively explored in cardiac stent applications.

Published literature on micro and nano particulate structures for cancer DDS is exhaustive, with a plethora of synthetic and natural polymers, and comprehensive usage of most of the existing chemotherapeutic agents. Chemoembolization with microspheres is an alternative practice in certain cancers, wherein the microspheres of sufficient size range are used to aid in sustained drug release, as well as blocking arterial supply to tumours. These systems known as Drug Eluting Microsphere-Transarterial Chemoembolization (DEM-TACE) were first conceptualised by Hori and Osuga using Sodium acrylate polyvinyl (SAP). Their improvised versions namely CE-approved HepaSphere and FDA-approved QuadraSphere microspheres are in market, for the treatment of primary and metastatic liver tumours. These embolic agents provided in a variety of size ranges (200-800  $\mu\text{m}$ ) have the capability to absorb 64 times their dry state volume and still maintain their spherical structure, thereby acting as arterial plugs (Rajput and Agrawal, 2010).

### 1.4. Theory of drug release

Drug release is the process by which a pharmacologically active agent leaves a DDS and becomes available for pharmacological action. To understand the drug release profile from any DDS, it is important to know about the various mass transport phenomena involved, as explained in the above section. Rapid release dosage forms such as tablets eliminate the active agents from them rapidly, resulting in overexposure of the drug. As time proceeds, this would gradually become underexposure, until the next dosage. Controlled drug delivery systems work towards increasing the presence of drug molecules within the therapeutic window, for longer durations (Bruschi and Luciano 2015). In many controlled devices, when they are initially brought in contact with the release medium, an excess amount of drug is eluted out and this phenomenon is known as burst release (Huang and Brazel, 2001). It is often desirable where a rapid initial dosage of the drug is required. But in case of devices that are designed to deliver longer release profiles, burst release is considered to be undesirable.

With the advances in formulation of various forms of DDS, mathematical modelling of drug delivery and release profile predictability is of huge commercial potential. *In silico* simulations to generate optimal designs by considering variables such as geometry and size of the DDS, solubility of the drug molecule incorporated, mode of erosion and degradation help increase predictability of temporal release profiles (Lao, Venkatraman and Peppas, 2008; Dash *et al.*, 2010). The parameters influencing release profiles vary, depending on the type of polymeric material used in DDS formulation, formulation technique, physiology, incorporated drug dose(s), types and amounts of excipients and degradation products (Siepmann and Siepmann, 2008). Generating predictive models can not only increase

accuracy and easiness of application, but also ensure pharmacokinetic safety, especially in the case highly potent drugs with narrow therapeutic windows (Siepmann and Siepmann, 2008). However, as in the case of purely diffusion-, or diffusion- and swelling-controlled release devices, mathematical modelling of erodible systems are not as advanced since these systems are more complex and are influenced by physicochemical processes apart from mass transport phenomena (Faisant, Siepmann and Benoit, 2002). Since it is not practical to consider all the contributing factors, often models take the most dominating phenomena into account (Faisant, Siepmann and Benoit, 2002). To compare drug release profiles from various DDS, there are a number of models available, most of which represent the fractional drug release as a function of time ( $f_t$ ). Many such models are based on Fick's laws describing mass transport per unit area. Fick's first law states that the amount of solid materials passing perpendicularly through a unit surface area per time from a DDS to its surrounding medium is directly proportion to the concentration gradient (Gouda, Baishya and Quing, 2017). According to this, a constant diffusion rate is achievable if the concentration gradient remains constant. Hick's second law states that a rate of change of concentration at a region is proportional to change in concentration gradient at that point. Release mechanisms are categorized into four, based on the mode of mass transport (Maderuelo, Zarzuelo and Lanao, 2011).

- 1). Fickian diffusion (type I): Drug release is dependent primarily upon diffusion
- 2). Polymer swelling (type II): Drug release is a result of swelling of the polymer that makes up the DDS
- 3). Anomalous / non Fickian diffusion: Drug release is dependent both on polymer swelling and diffusion

4). Super type II: Occurs in DDS where the surface gets hydrated and starts eroding.

While the quantitative representation of release from simpler forms of DDS can be facilitated by using generic equations such as in zero order (explained in section 1.4.1), in most cases theoretical analysis of the process doesn't suffice for an accurate prediction (Costa and Sousa Lobo, 2001). Release kinetics can be predicted in roughly two different ways; Empirical models that usually unify all the contributive parameters to a single zero-order process controlling the overall drug release rate, Mechanistic realistic mathematical models that consider diffusional mass transfer and/or chemical reactions (Faisant, Siepmann and Benoit, 2002). In the case of empirical models, the predictive power is considered to be low as the mathematical treatment is mostly descriptive, as opposed to the mechanistic models that take into account physical phenomena such as diffusion, dissolution, swelling, erosion, precipitation and/or degradation (Siepmann and Siepmann, 2008). Zero-order kinetics, first-order, Higuchi, Hixson-Crowell and Korsmeyer-Peppas are examples of some of the popular approaches employed.

### **1.4.1. Zero-order model**

In zero-order kinetics, the release of a drug from a DDS is directly proportional to time (Bruschi and Luciano 2015). Zero-order release kinetics is independent of the initial concentration. Constant release of active agent from the DDS is made possible along a concentration gradient and is mostly true for systems with a semipermeable coating. Osmosis property, dissolution, diffusion, and partition are identified as physical phenomena that can result in zero-order release of active agents from DDS (Bruschi and Luciano 2015). It is represented by the equation:

$$Q_t = Q_0 + K_0t$$

Where  $Q_0$  is the initial amount of drug in the solution it is being eluted to,  $Q_t$  is the amount of drug dissolved in time  $t$  and  $K_0$  is the zero- order constant (Dash *et al.*, 2010). Since for most systems  $K_0 \neq 0$ ,  $Q_t$  can be represented as a function of time ( $f(t)$ ), whose slope ( $\alpha$ ) is the zero- order constant  $K_0$  (Figure 1.5).

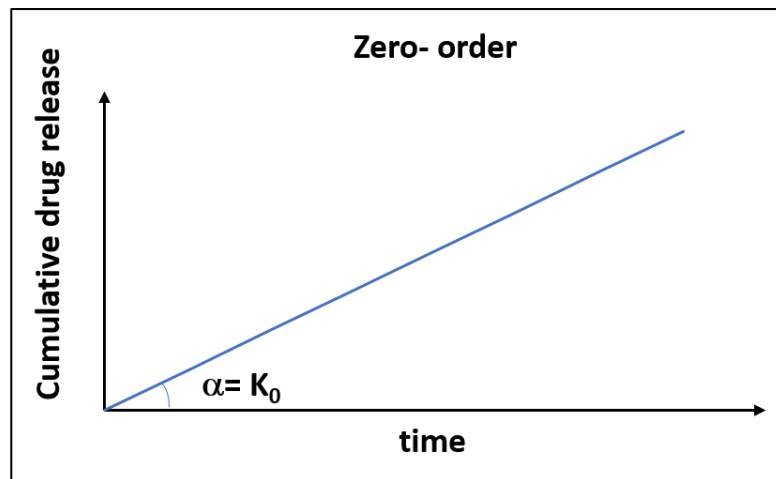


**Figure 1.5:** Graphical representation of drug release of zero- order release kinetics.

By this method, it is possible to release the same amount of drug per unit time and hence is pharmacologically preferred. Zero- order release is observed in DDS that do not disaggregate and contain matrices with low soluble drugs or osmotic systems in which the drug is protected by semi- permeable membranes (Dash *et al.*, 2010).

### 1.4.2. First- order model

In first- order kinetics, the change in concentration of the drug with time is dependent only on the concentration (Ramteke *et al.*, 2014). The release of a drug obeying first- order kinetics can be represented by the equation:

$$dC/ dT = -KC$$

where  $dC/dT$  is the change in concentration of with respect to time,  $K$  is the first- order constant and  $C$  is the concentration. This equation can also be represented as:

$$\log C - \log C_0 = Kt / 2.303$$

where  $C$  is the concentration of drug released at time  $t$ , and  $C_0$  is the initial amount of drug dissolved and  $K$  is the first- order constant. This means, a graph of log cumulative percentage of drug remaining vs. time will give a straight line with a slope of  $- K / 2.303$ , as given in **figure 1.6**. (Ramteke *et al.*, 2014).

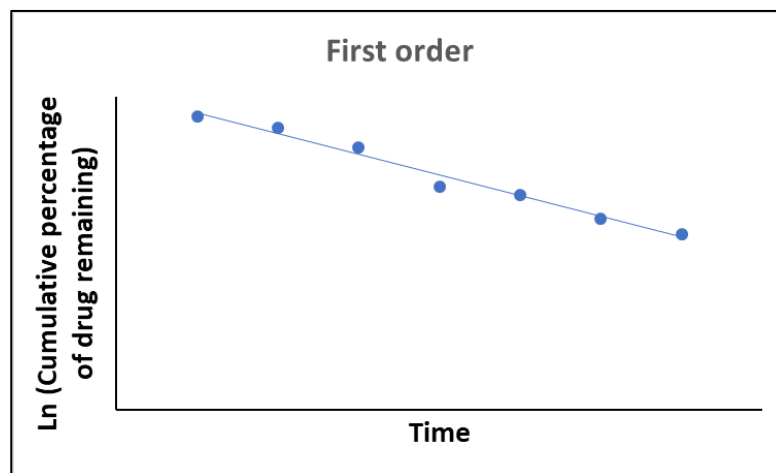


**Figure 1.6:** Graphical representation of drug release of first- order release kinetics First- order release kinetics is observed in DDS that are formulated as porous matrices containing water soluble drugs (Dash *et al.*, 2010).

### 1.4.3. Higuchi model

Higuchi can be considered as the pioneer of mathematical modelling in drug delivery, as he was the first scientist to propose a mathematical model, to describe the release of drugs from matrix systems in 1961 (Peppas and Narasimhan, 2014). Higuchi model was initially developed for planar systems such as ointments but was later extended to the release of soluble and partially soluble drug molecules from porous and matrix systems (Bruschi and

Luciano 2015). A simplified version of Higuchi model is represented by the following equation:

$$Q = K_H t^{1/2}$$

Where Q is the cumulative amount of drug released at time t and  $K_H$  is the Higuchi constant. Higuchi model, considering DDS of varying geometry proposes that the cumulative percentage of drug release when plotted against square root of time gives a straight line, with a slope that is equal to Higuchi dissolution constant (**Figure 1.7**) (Gouda, Baishya and Quing, 2017).

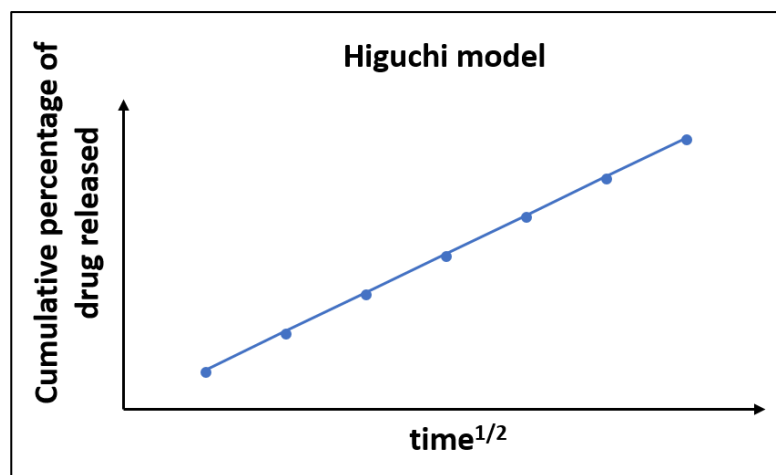


**Figure 1.7:** Graphical representation of drug release following Higuchi model

The Higuchi model assumes the following: 1). The matrices contain drug in an amount that is much higher than its solubility, 2). Diffusion is one dimensional, 3) Swelling is negligible and 4). Drug molecules are much smaller in size than the matrices (Dash et al., 2010).

#### 1.4.4. Hixson- Crowell model

Hixson- Crowell model is applicable to DDS where the surface area reduces as a function of time, without altering the geometry. This model assumes that the rate of release is a

property of dissolution, rather than diffusion (Bruschi and Luciano 2015). According to this model,

$$W_0^{1/3} - W_t^{1/3} = \kappa t$$

Where  $W_0$  is the initial amount of the drug,  $W_t$  is the remaining amount of drug at time 't', and  $\kappa$  is the Hixson- Crowell release constant incorporating the surface area and volume of the DDS (Gouda, Baishya and Quing, 2017). From the equation, it can be learned that a plot of cube root of percentage drug remaining unreleased vs. time would give a straight line with a slope ' $\kappa$ ' (**Figure 1.8**).

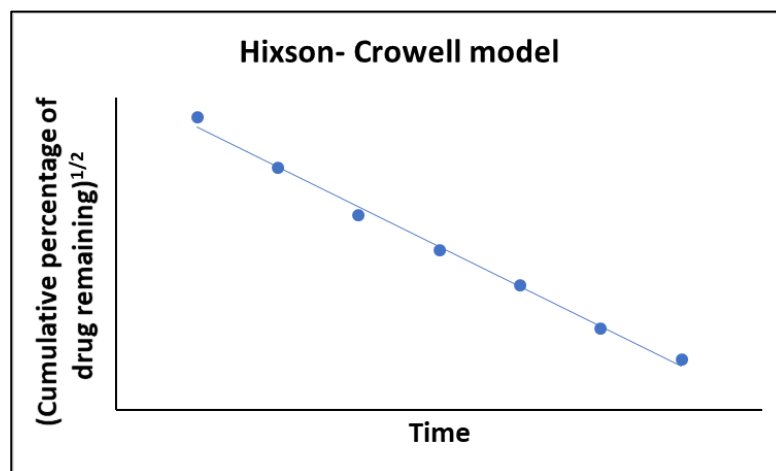


**Figure 1.8:** Graphical representation of drug release following Hixson- Crowell model. While Higuchi model establishes diffusion as the prime mechanism of mass transfer, Hixson Crowell gives an insight into what kind of diffusion mechanism is involved.

#### 1.4.5. Korsmeyer-Peppas model

Korsmeyer et al. (1983), developed a semi empirical model to describe drug release from polymeric systems. It is often used to linearize release data from microspheres and capsules (Bruschi and Luciano 2015). According to this model, the fraction of the drug released at any point is given by

$$Q_t/Q_0 = k t^n$$

Where  $Q_t$  is the amount of drug released at time  $t$ ,  $Q_0$  is the initial amount of drug and  $n$  is the release exponent. Therefore, a plot of  $\log(Q_t/Q_0)$  vs  $\log(t)$  should be able to provide the value of  $n$  from linear regression (**Figure 1.9**).

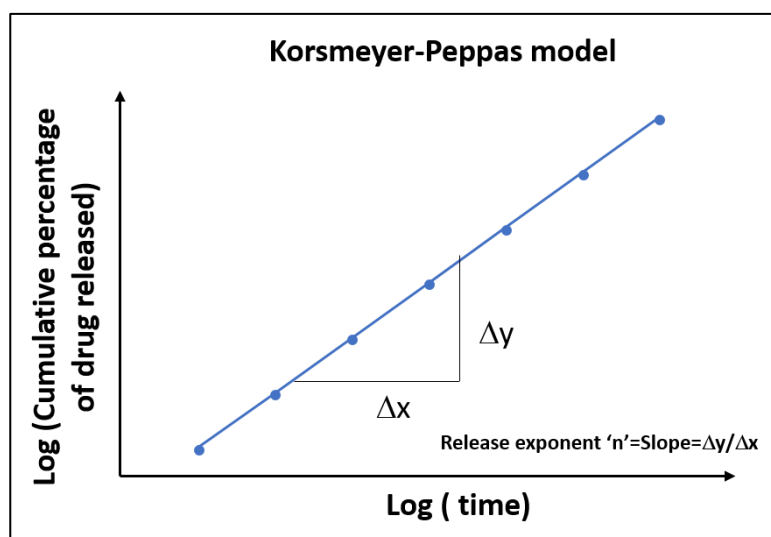


**Figure 1.9:** Graphical representation of drug release following Korsmeyer-Peppas model.

The  $n$  value characterizes the type of mass transport mechanism for various geometries. For spheres, release mechanisms corresponding to different  $n$  values are given below in **table 1.1**.

### 1.1.

Release exponent ( $n$ )	Release mechanism
0.43	Fickian diffusion
$0.43 < n < 0.85$	Anomalous transport
0.85	Type II transport

**Table 1.1:** Correlation between release exponent ' $n$ ' and release mechanism in spherical DDS, following Korsmeyer-Peppas model (Carbinatto et al., 2014).

## 1.5. Biodegradable polymers in drug delivery

### 1.5.1. Synthetic Polymers

Although both naturally derived and synthetic polymers have been explored in the context of biomedical applications, associated disadvantages of naturally derived polymers such as immunogenicity, complexities associated with purification and sterilisation have triggered a new wave of synthetic polymer engineering (Lutolf and Hubbell, 2005). Synthetic polymers are broadly defined as man-made polymers from petroleum sources. These include polyesters, polyamides, polyurethanes, polyureas, poly(amide-enamines) and polyanhydrides (Vroman and Tighzert, 2009). Synthetic biomaterials have also been developed equipped with features that promote cell interactions and respond to molecular cues. The development of Molecular Imprinting technology has also made it possible to synthesise polymers with specific molecular recognition sites. Molecular Imprinted Polymers or MIPs are prepared by mixing the template molecules and monomers, followed by crosslinking and polymerisation. The template is then extracted out, resulting in MIPs that have memory of the template molecule, which can be used as effective tools for drug delivery (Yan and Ho Row, 2006). The main advantage of this technology is high selectivity and adaptability. The same material can be used to recognise a multitude of biomolecules such as DNA, antibodies, amino acids and drugs. MIPs made using methacrylic acid (MAA) as a functional monomer for the controlled release of Propranolol (a  $\beta$ -adrenergic antagonist), have exhibited prolonged release as opposed to non -MIPs (Vasapollo *et al.*, 2011).

Synthetic polymers can be modified to have tailorable degradation rate, as in the case of Polylactic acid or PLA, usually obtained from polycondensation of D- or L-lactic acid or from

ring opening polymerization of lactide, a cyclic dimer of lactic acid (Vroman and Tighertz 2009). Both the stereoisomeric forms of PLA namely PDLA and PLLA and their racemic mixture PDLLA have been used for biomedical applications. These have been used extensively as resorbable sutures, stents, artificial skin, staples, orthodontic implants, oriented and blown films and tissue regenerative scaffolds (Mallakpour and Zadehnazari, 2011). However, drawbacks such as risk of toxicity due to acidic by-products have led researchers to consider alternatives.

### **1.5.2. Natural polymers**

Natural polymers are naturally occurring macromolecules such as polysaccharides, starch, collagen, fibrinogen and elastin. The advantage of natural polymers in their inherent biological recognition, including presentation of receptor-binding ligands and susceptibility to cell-triggered proteolytic degradation and remodelling make them good candidates in biomedical applications (Lutolf and Hubbell 2005). Since natural polymers make up extracellular matrix, they have an inherent ability to communicate with other cellular components and assist in routine cellular processes (Sell *et al.*, 2010). Cellulose, the most abundant material in nature, has been used as nanofillers for various polymers such as Polyvinyl alcohol (PVA), PLA and Polycaprolactone (PCL). Different aspect ratios of the fillers and different polymer/filler ratios have been evaluated and an improvement in the mechanical properties of the composites has been observed (Siqueira *et al.*, 2010). Chitin, one of the most abundant natural polymers, has been used to produce hydrogels, powders, fibres and porous scaffolds. Porous chitosan scaffolds prepared by transferring a homogenised, air bubbled solution of chitosan into sodium hydroxide to facilitate liquid hardening, have been used to incorporate either bone morphogenic proteins (BMP-2) or

insulin-like growth factor (IGF-1). *In vivo* studies on these scaffolds revealed that the ones with IGF-1 exhibited increased osteoblastic differentiation (Sampath *et al.*, 2016). Starch is another natural polymer extensively researched in this context and has been so since early 1970s. The applications of starch as biopolymers vary; the most prominent of them being in food industry. Corn starch and microcrystalline cellulose extrusions have been used to make edible films (Phan *et al.*, 2009). They are also used in various medical applications such as starch based biodegradable bone regeneration scaffolds and as hydrogels and microspheres in drug delivery (Lu *et al.*, 2009). Polyhydroxyalkanoates (PHAs), a group of naturally occurring biodegradable polyesters that are synthesised by microorganisms during unbalanced growth, have received much attention in the last decade, especially in biomedical applications. This is owing to their high biodegradability in varied environments and processing versatility (Bugnicourt *et al.*, 2014).

### **1.6. Polyhydroxyalkanoates (PHAs)**

PHAs are considered as potential alternatives for fossil fuel-based thermoplastics. These are bacterial storage polymers produced under nutrient limiting conditions such as nitrogen, phosphorous or potassium, but with excess carbon (Le Meur *et al.*, 2012). These are water insoluble, biodegradable and biocompatible polymers and accumulate as cytoplasmic inclusions in both Gram positive and Gram-negative microorganisms. PHAs are polyesters of 3-, 4-, 5-, 6- hydroxyalkanoic acids and generally consist of 1000-10000 monomer units (**Figure 1.10**).



low melting temperature, crystallinity, tensile strength and are extremely elastomeric in nature. The reason for the difference in crystallinity and melting point between SCL and MCL- PHAs could be the presence of larger pendant groups in MCL- PHAs that make the packing of polymer chains irregular. Crystallinity is a result of compact packing and SCL- PHAs with small regular pendant groups can pack in a more ordered manner, thus leading to increased crystallinity and melting point (Sánchez et al., 2013). Poly(3-hydroxybutyrate), P(3HB), poly(3-hydroxybutyrate-co-3-hydroxyvalerate), P(3HB-co-3HV), are some examples of SCL PHAs and poly(3-hydroxyhexanoate), P(3HHx), poly(3-hydroxyoctanoate), P(3HO), poly(3-hydroxydecanoate), P(3HD), poly(3-hydroxydodecanoate), P(3HDD) are some examples of MCL PHAs (Rai *et al.*, 2011a).

Homopolymers, block copolymers and random copolymers of PHAs are produced depending on the carbon source used, organism used and metabolic pathways. Sato *et al.*, suggested that even the homopolymer P(3HB) consists of less than 1% monomer units of 3-hydroxyvalerate (Sato *et al.*, 2005). A few examples of diversities in mechanical and thermal properties of PHAs are tabulated below in **Table 1.2**. These properties vary from highly elastomeric to highly brittle. These varied properties imply their application in a variety of biomedical devices such as scaffolds for hard tissue regeneration (bone regeneration) and soft tissue regeneration (cardiac regeneration), cardiovascular stents and nerve conduits.

Polymer	Melting Point (°C)	Tensile strength (MPa)	Young's modulus (GPa)	Elongation at break (%)
P(3HB)	175	40	3.5	5-6
P(3HB-co-3HV)	137-170	20-25	0.7-2.9	50
P(3HB-co-4HB)	152	26	-	444
P(4HB)	53	36	0.23	1000
P(3HHx-co-3HO)	61	9	0.008	380
P(3HB-co-3HHx)	52	20	-	850
P(3HO)	39-50	9.6	0.005	1300
Polypropylene	170	38	1.7	400

**Table 1.2:** Thermal and mechanical properties of some PHAs (Valappil et al., 2006)

These huge range of properties coupled with PHAs' excellent biocompatibility has paved way to their use as a suitable material in various biomedical applications. They are natural storage polymers for microorganisms and are also ubiquitous in plants and animals and their degradation products are compatible with and similar to cell metabolic products, such as in fatty acid metabolism. Hence the metabolic pathway of PHAs and their removal from the body is well understood, which gives them a clear advantage over other biomaterials. TephafLEX, an absorbable suture prepared from P(4HB) obtained FDA approval in 2007, a remarkable leap towards establishing PHAs as niche biomaterials in medical applications (Shrivastav *et al.*, 2013). The list of these applications includes hard tissue and soft tissue regeneration scaffolds, wound healing, cardiac patches, nerve conduits, heart valve and therapeutic delivery (**Table 1.3**). Advancements in material processing techniques have enabled newer avenues for PHAs in biomedical applications.

Modified/unmodified PHAs	Physical properties	Medical application
P3(HB)	Asymmetric patches	Subcutaneous patches Stomach wall patch
	Micro/ nanospheres	Drug delivery, chemoembolization
	Implantable rods	Peripheral nerve guide
Fibronectin and alginate conjugated P3HB	Fibres	Spinal cord injury
P(3HB-co-3HV)	Film	Drug delivery
	Design of a 3D microfibrinous material- formed by the blend and electrospun into fibre materials	Myocardial patch
	Chondrocyte seeded foams	Cartilage proliferation
	Sutures	Wound management
P(3HB-co-3HV)/P(3HB-co-4HB)	Micro/nanospheres and implantable rods	Drug delivery
P(3HB-co-3HHx)	Porous tube form	Nerve conduit
	Human adipose tissue embedded scaffolds	Cartilage proliferation
	Films	Blood vessels
	3 D scaffolds	Blood vessels

**Table 1.3:** Biomedical applications of PHAs (Nigmatullin et al., 2015)

### 1.6.1. P(3HB)

P(3HB), an SCL PHA is the best studied of PHAs, first discovered in *Bacillus megaterium*. P(3HB) is highly crystalline, hydrophobic, 100% biodegradable and, like most thermoplastics, can be processed by extrusion, injection, and melt press moulding, making it a suitable candidate for various processing methods (Pachekoski et al., 2013). Although its stability is compromised at higher temperatures, the biodegradation rate of P(3HB) increases when the polymer is processed at higher temperatures, which is explained by decreasing of the polymer crystallinity, which facilitates the capability of the extra-cellular enzymes responsible for P(3HB) degradation to attack its chains (Pachekoski et al., 2013). There is evidence to show that the degradation products of P(3HB) are not only biocompatible, but also growth promoting (Cheng et al., 2006).

### 1.6.2. P(3HB) Biosynthesis

P(3HB), as mentioned earlier is a storage molecule in response to physiological stress in various microorganisms. It is a linear polymer produced by both Gram positive and Gramnegative microorganisms such as *Cupriavidus necator*, several species of *Pseudomonas*, *Bacillus*, *Azotobacter* and also recombinant *Escherichia coli*, expressing the P(3HB) biosynthetic genes from *C. necator* and *A. vinelandii*. Gram positive bacteria such as *Bacillus spp.*, are specifically useful for medical applications due to the absence of lipopolysaccharides, a group of immunogens that coprecipitate with polymer extraction. P(3HB) is produced by fermentation either in batch, fed batch, continuous cultures, or multistage fermentation systems (Rai *et al.*, 2011). P(3HB) can be synthesised using inexpensive carbon sources such as beet and cane molasses, corn starch, alcohols, and vegetable oils. There are 3 main enzymes involved in the biosynthesis of P(3HB),

corresponding to 3 distinctive steps. The first step is the condensation of two molecules of acetyl-CoA to form acetoacetyl-CoA catalysed by the enzyme ketothiolase, encoded by the *phbA* gene. This is followed by the enzymatic action of an NADPH dependent acetoacetyl-CoA reductase (encoded by *phbB*) which catalyses the conversion of acetoacetyl-CoA to 3-hydroxybutyryl-CoA using NADPH. The enzyme PHA synthase (encoded by *phbC*) then polymerizes the 3-hydroxybutyryl-CoA monomers to P(3HB), liberating CoA (Rehm, 2003). Under non-limiting conditions acetyl CoA enters the TCA cycle, and the enzyme-ketothiolase is negatively regulated by CoASH (Figure 1.11) (Shrivastav *et al.*, 2013)

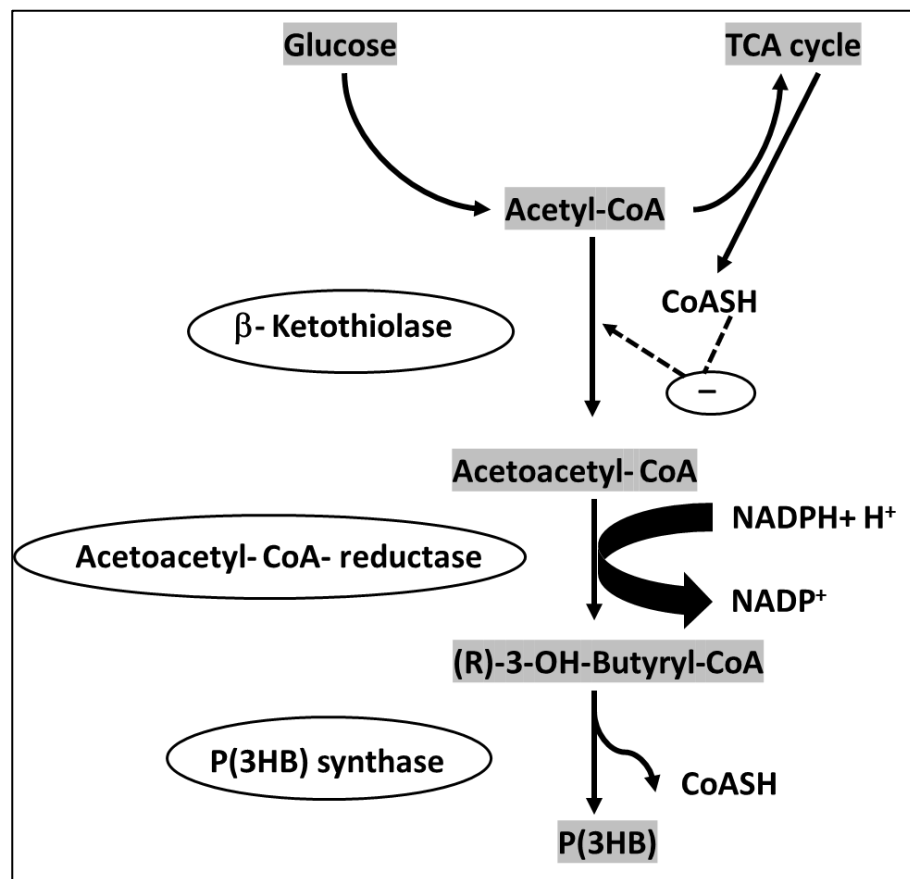


**Figure 1.11:** Biosynthetic pathway of P(3HB) in *C. necator* (adapted from Shrivastav *et al.*, 2013)

### **1.6.3. Thermal and physical properties of P(3HB)**

P(3HB), an isotactic homopolymer of 3-hydroxybutyrate is the most commonly known PHA. The molecular mass of P(3HB) (between 200-20,000 KDa) is pivotal in all its biomedical applications and the manipulation of this feature is key in improving and altering the properties relevant to biomedical applications (Peña et al., 2014). The thermoplastic and crystalline properties of P(3HB) vary with increasing molecular mass. P(3HB) is known to exhibit a melting temperature ( $T_m$ ) of 160 °C to 177 °C and a glass transition temperature ( $T_g$ ) of -4 to 15°C. The Young's modulus exhibited by P(3HB) is 400 MPa and compressive elastic modulus of 317 MPa. The properties of P(3HB) are comparable with petroleum-derived plastics with 60-80 % crystallinity (Valappil et al., 2007). P(3HB) is semi crystalline and often undergoes polymorphic crystallisation where the polymer crystallises into lamellar crystals and into zigzag crystals.

### **1.6.4. Biodegradability of P(3HB)**

The significance of using biodegradable polymers in medical applications is to ensure that there are no post-operative procedures required for the removal of these polymers or their degradation products from the body (Verlinden et al., 2007). The degradation rate depends on the nature of the polymer, composition, molecular weight, crystallinity, structure, thickness, surface properties and environmental conditions. As a critical element in biomedical applications of polymers is the development of a temporary physical and mechanical support for the regeneration of newly formed tissues over time, it is imperative to understand the degradation rates of the polymer in question (Manavitehrani et al., 2016).

Polyesters are primarily degraded through bulk and surface degradation brought about by hydrolysis and enzymatic activities. Hydrolytic degradation proceeds by autocatalysis that involves the hydrolysis of the ester linkages, and the enzymatic degradation explicitly depends on the specific enzyme that is responsible for the degradation of the ester linkage. 3-Hydroxybutyric acid, the degradation product of P(3HB) naturally occurs in mammals and it has been observed that P(3HB) undergoes 35% reduction in molecular weight after six months within the body (Manavitehrani et al., 2016; Kunze et al., 2006). An earlier study however reported only 1.4% reduction over a period of six months for P(3HB) implanted in mice (Verlinden et al., 2007). This variation is concurrent with the argument that rates of enzymatic degradation of P(3HB) by PHA depolymerase is largely dependent on the crystallinity of the polymer as well as the availability of the enzyme. The absorption isotherms of PHA depolymerases obey Langmuir adsorption model where the enzyme irreversibly binds to the surface of the substrate until a saturation point is reached (Numata et al., 2009). As the degradation of amorphous regions of the polymer is much faster, the degradation rate of P(3HB) is primarily controlled by its crystallinity including the size of crystals, and lamellar thickness (Numata et al., 2009).

#### **1.6.5. Biocompatibility of P(3HB)**

To be suitable for use in biomedical applications, materials must not induce any immunological reactions when in contact with soft tissue or blood of the host, during implantation/ administration or degradation. Widespread occurrence of low molecular weight P(3HB) as an oligomer in animals and humans lead to high biocompatibility of P(3HB). R-3-hydroxybutanoic acid, the degradation product and monomeric component of P(3HB), is an innate cell metabolic product during *de novo* fatty acid synthesis in the liver

mitochondria. Various structures fabricated using P(3HB) have been shown to be compatible in animal models. These include sutures, nerve conduits, drug delivery systems, implantable rods and 3D scaffolds. The earliest studies on *in vivo* studies on P(3HB) were carried out by WR Grace and Co., in the 1960s. Subcutaneously and intramuscularly implanted P(3HB) filmstrips on removal after 8 weeks revealed no signs of immunogenic reactions or damage to the underlying area (Valappil *et al.*, 2006). One of the longest *in vivo* investigations involving PHAs was conducted using P(3HB-co-3HV) films with 7, 14 and 22% of valerate content, implanted in sheep for up to 90 days (Williams and Martin 2005). Although after one week of implantation, numerous macrophages, neutrophils and fibroblasts concurrent with inflammatory responses were observed at the site, which decreased with time. These immune cells were found to be present in fibrous capsules around the site of implantation and consisted largely of lymphocytes towards the later stages of implantation. Similar observations of fibrous capsule formation were made in mice subcutaneously implanted with P(3HB) and P(3HB-co-3HV) samples. The fibrous capsules formed were of 100-200  $\mu\text{m}$  in diameter and reduced to 100  $\mu\text{m}$  in six months. It was revealed that the size of capsules increased with valerate content. Sterilization of P(3HB) does not interfere with mechanical properties or molecular weight of the polymer. There are many reported instances of P(3HB) supporting excellent cell proliferation (Brigham and Sinskey 2012). P(3HB-co-3HV-co-3HHx) was researched as a supporting matrix for mesenchymal stem cells and it was noted that the material's surface roughness and increased water contact angle contributed to enhanced adherence and cell proliferation (Guang-Zhen 2009). Most of the observed tissue responses elicited during implantation of P(3HB) based structures were found to be due to the implantation procedure, rather than its material properties. Even this was comparable with implants

made from silk or catgut materials currently used in surgical procedures. A study comparing immune responses elicited by PLA, P(3HB) and P(3HB-co-3HV) showed that P(3HB-co-3HV) elicited the least extent of immune response, followed by P(3HB) and then PLA, a biopolymer extensively used in commercial medical applications (Brigham and Sinskey 2012). This makes a strong case for the need for switching to PHA based biomedical implants with suitable surface modifications. Hemocompatibility of P(3HB) films were also found to be favourable for its use in biomedical applications as the polymer did not affect platelet response or activate the complement system, when in contact with mammalian blood. The associated responses if any, were found to be due to the bacterial cell wall, necessitating a requirement for better purification methods as polymer from Gram negative bacteria may contain lipopolysaccharides. The alternative is to use P(3HB) produced from Gram positive bacteria.

#### **1.6.6. Biomedical applications of P(3HB)**

Due to the favourable biodegradation and biocompatibility of P(3HB) in *in vitro* and *in vivo* studies, the use of P(3HB) as homopolymer, co-polymer and blends of other organic materials such as hydroxyapatite (HA) and polyglycolic acid (PGA) has gained momentum. An early research established that materials based on P(3HB) to be structurally robust with no extensive break down during implantation. Bone tissue adaptation response had no evidence of an undesirable chronic inflammatory response after implantation periods up to 12 months. Bone regeneration occurred in close proximity to the implant interface with subsequent structural organisation, with up to 80% of the implant surface lying in direct contact with the new bone (Doyle, Tanner and Bonfield, 1991). In a similar research, 10-50% compositions of HA with P(3HB) were analysed for its correlation to crystallinity and it

was observed that crystallinity increased from 77- 89% within this window. Ectopic bone formation assay performed *in vitro* and *in vivo* proved that the hybrid PHB/HA composites can function as scaffolds and that bone tissue develops on their surface and in pores (Shishatskaya, 2016). The other medical applications of P(3HB) are in the form of sutures, pericardial patches, stents, separating films, conduits, damaged tissue and dura mater substitutes, hard and soft tissue regenerative scaffolds and most extensively, drug delivery systems.

### **1.7. P(3HB) in drug delivery**

Although there are many polymers with comparable thermal and physical properties to P(3HB), its surface eroding mode of degradation and non-toxic degradation products make it highly relevant and useful in the area of controlled drug delivery. P(3HB) microspheres, vesicles of polymer with entrapped or encapsulated Active Pharmaceutical ingredient (API), are conventionally fabricated using solvent evaporation of water-in-oil-in-water emulsions. Briefly, the polymer is dissolved in organic solvents such as chloroform, dichloromethane and methyl chloride, and then emulsified in water containing chosen surfactants. The emulsion is allowed to stir, during which the organic solvent evaporates, leaving behind spherical matrices of the polymer. This method, although easy to achieve on a bench scale, have few shortcomings in the form of polydisperse particle size distributions and low encapsulation efficiency, especially in the case of hydrophilic drugs (Chew, Hinojosa and Arriaga, 2017).

Anaesthetics, antibiotics, anti-inflammatory agents, anticancer agents, hormones, steroids, and vaccines are some examples of the classes of APIs investigated in association with P(3HB) microspheres (Shrivastav *et al.*, 2013). Gangrade and Price had reported one of the

earliest applications of P(3HB) microspheres for the incorporation of progesterone as a model drug. P(3HB) microspheres and P(3HB-co-3HV) microspheres were compared with respect to release kinetics, and P(3HB-co-3HV) spheres being less porous than P(3HB), exhibited slower release of the drug. This group also compared the effect of chloroform and methyl chloride as organic phases in the emulsion and it was found that the spheres formed using methyl chloride had smoother surfaces compared to the ones with chloroform (Gangrade and Price, 1992).

Over the years, a lot of research has been carried out in antibiotic pharmacokinetics using P(3HB) microspheres. Francis *et al.*, reported encapsulation of gentamycin, a hydrophilic aminoglycoside used against Gram positive and Gram-negative inflammatory bacteria, especially in the treatment of osteomyelitis. Systemic delivery of gentamycin extending up to 4-6 weeks is required for efficient control of infection and oral and parenteral delivery has been known to cause patient discomfort. This was proposed to be ameliorated by the use of P(3HB) microspheres, intended to be incorporated into 3D scaffolds for localised delivery. Uniform sized microspheres ranging from 1-2  $\mu\text{m}$  in diameter were obtained with an encapsulation efficiency of 48%. X- ray diffraction studies indicated the presence of surface adsorption of gentamycin that led to a burst release of about 60% and the remaining drug content was released in an almost zero order fashion within 24 hours (Francis *et al.*, 2011). The same group followed up on these results with the incorporation of gentamycin encapsulated P(3HB) microspheres in 45S5 Bioglass<sup>®</sup>-based composite scaffolds, to be used in bone tissue engineering (Francis *et al.*, 2010). The release kinetics of gentamycin from free microspheres compared with microspheres coated on the bioglass clearly showed a reduction in burst release, from 60% to 24% and was extended for 30 days

as opposed to the 24 -hour long deliveries from free microspheres (Francis *et al.*, 2010). In a more recent study, titanium implants coupled with antibiotic loaded P(3HB) and PEG microspheres have also been reported with the same intent of post-operative infection prevention, which successfully rendered the titanium implants with antibacterial properties (Rodríguez-Contreras *et al.*, 2016).

One of the earlier reported studies involving P(3HB) in anticancer drug delivery has been the encapsulation of 5-fluorouracil in microspheres fabricated using the copolymer P(3HB-co-3HV), with a molar ratio of 85:15. Encapsulation efficiency of the microspheres prepared using water-in-oil-in-water (W/O/W), oil-in-water (O/W) and oil-in-oil (O/O) solvent evaporation method differed dramatically with 1% in the case of (W/O/W), 7% in the case of O/W and 80% in the case of O/O (Khang *et al.*, 2001). The effect of acylglycerols on the release rate of the anticancer drug Lastet from P(3HB) microspheres (Abe, 1992), rifampicin loaded microspheres as chemoembolization agents (Kassab, 1997), the effect of fatty acids and alkyl esters on the release rate of anthracycline anticancer drug and aclarubicin from microspheres (Kazuhiko, Masahiro and Miko, 1986) are some of the noteworthy research in this context.

Nanoparticles intended for drug delivery are submicron particles in which API is dissolved, adsorbed, dispersed, or encapsulated. The advantages of using nanoparticles include high stability, high carrier capacity, feasibility of incorporating both hydrophilic and hydrophobic drugs, and the feasibility of subcutaneous, and oral administration and inhalation (Gelperina *et al.*, 2005). Polymeric nanoparticles have attracted huge interest due to the ease of surface modification, a strategy for target specific drug delivery. The specific advantage of nanospheres due to their smaller size range is that they can reach tissue

spaces that larger carrier systems cannot penetrate. *In vitro* and *in vivo* transdermal permeation of P(3HB-co-3HV) micro and nanospheres were compared by Eke *et al.*, with the use of fluorescent Nile red to observe permeability. It was observed that while particles larger than 1.9  $\mu\text{m}$  were not suitable for intracellular uptake, nanoparticles were taken up by macrophages using phagocytosis (Eke *et al.*, 2014). Along the same lines, a comparative study on P(3HB), P(3HBHHx) and PLA nanospheres of size 160, 250 and 150 nm were conducted to analyse cellular uptake, in this case using rhodamine B isothiocyanate (RBITC) as a fluorescent label. The study that demonstrated intracellular uptake of PHA nanospheres for the first time, established that PHA nanospheres had higher sustained release of 20 days as opposed to 15 days of release using PLA, and 7 days using free drug administrations. PHA nanospheres also exhibited 75% encapsulation efficiency of the hydrophilic dye (Xiong *et al.*, 2010). P(3HB) and its copolymers are also employed in targeted drug delivery. Addition of PHA binding proteins, folate mediated targeting and PEGylation are some examples for strategies applied in targeted drug delivery using these.

### **1.7.1. Addition of PHA binding proteins**

This strategy involves biochemical engineering of the PHA biosynthetic enzymes to incorporate favourable ligands or molecules that can help direct PHA granules to the designated delivery site. Two enzymes, namely PHA granule-associated proteins (PhaP) and PHA synthase (PhaC) were involved in this process. The former is a small molecular weight amphiphilic protein, which helps in stabilising the hydrophobic PHA granules in the aqueous environment of the bacterial cytoplasm and the latter covalently binds to cysteine residues of the PHA granules during polymerisation. Both these proteins are viable targets for modification of the granules, in creating fusion proteins (Nigmatullin *et al.*, 2015).

Hepatocellular carcinoma is distinguished by overexpression of the epidermal growth factor receptor (EGFR). Yao *et al.*, engineered PhaPs linked with recombinant human epidermal growth factor (rhEGF) and these were adsorbed on P(3HB-co-HHx) nanoparticles encapsulated with RBITC. *In vivo* studies in mice models demonstrated selective accumulation of the nanoparticles in tumour tissues, confirming the targeting ability of these constructs (Yao *et al.*, 2008). In a similar study, P(3HB) nanoparticles surface functionalized with RGD4C coupled with PhaC were used to analyse the permeability of these nanoparticles in the breast cancer cell line MDA-MB 231. These Nile Red encapsulated particles exhibited effective internalization, emphasizing the feasibility of P(3HB) nanoparticles in surface modification to aid targeting (Lee *et al.*, 2011). Following this, Kwon *et al.*, incorporated A33scFv, specific to the A33 antigen overexpressed in colorectal cancers. The accumulation of particles was observed using fluorescence microscope and specificity was confirmed as cancerous cells accumulated increased amount of the nanoparticles (Kwon *et al.*, 2014).

### **1.7.2. Folate mediated targeting**

Cancer, by definition, is uncontrolled cell division. Folate, a molecule used in the biosynthesis of DNA bases, is abundantly used by continuously dividing cancer cells, and hence, certain cancer cells overexpress folate receptors. The density of these receptors on the cell surfaces is found to be linear with disease progression. Therefore, folate target is one of the most popular approaches in targeted delivery of anticancer agents (Nigmatullin *et al.*, 2015). Zhang *et al.* compared inhibitory concentrations ( $IC_{50}$ ) of free doxorubicin, P(3HB-co-3HO) nanoparticles encapsulating doxorubicin, and folate-conjugated P(3HB-co-3HO) nanoparticles encapsulating doxorubicin (DOX/FA-P(3HB-co-3HO)) and the  $IC_{50}$  were

found to be  $2.8 \mu\text{mol L}^{-1}$ ,  $27.3 \mu\text{mol L}^{-1}$  and  $0.87 \mu\text{mol L}^{-1}$  respectively. The drastic change in  $\text{IC}_{50}$  with folate incorporation affirms its role in cellular uptake of particles (Zhang *et al.*, 2010). In a similar study Hazer *et al.*, compared etoposide encapsulated P(3HB-co-3HHx) nanoparticles conjugated with folate and free etoposide and found that the former elicited 32% cytotoxicity and the latter only 12%. The comparatively low cytotoxicity may have been due to the reduced folate receptor expression on L929 cells used in this study (Hazer *et al.*, 2011). Folate conjugation of DDS is far more efficient than folate conjugation of free drug as receptor saturation is sooner to occur with small molecules and therefore comparatively less amount of drug would be endocytosed, whereas when the entire DDS is endocytosed, it would have larger amount of the drug encapsulated in it.

Folate mediated targeting has certain limitations. First of all, not all cancer types over express folate receptors (example: prostate cancer). Due to high affinity of folate to its receptors, the folate conjugated DDS particle might not be able to release the drug cargo at a rate that would achieve the desired therapeutic window (Garcia-Bennett, Nees and Fadeel, 2011). Folate can also be competitively inhibited by serum folate binding (Xing *et al.*, 2018).

### **1.7.3. Other surface functionalization strategies**

With growing understanding of the metabolics and genomics of cancer, it has been easier to strategize the development of various theranostic nanoparticles. PEGylation is such a common strategy, which enhances retention time by increasing serum circulation, solubility and to some extent, targeting (Mishra *et al.*, 2016). However, PEG is a non-biodegradable polymer and therefore it is put to best use when in combination with biodegradable polymers, in small quantities. Marine bacterial enzyme glutaminase, which

inhibits cancer proliferation by inducing glutamine deprivation was immobilized on PEGylated P(3HB) nanoparticles. These were tested on HeLa cells for the effect of the immobilized enzyme on cancer proliferation. Concomitantly, the cells were also subjected to growth in glutamine free medium. The results obtained were comparable with similar dented anatomy of cells and shrunken nucleus (Pandian *et al.*, 2015). Other targeting strategies include the use of markers specific for receptors such as HER-2 (breast), CD 44+ (breast, head and neck, ovarian, pancreas), CD 133+ (colon, pancreas), CD34+, CD 38- (Acute Lymphoblastic Leukemia) and CD 34+ (Multiple Myeloma) (Schatton, Frand and Frank, 2010).

### **1.8. Aims and objectives**

The aim of this project was to produce LPS free P(3HB) from *B. cereus* SPV and *B. subtilis* OK2, and to optimise the production of microspheres and nanospheres from them, for various drug delivery applications. The specific objectives of this research are as follows:

- 1) Large scale production of P(3HB) from *B. cereus* SPV and *B. subtilis* OK2, and characterisation:** The polymer will be produced from these two microorganisms to obtain LPS free P(3HB). The polymer thus obtained will be characterised for their structural properties using FTIR, chemical properties using NMR and thermal properties using DSC. The molecular weight of the polymer produced will be analysed using GPC
- 2) Optimisation of the synthesis of P(3HB) microspheres and nanospheres:** The polymer produced will be used to synthesise microspheres and nanospheres of varying size ranges. Process parameters such as polymer concentration, PVA concentration and stirrer speed will be manipulated to obtain optimum conditions,

using Box-Behnken Response surface methodology. The spheres produced will be characterised for particle diameter, porosity, surface hydrophobicity and degradation.

- 3) Encapsulation of cardiovascular drugs:** Antiproliferative drugs namely rapamycin and tacrolimus will be encapsulated in P(3HB) spheres. P(3HB) microspheres encapsulated with rapamycin will be compared against PLLA microspheres with respect to fabrication process and physical characteristics. The drug release profile of these will be compared using widely published mathematical and kinetic models. Release of tacrolimus from P(3HB) microspheres and nanospheres will be analysed the same way as mentioned above. Finally, VEGF release from P(3HB) microspheres and nanospheres will be compared with their counterparts embedded in collagen.
- 4) Encapsulation of porphyrin derivatives and analysis of their effectiveness in targeted anticancer therapy:** P(3HB) microspheres will be encapsulated with 3 different porphyrin derivatives and their effectiveness in reducing cell viability will be tested. The data generated will be compared against the same formulations conjugated with the anticancer marker anti-HER-2.
- 5) Optimisation of microsphere synthesis from P(3HB)- HA conjugate:** The amphiphilic conjugate will be used to produce microspheres using cross-linking method in oil-in-water emulsion. Hydrophilic drugs (aspirin and gentamicin) and hydrophobic drug (curcumin) will be encapsulated in these and their drug release profile will be compared. The formulations with encapsulated curcumin will be tested for their antimicrobial activity against MRSA.

# **Chapter 2.**

# **Materials and**

# **Methods**

## 2.1. Materials

### 2.1.1. Water

Deionised water was used for media preparation and High-Performance Liquid Chromatography grade water was used in all other experiments.

### 2.1.2. Chemicals and Reagents

All the chemicals for growth and production media were purchased from Sigma-Aldrich or Thermo Fisher Scientific UK or VWR (Leicestershire, UK) except for nutrient broth and yeast extract, which was obtained from DIFCO (BD UK Ltd., Oxford, UK). Antifoam (FG-10) was purchased from DOW corning (Edison, NJ, USA) for use in fermentation studies. For analytical experiments, such as GC-MS and HPLC, analytical grade reagents were used. Cell culture studies were carried out using cell culture grade media and reagents from Sigma-Aldrich, UK, and Lonza, UK. Human Vascular Endothelial Growth Factor (VEGF) was purchased from Sigma- Aldrich and VEGF ELISA kit was purchased from Thermo Fisher Scientific UK.

### 2.1.3. Bacterial strains and cultures

P(3HB) was extracted from the Gram-positive bacteria *Bacillus cereus* SPV and *Bacillus subtilis* OK2, both of which were obtained from the culture collection of University of Westminster, London, U.K. Methicillin Resistant *Staphylococcus aureus* (MRSA) was obtained from the culture collection of University of Westminster, London, U.K. All chemicals required for the polymer production from the two bacteria and extraction of polymer from the bacterial cells were obtained from Sigma-Aldrich Company Ltd. and VWR Chemicals (England).

#### **2.1.4. Cell lines and maintenance**

Human dermal microvascular endothelial cells (HMEC-1), used for biocompatibility studies were obtained from the University of Westminster cell line collection. Cell culture studies for assessing photodynamic activity of the porphyrin-encapsulated microspheres by quantifying cytotoxicity were carried out on SK-BR-3 cells obtained from the University of Westminster cell line collection.

#### **2.1.5. Plasmids**

The red fluorescent protein containing Anti-HER-2 plasmid was obtained from Dr. Anatoly Markiv, University of Westminster.

#### **2.1.6. Porphyrins**

Protoporphyrin IX (PP) was purchased from Sigma- Aldrich. Hematoporphyrin ether (HP) and Tetraphenyl porphyrin (TPP) were synthesised by Dr. Eugen Stulz's Group at the University of Southampton.

#### **2.1.7. Reagents used for the *in vitro* drug release and *in vitro* degradation studies**

##### **2.1.7.1. Phosphate buffered saline solution (PBS):**

Phosphate buffered saline solution (PBS) purchased from Sigma-Aldrich, (Dorset UK) was used for the *in vitro* drug release studies, one tablet in 200 mL of water.

##### **2.1.7.2. Simulated body fluid (SBF):**

SBF was prepared using the components, HPLC grade water 1500 mL, sodium chloride 15.92g, sodium bicarbonate, 0.72g; potassium chloride, 0.44g; potassium phosphate dibasic trihydrate 0.45g; magnesium chloride hexahydrate, 0.61g; calcium chloride, 0.55g;

sodium sulphate, 0.142g; TRIZMA<sup>®</sup> base, 12.11g; and hydrochloric acid to adjust pH to 7.25.

### **2.1.8. Buffers and Reagents**

#### **2.1.8.1. Buffers for SDS-PAGE:**

*2X sample buffer for sodium dodecyl sulphate-Polyacrylamide gel electrophoresis (SDS-PAGE)*

The components were 0.125 M Tris-HCl, pH 6.8, 15% glycerol (v/v), 6% SDS, and 0.005% bromophenol blue. 50  $\mu$ L of  $\beta$ -mercaptoethanol was added to 1 mL of sample loading buffer.

#### **2.1.8.2. Resolving gel buffer**

The components were 1.5 M Tris-HCl, 0.4% SDS

#### **2.1.8.3. Stacking gel buffer**

The components were 0.5 M Tris-HCl, 0.4% SDS

#### **2.1.8.4. 5X Reservoir Buffer**

The components are Tris Base 15g, 72g glycine, 5g SDS (g/L)

#### **2.1.8.5. Coomassie brilliant blue stain (for staining SDS-PAGE gels)**

0.025% Brilliant Blue R stain dissolved in 10 mL acetic acid (100%) and 90 mL water.

#### **2.1.8.6. Destaining solution (for destaining SDS-PAGE)**

10% acetic acid (100%) in water.

#### **2.1.8.7. 5X TBE, pH 8.0, (g/L)**

The components are Tris Base 54, Boric acid 27.5, EDTA 4.5

### 2.1.9. Media components

*Kannan and Rehacek media (g/L)*: Yeast extract 2.5, Potassium chloride 3, Ammonium sulphate 5 and Soybean dialysate 100 mL/L

*Soybean dialysate*: Dialysis of 10 g of defatted soybean flour in 1L of distilled water for 24 hr. at 4°C.

Glucose (20g/L for *B. cereus* SPV and 30g/L for *B. subtilis* OK2)

## 2.2. Experimental methods:

### 2.2.1. Production of P(3HB)

The P(3HB) polymer production was carried out in Kannan and Rehacek media using glucose as a sole carbon source (Rai, 2010). To this end, a single colony of either *B. cereus* SPV or *B. subtilis* OK2 was used to inoculate nutrient broth and the culture was grown at 30 °C and 200 rpm until mid-log phase (O.D. 3 at 600nm) was reached. This culture was then used to inoculate the PHA production media. P(3HB) production was carried out in 20 L fermenter with a 14 L working volume with an inoculum of 1.4 L culture, which was prepared using a single bacterial colony obtained from a nutrient agar plate. The fermenters containing only the salts of the production medium were sterilized separately without the addition of glucose and soybean dialysate to avoid any caramelisation. These were added later at the time of inoculation. The media components were maintained at a pH of 6.8 using 1 N NaOH or 1 N HCl. The fermentation was run with an initial 100% Dissolved Oxygen tension (DOT), airflow rate at 1.0 vvm (volumetric air flow rate), impeller speed of 200 rev/min and at a temperature of 30°C. The pH, DOT, glucose concentration

and optical cell density were monitored throughout the run by taking samples every 3 hours. Polymer yield over time was recorded as a fraction of dry cell weight. The temporal profile of polymer production from the two bacteria was plotted using SYSTAT Software Inc. Sigma-Plot 12.5.

### **2.2.2. Optical density**

The optical density of the inoculum was measured at all instances using nutrient broth as blank. OD readings were taken at 600 nm (absorbance) in a standard spectrophotometer (Novaspec II visible spectrophotometer, UK). The mid log phase was used for the inoculation of production media.

### **2.2.3. Temperature, pH and dissolved oxygen tension (DOT)**

Temperature and DOT levels were monitored online using the temperature and DOT probes (polarographic oxygen-sensing probe (Inglold, Metler-Toledo Ltd., Beaumont Leys, Leicester, UK) which were connected to the fermenter vessel. The pH of the production medium was measured offline (Jenway pH meter 3305, UK) by collecting samples from the fermenter at regular intervals. 1 mL of samples drawn at every 3 hours were used to record OD. These samples were then centrifuged at 13,000 rpm for 10 minutes and the supernatant was used to record pH and the pellets were lyophilised to quantify periodic dry cell weight accumulation. 50 mL samples drawn from 4 different time periods during growth were used to quantify polymer yield over time.

## 2.2.4. Polymer extraction techniques

### 2.2.4.1. Extraction of PHA by chloroform/ sodium hypochlorite dispersion

The culture was harvested after 48 hours of growth and then was centrifuged at 4600 rpm for 30 min. The cell pellet obtained was then washed with deionised water and lyophilised. The lyophilised cell biomass was thoroughly ground and incubated in a dispersion containing 80% of sodium hypochlorite and chloroform in 1:4 ratio at 30°C, for two hours at 150 rpm. The resulting slurry was then centrifuged at 4600 rpm for 20 min, to obtain 3 layers, of which the first layer was that of the sodium hypochlorite solution, the middle layer was that of the cell debris and the bottom most layer was that of the chloroform containing the dissolved polymer (**Figure 2.1**).



**Figure 2.1:** Layers containing sodium hypochlorite with cell debris and chloroform with polymer

The chloroform layer was separated by manually removing the first two layers using spatula and filters. This layer of chloroform containing the dissolved polymer was then concentrated to an oily consistency using the rotary vacuum evaporator. The dissolved polymer was precipitated using ten volumes of ice-cold methanol under continuous stirring, on a magnetic stirrer (Rai *et al.*, 2011).

#### **2.2.4.2. Soxhlet extraction method**

The lyophilised biomass was thoroughly ground using mortar and pestle and filled in cellulosic thimbles up to half way. This was set up in a soxhlet apparatus with methanol as the first solvent, to dissolve the cell membrane to expose the polymer. This was allowed to reflux until the condensed methanol flowing down the side arm was colourless. The methanol was then replaced with chloroform and was refluxed for a further 24 hours to allow the polymer to be dissolved in chloroform. This chloroform was then filtered and subjected to differential precipitation using ice cold methanol as explained in the section above.

#### **2.2.5. Characterization of the P(3HB) produced**

##### **2.2.5.1. Fourier Transform Infrared Spectroscopy (FTIR)**

The FTIR spectra of the polymers were recorded using Perkin-Elmer Spectrum Two Spectrometer in the range between 4000 to 450  $\text{cm}^{-1}$ . The spectral resolution was 4  $\text{cm}^{-1}$ .

##### **2.2.5.2. Nuclear Magnetic Resonance Spectroscopy (NMR)**

NMR spectra were analysed using the MestRec software package, at Eastman Dental Institute, University College London, UK. 20mg of polymer samples were prepared by dissolving in 1 mL of deuterated chloroform. Chemical shifts are referenced against residual solvent signal (7.26 ppm and 77.0 ppm for  $^1\text{H}$  and  $^{13}\text{C}$  respectively). Bruker AV400 (400 MHz) spectrometer was used for analysis.

##### **2.2.5.3. Molecular weight analysis**

Molecular weight analysis was done using Agilent 1260 Infinity system equipped with a refractive index detector (Agilent Technologies, UK). PLgel 5um MIXED-C (300 x 7.5 mm) column was calibrated using polystyrene standards (Easivial PS-H, Agilent Technologies,

UK) of narrow molecular weights from 162 Da to 7.0 kDa. Chloroform was used as a mobile phase at a flow rate of 1 mL/min. 2 mg/mL polymer solutions in chloroform were used for the analysis and injection volume was 50  $\mu$ L.

## 2.2.6. Production of P(3HB) micro/nanospheres

### 2.2.6.1. Solid-in-oil-in-water emulsion technique

Micro/nanospheres were synthesised as follows: 20 mL P(3HB) solutions of specified concentrations in chloroform were prepared by dissolving the polymer in air tight bottles for 15 hours. The solutions were then homogenised for 5 minutes, with 40 mL of Polyvinyl alcohol (PVA), of specified concentration. This was then transferred drop wise to 100 mL of polyvinyl alcohol (PVA) solution of specified concentrations and stirred at specified speed for 10 minutes, to allow evaporation of the chloroform. Alternatively, according to different methods tried, the polymer solution was directly added to PVA solution and homogenised for 5 minutes. This was further transferred to 500 mL of PVA solution and stirred for 4 hours at the specified speed. The process was carried out in the dark where photosensitizers were involved. The microspheres were centrifuged at 4600 rpm for 5 min and then washed with 10% ethanol once and distilled water three times, and freeze dried (Savant Modulyo D Freeze drier, Thermoelectron Corp, UK) (Francis *et al.*, 2011).

The drug-loaded microspheres were also prepared using the same solid-oil-in water emulsion technique. For this the drugs were added to the first water-in-oil emulsion (w/o) of aqueous polyvinyl alcohol (PVA) solution, in the case of hydrophilic drugs and then transferred to a second water-in-oil-in water emulsion (w/o/w) aqueous PVA solution. In the case of hydrophobic drugs, these were added directly to the polymer solution and homogenised. Following centrifugation, the microspheres were lyophilised and stored at

4°C for further use. The different drugs/proteins loaded during P(3HB) microsphere production is shown in **Table 2.1**.

Drug	Amount
Rapamycin	1 & 5%
Tacrolimus	1, 5 and 10 %
Protoporphyrin IX	1, 5 and 10 %
Hematoporphyrin ether	1, 5 and 10 %
Tetraphenyl porphyrin	1, 5 and 10 %
Gentamycin	10 %
Aspirin	10 %
Curcumin	10 %
VEGF	10 µg/ 0.13g

**Table 2.1:** Drugs encapsulated and their wt.% with respect to polymer

#### 2.2.6.2. Optimisation of microsphere production

Based on literature research and previous established results by Francis *et al.*, 2011, 3 factors, namely polymer concentration, surfactant concentration and revolutions per minute were considered as the most significant contributing factors and a set of pilot experiments were carried out to establish boundary limits. A Box-Behnken Response surface methodology design was generated using MiniTab software 6.0 (trial version). Particle size was set as the response and the significant effects were analysed to obtain optimized results.

## **2.2.7. Preparation of Amphiphilic HA- P(3HB) microspheres**

### **2.2.7.1. Hydrolytic depolymerisation of P(3HB) and HA conjugation**

Oligomeric derivatives of P(3HB) was obtained via partial depolymerisation as follows. 3 g of dry P(3HB) was added to a mixture of 166 mL of glacial acetic acid and 34 mL of distilled water. The mixture was refluxed at 100-105°C for up to 30 hours. Resulting polymer was precipitated into excess of cold methanol and washed several times with distilled water. This was then lyophilised to obtain dry polymer. Dr. Rinat Nigmatullin conducted this part of the experiment, with the researcher's minor contributions. This product was sent to ContiPro a.s. in Czech Republic for conjugation to hyaluronic acid (HA). The HA- P(3HB) conjugate thus produced was chemically characterised at ContiPro a.s.

### **2.2.7.2. Amphiphilic HA- P(3HB) microsphere preparation**

Microsphere production using a water-in-oil (w/o) dispersion method was optimised through use of varying polymer concentrations, oil phases, surfactants and crosslinking agents shown in the Table. Polymer was first dissolved in a specified volume of 1.7% acetic acid and homogenised in paraffin oil containing specified surfactants. Encapsulated drugs, that include aspirin, gentamicin, and curcumin were added to polymer solution before homogenisation. The homogenised solution was added slowly to a specific volume of paraffin oil and surfactant under constant stirring at 1000 rpm. Effect of crosslinking agents such as Glutaraldehyde Saturated Toluene (GST) and 1% Glutaraldehyde were analysed by adding at specified time intervals (**Table 2.2.**). The spheres were subsequently centrifuged (4600 rpm) and washed four times with the desired oil-removing solvent, the final wash using acetone. Three separate solvents were trialled: hexane, isopropanol and petroleum

ether, with only the isopropanol effectively removing residual oils. The spheres were then lyophilised for 48 hours before visualisation and/or subsequent experimentation.

Polymer concentration (g/mL)	Oil- Phase	Surfactant	Crosslinking Agent
0.01	Ethyl acetate	Nil	Nil
0.05	Ethyl acetate	Nil	Nil
0.01	Ethyl acetate	Nil	GST
0.01	Ethyl acetate	Span 80	GST
0.01	Paraffin oil/ Petroleum ether	Tween 80	GST
0.01	Paraffin oil/ Petroleum ether	Span 80 (1% v/v)	GST
0.01	Paraffin oil	Tween 80	1% Glutaraldehyde
0.01	Paraffin oil	1% Span 80	1% Glutaraldehyde
0.01	Paraffin oil	Span 80 (0.1% v/v)	Heat
0.01	Paraffin oil	Span 80 (0.1% v/v)	GST

**Table 2.2:** Optimization conditions for Amphiphilic microspheres

## 2.2.8. P(3HB) microsphere: physical characterization techniques

### 2.2.8.1. Microstructural studies using Scanning Electron Microscopy (SEM)

The surface morphology and size distribution of the microspheres were observed and imaged using FEI XL30 FEG Scanning Electron Microscope at Eastman Dental Institute, UCL,

UK. The samples placed on 8 mm diameter aluminium stubs were coated with gold using a sputtering device (Polaron E5000 Sputter Coater).

#### **2.2.8.2. Particle size analysis**

Image J software was used to quantify particle distribution using images captured using SEM. The images were appropriated to suitable thresholds and the analysis was calibrated using pixel to scale bar. Distribution curves were plotted using MS Excel, using data generated from particle size analysis on Image J.

#### **2.2.8.3. Porosity**

The porosity ( $\epsilon$ ) of the microspheres was measured using liquid displacement method. 5 mL of ethanol was added to a pre-weighed measuring cylinder and weighed. A certain weight of microspheres was added to this ethanol and sonicated to assist penetration of methanol into the pore spaces. Excess ethanol above the 5 mL mark was removed, and the cylinder was weighed again. Following this, the microspheres were removed from ethanol by decanting and the weight of the ethanol and cylinder were recorded. Porosity was calculated using the formula,

$$\epsilon = (W_2 - W_3 - W_s) / (W_1 - W_3)$$

$W_1$  is the weight of the cylinder filled with ethanol before the immersion of the microsphere sample,  $W_2$  is the weight of the cylinder, the ethanol and the sample after removing the excess ethanol above the 5 mL mark,  $W_3$  is the weight of the cylinder and ethanol after removing the microsphere sample saturated with ethanol, and  $W_s$  is the weight of the microsphere sample used in the measurement (Francis *et al.*, 2011).

#### 2.2.8.4. Determination of Residual PVA content

Iodine can form a coloured complex between the adjacent hydroxyl groups of PVA and this property is exploited in quantifying residual PVA (Yang *et al.*, 2008). 2mg of microsphere samples were treated with 2 mL of 0.5 M sodium hydroxide (NaOH) for 15 minutes at 60 °C followed by neutralization with 900µL of 1 N hydrochloric acid (HCl). The volume was adjusted to 5 mL with distilled water. To each of the samples, 3 mL of 0.65 M solution of boric acid, 0.5 mL of iodine solution (I<sub>2</sub>)/Potassium iodide (KI) (0.05 M/0.15 M) and 1.5 mL of distilled water were then added. The absorbance of this complex was measured at 690 nm (Novaspec II Visible spectrophotometer, UK) after 15 mins of incubation. A standard plot of PVA was also prepared under identical conditions (Francis *et al.*, 2011).

#### 2.2.8.5. Determination of surface hydrophobicity

1 mg microsphere samples were incubated with different concentrations of Rose Bengal dye (0-50 g/mL) for 3h at room temperature. Dye solutions of all the concentrations, without any microspheres were used as controls. The samples were then centrifuged at 13,000 rpm for 30 minutes in a microcentrifuge (Sorvall legend RT, UK). The supernatant was analysed at 542.7nm (Novaspec II Visible spectrophotometer, UK) to determine the unbound dye. Dye bound on microspheres were calculated with reference to each of the control.

#### 2.2.8.6. Protein adsorption studies

20 mg of samples prepared under different conditions were immersed in a BSA solution of 0.2mg/mL concentration. These were incubated for 24 hours at 37 °C. The samples were centrifuged at 12,000 rpm and the supernatant was subjected to Bradford assay to determine the amount of unbound BSA. The basic principle is that amino acid residues such

as arginine, lysine and histidine bind with Coomassie blue of the Bradford's reagent under acidic conditions to give a coloured complex. Briefly 1.5 mL of Bradford's reagent was added to 30  $\mu$ L of diluted samples and standards. This was incubated at room temperature for 5 minutes and absorbance was measured at 280nm. Protein adsorbed on the surface of the samples was calculated using the following equation

$$Q = (C_i - C_f)V/m$$

Where  $C_i$  is the initial concentration of BSA and  $C_f$  is the final BSA concentration in the supernatant after centrifugation,  $V$  is the total volume of the solution and  $m$  is the weight of the samples.

#### **2.2.8.7. In vitro degradation**

*In vitro* degradation studies were carried out by incubating 10mg of micro/nanosphere samples in 1 mL of PBS, at 37 °C, in a shaken incubator. Samples were removed at specified time points and analysed for water adsorption (% WA) and weight loss (%WL) and weight loss as described below. pH changes of the samples in PBS were also periodically recorded.

#### **2.2.8.8. Water uptake and weight loss measurement**

The dry weight samples were measured before incubation and recorded ( $M_o$  dry, initial dry weight). These were then incubated in PBS for time periods ranging up to 12 months and samples were periodically removed. The micro/nanosphere samples were centrifuged at 4600 rpm for 5 minutes and supernatant was removed, and the weights of the samples were recorded ( $M_t$  wet). The samples were then dried in an incubator overnight at 37 °C and the weight was recorded ( $M_t$  dry). Water uptake and weight loss were calculated using the following equations.

$$\%WA = (M_t \text{ wet} - M_t \text{ dry}) / (M_t \text{ dry})$$

and

$$\%WL = (M_o \text{ dry} - M_t \text{ dry}) / (M_t \text{ dry})$$

Where ( $M_o$ , dry) is the weight of the samples before immersion ( $M_t$ , wet) is the weight of the wet samples ( $M_t$ , dry) is the weight of the samples after drying.

#### 2.2.8.9. Swelling studies on HA-P(3HB) microspheres

HA-P(3HB) microsphere samples were subjected to swelling studies under various physical conditions such as different ionic strengths (Five NaCl solutions (pH = 7.4) of ionic strength 0.0001-1 M), pH (3, 6, 6.8, 7.4 and 10) and temperature (20, 30 and 37 °C). Briefly, Pre-weighed ( $M_d$ ) samples were immersed in respective solutions and were periodically removed and mass of the swollen state ( $M_s$ ) was measured. Swelling ratio was calculated using the formula

$$Q = (M_s - M_d) \times 100 / M_d.$$

Water content in the amphiphilic microspheres were calculated using the formula

$$\text{Water content} = M_s \times 100 / M_d$$

Where  $M_d$  is the dry weight of the microspheres and  $M_s$  is the weight of the microspheres in swollen state.

### 2.2.8.10. Biocompatibility studies

#### I. Cell culture maintenance of HMEC-1

To establish biocompatibility of the micro/ nanospheres prepared, they were subjected to cell viability assays on HMEC-1 cells. All media components and trypsin were filter sterilized and pre-warmed to 37 °C prior to use. Cells stored in liquid nitrogen were thawed to 37 °C and seeded in 75 cm<sup>2</sup> tissue culture grade flask in Dulbecco's Modified Eagle Medium (DMEM), supplemented with 10% foetal calf serum, 2 mM L-glutamine and 1% w/v penicillin and 1% w/v streptomycin solution. The cells were incubated at 37 °C, 5% CO<sub>2</sub>, and intermittently changing media every 2 days. The cells were observed for confluency using a microscope and were trypsinised to allow for cell detachment. Fresh media was added to detached cells and was centrifuged at 500g for 10 minutes. Supernatant was removed, and fresh media was added to cells and seeded into new flasks.

#### II. Sample sterilization

Samples were placed using sterilized spatula in 24-well plates and subjected to UV sterilization, as alcohol sterilization of samples has been known to compromise sample properties. Shortwave 254nm UV sterilization was used in a SI-950 UV Benchtop incubator with a height of 18 inches, for 30 minutes.

#### III. Cell seeding

60-70% confluent cells were detached by trypsinisation and added to sterilised samples at a cell seeding density of 20,000 cells/cm<sup>2</sup>. Cell proliferation up to day 21 was quantified using the MTT assay. Standard tissue culture plate was used a positive and 4% hydrogen peroxide was used as negative control. The plates were incubated under the same conditions as mentioned in the above section. Cell viability was expressed as

Cell viability= mean absorbance of cells on samples/ mean absorbance of cells on tissue culture plates.

### **2.2.9. Drug quantification methods**

#### **2.2.9.1. Determination of the drugs: encapsulation efficiency**

The percentage encapsulation efficiency of the drugs was calculated using the formula

$\%EE = \text{Experimental drug loading} / \text{Actual drug loading}$ .

The supernatant from washing step in the preparation of microspheres were collected to analyse drug loading. Standard plots of each of the drug were prepared using varying concentrations, in triplicates. From the linear regression, the amount of drug leached out in the supernatant was calculated. This was subtracted from the actual amount of drug loaded to get experimental drug loading.

##### **i. High Performance Liquid Chromatography (HPLC) for Rapamycin**

Isocratic elution at a flow rate of 1.0 mL/min was employed on a C18 60 RP column (250x4.6mm, 5 $\mu$ m in particle size) column at 25 °C. The mobile phase consisted of acetonitrile: methanol 20:80 (V/V). The UV detection wavelength was 272nm and 20 $\mu$ L sample was injected.

##### **ii. HPLC for Tacrolimus**

HPLC analysis was carried out using a C18 60 RP column (dimensions 250 mm x 4.6 mm, 5 $\mu$ m in particle size). The UV detection wavelength was 210 nm and 20  $\mu$ L sample was injected (Dionex HPLC). The detector temperature was set at 37 °C. Mobile phase used was Acetonitrile (100%) and flow rate was 1 mL/min.

**iii. Fluorescence spectrometry for Porphyrin quantification**

The amount of porphyrin encapsulated was quantified using a fluorescence spectrophotometer (Eppendorf Biophotometer, U.K). the encapsulated porphyrin derivatives were quantified under the following condition: PP:  $\lambda$  excitation: 400 nm;  $\lambda$  emission: 632 nm; HP  $\lambda$  excitation: 395 nm;  $\lambda$  emission: 630 nm and TPP was  $\lambda$  excitation: 420 nm;  $\lambda$  emission: 651 nm; all three with a bandwidth of 0.5 nm and excitation and emission slit: 10/10.

**iv. UV-VIS spectrometry for Curcumin quantification**

Curcumin was quantified using UV spectroscopy (Eppendorf Biophotometer, U.K), at 422 nm.

**v. UV-VIS spectrometry for Gentamycin quantification**

Gentamycin extracted in the water phase was treated with equal volume of ninhydrin and subjected to heat treatment in a water bath at 95 °C for 15 minutes and cold treatment in ice cold water for 10 minutes. This complex was subjected to UV spectrophotometry evaluation with the wavelength of 418 nm (Ismail *et al.* 2016).

**vi. UV-VIS spectrometry for Aspirin quantification**

Aspirin was quantified using UV spectroscopy (Eppendorf Biophotometer, U.K), at 299 nm.

**vii. VEGF quantification using VEGF human ELISA kit**

VEGF encapsulated was calculated using the VEGF human ELISA kit. The samples and controls were added to ELISA plates with immobilized antibody. The VEGF antibody complex was washed to remove any unbound samples and then subjected to treatment with a second detector antibody with a conjugate enzyme, that binds to a different epitope

on the target antibody. The microplates were then washed to remove any unbound substances and a substrate specific to the enzyme, was added, resulting in a coloured complex. The absorbance of this complex was read at 540 nm.

### 2.2.10. Drug release kinetics

10mg each of drug-encapsulated microspheres were immersed in 2 mL of PBS and incubated at 37 °C. 1mL samples were drawn periodically and 1mL fresh PBS was added to the samples. Drug release was detected using the methods described as above.

### 2.2.11. Application of drug release data on mathematical models

The cumulative drug release (of each of the DDS prepared) at each time point was expressed as a fraction of the actual drug loading. The data generated were fitted in zero-order, first- order, Higuchi, Hixson- Crowell and Korsmeyer-Peppas models. All equations were fitted to the whole release profile, except for Korsmeyer-Peppas in which only 60% was fitted. To linearize the obtained data, the following plots were generated (**Table 2.3**) and the  $R^2$  value of each of them was compared. The model with the highest  $R^2$  value was identified as the best fit for each drug release.

Model	Graph
Zero- order	% Cumulative release vs time
First- order	Log (% cumulative drug remaining) vs time
Higuchi	% Cumulative release vs time <sup>1/2</sup>
Hixson- Crowell	% cumulative drug remaining <sup>1/3</sup> vs time
Korsmeyer-Peppas	Log (% Cumulative release) vs Log (time)

**Table 2.3:** Drug release models

### 2.2.12. Protein expression and purification

To express the RFP-anti HER-2, Rosetta gami B(DE3) *E. coli* (EMD Chemicals Inc., Gibbstown, NJ) cells were transformed with the appropriate plasmid and grow on LB agar supplemented with carbenicillin and chloramphenicol (100 µg/ mL and 34 µg/mL final concentration respectively), 37°C for 18 hours. A single colony was inoculated into 10 mL of LB media (with antibiotics) and grown at 37°C (with shaking at 250 rpm) for 16 hours. 10 mL of this was then added to 200 mL of pre-warmed LB media, prepared in 1 L conical flasks (with antibiotics) and incubated at 37°C and 250 rpm, to O.D. 0.5 at 600 nm. The culture was then placed on ice for 30 minutes and isopropyl β-D-1- thiogalactopyranoside (IPTG) added to a final concentration of 1mM to induce expression. This was then incubated at 20°C for 20 hours at 250 rpm. 50 mL aliquots of the culture were centrifuged for 20 minutes, 5,000 rpm at 4°C (using Sorvall SuperT 21 bench top centrifuge, with SL-250T rotor) and the pellets were used for cytoplasmic protein extraction. Using immobilised metal ion chromatography (IMAC), the proteins were enriched from the cell lysate on 1 mL HisTrap HP Ni Sepharose™ column using the ÄKTAprime™ plus purification system. The fractions were then analysed with 12% SDS-PAGE Tris- glycine gels stained with Coomassie blue (Markiv *et al.*, 2011). Concentration of the protein purified was calculated by the spectrometric method using Thermo Scientific™ NanoDrop.

### 2.2.13. Surface adsorption of anti-HER2 on porphyrin encapsulated microspheres

Microspheres were dispersed in PBS, pH 5.0, (10 mg/mL) and a 600 µL aliquot was mixed with 200 µL of a solution of anti-HER-2 (2 mg/mL) and adjusted to the volume of 500 µL with phosphate buffer. Monoclonal antibody (anti-HER-2) was adsorbed onto the

microspheres at 4°C for 24 h, and then centrifuged at 10,000 rpm for 15 min (microcentrifuge Sorvall legend RT, UK) to separate microspheres from free anti-HER-2. The pellet was washed with phosphate buffer saline (PBS), pH 7.4, and re-dispersed in 500 µL of PBS, pH 7.4. The control was run the same way as the sample, but PBS was used instead of anti-HER-2 solution. The supernatant was subjected to Bradford's assay to quantify anti-HER-2 adsorbed on the microspheres (Kocbek *et al.*, 2007). Briefly 1.5 mL of Bradford's reagent was added to 30 µL of diluted supernatants and standards. This was incubated at room temperature for 5 minutes and absorbance was measured at 280nm. Protein adsorbed on the surface of the samples was calculated using the following equation

$$Q = (C_i - C_f)V/m$$

Where  $C_i$  is the initial concentration of anti-HER-2 and  $C_f$  is the final concentration of anti-HER-2 concentration in the supernatant after centrifugation,  $V$  is the total volume of the solution and  $m$  is the weight of the samples.

## **2.2.14. Cell viability studies**

### **2.2.14.1. Cell culture maintenance of SK-BR-3**

SK-BR-3 cells (Fogh, Wright and Loveless, 1977) were grown in McCoy's 5A media, supplemented with 10% foetal calf serum, and 1% w/v penicillin and 1% w/v streptomycin solution, as described by ATCC (Wu *et al.*, 2003). The medium was changed every 2-3 days. The cell cultures were maintained at 37 °C, 5% CO<sub>2</sub> and passaged, on 60-70% confluence, by trypsin treatment for 10 minutes. Following cell detachment, fresh medium was added to the cell suspension, which was then centrifuged at 1000 rpm for 10 minutes. The resulting cell pellet was suspended in fresh medium and transferred to 75 cm<sup>2</sup> tissue culture flasks.

#### **2.2.14.2. Metabolic activity assay**

Metabolic activity of the SK-BR-3 cells when treated with microspheres encapsulated with porphyrin derivatives was quantified using the MTT assay. The cells were incubated at a density of  $1 \times 10^4$  in the presence of 2mg porphyrin derivative encapsulated microspheres, for 48 hours, in dark. The tissue culture plates were covered in aluminium foil to prevent light exposure. These were then exposed to white light 30 minutes, to allow for photoexcitation. The cytotoxic effect was quantified using cell viability calculations, as indicated by the MTT assay. Briefly, the media was aspirated from the wells and 1mg/mL MTT in 200 mL serum free media (media without addition of FBS) was added. This is then incubated for 3 hours, after which the MTT solution was removed and an equal volume of isopropanol was added. The plate was then covered with aluminium foil and absorbance was read at 540nm.

#### **2.2.14.3. Calculation of Inhibitory concentration (IC50)**

Varying concentrations (0.05, 0.1, 0.2, 0.5, 1, 2 and 3mg/mL) of the microspheres were incubated in SK-BR-3 and cytotoxicity was quantified using the MTT assay. Linear regression of the variables was used to analyse the inhibitory concentration for 50% cytotoxicity.

#### **2.2.15. Confocal imaging**

For confocal imaging, Promokine Live/Dead Cell Staining Kit II containing two fluorescent dyes, Calcein-AM and Ethidium homodimer III (EthD-III) were used. The virtually non-fluorescent Calcein-AM attains green fluorescence by the ubiquitous esterase activity that characterizes live cells. EthD-III selectively excludes intact live cells and enters damaged cells and binds to nucleic acids, resulting in red fluorescence (Probes, 2005). Stained cells were observed and imaged using the confocal microscope Leica TCS SP2 50.

---

**2.2.16. Determination of the Minimum Inhibitory Concentration (MIC) of HA-P(3HB) with encapsulated curcumin against Methicillin Resistant *Staphylococcus aureus***

MIC is defined as the minimum concentration of an antimicrobial agent that can cause an inhibitory effect. To estimate MIC, a single colony of MRSA was grown in LB medium at 37 °C and 250 rpm and an optical density at 595nm was recorded to observe its growth profile. At mid log phase 1 mL aliquots of the culture was further inoculated into 10 mL of media and this was then allowed to grow in 96 well plates, in the presence of different concentrations of microspheres (500, 250, 125, 62.5, 31.25, 16, 8, 4, 2, 1 µg /mL of curcumin respectively). The growth profile was observed, with O.D recorded at 595nm at intervals of 1 hour, with free inoculum as control. MIC was determined as the lowest concentration at which bacterial growth was inhibited (Ortiz & Torres 2014).

**2.2.17. Determination of Minimum Bactericidal Concentration (MBC) of curcumin encapsulated HA-P(3HB) against Methicillin Resistant *Staphylococcus aureus***

MBC is defined as the minimum bactericidal concentration to kill 100% of the bacteria. The lowest concentration that exhibited the absence of viable microorganisms was reported as MBC. The contents of each well (200 µL) as described in the section above was transferred into 2 mL of fresh LB medium and grown for 12 hours. The tubes were observed for turbidity and 20µL of the culture from the least turbid looking tubes were inoculated on LB Agar plates and incubated at 37°C for 24 hours. The concentration of microspheres

corresponding to absolute absence of colonies was recorded as MBC (Ortiz and Torres 2014).

### **2.2.18. Statistical analysis**

All experiments were done in triplicates and data is expressed along with their mean standard deviation. The data, where appropriate, were compared using the student's t-test and ANOVA and was used to analyse significant differences amongst factors assessed. The differences were considered significant when  $*p < 0.05$ , very significant when  $**p < 0.01$  and highly significant  $***p < 0.001$ , respectively. Any p-value higher than 0.05 ( $p > 0.05$ ) was insignificant. The statistical analysis for comparing drug release models was done using ANOVA on excel Analysis ToolPak, within 95% confidence interval.

# **Chapter 3**

## **Polyhydroxybutyrate microspheres and nanospheres as drug delivery systems: Process optimisation**

### 3.1. Introduction

Micro/Nano encapsulations are one of the most common and developing strategies of drug delivery. Geometrically, spherical constructions are superior for efficient drug delivery as they have higher specific surface area and hence higher therapeutic coverage (Kim and Pack, 2006). The advantages of spheres over other DDS are several; they can be tailored to have uniform size and geometry, they can have external or internal interconnected pore networks and their porosity can be modulated, degradation rate is linear in the case of surface eroding polymers and can be made stand alone or in combination with other 3-D structures (Hossain, Patel and Ahmed, 2014). Sphericity is thought to improve cell attachment, especially with low density spheres that have interconnected pore networks. Spherical geometry also enhances ease of subcutaneous administration via injections.

Depending on the nature of the drug to be encapsulated, single or double emulsion methods can be approached for hydrophobic and hydrophilic drugs, respectively. In single emulsion method, the polymer is dissolved in a water immiscible, volatile solvent and emulsified with water containing an appropriate surfactant/ emulsifier forming an oil/water (O/W) emulsion. The organic solvent is then allowed to evaporate under agitation, and this leaves behind solid spherical microspheres with a polymeric inner core (**Figure 3.1**). In the case of hydrophilic drugs, a double emulsion of water/oil/water is preferred as in W/O method, there are increased chances of the hydrophilic drug to partition into the aqueous phase. In double emulsion method, the hydrophilic drug is dissolved in a water phase and then emulsified with the oil phase containing polymer solution. This is then transferred to an excess amount of water to form a secondary emulsion. During solvent evaporation, the polymer starts decreasing in volume towards

the core, also entrapping microdroplets of the emulsion, which coalesce to form a honeycomb structure characterised with hydrophilic points (Vilos and Velasquez, 2012).

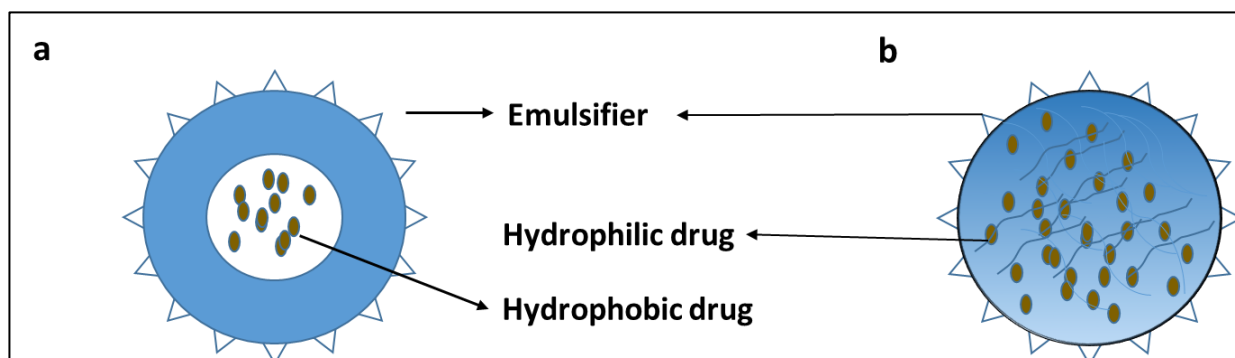


**Figure 3.1:** Schematic representation of polymeric particles prepared by a) single emulsion method and b) double emulsion method (Adapted from (Vilos and Velasquez, 2012)).

Subsequently, with a variety of determinants to consider, it is essential for a polymer to be used in an application as specific as drug delivery, to have predictive models for process parameters. Bearing this in mind, in this study, a select set of pilot experiments were carried out to establish boundary conditions of each of the parameters analysed (Polymer concentration, PVA concentration and stirrer speed), within the limits of practical feasibility. Having set these boundary limits, Box–Behnken experimental design and response surface methodology (RSM) were applied to predict process parameters for a set goal of particle size range. RSM is a strategy to device or design of experiments that can correlate interactions between variables and map a response surface that can provide optimal parameter settings. Box- Behnken is the least expensive RSM strategy, that takes into account three variables and three representatives of each of the variables at their extremities and midpoints (Joseph and Manohar, 2013). There are 15 sets of experiments

in three-factor Box-Behnken design, as represented by the points on the Figure below (Figure 3.2).

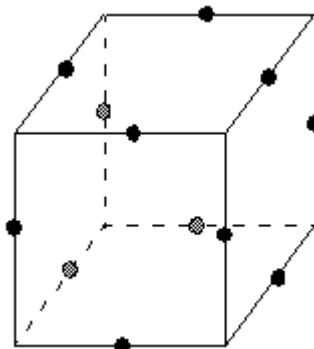


**Figure 3.2:** Representation of experimental runs on a Box-Behnken design.

RSM follows 4 steps to generate a predictive model where the first step is to design a series of experiments to generate reliable measurement of the intended response. This is followed by the development of a second order, best-fitted response surface, to find an optimal set of parameters for predictive responses and finally, generation of plots to correlate the variables and responses. Validation of this method can be done by comparing the prediction models with the experimental results (Joseph and Manohar, 2013).

In this chapter, P(3HB) was produced using *B. cereus* SPV and was chemically well characterised. This was used for the optimization of microsphere production, using PVA as the surfactant. The effect of polymer concentration, PVA concentration, stirrer speed, nature of the solvent used, and temperature were initially observed to set boundary limits for RSM, and of these three most influential variables on determining particles formation were identified. A Box- Behnken design was then generated using the software Design expert and a set of 15 experiments were run, keeping particle size as the response analysed. (The microspheres produced were also characterised for other parameters, but in the

interest of its efficient applications, particle size was identified as the most desirable response that necessitated optimising). The predicted model was then validated using a set of experiments.

*B. cereus* SPV is known to produce emetic toxins and enterotoxins, leading to food poisoning (Granum and Lund, 1997). Although, the purity of the polymer extracted from this organism is ensured by complete removal of cell content during polymer extraction, this factor can be a hindrance in the use of these polymers for biomedical applications. Therefore, P(3HB) extracted from *B. subtilis* OK2, which has a higher molecular weight was also used in this project to produce micro and nanospheres. P(3HB) from *B. subtilis* OK2 is of higher molecular weight as compared to that produced using *B. cereus* SPV, production of relatively larger microspheres were expected in this case.

## 3.2. Results

### Part I: Statistical optimisation of synthesis of P(3HB) microspheres

#### 3.2.1. Production of P(3HB) from *B. cereus* SPV

Figure 3.3 represents the temporal growth profile obtained from the culture of *B. cereus* SPV for P(3HB) production, in a 5 L Bioreactor using Kannan and Rehacek (KR) nitrogen-limiting media. This was carried out to analyse the temporal pattern of biomass and P(3HB) accumulation to establish a production strategy and ensure a reasonable yield. This pattern was found to correlate with changes in optical density, pH and estimated glucose consumption. The initial lag phase was not visible, possibly suggesting it might have been either less than 3 hours or absent. OD<sub>600</sub> increased sharply until the 36<sup>th</sup> hour, clearly indicating log phase of growth. A decrease in OD<sub>600</sub> was observed at the 36<sup>th</sup> hour due to

excess foaming and increased again on addition of antifoam and plateaued around a value of 17, until the 72<sup>nd</sup> hour, indicating a stationary phase of growth. The intermittent dips in the OD<sub>600</sub> profile were observed to correspond with excessive foaming. As expected, there is a direct correlation observed between OD<sub>600</sub> and biomass. The pH decreased throughout the experiment from  $6.8 \pm 0.3$  and reached a value of  $3.7 \pm 0.4$  at 48 hours. Dissolved Oxygen Tension (DOT) was observed to decrease rapidly until the 9<sup>th</sup> hour when it reached a minimum and a steady rise was observed between 48 and 72 hours. The decrease in DOT overlapped with the log phase, confirming oxygen consumption during growth. P(3HB) accumulation demonstrated a positive correlation with time. After 72 hours, a P(3HB) yield of 26.3% dry cell weight was observed.

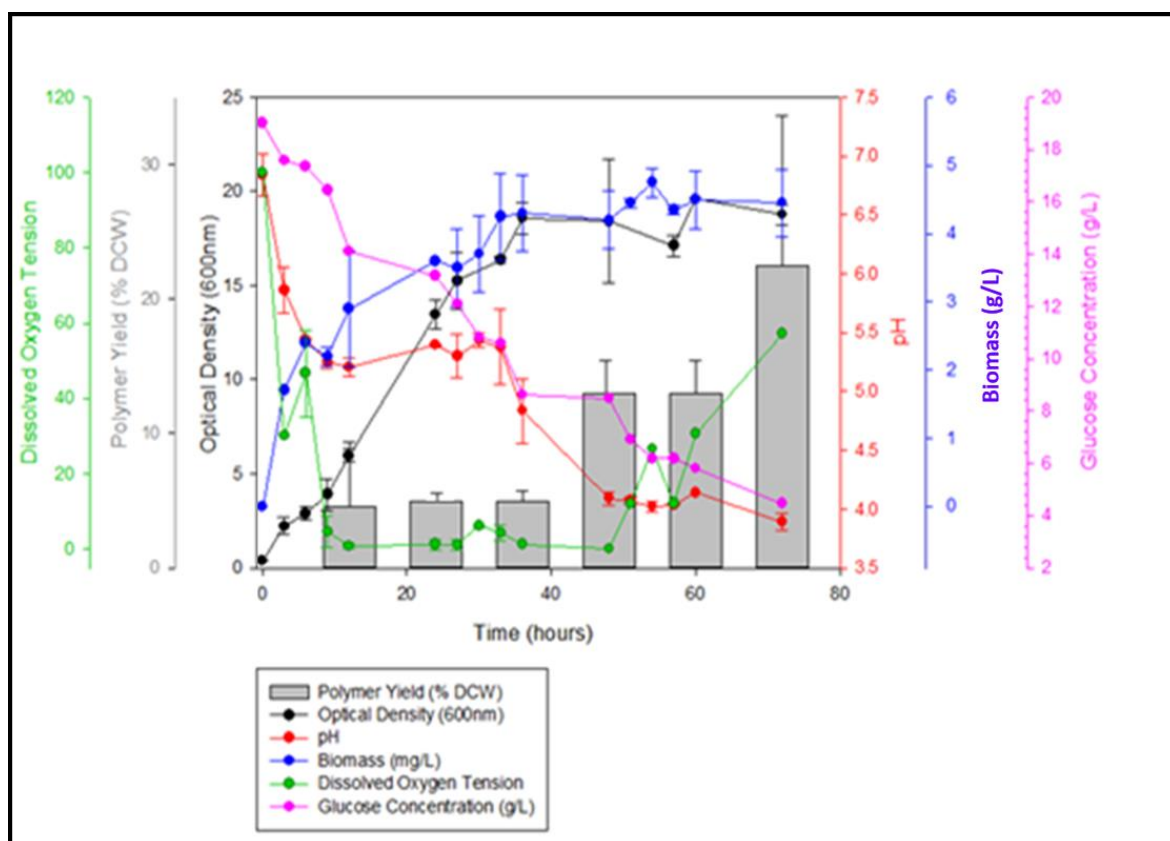


**Figure 3.3:** Temporal growth profile of *B. cereus* SPV for the production of P(3HB) in 5L bioreactors

### 3.2.2. Characterisation of the polymer

The P(3HB) thus produced was extracted using the soxhlet method with methanol and chloroform as solvents and was precipitated using differential precipitation.

#### 3.2.2.1. FTIR analysis of P(3HB) produced using *B. cereus* SPV

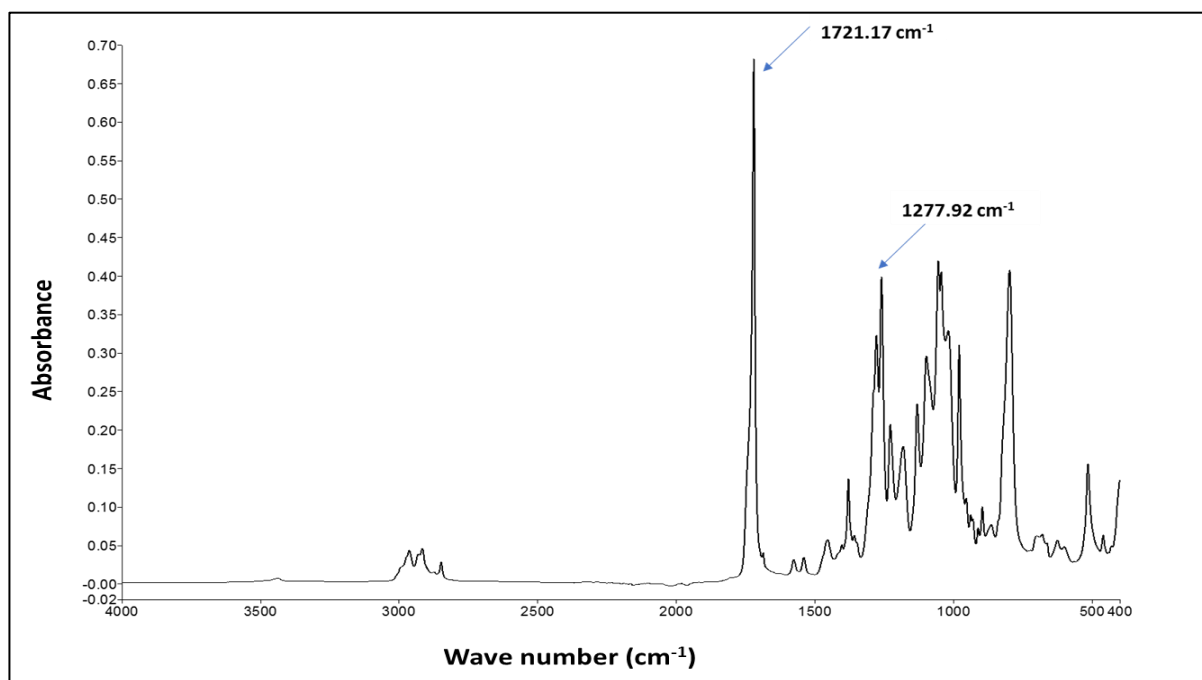


**Figure 3.4:** FTIR spectra of P(3HB) produced using *B. cereus* SPV

Preliminary confirmation of the polymer produced was obtained using the FTIR spectra. The FTIR spectrum showed two distinct peaks at wavenumbers  $1721.17\text{ cm}^{-1}$  and  $1277.92\text{ cm}^{-1}$ , corresponding to the ester carbonyl group and the  $-\text{CH}$  group, respectively, which is characteristic of SCL PHAs (**Figure 3.4**).

#### 3.2.2.2. Nuclear Magnetic Resonance

The proton NMR shows peaks corresponding to 3 different hydrogen environments (**Figure 3.5.a**). These are manifested as a duplet at 1.26 ppm, a multiplet around 2.5 ppm and a

sextet around 5.2 ppm.  $^{13}\text{C}$  NMR shows four different peaks corresponding to four separate carbon environments. The chemical shifts respectively are at 169 ppm corresponding to  $\text{C}_3$  ( $\text{C}=\text{O}$  group), 68 ppm corresponding to  $\text{C}_1$  ( $-\text{CH}$  group), 41 ppm corresponding to  $\text{C}_2$  ( $-\text{CH}_2$ ) and the 19 ppm corresponding to  $\text{C}_4$ , which is the part of the  $-\text{CH}_3$  group (**Figure 3.5.b**).

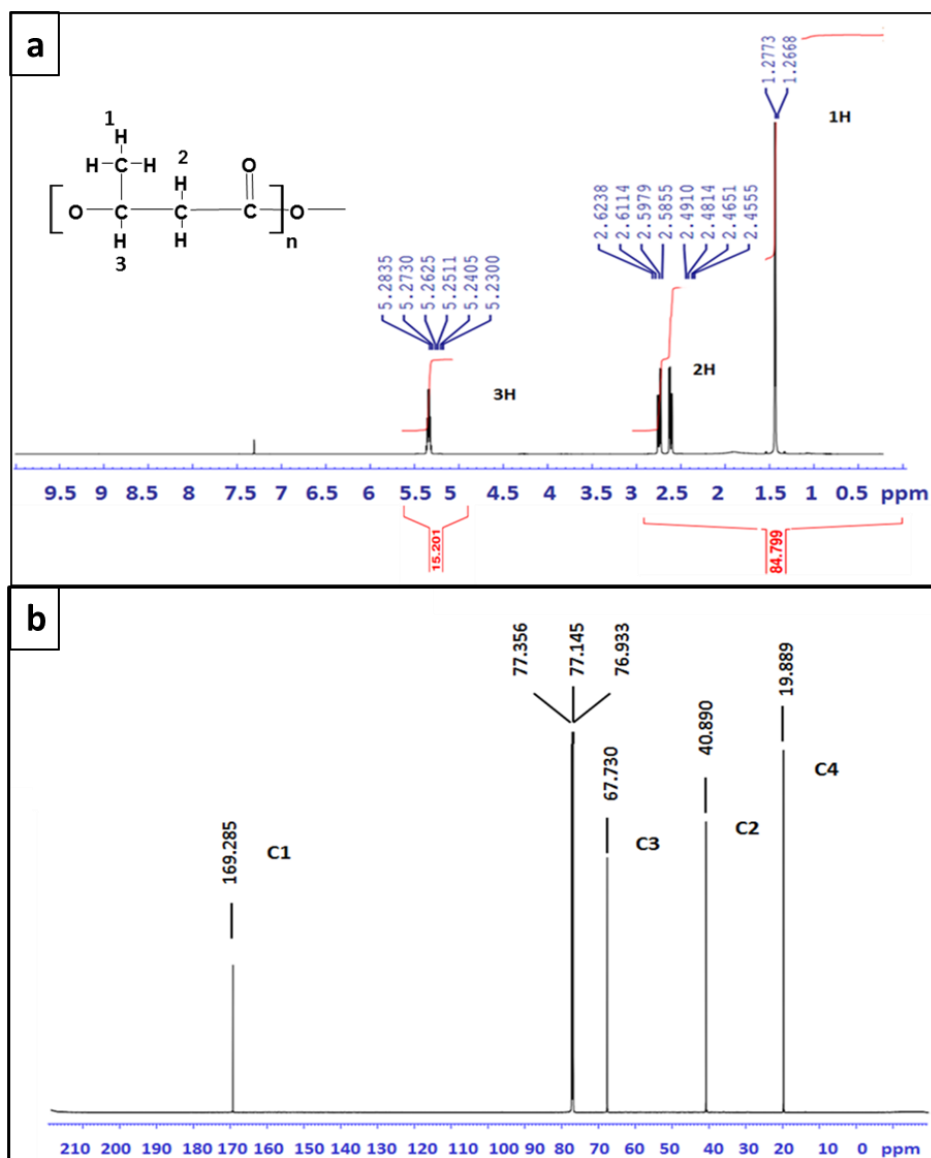


**Figure 3.5:** a) Proton NMR and b)  $^{13}\text{C}$  NMR spectra of P(3HB) produced using *B. cereus* SPV

### 3.2.2.3. Molecular weight analysis

The polymer produced and purified was subjected to molecular weight analysis using gas permeation chromatography (GPC). The molecular weight of the polymer was found to be 158kDa with a polydispersity Index of 1.73.

### 3.2.3. Optimisation of microsphere production

#### 3.2.3.1. Pilot experiments

A set of pilot experiments were (not statistically optimised) carried out by varying the process parameters, namely, type of organic solvent used, concentration of polymer in the organic solvent, PVA concentration, fabrication method, mode of drying and stirrer speed, some of which are as represented in the Table below (**Table 3.1**).

Expt. number	P(3HB) concentration (mg/mL)	Solvent	PVA concentration (%)	Fabrication method	Drying
1	2.5	Dichloro-methane	0.5	Magnetic stirring at 800 rpm	Freeze drying
2	30	Dichloro-methane	0.5	Magnetic stirring at 800 rpm	Air drying
3	50	Dichloro-methane	0.5	Homogenization, and magnetic stirring	Freeze drying
4	35	Chloroform	1	Sonication for 10 s, maximum power	Freeze drying
5	50	Chloroform	0.5	Sonication for 10 s, maximum power	Air drying
6	62.5	Chloroform	1	Magnetic stirring at 1000 rpm	Air drying
7	5	Chloroform	0.01	Magnetic stirring at 500 rpm	Freeze drying
8	50	Chloroform	0.5	Magnetic stirring at 800 rpm	Freeze drying
9	35	Chloroform	0.5	Magnetic stirring at 1000 rpm	Freeze drying

**Table 3.1:** Conditions used for pilot experiments in making P(3HB) microspheres

The P(3HB) microspheres were prepared by the solid-in-oil-in-water (s/o/w) technique and their surface morphology was analysed using SEM. It was found that microspheres produced using DCM as the solvent did not yield spheres with good morphology. The spheres formed were polydisperse in size, forming occasional structures that looked like agglomerations of smaller spheres. For the most part, the polymer did not yield spherical structures, when dissolved in DCM. Sonicated emulsion did not yield any microspheres and the polymer was found to precipitate from the emulsion on to the sides of the liquid vessel in which the experiments were being carried out. Air drying resulted in microspheres with extensive interconnecting water channels that assumed the shape of the surface on which they were placed for drying. These did not yield free flowing powder forms at all and hence weren't imaged.

SEM images corresponding to experiment numbers 1-10 (**Table 3.1**) are represented below (**Figure 3.6 a & b**):

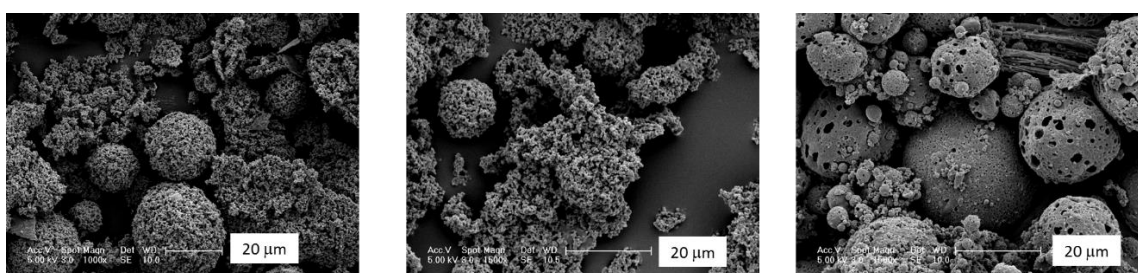


**Figure 3.6.a:** SEM images of microspheres corresponding to experiments 1,3&4

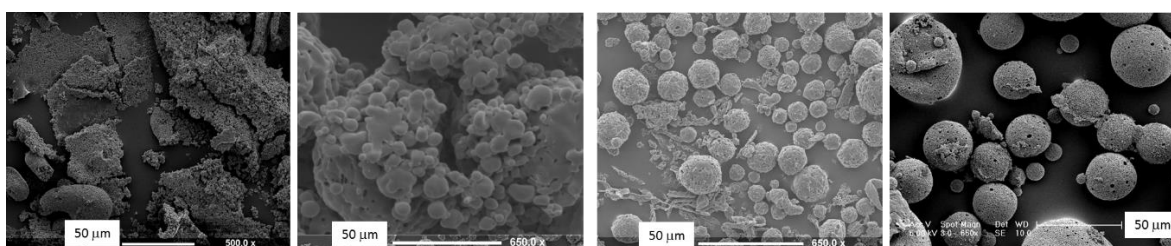


**Figure 3.6.b:** SEM images of microspheres corresponding to 7-10

### 3.2.3.2. Design of experiments

A set of pilot experiments were carried out using varying polymer concentrations, PVA concentrations and stirrer speeds. Microspheres of appreciable spherical shape and yield were produced within the concentration range of 0.3- 0.8 g of polymer in 8 mL of chloroform, using 0.5-1% solution of PVA as the aqueous phase, under circular agitation using a magnetic stirrer between stirrer speeds of 500 to 1000 rpm (**Table 3.2**).

	Polymer concentration (%)	PVA concentration (%)	Stirrer speed (rpm)
Level 1 (-1)	0.0375	0.5	500
Level 2 (0)	0.0625	0.8	800
Level 3 (+1)	0.1	1	1000

**Table 3.2:** Boundary conditions for microsphere optimization

Therefore, based on the preliminary experimental trials, the tabulated process parameters and three levels for each of them were assigned. Based on these three parameters a Box-Behnken design with 15 runs for modelling a response surface was generated using the software MiniTab Express (**Table 3.3**).

	Pattern	Polymer concentration (mg/mL)	PVA concentration (%)	Stirrer speed (rpm)
1	0+-	0.0625	1	500
2	+0+	0.1	0.8	1000
3	000	0.0625	0.8	800
4	-0+	0.1	0.8	1000
5	+0-	0.1	0.8	800
6	0--	0.0625	0.5	500
7	-+0	0.1	1	800
8	+0-	0.1	0.8	500
9	++0	0.1	1	800
10	-0-	0.1	0.8	500
11	0+-	0.0625	0.5	1000
12	000	0.0625	0.8	800
13	--0	0.1	0.5	800
14	0++	0.0625	1	1000
15	000	0.0625	0.8	800

**Table 3.3:** Design of experiments generated using MiniTab Express

### 3.2.4. Surface morphology and particle size analysis

Morphological characterisation of microspheres produced was done by observing SEM images under different magnifications (**Figure 3.7**).

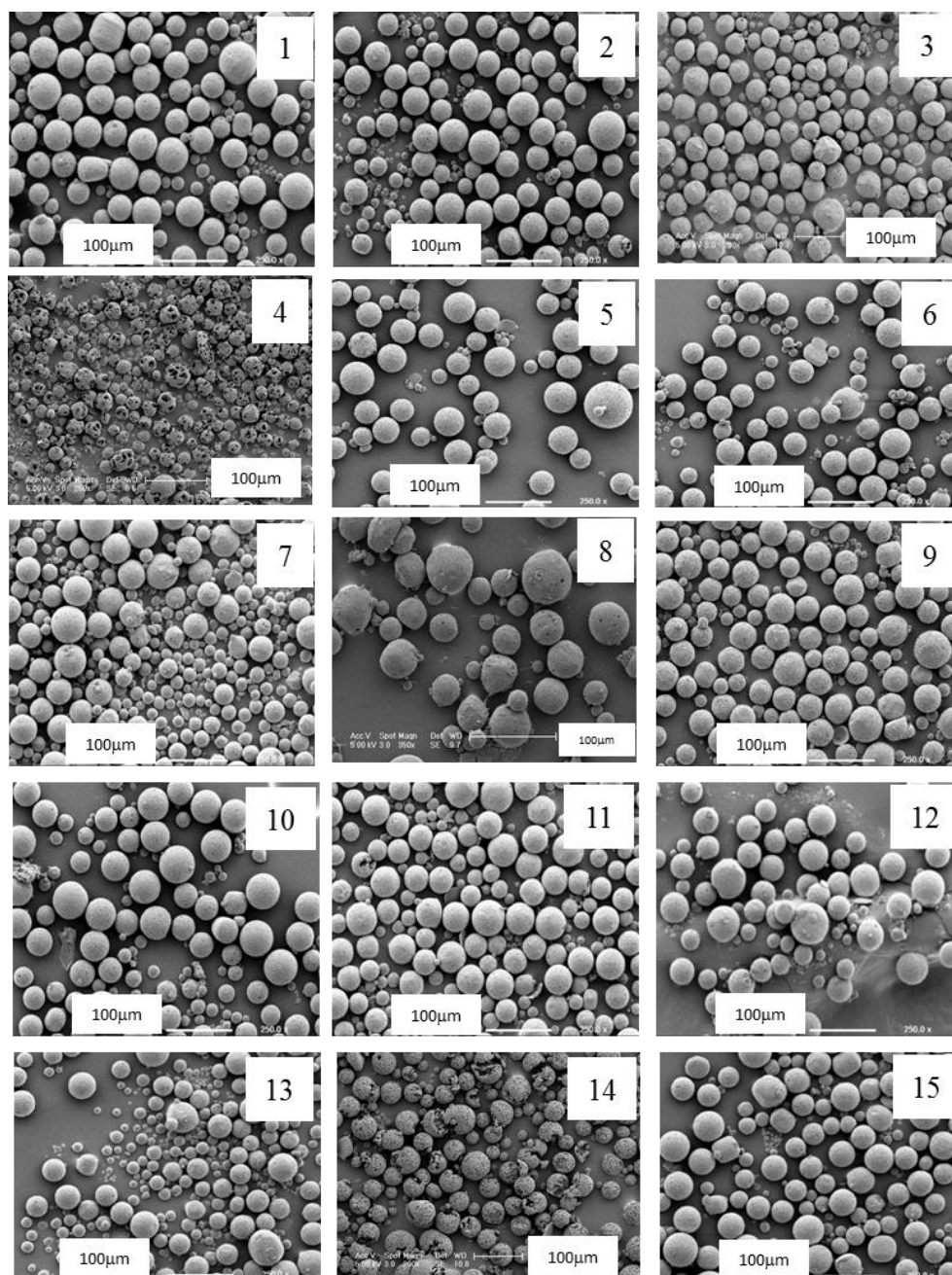


**Figure 3.7:** SEM images of microspheres corresponding to experiments 1-15.

Of the 15 runs, all except, experiment number 4 and 14, gave well- formed microspheres of defined spherical shape and smooth surface. The microspheres corresponding to experiment number 4 was found to be extremely porous with a ruptured wall revealing an empty core. Diameter of the microspheres corresponding to each experiment run was calculated after analysing the SEM images on ImageJ software. SEM images of varying magnifications corresponding to each experiment run were adjusted to the right threshold and gain, and the analysis tool was calibrated using the size bar of the SEM images against pixels. From the surface area output, diameters of the images were calculated, and an average value was recorded (**Figure 3.8**).

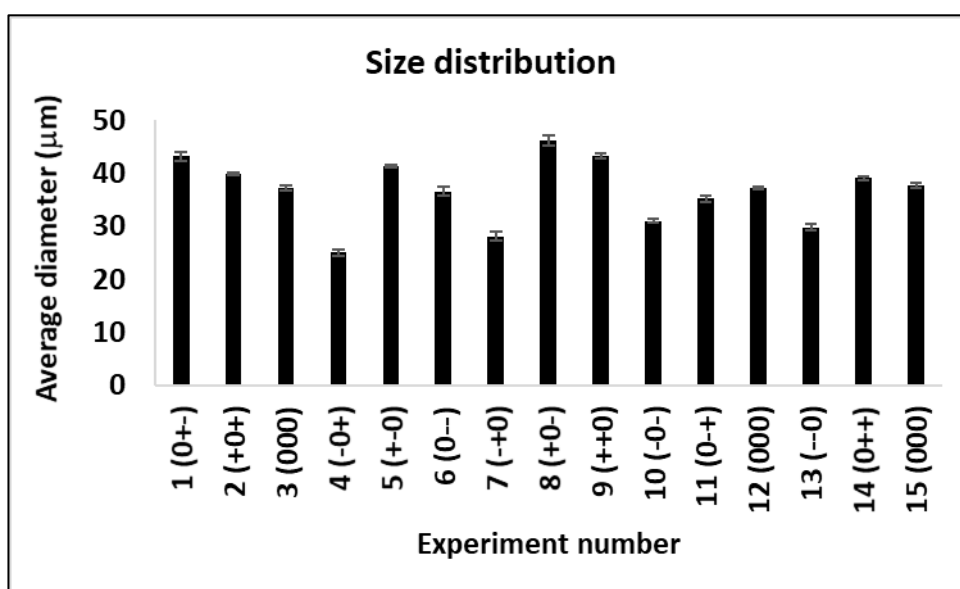


**Figure 3.8:** Average diameter of microspheres corresponding to experiments 1-15 [code (polymer concentration: PVA concentration: Stirrer speed); For polymer concentration, -= 0.0375, 0= 0.0625 and += 0.1 g/mL; PVA concentration, -= 0.5, 0= 0.8 and += 1 % w/v and stirrer speed, -= 500, 0= 800 and += 1000 rpm]. (n=3, error bars= ±SD)

In all the preparations, microspheres were found to be largely polydisperse in size. Microspheres corresponding to experiment number 4, 7 and 13 were found to be the smallest (with mean diameter of 25.5, 28.1 and 29.8 μm respectively) and the factor

common to these conditions is that they were synthesised using the least concentration of P(3HB) used in the design. Images corresponding to experiment number 1, 8 and 9 were found to be of the largest (with diameter of 46.02, 43.1 and 41.733  $\mu\text{m}$  respectively) and the common factor amongst was the highest polymer concentration. However, experiment number 11, although was run with the least polymer concentration, and least stirrer speed, was of an average diameter of 35.2  $\mu\text{m}$ . The microspheres corresponding to experiment number 4, although were small, were found to be visibly highly porous, and lacking a spherical shape.

### 3.2.5. Modelling of response surface

Based on the input parameters under the 15 conditions given by the Box- Behnken design, microspheres were prepared. The average diameter obtained from each of the trials was recorded as output parameter. The table below (**Table 3.4**) summarizes the values for the experimental output (observed value as represented in Figure 3.8) and predicted output (fitted value). A total of 15 experiments were run as randomized trials as generated by the Box- Behnken design and the relationship between input variables and expressed outcome was analysed. On running the 3- level, 3- factor design, the relationship between independent variables and dependent variables were statistically analysed using ANOVA. The variables and variable interactions with a p value  $<0.05$  was considered highly significant. Variables and variable interactions with regression coefficients of a positive value were thought to have an agonistic and with regression coefficients of negative value were considered to have antagonistic effects on the lowering of particles size. When the coefficient of determination ( $R^2$ ), approached 1, the model was considered to be more fitting.

Expt. number	Concentration of P(3HB) (g/mL)	PVA concentration (%)	Stirrer speed (rpm)	Observed value ( $\mu\text{m}$ )	Fitted value ( $\mu\text{m}$ )
1	0.0625	1	500	43.21	42.84
2	0.1	0.8	1000	39.83	39.31
3	0.0625	0.8	800	37.20	37.1990
4	0.0375	0.8	1000	25.09	28.82
5	0.1	0.8	800	41.33	39.80
6	0.0625	0.5	500	36.61	36.69
7	0.0625	1	800	28.13	25.35
8	0.0375	0.8	500	46.21	45.69
9	0.1	1	800	43.37	44.18
10	0.1	0.8	500	31.02	30.76
11	0.0375	0.5	1000	35.23	35.25
12	0.0625	0.8	800	37.19	37.19
13	0.0375	0.5	800	29.82	28.05
14	0.0625	1	1000	39.05	37.60
15	0.0625	0.8	800	37.68	37.19

**Table 3.4:** The observed and fitted value for particle diameter

**Table 3.5** shows the result of variance of analysis performed for mean particle size. From the analysis, based on p value, Polymer concentration was found to have the highest F ratio and the least p value, making it the most significant variable. Table 3.6 below represents the analysis of variance for the independent variables and the parameters are coded as A: Polymer concentration, B: PVA concentration, and C: Stirrer speed.

Variable	Regression Coefficient	P value
Constant	24.203	<0.001
A	195.73	<0.001
B	5.734	0.00854
C	-0.008134	0.0214
A.A	4.102	0.0009
A.B	-4.95	0.0101

**Table 3.5:** Analysis of variance for factors and factor interactions influencing particles size, performed using the JMP software. A: Polymer concentration, B: PVA concentration, and C: Stirrer speed.

### 3.2.5.1. Mathematical modelling and effect of independent variables on the particle properties

The results obtained from statistical analysis confirmed that all the tested parameters namely polymer concentration, PVA concentration and stirrer speed have significant effect in determining the size of particles. Using regression coefficients of factors and factor interactions with p values less than 0.05, a model was designed to predict the effects of input variables on the output response. The model considered individual independent variables and their interactions. The equation generated has linear terms corresponding to single factor effects and second order terms corresponding to interactions, used to express nonlinearity of the response. The equation generated for the model given below:

$$\text{Mean particle size} = 24.203 + (195.73 * A) + (5.734 * B) - (0.008134 * C) + (4.102 * A * B) - (4.95 * A^2)$$

Where A= Polymer concentration

B= PVA concentration

C=Stirrer speed.

The linear regression plot corresponding to experimental values and predicted values for mean particle diameter are given below. As the predicted values come closer to the actual values, the points on the scatterplot fall closer to the red line. (**Figure 3.9**). Because the points are all very close to the line, it can be concluded that the model predicts particle size based on the defined parameters very well. The  $R^2$  value was found to be 0.91, which is very close to 1, hence concluding the model to be adequate for predicting mean particle size.

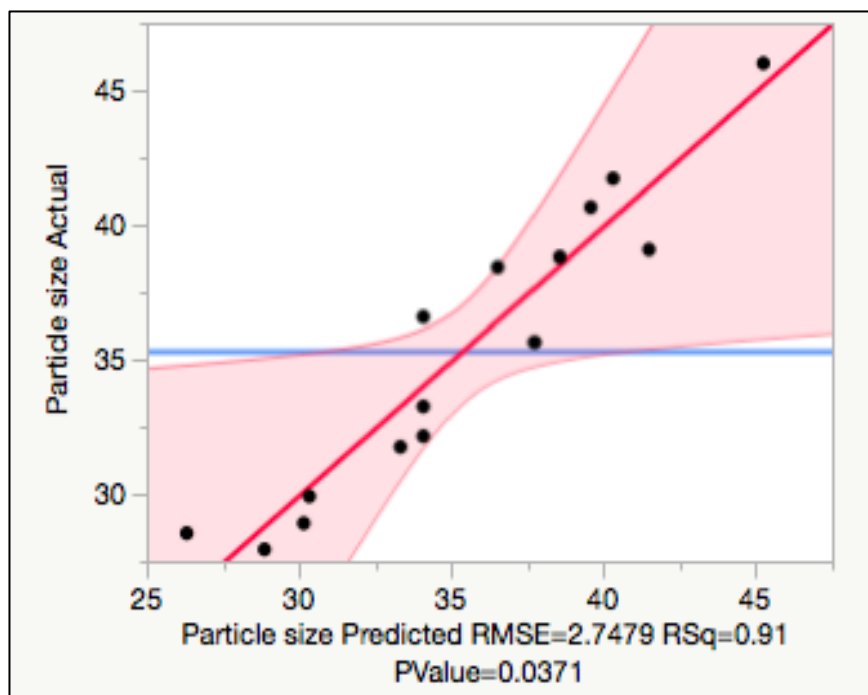


**Figure 3.9:** Linear regression plot correlating the actual value and predicted value for mean particle diameter.

### 3.2.5.2. Graphical representation of significant effect of independent variables

The significance of the independent variables on particle size was graphically demonstrated by using 3-D plots. The plots were generated by keeping one of the parameters constant and mapping the response as a function of interaction between the other two parameters. These plots are useful in analysing the influence of two independent parameters on the response, simultaneously. The 3-D plot representing the effects of P(3HB) concentration and PVA concentration, P(3HB) concentration and stirrer speed and PVA concentration and stirrer speed are represented below (**Figure 3.10 a, b &c**).

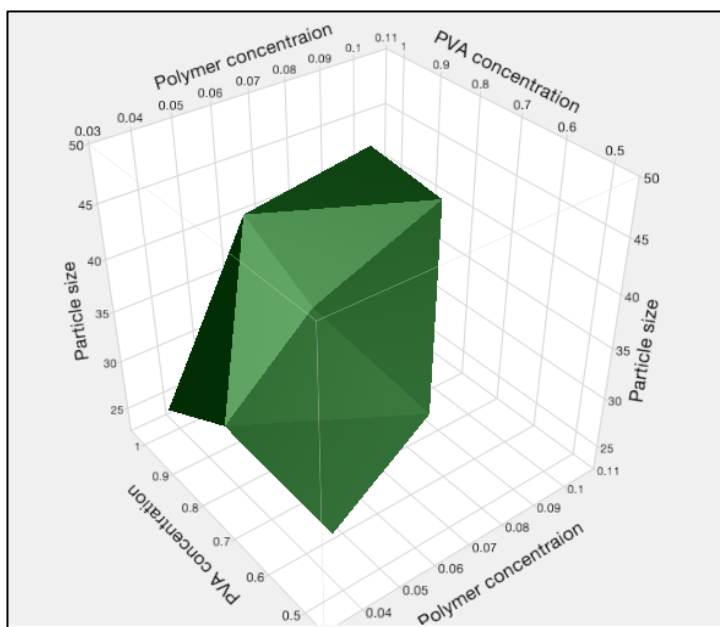


**Figure 3.10.a:** response surface plots showing the effect of PVA concentration and polymer concentration on particle size

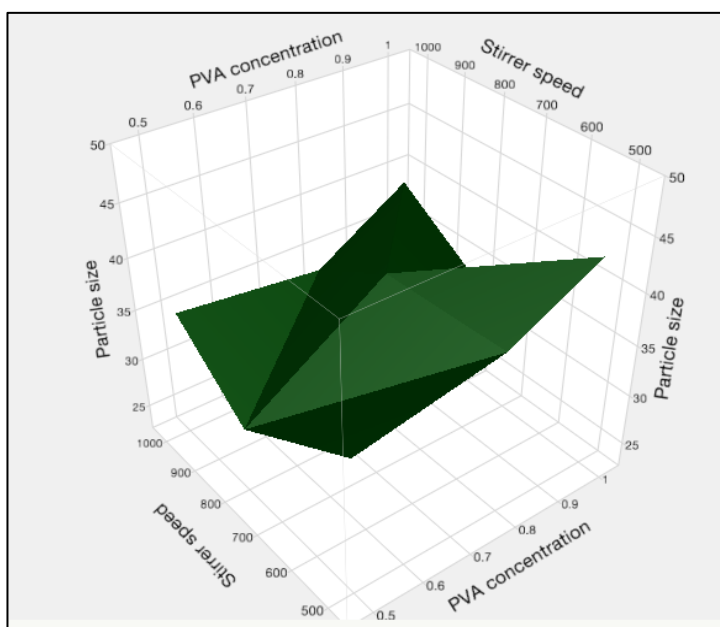


**Figure 3.10.b:** response surface plots showing the effect of PVA concentration and stirrer speed on particle size

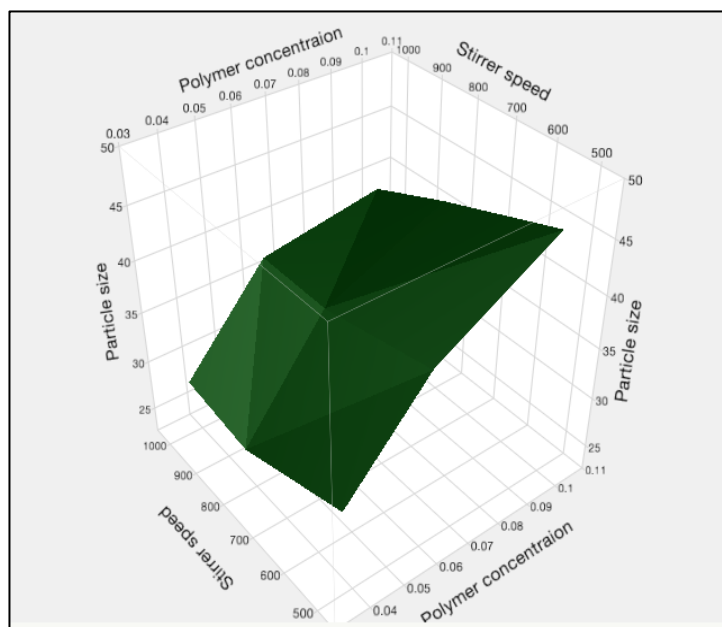


**Figure 3.10.c:** 3- D response surface plots showing the effect of polymer concentration and stirrer speed on particle size.

### 3.2.5.3. Validation of method

The optimisation design was intended to minimise particle size and the optimal conditions were found to be 0.0375% of polymer concentration, 0.5% PVA concentration and 1000 rpm and surface morphology was observed under SEM (**Figure 3.11.a&b**).

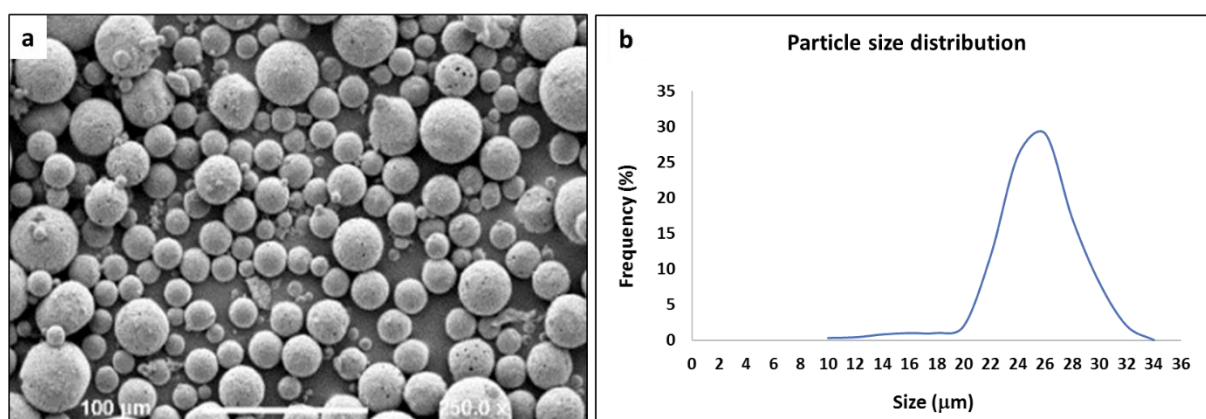


**Figure 3.11:** a) SEM images of microspheres prepared using 0.0375% of polymer concentration, 0.5% PVA concentration and 1000 rpm b) Particle size distribution curve.

The predicted results were compared with experimental results and error was calculated. The predicted result gave a particle diameter of 26.3  $\mu\text{m}$ , and the experimental result was  $25.2 \pm 1.12 \mu\text{m}$ , hence the error was 4.41% (**Figure 3.11 & b**).

### **3.2.6. P(3HB) microsphere characterization**

**Note: In the following sections, experiment number 12 and 15 are omitted as they correspond to the same data as experiment number 3 (This is because the design considered triplicates of the mid- level parameters and experiments corresponding to numbers 3, 12 and 15 are carried out under the same parameters).**

#### **3.2.6.1. Porosity**

Porosity of the microspheres prepared was calculated using the liquid displacement method. The microspheres were found to have porosity within the range of 48-60%. Porosity was observed to increase with stirrer speed. P(3HB) microspheres, prepared with a low concentration of polymer and high stirrer speed were found to be the most porous, corresponding to experiment number 4. These were prepared with 0.0375 g/mL polymer concentration at 1000 rpm. However, increasing the polymer concentration appeared to have a deleterious effect on porosity as in the second experiment prepared with 0.1 polymer at a stirrer speed of 1000 rpm was found to have a porosity of  $49 \pm 4.1\%$  compared to the porosity corresponding to experiment number 4, which was  $62 \pm 1.5\%$ . PVA concentration was not found to have a significant effect on porosity. Between experiment number 2 and 8, both polymer concentration and PVA concentration was kept constant, but stirrer speed was decreased from 500 to 100 rpm, which was found to decrease porosity of the respective microspheres from 49 to 43%. The effect of polymer concentration and stirrer speed were analysed separately, keeping the other 2 variables

constant, and it was found that stirrer speed has a positive influence and polymer concentration has a negative influence on porosity and the differences were statistically significant (Figure 3.12.a, b and c).

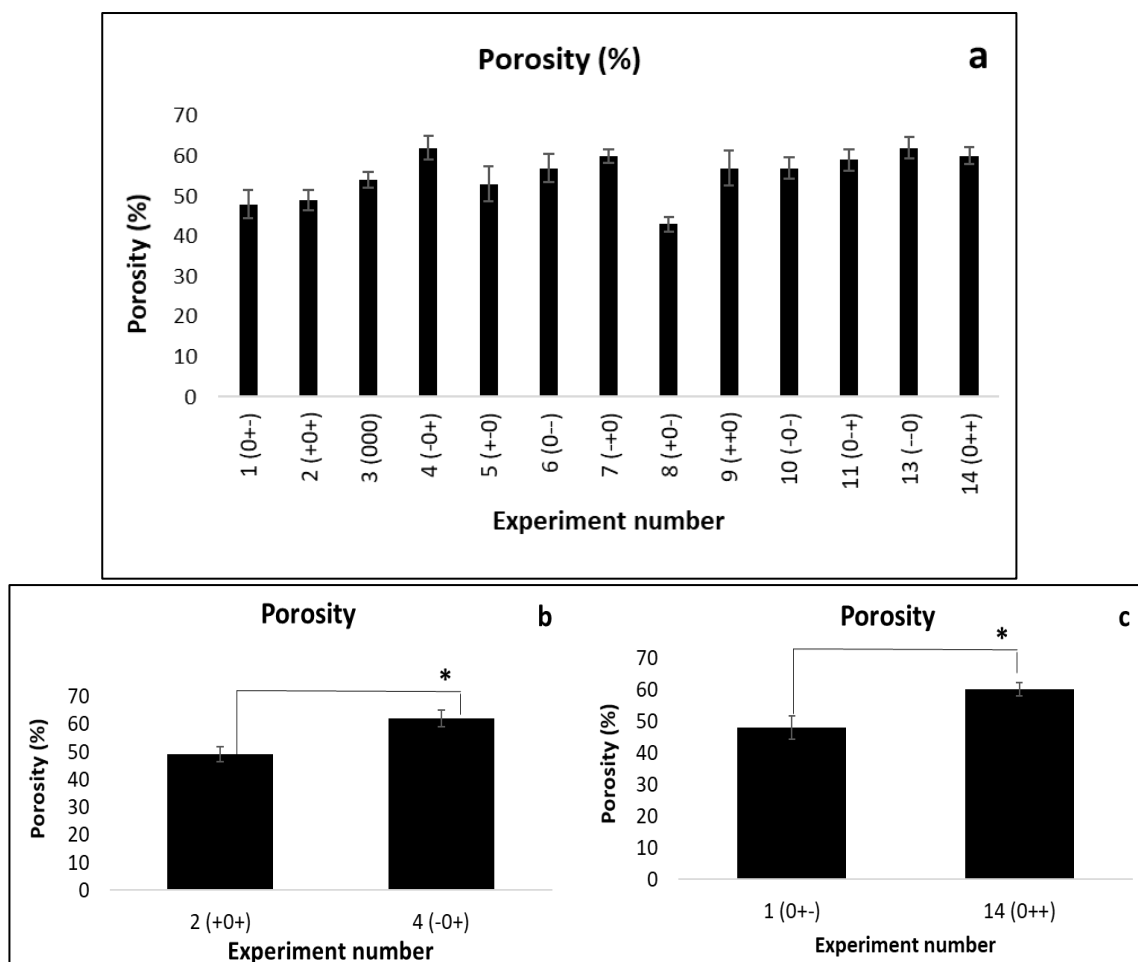


**Figure 3.12:** a) Porosity of microspheres corresponding to experiment number 1-11 and 13 and 14 b) Comparison of effect of stirrer speed on porosity c) Comparison of effect of polymer concentration on porosity [code (polymer concentration: PVA concentration: Stirrer speed); For polymer concentration, -= 0.0375, 0= 0.0625 and += 0.1 g/mL; PVA concentration, -= 0.5, 0= 0.8 and += 1 % w/v and stirrer speed, -= 500, 0= 800 and += 1000 rpm]. (n=3, error bars=  $\pm$ SD)

### 3.2.6.2. Surface residual PVA

Surface residual PVA of the microspheres prepared was measured by the method described in section 2.2.8.4. Residual PVA was expressed as a percentage of mass of PVA per mass of

microspheres. There was a clear correlation between the concentration of PVA used in the preparation and the amount of residual PVA on the surface of microspheres (**Figure 3.13**).

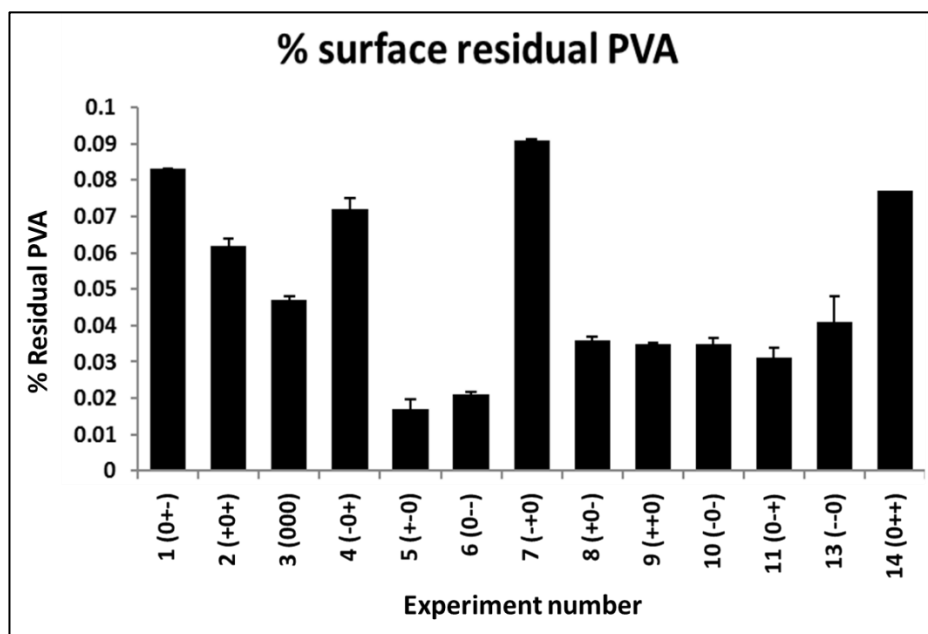


**Figure 3.13:** Surface residual PVA of microspheres corresponding to experiment numbers 1-13 and 14 [code (polymer concentration: PVA concentration: Stirrer speed); For polymer concentration, -= 0.0375, 0= 0.0625 and += 0.1 g/mL; PVA concentration, -= 0.5, 0= 0.8 and += 1 % w/v and stirrer speed, -= 500, 0= 800 and += 1000 rpm]. (n=3, error bars=  $\pm$ SD)

The highest amount of surface associated PVA was 0.091% w/w, corresponding to microspheres prepared under process conditions as in experiment number 7. Here, 0.0375g/mL polymer concentration and 1% PVA concentration was used at a stirrer speed of 800 rpm. The second highest amount of residual PVA ( $0.083 \pm 0.002$  % w/w) corresponded to microspheres prepared with process conditions under experiment number 1, with 0.0625 g/mL of polymer, 1% PVA concentration and 500 rpm stirrer speed. This was followed by a residual PVA of  $0.077 \pm 0.0012$  % w/w, in the case of microspheres prepared as per conditions corresponding to experiment number 14, with 0.0625 g/mL polymer concentration, 1% PVA concentration and 800 rpm stirrer speed. It follows that

the highest amounts of residual PVA calculated corresponded to microspheres prepared with process conditions as per 7, 1, 14, 4 and 9. These are the 4 experiments in the design, which were conducted with the maximum PVA concentration. On the other hand, the least amount of residual PVA was found associated with microspheres corresponding to experiment number 5 ( $0.017 \pm 0.0027$  % w/w), 6 ( $0.021 \pm 0.0007$  % w/w), 11 ( $0.031 \pm 0.0029$  % w/w) and (13  $0.041 \pm 0.0071$  % w/w) respectively, all of which were prepared with the minimum concentration of PVA.

#### **3.2.4.1. Hydrophobicity and correlation between residual PVA and hydrophobicity**

Surface hydrophobicity was estimated as a function of the amount of Rose Bengal dye adsorbed on the surface of microspheres. The amount of Rose Bengal dye bound is directly proportional to the hydrophobicity of the microspheres (**Figure 3.14**). It was found that there is an inverse proportionality between the amount of surface residual PVA and hydrophobicity of microspheres. The least amount of surface associated PVA corresponded to experiment number 5, and 6 and 11 and in the case of hydrophobicity, these had the highest amount of surface bound Rose Bengal dye ( $0.91 \pm 0.001$  and  $0.72 \pm 0.01$   $\mu\text{g}/\text{mg}$  respectively). The least amount of surface bound Rose Bengal dye corresponded to experiment number 7 and 1, ( $0.13 \pm 0.21$  and  $0.20 \pm 0.02$   $\mu\text{g}/\text{mg}$  respectively) both of which had belonged to the group of microspheres with highest amount of surface residual PVA.

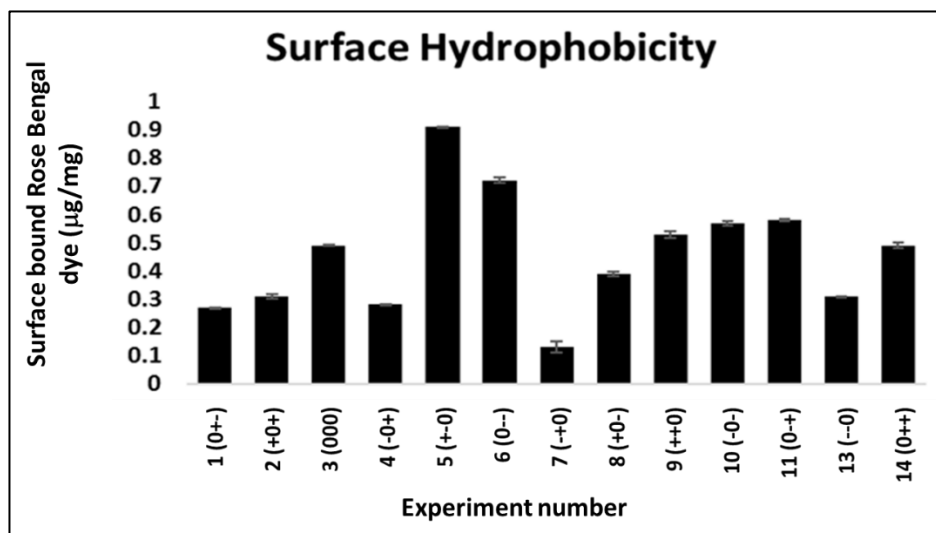


**Figure 3.14:** Surface hydrophobicity microspheres corresponding to experiment number 1-3 & 14, represented as a function of amount of surface bound Rose Bengal dye at saturation [code (polymer concentration: PVA concentration: Stirrer speed); For polymer concentration, -= 0.0375, 0= 0.0625 and += 0.1 g/mL; PVA concentration, -= 0.5, 0= 0.8 and += 1 % w/v and stirrer speed, -= 500, 0= 800 and += 1000 rpm] (n=3, error bars= SD).

### 3.2.7. Optimisation of production parameters for microspheres and nanospheres of varying size ranges.

The model generated demonstrated that to lower particle size, the main parameter to vary was the concentration of P(3HB). The model generated was tested for a range of microsphere sizes from 20 µm to 100 µm and was proven to be fitting. Although the model had very good predictability, the model was impractical to implement for lower working concentration since the resulting yield of microspheres would be too low. Therefore, a series of other process parameters were tested, mainly focusing to reduce the viscosity of the emulsion and thereby to reduce the size of the microspheres, even to nanoscale ranges. Varying P(3HB) concentrations, PVA concentrations, stirrer speed as well as homogenisation techniques were employed (Table 3.6).

Experiment number	P(3HB) concentration (g/mL)	PVA concentration (%)	Fabrication method	Drying
1	0.0065	0.05	Magnetic stirring at 800 rpm	Freeze drying
2	0.0065	0.25	Magnetic stirring at 1000 rpm	Freeze drying
3	0.0065	0.25	Homogenization for 5 minutes, followed by	Freeze drying with 1 mL of 0.5% trehalose dihydrate
4	0.009	0.05	Magnetic stirring at 800 rpm	Freeze drying
5	0.009	0.25	Magnetic stirring at 1000 rpm	Freeze drying
6	0.009	0.25	Homogenization for 5 minutes, followed by	Freeze drying with 1 mL of 0.5% trehalose dihydrate
7	0.015	0.25	Magnetic stirring at 1000 rpm	Freeze drying
8	0.015	0.5	Magnetic stirring at 1000 rpm	Freeze drying
9	0.03	0.25	Magnetic stirring at 1000 rpm	Freeze drying
10	0.035	0.5	Magnetic stirring at 800 rpm	Freeze drying

**Table 3.6:** Conditions for the optimization of micro and nanospheres of varying size ranges

### 3.2.7.1. Surface morphology of nanospheres and microspheres under SEM

Nanospheres and microspheres of P(3HB) were successfully produced in 4 different size ranges. Surface morphology of these were observed under SEM at different magnifications.

The spheres produced appeared to be of good spherical shape in general, except for the

intermittent disc shaped structures amongst the nanospheres. The process conditions corresponding to experiment number 1-3 involved a very low polymer concentration of 0.001 g/mL and the spheres produced with these were of the size range 400-800 nm. Experiment number 1 was set up with a polymer concentration of 0.0065 g/mL, PVA concentration of 0.05 %w/v at 1000 rpm. The spheres produced were highly interconnected and completely lacked the spherical shape. In the second experiment, the same conditions with respect to polymer concentration and stirrer speed were maintained, but PVA concentration was increased to 0.25 %w/v. This was found to decrease the appearance of interconnecting water channels; however, they were not entirely absent, and the spheres lacked sphericity. The SEM images of spheres produced using process parameters corresponding to experiment number 1 and 2 are given in **Figure 3.15 a & b**. In the third experiment, the emulsion was first subjected to homogenisation for 5 minutes before being subjected to magnetic stirring and the resulting spheres were lyophilised in the presence of the cryoprotectant trehalose dihydrate. The resultant spheres were of appreciable sphericity with no interconnecting water channels (**Figure 3.18.a**).

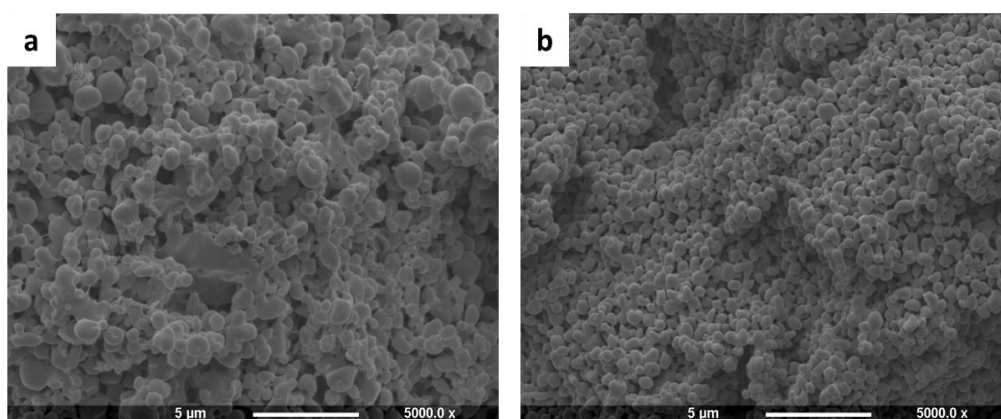


**Figure 3.15:** SEM images of nanospheres prepared under process conditions corresponding to **a)** experiment number 1, **b)** experiment number 2

Experiment number 4 -6 involved the use of 0.009 g/mL polymer concentration. Spheres produced under conditions corresponding to experiment number 4 (PVA concentration 0.05 %w/v, stirrer speed 800 rpm) produced microspheres within the range of 1-2  $\mu\text{m}$ , with intermittent spheres of about 5  $\mu\text{m}$  in diameter (**Figure 3.16.a**). The spheres lacked in sphericity and had interconnecting water channels although not as extensive as in the case of spheres produced using conditions under experiment number 1. In experiment number 5, PVA concentration was increased to 0.25% and stirrer speed of 1000 rpm applied. This was found to be effective in achieving uniformity of size distribution and improved sphericity, although not ideal (**Figure 3.16.b**). In experiment number 6, the emulsion was homogenised for 5 minutes and then was subjected to magnetic stirring at 800 rpm and lyophilised with the presence of the cryoprotectant. This experiment produced microspheres in the size range of 1-2  $\mu\text{m}$ , with good sphericity, even size distribution and appreciable separation (**Figure 3.8.b**).

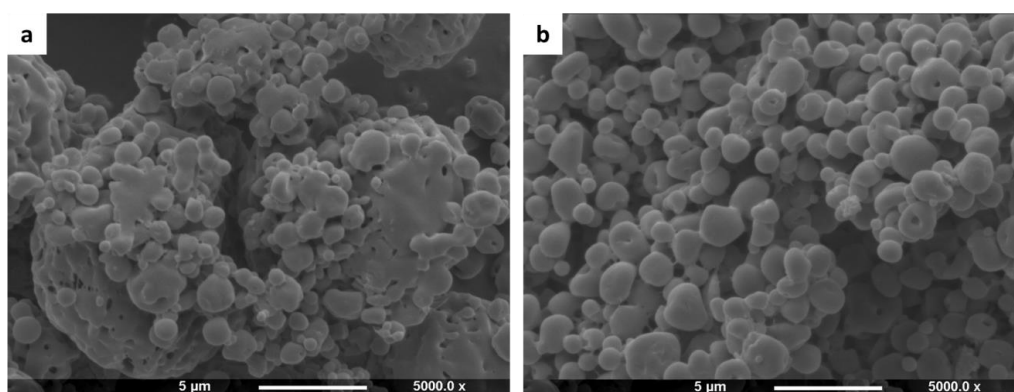


**Figure 3.16:** SEM images of microspheres produced using process parameters corresponding to **a)** experiment number 4, **b)** experiment number 5.

Experiment number 7 and 8 were carried out using 0.015 g/mL concentration of polymer solution at 1000 rpm, with 0.25 and 0.5 % PVA solution respectively. The microspheres

produced with 0.25% of PVA had a shrunken appearance and lacked in sphericity (**Figure 3.17 a**). However, the microspheres produced with 0.5% PVA solution were of excellent sphericity and smoothness, in a size range of 4-10  $\mu\text{m}$  in diameter (**Figure 3.18.c**). No interconnecting water channels were observed in both the cases.

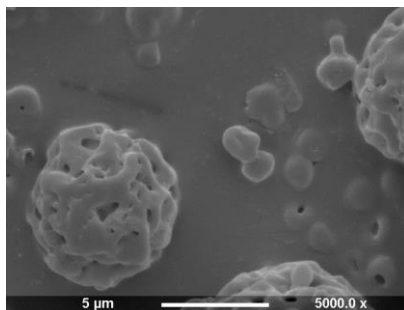


**Figure 3.17.a:** SEM image of microspheres prepared under process conditions corresponding to experiment number 7.

Finally, experiment number 9 and 10 involved the use of 0.03 and 0.0035 g/mL concentration of polymer solution at 1000 rpm with 0.25% and 0.5% PVA solutions respectively. The results obtained were similar to the case of experiment number 7 and 8, with extremely shrunken and uneven surface morphology of microspheres in the case of lower concentration of PVA (**Figure 3.17.b**).

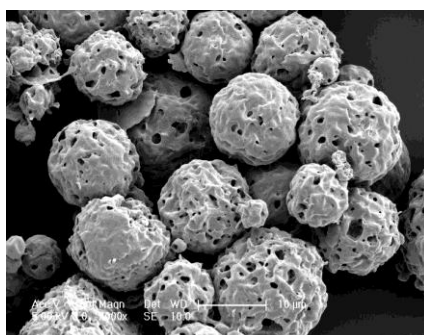


**Figure 3.17.b:** SEM image of microspheres corresponding to experiment number 9 (magnification X2000).

In experiment number 10, sphericity had improved considerably, but the surface of the spheres appeared to be comparatively porous and coarse (**Figure 3.18.d**).

Process conditions corresponding to experiment number 3 resulted in the successful nanospheres in the size range of 400-800 nm, and process conditions corresponding to experiment number 6, 8 and 10 resulted in the successful production of microspheres in the size range of 1-2  $\mu\text{m}$ , 4-10  $\mu\text{m}$  and 15-25  $\mu\text{m}$  respectively. The SEM images of these microspheres under X2000 magnification are given in **Figure 3.18**.

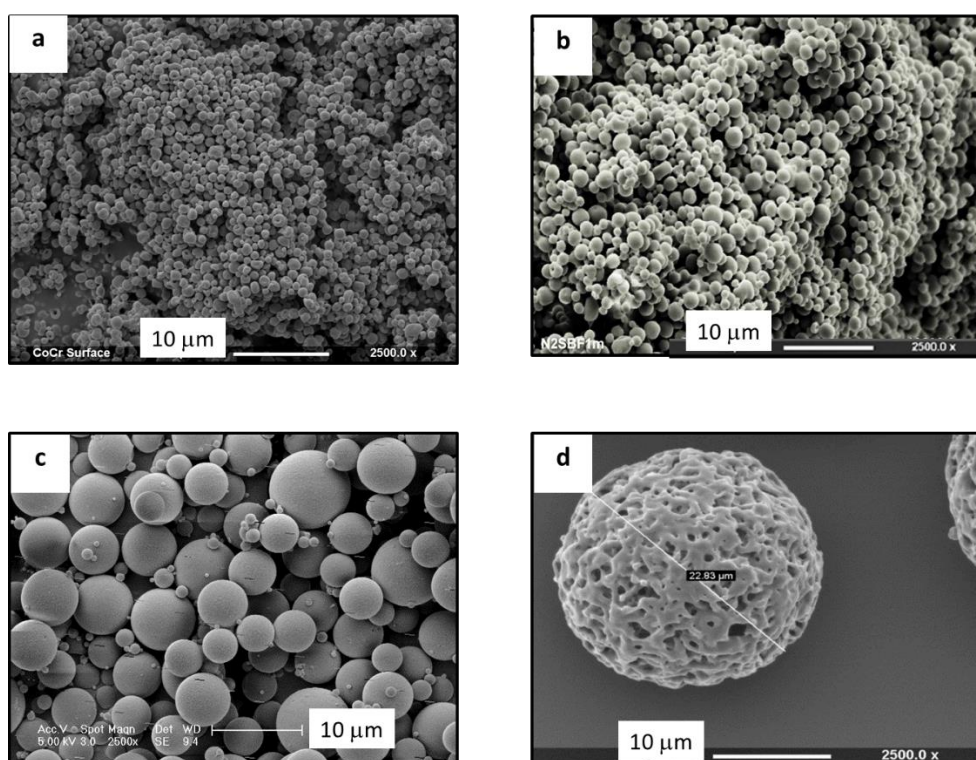


**Figure.3.18:** SEM images of a) Nanospheres prepared under conditions corresponding to experiment 3, microspheres prepared under conditions corresponding to experiment number b)6, c)8, and d)10

## Part II: Optimisation of nanospheres production from P(3HB) extracted using *B. subtilis* OK2.

### 3.2.8. P(3HB) production using *B. subtilis* OK2

Figure 3.19 represents the temporal growth profile obtained from the culture of *B. subtilis* OK2 for P(3HB) production, in a 5 L Bioreactor using Kannan and Rehacek (KR) nitrogen-limiting media with 30g/L glucose as the carbon source. This was carried out to analyse the pattern of biomass and P(3HB) accumulation in order to establish a production strategy and ensure a reasonable yield. This pattern was found to correlate with changes in optical density, pH and estimated glucose consumption. The initial lag phase was not visible, possibly suggesting it might have been either less than 3 hours or missing. OD600 increased sharply until the 32nd hour, clearly indicating a prolonged log phase of growth. Beyond this O.D started declining with no clear indication of a stationary phase.

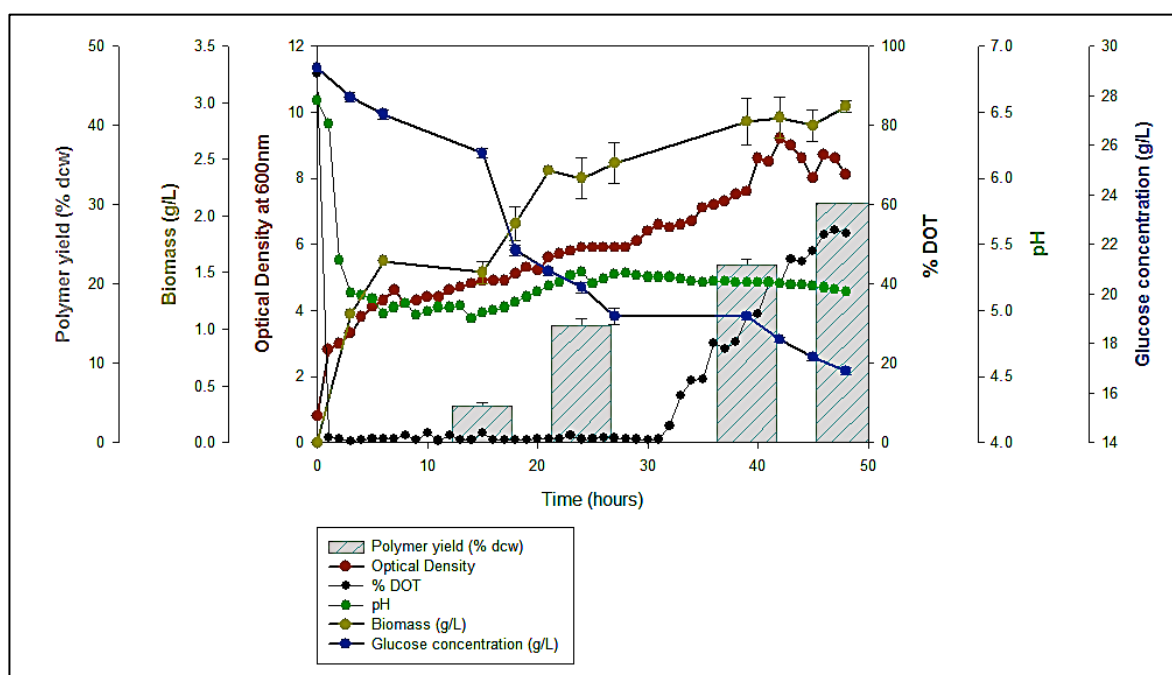


**Figure 3.19:** Temporal growth profile of *B. subtilis* OK2 for the production of P(3HB) in 5L bioreactors

As expected, there is a direct correlation observed between OD<sub>600</sub> and biomass. Biomass was found to increase throughout the profile, peaking at 48 hours with a maximum biomass accumulation of 3.2 g/L. The pH decreased throughout the experiment and dropped from 6.6 to 5.1 by the end of 48 hours. Dissolved Oxygen Tension (DOT) was observed to decrease rapidly until 9<sup>th</sup> hour when it reached a minimum and a steady rise was observed between 48 and 72 hours. The decrease in DOT overlapped with the log phase, confirming oxygen consumption during microbial growth. P(3HB) accumulation demonstrated a positive correlation with time. After 48 hours, a P(3HB) yield of 26.3% dry cell weight was observed. Slow glucose depletion was experienced as the glucose concentration dropped from the initial 30g/L to 16 g/L at the end of 48 hours. Polymer yield over the period of 48 hours was found to be steady, with a maximum of 30.2 % dcw.

### **3.2.9. Characterisation of the polymer**

The P(3HB) thus produced was extracted using the soxhlet method with methanol and chloroform and was purified using the differential precipitation.

#### **3.2.9.1. FTIR analysis of P(3HB) produced using *B. subtilis* OK2**

Preliminary confirmation of the structure of the polymer produced was obtained using FTIR. The FTIR spectrum showed two distinct peaks at wavenumber of 1719.69 cm<sup>-1</sup> and 1276 cm<sup>-1</sup>, corresponding to the ester carbonyl group and the-CH group, respectively which is characteristic of SCL PHA (3.20).

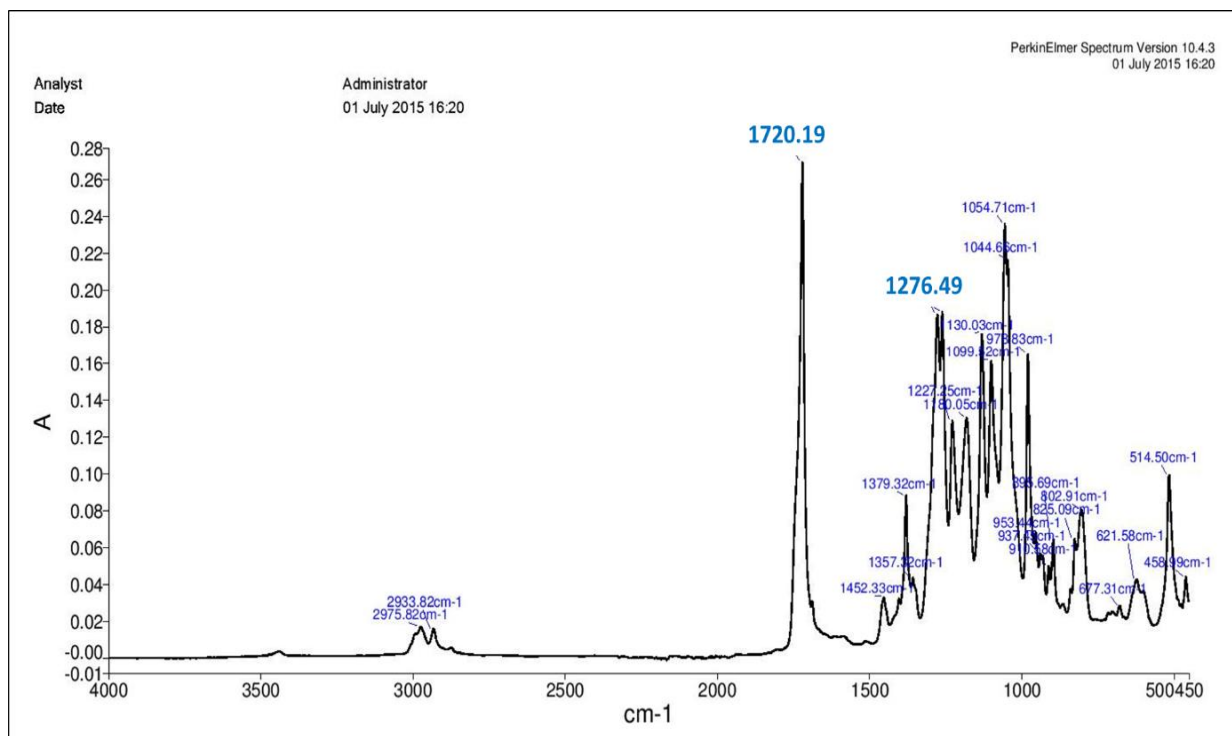


**Figure 3.20:** FTIR analysis spectrum of P(3HB) produced from *B. subtilis* OK2

### 3.2.9.2. Nuclear Magnetic Resonance

The proton NMR showed peaks corresponding to 3 different hydrogen environments (**Figure 3.21a**). These were observed as a duplet at 1.26 ppm, a multiplet around 2.5 ppm and a sextet around 5.2 ppm.  $^{13}\text{C}$  NMR shows four different peaks corresponding to four separate carbon environments (Figure 4b). The chemical shifts respectively are at 169 ppm corresponding to  $\text{C}_3$  (C=O group), 68 ppm corresponding to  $\text{C}_1$  (-CH group), 41 ppm corresponding to  $\text{C}_2$  (- $\text{CH}_2$ ) and the 19 ppm corresponding to  $\text{C}_4$ , which is the part of the - $\text{CH}_3$  group (**Figure 3.21.b**).

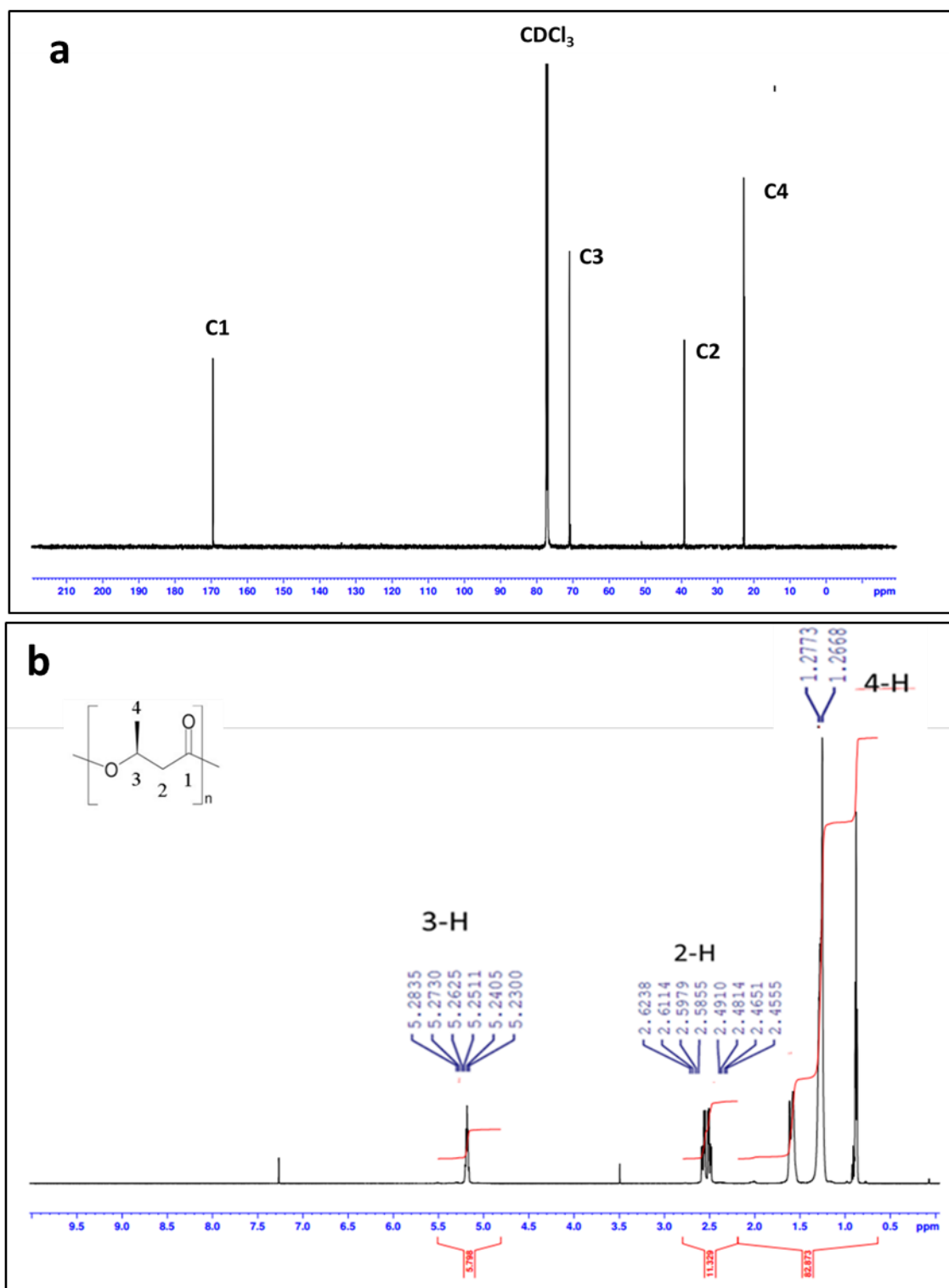


Figure 3.21: a) Proton NMR and b) <sup>13</sup>C NMR of P(3HB) produced using *B. subtilis* OK2

### 3.2.9.3. Molecular weight analysis

The polymer produced and purified was subjected to molecular weight analysis using gas permeation chromatography (GPC). The molecular weight of the polymer was found to be 868kDa with a polydispersity Index of 3.674.

### 3.2.10. Optimisation of nanospheres production using P(3HB) extracted from *B. subtilis* OK2

The process conditions for nanosphere fabrication were optimised as shown in **Table 3.7**.

Experiment number	P(3HB) concentration (mg/mL)	PVA concentration (%)	Fabrication method	Drying
1	1	0.25	Homogenization for 5 minutes, followed by Magnetic stirring at 1000 rpm	Freeze drying with mL of 0.5% Trehalose dihydrate
2	1	0.25	Homogenization for 5 minutes, followed by Magnetic stirring at 1000 rpm	Freeze drying with mL of 0.1% Trehalose dihydrate
3	1	0.3	Homogenization for 5 minutes, followed by Magnetic stirring at 1000 rpm	Freeze drying with mL of 0.5% Trehalose dihydrate
4	1	0.3	Homogenization for 5 minutes, followed by Magnetic stirring at 1000 rpm	Freeze drying with 1 mL of 1% Trehalose dihydrate
5	0.75	0.3	Homogenization for 10 minutes, followed by Magnetic stirring at 1000 rpm	Freeze drying with mL of 1% Trehalose dihydrate
6	0.75	0.35	Homogenization for 10 minutes, followed by magnetic stirring at 800 rpm	Freeze drying with mL of 1% Trehalose dihydrate
7	0.5	0.35	Homogenization for 10 minutes, followed by magnetic stirring at 800 rpm	Freeze drying with mL of 1% Trehalose dihydrate

**Table 3.7:** Process conditions for the preparation of nanospheres using P(3HB) extracted from *B. subtilis* OK2.

This is because, P(3HB) from *B. subtilis* OK2 being of higher molecular weight was assumed to result in nanospheres of increased size distribution. Hence, the conditions optimised from nanospheres production of P(3HB) extracted from *B. cereus* SPV were employed here for the purpose of comparison. However, the resulting nanospheres were of much larger size range.

### 3.2.10.1. Observation of surface morphology under SEM

Condition 1 was carried out with a polymer concentration was 1mg/mL, with a PVA concentration of 0.25% and a stirrer speed of 1000 rpm, following a five minutes' homogenization. The spheres thus produced were lyophilised using 0.5% of trehalose dihydrate as a cryoprotectant. These samples were subjected to TEM to observe the nature and sphericity of spheres that might have formed between these water channels and they appeared to be roughly of 300nm and of good sphericity (**Figure 3.22**)

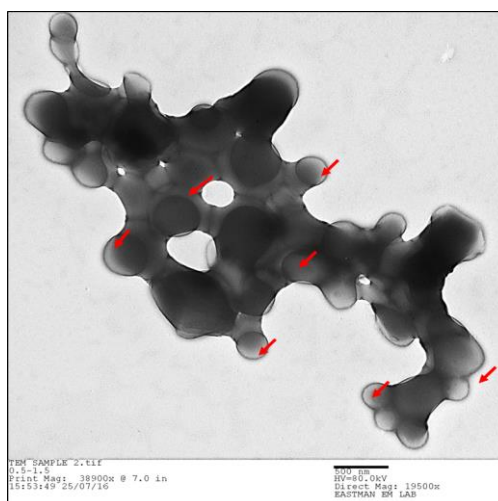


**Figure 3.22:** TEM images of nanospheres prepared under process conditions corresponding to Experiment number 1. The arrows point towards spheres trapped between interconnecting water channels (Size bar= 500nm).

The size range of nanospheres produced was observed to have been reduced, however, they were not well separated and appeared agglomerated, forming a mesh of interconnected channels.

In condition 2, the polymer concentration was kept at 1mg/mL and increased amount of cryopreservants were added. Although the water channels were found to have disappeared. However, the sphericity of the nanospheres formed were compromised and to circumvent this, PVA concentration was increased as in condition 3, and this however, resulted in the formation of water channels once again. In condition 4, the same condition was repeated, this time increasing the concentration of cryoprotectant to 1%, which resulted in better separation of the spheres (**Figure 3.23**).

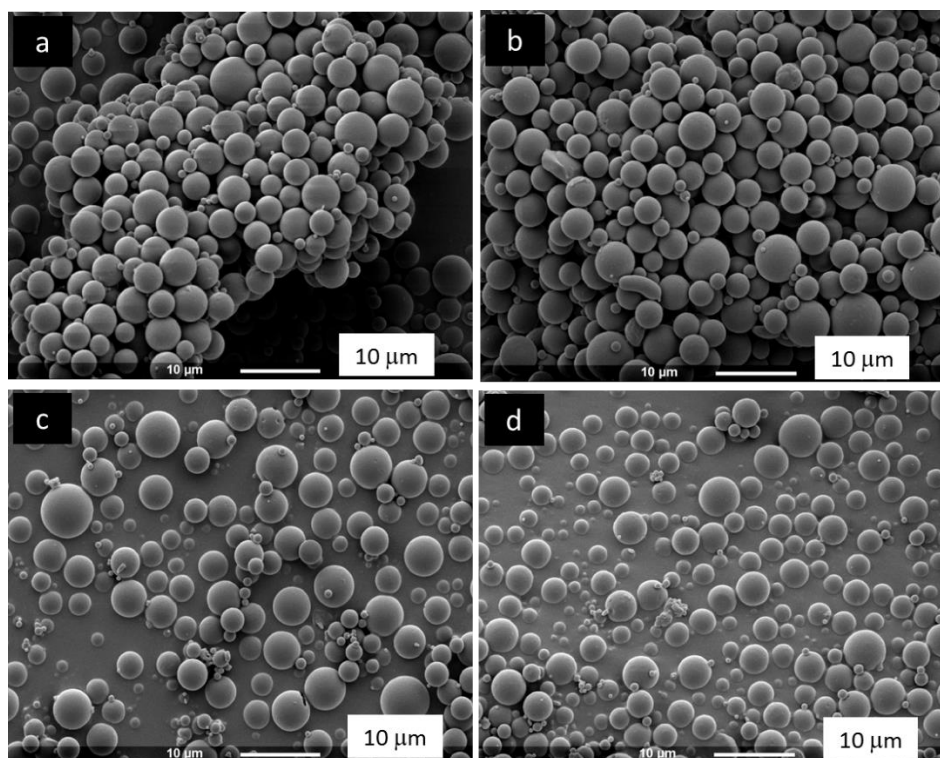


**Figure 3.23:** SEM images of spheres prepared using process conditions corresponding to experiment number a)1, b) 2, c)3 and d)4.

Following these results, further attempts were made to reduce particle size, by altering the polymer concentration and increasing the time of homogenisation. Experiment number 5 was prepared with 0.5 mg/mL polymer concentration, 0.3% PVA concentration, homogenization of the emulsion for 10 minutes followed by magnetic stirring at 1000 rpm and then lyophilisation with 1% cryoprotectant. However, although the spheres were well separated, the spheres formed had a shrunken morphology and were of the size range ~500-800 nm (**Figure 3.24.a**). In experiment number 6, polymer concentration was reduced to 0.75 mg/mL and PVA concentration was increased to 0.3%. The nanospheres formed was of a smaller size range and had better sphericity (**Figure 3.24.b**). Finally, in experiment number 7, polymer concentration was further reduced to 0.5 mg/mL and the resulting nanospheres had a size range of 100-200 nm with appreciable sphericity (**Figure 3.24.c**).

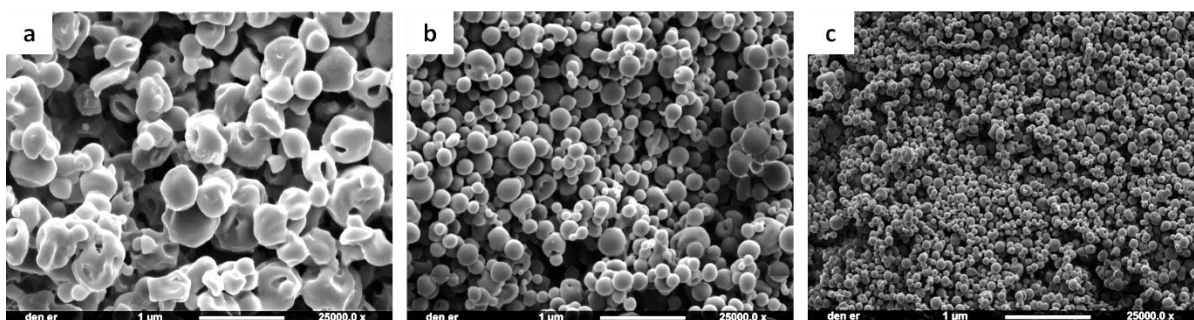


**Figure 3.24:** SEM images of nanospheres prepared under process conditions corresponding to experiment number a)5, b)6, and c)7.

### **Part III: Comparison of nanospheres and microspheres prepared using**

#### **P(3HB) extracted from *B. cereus* SPV and *B. subtilis* OK2**

*Note: These experiments were carried at different stages of optimisation, during encapsulation of various drug molecules mentioned in following chapters. Therefore, they are not fabricated using the same parameters.*

### 3.2.11. Characterisation

The microspheres and nanospheres produced using P(3HB) extracted from *B. cereus* SPV and *B. subtilis* OK2 were compared with respect to their particle size, porosity, surface residual PVA, hydrophobicity, protein adsorption and degradation profile. For ease of understanding, the samples used in this comparison study are coded, as given in **Table 3.8**.

Sample	P(3HB) concentration (mg/mL) and origin	PVA concentration (%)	Fabrication method	Drying
A	0.5, from <i>B. subtilis</i> OK2	0.35	Homogenization for 10 minutes, followed by magnetic stirring at 800 rpm	Freeze drying with 1mL of 1% trehalose dihydrate
B	6.5, from <i>B. cereus</i> SPV	0.25	Homogenization for 5 minutes, followed by Magnetic stirring at 1000 rpm	Freeze drying with 1mL of 0.5% trehalose dihydrate
C	9, from <i>B. cereus</i> SPV	0.25	Homogenization for 5 minutes, followed by magnetic stirring at 800 rpm	Freeze drying with 1mL of 0.5% trehalose dihydrate
D	15, from <i>B. cereus</i> SPV	0.5	Magnetic stirring at 1000 rpm	Freeze drying
E	35, from <i>B. cereus</i> SPV	0.5	Magnetic stirring at 800 rpm	Freeze drying

**Table 3.8:** Coding for microspheres used in comparative study and their corresponding fabrication methods

#### 3.2.11.1. Particle size distribution

Particle size of both nanospheres and microspheres were found to depend primarily on the viscosity of the oil phase, either as an effect of concentration or molecular weight. The nanospheres prepared with 2.5 mg/mL of polymer concentration using P(3HB) from

*B. subtilis* OK2 were found to be of the smallest size range, of 50-200 nm. It was observed that increasing polymer concentration of P(3HB) extracted from *B. cereus* SPV corresponded to an increase in particle size, from a mean particle size of  $728 \pm 32.96$  nm to  $22.83 \pm 1.21$   $\mu\text{m}$ . **Figure 3.25** represents particle size distribution of the nanospheres and microspheres A- E and **Table 3.9** represents the mean particles size of the same.

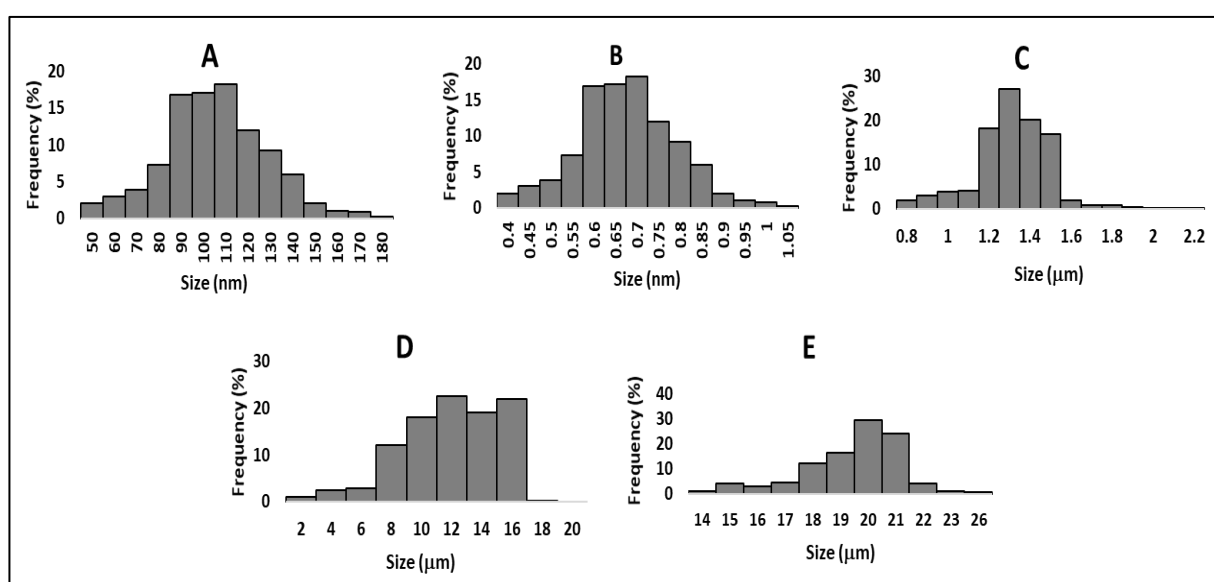


**Figure 3.25:** Size distribution charts of nanospheres and microspheres prepared from A) *B. subtilis* OK2 B-E) *B. cereus* SPV, corresponding to conditions in table 3.8

Sample code	Mean particle size
A	$118 \pm 12.3$ nm
B	$728 \pm 32.96$ nm
C	$1.6 \pm 0.13$ $\mu\text{m}$
D	$9.8 \pm 2.18$ $\mu\text{m}$
E	$22.83 \pm 1.21$ $\mu\text{m}$

**Table 3.9:** Table representing the mean particle size of nanospheres prepared using P(3HB) extracted from *B. subtilis* OK2 and nanospheres and microspheres prepared using polymer extracted from *B. cereus* SPV, corresponding to conditions in table 3.8.

### 3.2.11.2. Porosity

Porosity of the nanospheres and microspheres prepared using P(3HB) of two different molecular weights were estimated using the liquid displacement method. Of the 5 samples compared, nanospheres corresponding to sample code A was found to be the most porous with a porosity of  $81.32 \pm 1.98\%$ . Porosity was influenced by polymer concentration and stirrer speed. Lower polymer concentration and higher stirrer speed contributed to increased porosity. Sample B with a polymer concentration of 1 mg/mL prepared at 1000 rpm had a porosity of  $77.908 \pm 2.93\%$ , while sample C prepared with 2 mg/L polymer concentration at 800 rpm had a porosity of  $73.183 \pm 1.89\%$ . Sample D prepared with 5 mg/L polymer concentration at 1000 rpm was found to have a porosity of  $71.093 \pm 4.18\%$  and sample E prepared with 35 mg/L polymer concentration at 800 rpm had a porosity of  $68.243 \pm 3.93\%$  (Figure 3.26).

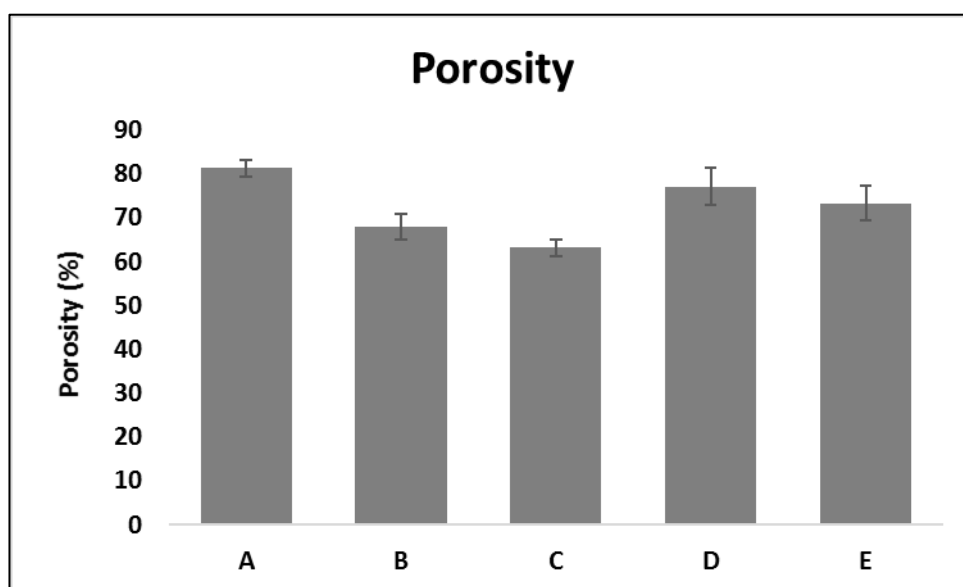


**Figure 3.26:** Porosity of nanospheres prepared using P(3HB) extracted from *B. subtilis* OK2 and nanospheres and microspheres prepared using *B. cereus* SPV, corresponding to conditions in table 3.8

### 3.2.11.3. Surface residual PVA

Surface residual PVA is expressed as the percentage of the mass of PVA on unit mass of microspheres. Surface residual PVA was found to vary, primarily as a function of the concentration of PVA used during the fabrication process. The highest amount of surface associated PVA was found on sample D and E, prepared with 0.5% PVA. This was followed by sample A, prepared with 0.35% PVA. Between sample B and C, both of which were prepared with 0.25% of PVA, sample B had a higher amount of surface residual PVA (Figure 3.27).

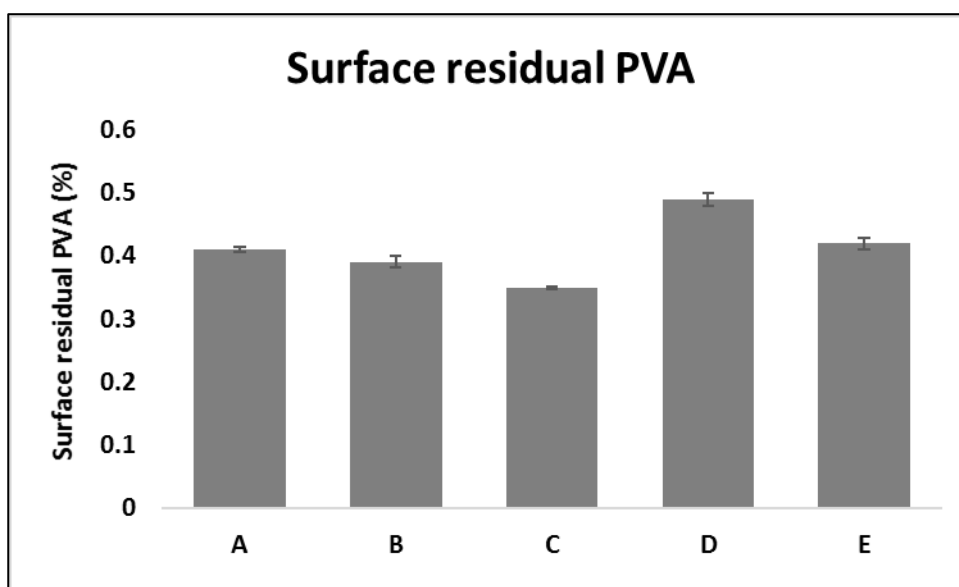


**Figure 3.27:** Representation of percentage residual PVA on nanospheres prepared using P(3HB) extracted from *B. subtilis* OK2 and nanospheres and microspheres prepared using *B. cereus* SPV, corresponding to conditions in table 3.8

### 3.2.11.4. Hydrophobicity

Hydrophobicity of the nanospheres and microspheres prepared from P(3HB) of 2 different molecular weights were estimated using Rose Bengal assay and was expressed as a function of the amount of Rose Bengal dye bound at saturation. Hydrophobicity was found to have an inverse proportionality with the amount of surface residual PVA. Samples D and E,

prepared with 0.5% PVA, had the least amount of surface bound Rose Bengal dye and amongst these, sample D had a lower amount than sample E. Sample C was found to have the highest amount of surface bound Rose Bengal dye (**Figure 3.28**).

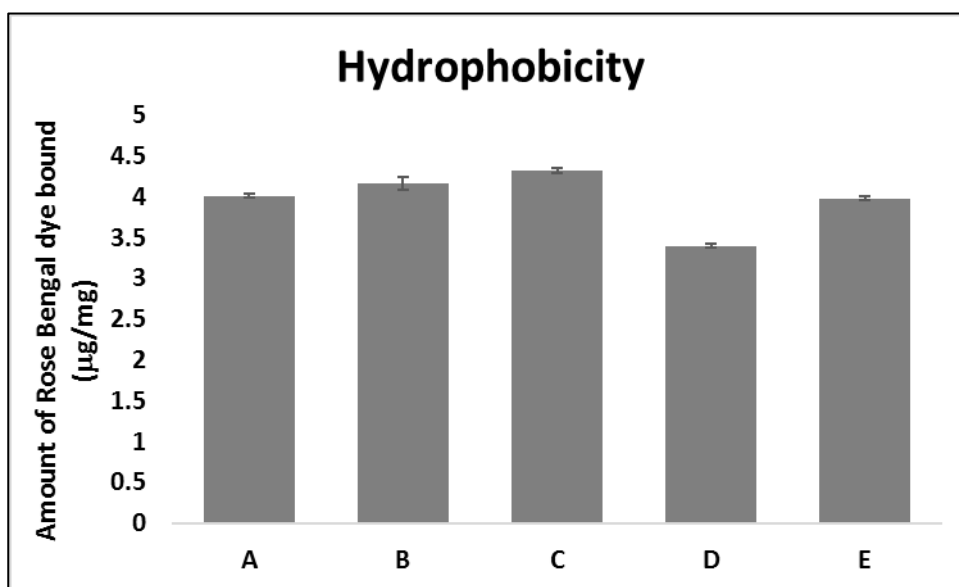


**Figure 3.28:** Comparison of hydrophobicity of nanospheres prepared using P(3HB) extracted from *B. subtilis* OK2 and nanospheres and microspheres prepared using *B. cereus* SPV, corresponding to conditions in table 3.8

### 3.3. Discussion

The use of P(3HB) in the development of various biomedical devices is gaining momentum and the results obtained across the spectrum look promising. The fact that it has great processability, proven by the demonstration of its manipulation using techniques such as spray coating, electrospinning and 3-D printing, combined with its natural origin makes it a suitable candidate for a great variety of biomedical applications. P(3HB) of consistent molecular weight has been achieved to be produced, ensuring reproducibility of results, in the fabrication of biomedical structures. In this study, optimisation of the preparation of P(3HB) microspheres using polymer produced using *B. cereus* SPV was achieved. A surface response methodology using Box- Behnken design was followed.

Polymer concentration was established as the most significant variable in controlling particle size and further optimisations based on this parameter to obtain spheres of different size ranges were attempted. These were well characterised and the results of these were compared with spheres synthesised using P(3HB) using *B. subtilis* OK2.

### **3.3.1. Effect of process parameters on particle size and morphology**

An initial set of pilot experiments were used to set suitable boundary conditions and solvent to be used. Based on experiments, a randomized Box-Behnken design was generated and according to this, 15 different experiments were carried out. The optimisation experiments intended to lower the size diameter of particles formed showed that a lower concentration of polymer with intermediate PVA concentration and intermediate stirrer speed (with respect to the boundary limits employed in this study) gave the best results. The rheology of the emulsion varies considerably based on the polymer concentration, interaction between the two phases (chloroform and PVA) of the emulsion and stirring speed (O'Donnell and McGinity 1997, Errico *et al.*, 2009). These, along with the rate of chloroform evaporation have a significant influence on how well the microspheres can be formed.

Polymer concentration has a linear effect on the viscosity of the emulsion and hence, an increased polymer concentration would result in an emulsion that is increasingly viscous and therefore more resistant to shear forces (Chen, Zhain and Schreyer 2013). This means, unless there is an increased source of energy or force to oppose this resistance, it becomes difficult to overcome the viscous forces and larger emulsion droplets would be formed. The process optimisation of microspheres production was carried out by a set of experiments designed using MiniTab express software as described in section 2.2.6.2. Microspheres

corresponding to experiment number 7, 4 and 3 prepared using the lowest concentration of polymer (0.0375g/mL) were found to be the smallest (with diameter of 25.5, 28 and 28.6  $\mu\text{m}$  respectively). Subsequently microspheres corresponding to experiment number 10, 8 and 5 prepared using the highest concentration of polymer (0.1g/mL) were found to be of the largest (with diameter of 46.02, 43.1 and 41.733  $\mu\text{m}$  respectively). However, experiment number 10, although was run with the least polymer concentration, and least stirrer speed, was of an average diameter of 32  $\mu\text{m}$ . This is probably due to the fact that the stirrer speed in this case was 500 rpm, and although the viscosity of the emulsion was lowered due to low polymer concentration, the stirrer speed might not have been sufficient to break down the emulsion droplets to a small enough size.

There are several studies corroborating this finding as that of Farhangi, Dadashzadeh and Bolourchian who in their study on the effect of formulation variables in the synthesis of gelatin microspheres observed 1.5-1.8 times increase in diameter of microspheres, when polymer concentration was increased from 25 w/v% to 45 w/v% (Farhangi, Dadashzadeh and Bolourchian, 2017).

This effect was also exemplified when spheres were synthesised using P(3HB) produced from *B. subtilis* OK2. Molecular weight of P(3HB) produced using *B. subtilis* OK2 is around  $\sim 850$  kDa, while that of *B. cereus* SPV is  $\sim 150$  kDa. P(3HB) from *B. subtilis* OK2 being of higher molecular weight resulted in increased viscosity of the oil phase and hence produced nanospheres of increased size distribution. In comparison with nanospheres prepared under the same conditions as that of P(3HB) produced using *B. cereus* SPV, nanospheres prepared using P(3HB) from *B. subtilis* OK2 resulted in nanospheres of much larger size range. However, when the concentration was lowered, this resulted in reduction of particle

size. These spheres appeared to be clumped, with the presence of an intensive network of water channels. The issue of interconnecting water channels was circumvented by the use of the cryoprotectant trehalose dihydrate. Spheres, especially of smaller diameters, tend to aggregate due to many reasons. These may not separate in suspension, eventually resulting in embolization, during intravenous administration. Cryoprotectants coat the nanospheres during freeze drying stage and protect them from mechanical stress of ice crystals. Trehalose dihydrate is a commonly used cryoprotectant due to the following advantages; less hygroscopicity, an absence of internal hydrogen bonds which allows more flexible formation of hydrogen bonds with nanoparticles during freeze-drying and very low chemical reactivity (Abdelwahed *et al.*, 2006).

The P(3HB) microspheres as expected were found to be quite porous in nature ranging between ~40-80% porosity. Lower polymer concentration, lower PVA concentration and increased stirring speed were observed to be contributing factors for porosity. Yang *et al.*, 2001, are of the opinion that during the synthesis of microspheres, after the solvent has evaporated, water droplets collect within the spheres (Yang *et al.*, 2001). Thus, rapid evaporation of the solvent would result in rapid entrapment and coalescing of the water droplets forming uneven pores. This can be contributed by high temperature, increased stirring speed and lower polymer concentration. However, at higher concentration of PVA, the surfactant might occupy the interstitial spaces not allowing for water droplets to collect, thus decreasing porosity (Yang *et al.*, 2001).

PVA, the surfactant used for the emulsion is amphiphilic and binds to the polymer by means of its hydrophobic end. During microsphere formation, when the organic phase is at its highest miscibility with the water phase, the hydrophobic vinyl acetate end of PVA binds

irretrievably with the polymer leaving the hydrophilic end of PVA exposed on the surface of the spheres (Sahoo *et al.*, 2002, Lee *et al.*, 1999). Hence, there is an inverse correlation between percentage surface residual PVA and hydrophobicity of the spheres, which has been exemplified in this study. Rose Bengal dye, which is a hydrophobic dye, binds to hydrophobic surfaces. The amount of Rose Bengal dye bound on the surface of the microspheres were inversely proportional to the % residual PVA on the microspheres. The exposed hydrophilic end renders hydrophilicity to the microspheres, if excess of residual PVA is present on them. This can have a direct impact on uptake of these particles as increased hydrophobicity is desirable for increased uptake. Therefore, it is essential to get rid of the excess PVA and this was achieved by washing the microspheres with 10% ethanol. The resulting % residual PVA was estimated and correlated with the hydrophobicity, which was expressed as a function of the hydrophobic Rose Bengal dye bound on the surface at a maximum concentration (50 µg/mL).

Percentage surface residual PVA exhibited a positive correlation with the PVA concentration employed in each experimental condition. Where a higher concentration of PVA was used, a higher residual PVA concentration was observed. This was also in accordance with the previous argument of increased PVA concentration resulting in decreased porosity.

The significance of surface residual PVA is a key factor in determining one of the very important features of a drug delivery system, hydrophobicity. Hydrophobicity is a desired feature for cancer drug delivery systems as tumour tissues have increased affinity for hydrophobic substances, due to the presence of increased LDL receptors than the normal tissues. Hydrophobic drug delivery systems entering the blood stream primarily attach

themselves to serum lipoproteins such as LDL and HDL. Due to the abundance of LDL receptors on tumour tissues, uptake of hydrophobic delivery systems becomes easier (Warren *et al.*, 2009). Oenbrink, Jurgenlimke, and Gabel, 1988 reported a positive correlation between hydrophobicity and tumour uptake of porphyrin derivatives (Oenbrink, Jurgenlimke, and Gabel, 1988).

The residual PVA content reported in these experiments are much lower than the ones reported in literature. Zielhuis *et al.*, 2005, reported residual PVA concentration of the order of 0.2-0.3% on PLGA microspheres and Francis *et al.*, 2011 reported PVA concentration of the order of 0.1-0.6% on P(3HB) microspheres (Zielhuis *et al.*, 2005, Francis *et al.*, 2011). The reason for lowered amount of residual PVA in this work could be the additional ethanol wash step involved that helped in removing PVA.

# **Chapter 4**

## **Production optimization and characterization of cardiovascular drug encapsulated microspheres**

## 4.1. Introduction

Cardiovascular diseases (CVD) are listed as the number one cause of mortality worldwide, as listed by World Health Organization (WHO). CVDs are characterised by occlusion or narrowing of blood flow to any part of the body and is primarily caused by atherosclerosis. Atherosclerosis is the condition where arterial walls thicken because of plaque accumulation comprising of calcium, cholesterol, fat and inflammatory components, along the arterial walls, which reduces blood flow (Mitra and Agrawal 2006; Daemen and Serruys 2007; Charpentier *et al.*, 2015). This can result in Angina, which is a discomfort in the chest due to reduced blood supply to the heart, myocardial infarction (MI) where blood supply to the heart is blocked, stroke where the blood supply to parts of brain is stopped and Peripheral Arterial Diseases where blood supply to leg, calves and hip muscles are blocked. Disease management for CVDs commonly involve strategies to increase blood flow to vascular beds and vary depending on the severity of the condition (Deveza, Choi and Yang, 2012). The most progressed stages of CVDs often necessitate the use of vascular stents, which are devices inserted in the lumen of the arteries to keep them open.

In-stent restenosis is elicited by the endothelial injury that the mechanical placement of the stent initiates, followed by thrombus formation and fibrin and platelet accumulation, which leads to classic anti-inflammatory agglomerates (Mitra and Agrawal 2006). To ameliorate these issues associated with bare metal stents, the second-generation stents with antiproliferative drugs such as rapamycin and paclitaxel incorporated on bare metal stents were introduced, which again had the problems of late restenosis and thrombosis. These drug eluting stents while helped in activation of signal-transduction pathways and inhibition of proliferation of vascular smooth muscle cell proliferation, also impaired



increased. The improved performance of these stents led to the consideration of other bioresorbable polymers such as PHAs, which compared to PLLA offers, less acidic degradation products, higher toughness/elongation at break and a surface erosion vs the bulk erosion of PLLA. A strategy to render the stents drug eluting has been to coat the stent surface with drug incorporated synthetic polymers such as PDLLA, as in the case of Abbott ABSORB. However, there are disadvantages associated with spray coating stent surfaces as these do not lead to controlled delivery of the incorporated drugs. This is because the release of drug depends on the degradation of the coated polymer and this can exert design constraints on stent development, and the overall modulation of drug release. Particulate systems such as micro and nanospheres offer better tunability of drug delivery, and they can be modified to be target specific and responsive to external stimuli (Dawson, Puranik and Peppas 2013).

In the first part of this chapter, a comparison of P(3HB) microspheres versus PLLA microspheres with encapsulated rapamycin, a well investigated antiproliferative and immunosuppressant drug was carried out. These were then characterized to determine the effect of drug loading on their physical properties. In the second part, P(3HB) microspheres of two different sizes encapsulated with Tacrolimus- another antiproliferative drug in the context of drug eluting stents- are compared with respect to their physical properties and drug release kinetics.

While antiproliferative drugs are administered to prevent the occurrence of MI as a result of atherosclerosis, an approach antagonistic to this is adopted in patients post MI. Rupture of atherosclerotic plaque leads to blocked blood supply to and hence nutrients and oxygen to any part of cardiac tissues and causes ischemia followed by MI. As the heart is a dynamic

---

organ and the function of the heart is vital to the functioning of the entire organism, several significant advancements have been made to circumvent the occurrence of tissue necrosis resulting in the loss of functionality in the case of MI. VEGF is a soluble, diffusible protein, first extracted from the medium conditioned by bovine pituitary folliculo-stellate cells by Henzel and Ferrara (Henzel, Ferrara and Winer, 1992). Since its discovery, a tremendous amount of research has been invested in the use of VEGF both in the perspective of angiogenesis and pro- angiogenesis. Vasculogenesis and succeeding angiogenesis are required to maintain a tissue's oxygen supply and support its functionalities (T Shoji *et al.*,2010). Therefore, VEGF plays a vital role in sustaining functionality of tissues and this is particularly relevant in the case of myocardial infarctions. The third part of this chapter discusses collagen scaffolds embedded with VEGF encapsulated microspheres of various sizes. VEGF encapsulated P(3HB) microspheres and nanospheres were synthesised and characterised and these were embedded in collagen scaffolds. The release kinetics of VEGF from neat spheres and spheres embedded in collagen scaffold were compared. Two different sizes of P(3HB) spheres were considered to analyse the changes in release profile, with respect to particle size.

To summarise, this study considered encapsulation and controlled release of therapeutic agents relevant before and after the occurrence of MI. The results of these were compared with existing alternatives in determining their efficacy for controlled delivery.

## 4.2. Results

### Part I: Comparison of P(3HB) and PLLA microspheres in the encapsulation and controlled release of rapamycin

#### 4.2.1. Hydrolytic depolymerisation of P(3HB)

P(3HB) was subjected to hydrolytic depolymerisation with acetic acid, for 8 and 12 hours of reflux respectively. These were then precipitated in excess of methanol and washed, centrifuged and lyophilised. Molecular weight analysis and polydispersity index (PDI) of polymers thus produced and non-hydrolysed polymer were determined using Agilent 1260 Infinity system equipped with a refractive index detector (Agilent Technologies, UK). Molecular weights decreased with time, however the PDI of the hydrolysed polymers were considerably high (**Table 4.1**).

Hydrolysis time (h)	$M_n$ , Da	$M_w$ , Da	PDI
0	27914	98628	1.674
8	12724	19820	3.71
12	6921	9341	4.18

**Table 4.1:** Molecular weight analysis of P(3HB) subjected to hydrolytic depolymerization.

#### 4.2.2. Optimisation of the process of microsphere production using solid-in-oil-in-water emulsion technique

Initial optimisation experiments were carried out using PLLA of three different molecular weights such as 30-50 KDa, 80-100 KDa and 300-400 KDa. Three different volumes of the dispersion phase (chloroform) were used to vary the polymer concentration. P(3HB)

subjected to hydrolytic depolymerization for 8 hours and 12 hours and non-hydrolysed P(3HB) were used to carry out the optimisation of microsphere production. Three different volumes of the dispersion phase (chloroform) were used to vary the polymer concentration (Table 4.2).

PLLA		P(3HB)	
Molecular weight of PLLA (KDa)	Polymer concentration in dispersed phase, 0.3g in	Molecular weight of P(3HB) (Da)	Polymer concentration in dispersed phase, 0.3g in
30-50	20 mL	98628	20 mL
	40 mL		40 mL
	60 mL		60 mL
80-100	20 mL	19820	20 mL
	40 mL		40 mL
	60 mL		60 mL
300-400	20 mL	9341	20 mL
	40 mL		40 mL
	60 mL		60 mL

**Table 4.2:** Processing conditions for the optimization of PLLA and P(3HB) microspheres.

### 4.2.3. Characterisation of PLLA and P(3HB) microspheres

#### 4.2.3.1. Surface morphology under SEM

Microspheres were successfully synthesized using PLLA of molecular weight 30-50 KDa and non-hydrolysed P(3HB) in 60 mL of chloroform. These two combinations were chosen for further characterisation. Microspheres prepared using other combinations resulted in

either polydisperse or poorly formed microspheres and in some cases, microspheres were not formed at all. Hydrolysis of P(3HB) was carried out to compare using P(3HB) of much lower molecular weight. However, the microspheres formed of hydrolysed polymer were widely polydispersed with lumps of polymer found intermittently with partially-formed microspheres (**Figure 4.2**).

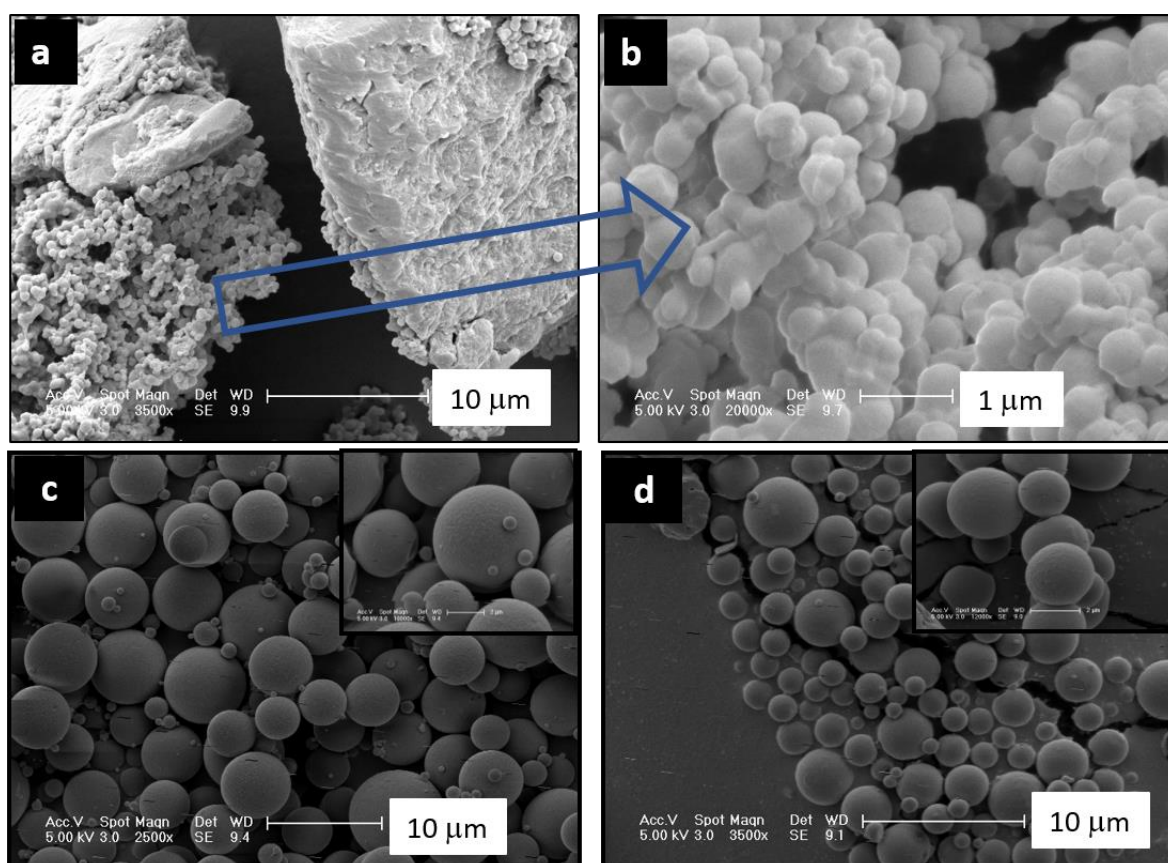


**Figure 4.2:** SEM images of a) microspheres produced using P(3HB) of Mw 9341 Da, b) magnified image of intermittent nanospheres c & d) microspheres produced using P(3HB) (98,268 Da) and PLLA (30-50 kDa).

These intermittent spheres were in the nanospheres range and were found to be clumped together with interconnecting channels, as discussed in Chapter 3. P(3HB) hydrolysed for 8 hours did not yield any microspheres at all. P(3HB) hydrolysed for 12 hours resulted in microspheres, when the organic phase contained 0.1 g of the polymer in 60 mL of

chloroform, but highly polydispersed. This indicated that further optimisation in the hydrolysis process was required. However, both PLLA and P(3HB) at a concentration of 0.1g/ 60 mL of chloroform resulted in excellent P(3HB) microspheres, within the size range of 1- 8  $\mu\text{m}$  and PLLA within the range of 1-5.5  $\mu\text{m}$ .

#### 4.2.3.2. Rapamycin encapsulation in P(3HB) and PLLA microspheres: Surface morphology under SEM

5wt% and 10wt% respectively of rapamycin was added to the polymer solution and was homogenized for 5 minutes and then emulsified with 0.5 % w/v PVA. Microstructural studies of chosen PLLA and P(3HB) microspheres were carried out using Scanning Electron Microscopy (SEM) as shown in **Figure 4.3.a &b**.

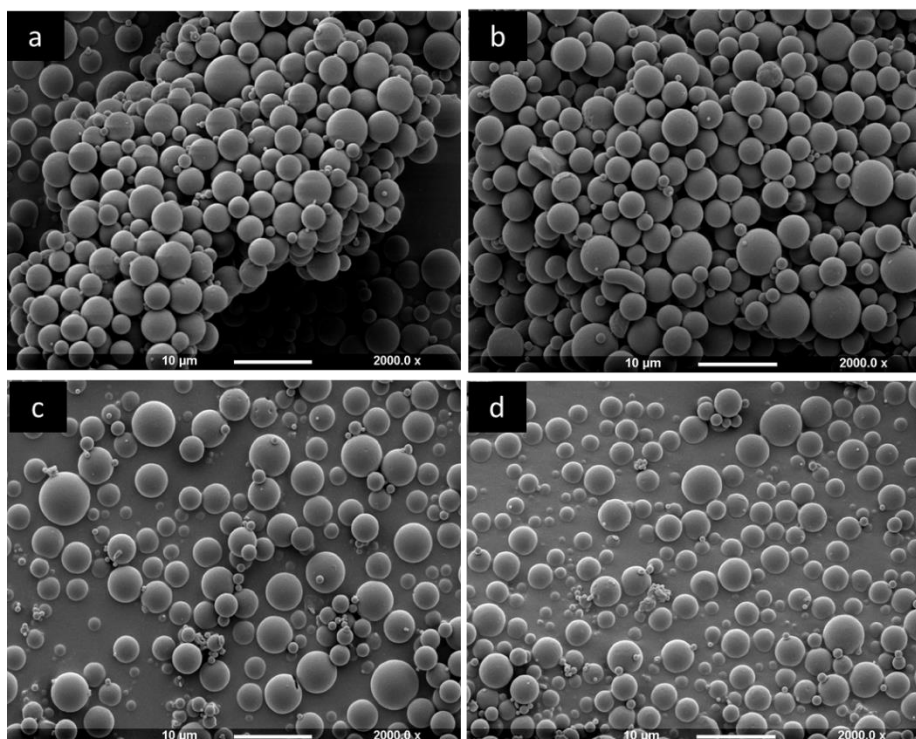


**Figure 4.3:** a) P(3HB) microspheres with 5 wt% Rapamycin, b) P(3HB) microspheres with 10 wt% Rapamycin, c) PLLA microspheres with 5 wt% Rapamycin, d) PLLA microspheres with 10 wt% Rapamycin

SEM studies revealed microspheres that were well formed with smooth surface and good spherical shape. The particles were free flowing and well separated from one another without the presence of interconnecting water channels.

#### 4.2.3.3. Particle size analysis

Microsphere images obtained under various magnifications were adjusted to appropriate threshold and analysed using the ImageJ software, calibrated with size bars of each of the image captured. The particle size distribution curve of microspheres corresponding to free P(3HB) and PLLA microspheres, P(3HB) and PLLA microspheres encapsulated with 5wt% of Rapamycin and P(3HB) and PLLA microspheres encapsulated with 10wt% Rapamycin are represented below (**Figure 4.4**). **Table 4.3** summarises the percentage distribution of microsphere into smaller and larger size range to analyse the influence of drug loading and type of polymer used. **Figure 4.4** and **Table 4.3** shows that the both free and Rapamycin encapsulated PLLA microspheres are smaller than P(3HB) microspheres. 20.73% of PLLA microspheres fall under the smaller size range of 1-3  $\mu\text{m}$  while only 12.5% of P(3HB) microspheres are in this range. In the case of PLLA, with Rapamycin encapsulation, although particle size range remained within 1-5.5  $\mu\text{m}$ , the percentage of microspheres in the larger size range of 3-5.5  $\mu\text{m}$  increased with drug/polymer ratio. The trend observed was the same in the case of P(3HB) microspheres with the cumulative frequency of larger microspheres increasing with drug/polymer ratio. It was observed that the frequency of P(3HB) microspheres in the 1-3  $\mu\text{m}$  range decreased from 18.77% to 8.5 % with 10 wt% Rapamycin encapsulations. 11.56% microspheres of 10 wt% Rapamycin encapsulated P(3HB) were in the size range of 5.5-7  $\mu\text{m}$ . The change in size distribution of PLLA was not

as pronounced with Rapamycin encapsulation, with a reduction of only 2.9% in the smaller size range, with Rapamycin encapsulation.

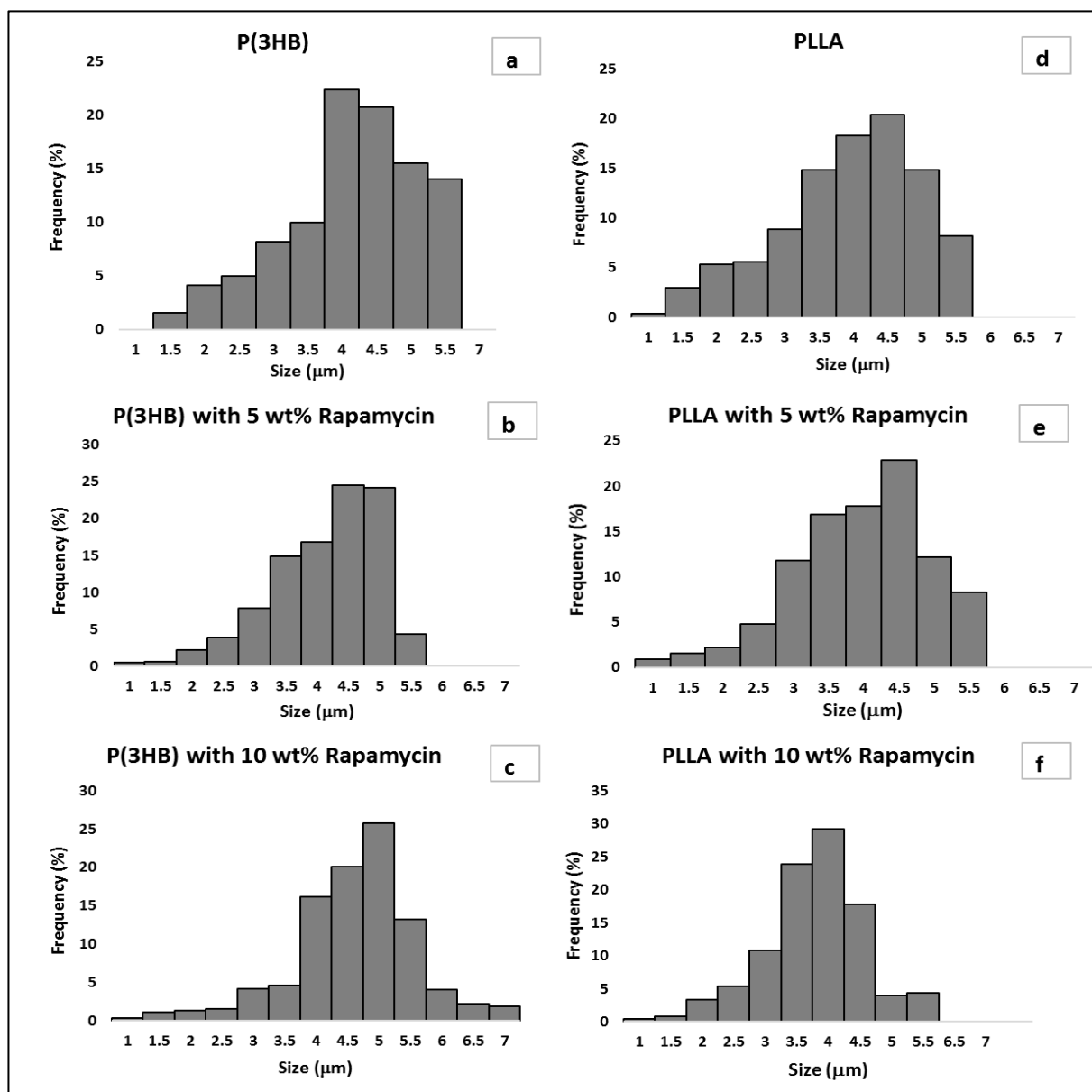


**Figure 4.4:** Size distribution analysis of a) neat P(3HB) microspheres, b) P(3HB) microspheres with 5 wt% rapamycin, c) P(3HB) microspheres with 10 wt% rapamycin, d) neat PLLA microspheres, e) PLLA microspheres with 5 wt% rapamycin, f) PLLA microspheres with 10 wt% rapamycin

	1-3 $\mu\text{m}$	3-5.5 $\mu\text{m}$
<b>P(3HB)</b>	18.77	80.73
<b>P(3HB) with 5 wt% Rapamycin</b>	15	84.7
<b>P(3HB) with 10 wt% Rapamycin</b>	8.5	79.94
<b>PLLA</b>	23.21	76.54
<b>PLLA with 5 wt% Rapamycin</b>	21.3	78.1
<b>PLLA with 10 wt% Rapamycin</b>	20.73	79.26

**Table 4.3:** Size distribution analysis of P(3HB) and PLLA microspheres with and without encapsulated rapamycin.

#### 4.2.3.4. Porosity

The optimization studies revealed that PLLA microspheres were  $15 \pm 1.1\%$  porous whereas P(3HB) microspheres amounted to a significant  $37.5 \pm 3.12\%$  porosity (**Figure 4.5**).

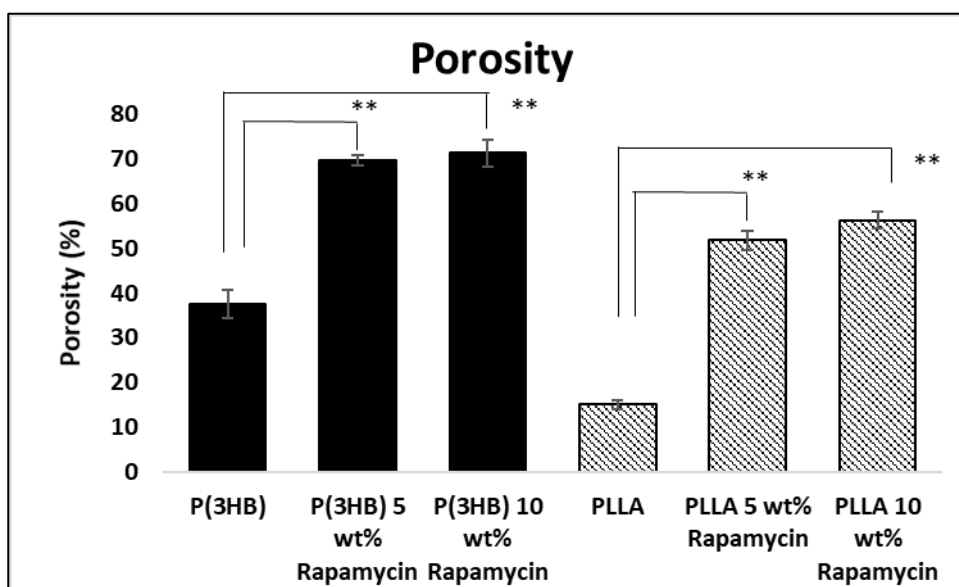


**Figure 4.5:** Porosity measurements of microspheres prepared using P(3HB) and PLLA with and without Rapamycin encapsulation ( $n=3$ ; error bars=  $\pm$ SD). The data was compared using t- test and the differences were considered very significant (\*\* $p < 0.01$ )

However, the rapamycin encapsulated microspheres of both the polymers exhibited much higher porosity. Rapamycin encapsulated PLLA microspheres exhibited porosity in the

range of ~50- 56% with a direct correlation between porosity and drug loading. Rapamycin encapsulated P(3HB) microspheres exhibited a similar trend, however, with a very high porosity range of ~69-71% porosity.

#### 4.2.3.5. Surface residual PVA

Surface residual PVA associated with free and Rapamycin encapsulated microspheres were quantified using the method described in section 2.2.8.4 (Figure 4.6).

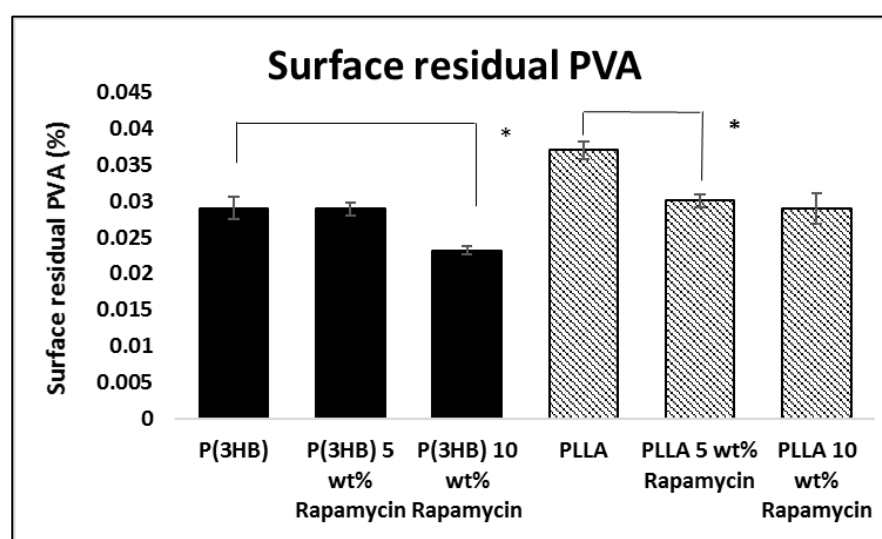


**Figure 4.6:** Surface residual PVA measurements of microspheres prepared using P(3HB) and PLLA with and without Rapamycin encapsulation (n=3; error bars=  $\pm$ SD). The data was compared using t- test and the differences were considered significant (\*p<0.05)

Free P(3HB) microspheres had  $0.029 \pm 0.0012$  % residual PVA associated on the surface when compared to the  $0.037 \pm 0.0012$ % residual PVA associated on the PLLA microsphere surface. % Surface residual PVA decreased with increasing drug loading and the decrease was significant between free P(3HB) microspheres and P(3HB) microspheres encapsulated with 10 wt% Rapamycin. Same trend was observed between free PLLA microspheres and PLLA microspheres encapsulated with Rapamycin. The decrease in % residual PVA between

free PLLA microspheres and PLLA microspheres encapsulated with 5 wt% Rapamycin ( $0.037 \pm 0.0012\%$  and  $0.030 \pm 0.009\%$  respectively) was found to be statistically significant but the differences between PLLA microspheres encapsulated with 5 wt% and 10 wt% Rapamycin ( $0.030 \pm 0.009\%$  and  $0.029 \pm 0.0021$  respectively) were statistically insignificant.

#### 4.2.3.6. Surface hydrophobicity

The surface hydrophobicity of the microspheres fabricated using P(3HB) and PLLA with and without the incorporation of Rapamycin was determined by comparing the amount of Rose Bengal dye that was adsorbed per mg of the microspheres. As shown in **figure 4.7**, P(3HB) microspheres are markedly more hydrophobic than PLLA microspheres with  $3.3 \pm 0.051 \mu\text{g}$  of surface bound Rose Bengal dye as opposed to a  $1.43 \pm 0.188 \mu\text{g}$  of PLLA microspheres.

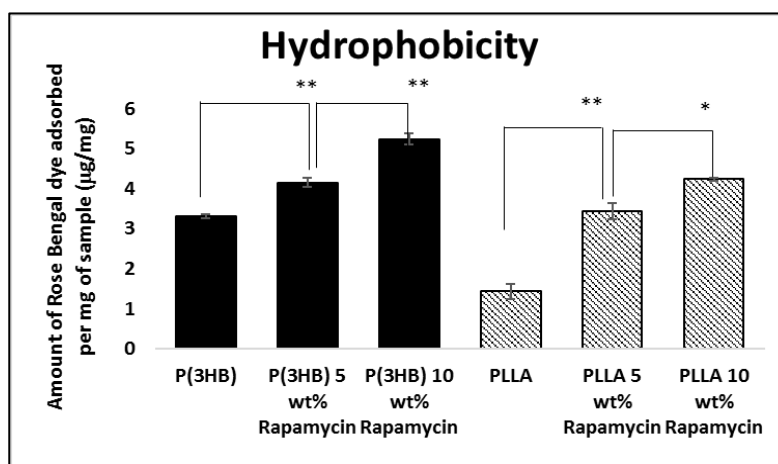


**Figure 4.7:** Hydrophobicity expressed as a function of surface bound Rose Bengal dye for microspheres prepared using P(3HB) and PLLA with and without Rapamycin encapsulation ( $n=3$ ; error bars =  $\pm$  SD). The data was compared using t- test.

Hydrophobicity expressed as a function of surface bound Rose Bengal dye was found to increase with drug loading and the differences were statistically very significant amongst P(3HB) microspheres ( $3.3 \pm 0.051 \mu\text{g/mg}$  on free microspheres,  $4.15 \pm 0.148 \mu\text{g/mg}$  on P(3HB) microspheres with 5 wt% Rapamycin and  $5.23 \pm 0.148 \mu\text{g/mg}$  on P(3HB)

microspheres with 10 wt% rapamycin, respectively). The trend was observed to be the same between free and Rapamycin encapsulated PLLA microspheres. The amount of Rose Bengal dye bound increased to  $3.43 \pm 0.200 \mu\text{g}/\text{mg}$  with 5 wt% Rapamycin encapsulations and the difference was found to be statistically very significant and the amount increased to  $4.24 \pm 0.04 \mu\text{g}/\text{mg}$  with 10 wt% of Rapamycin encapsulations.

#### 4.2.3.7. Protein adsorption

Passive protein adsorption on the surface of microspheres was estimated by immersing samples in BSA solution for 24 hours and subjecting the supernatant to Bradford assay (Figure 4.8).

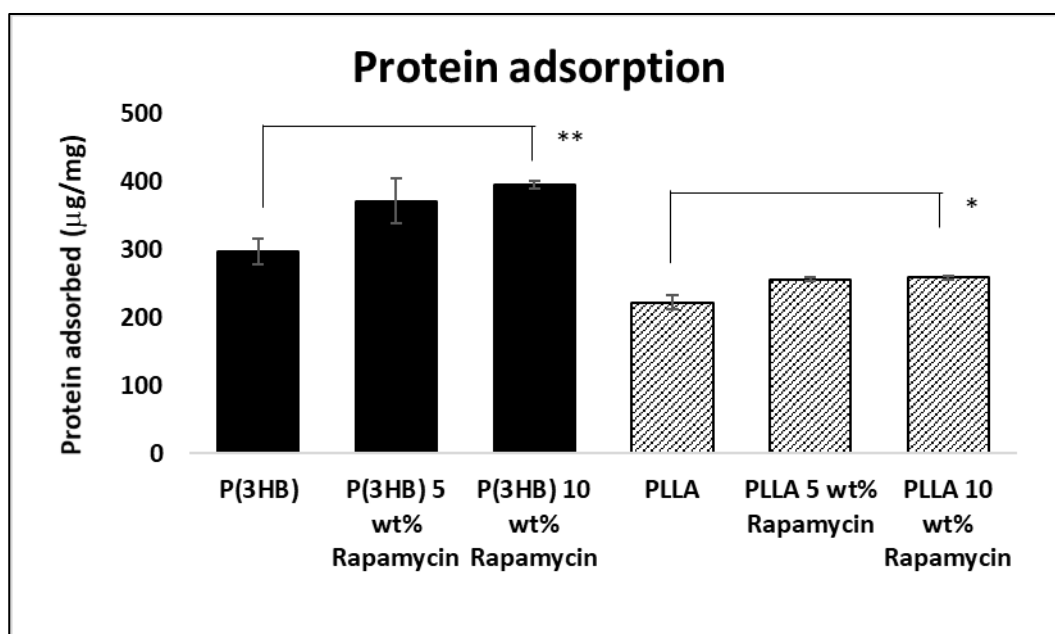


**Figure 4.8:** Protein adsorption on the surface of microspheres prepared using P(3HB) and PLLA with and without Rapamycin encapsulation ( $n=3$ ; error bars =  $\pm$  SD).

In comparison with PLLA microspheres ( $221.67 \pm 10.21 \mu\text{g}/\text{mg}$ ), protein adsorption on P(3HB) microspheres was found to be higher ( $297 \pm 19.31 \mu\text{g}/\text{mg}$ ). Rapamycin incorporation was found to have a positive correlation with protein adsorption in the case

of both P(3HB) and PLLA microspheres. In the case of PLLA,  $255.67 \pm 2.8 \mu\text{g}/\text{mg}$  was adsorbed on microspheres with 5 wt% drug loading and  $258.66 \pm 3.05 \mu\text{g}/\text{mg}$  was adsorbed on microspheres with 10 wt% drug loading. In the case of P(3HB), this was  $371.33 \pm 33.21 \mu\text{g}/\text{mg}$  and  $396.38 \pm 5.68 \mu\text{g}/\text{mg}$  respectively.

#### 4.2.3.8. In vitro Degradation of P(3HB) and PLLA microspheres

##### I. Water uptake and weight loss analysis

*In vitro* degradation of P(3HB) and PLLA microspheres with and without encapsulated Rapamycin was analysed using data from water uptake and water loss measurements. In the case of unloaded P(3HB), water uptake was gradual from 201% to 405% over a span of 36 days. This trend was followed even in the case of Rapamycin loaded P(3HB), with a maximum water uptake of 402% in the case of both 5 wt% and 10 wt% rapamycin encapsulations (**Figure 4.9**).

Maximum weight loss in the case of unloaded P(3HB) microspheres was 11.9%, followed by a 10.5% in the case of 5 wt% Rapamycin encapsulated microspheres and 10.2% of 10 wt% Rapamycin encapsulated microspheres. PLLA microspheres were found to show increased water uptake in comparison with P(3HB) microspheres, starting with 248% on day 3 and ending at a maximum of 583 on day 36 (**Figure 4.9**). 5 wt% rapamycin encapsulated PLLA microspheres showed a maximum water uptake of 560% and 10 wt% Rapamycin encapsulated PLLA microspheres showed a maximum water uptake of 555%. Weight loss also was found to be more in the case of PLLA, with a maximum of 14.3% in unloaded PLLA microspheres, and a minimum of 13.8% in 10 wt% Rapamycin encapsulated microspheres respectively.

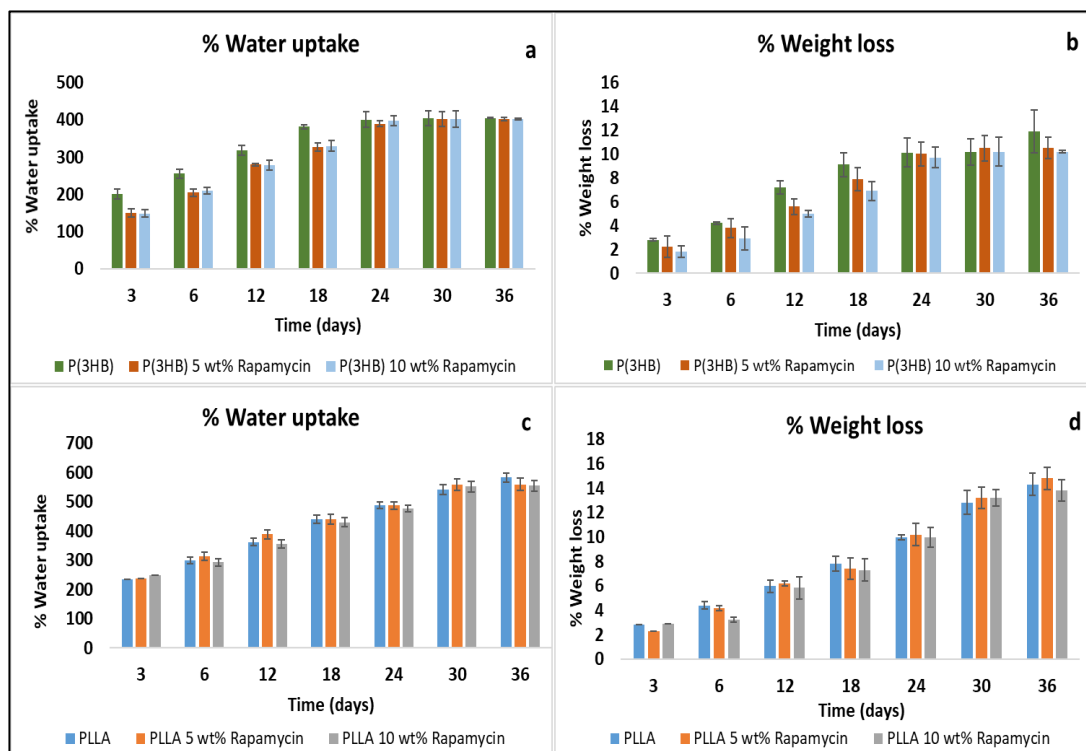


**Figure 4.9:** Water uptake and weight loss measurements in measurements in a & b) unloaded P(3HB) microspheres P(3HB) microspheres with 5 wt% Rapamycin and 10 wt% Rapamycin, and c & d) Water uptake measurements in unloaded PLLA microspheres, PLLA microspheres with 5 wt% rapamycin and PLLA microspheres with 10 wt% Rapamycin and (n=3; error bars=  $\pm$ SD)

#### i. pH changes

Rapamycin loaded and unloaded P(3HB) and PLLA microspheres were immersed in PBS at pH 7.4 and pH changes over time was recorded (**Figure 4.10**). It was observed that while pH changes in P(3HB) microspheres over a span of 36 days remained within the range on 7.2-6, PLLA microspheres showed drastic pH changes from 7.2 to 3.1. in the case of P(3HB), the degradation products of rapamycin encapsulated microspheres were found to be even more acidic compared to unloaded microspheres while no such differences were observed in the case of PLLA microspheres.

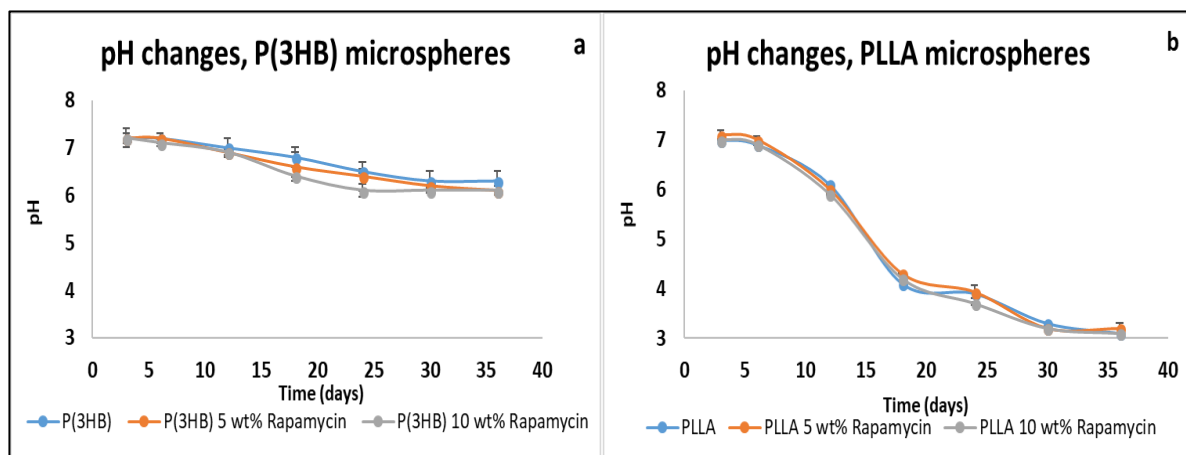


**Figure 4.10:** pH changes observed in the PBS solution containing a) unloaded and rapamycin loaded P(3HB) microspheres and b) unloaded and rapamycin loaded PLLA microspheres, (n=3; error bars = SD).

#### 4.2.4. Rapamycin encapsulation and release kinetics

##### 4.2.4.1. Encapsulation efficiency

The best optimised microspheres were chosen to incorporate 5 wt% and 10 wt% drug loadings of Rapamycin. Briefly, 0.1g of each polymer was dissolved in 20 mL of chloroform and 5 wt% and 10 wt% each of Rapamycin was added to this solution, followed by homogenization, at 4 °C. Microspheres prepared using this organic phase was lyophilized and was observed for release kinetics. Prior to that the experimental loading of encapsulation in these microspheres were quantified using HPLC (**Figure 4.11**).

The release profile in both the cases were found have a pronounced burst release in the first 48 hours, for up to 11% cumulative release. P(3HB) microspheres exhibited a slightly faster release when compared to PLLA microspheres, with 5 wt% Rapamycin loaded P(3HB) microspheres releasing up to 22.70% and 10 wt% rapamycin loaded P(3HB) microspheres

releasing up to 22.97% in 30 days. This was found to be 19.01 and 22.02 respectively, in the case of 5 wt% and 10 wt% loaded PLLA microspheres.

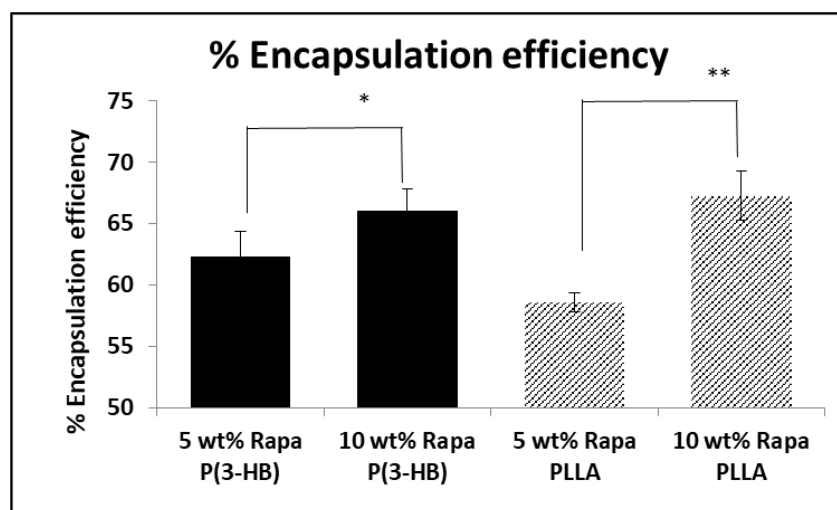


**Figure 4.11:** Encapsulation efficiency of P(3HB) and PLLA microspheres at 5 wt% and 10 wt% rapamycin loading (n=3; error bars = SD).

At 5 wt% loading (5mg of rapamycin), P(3HB) microspheres had a higher encapsulation efficiency of 62.37% compared to the 58.58% of PLLA microspheres. However, at 10 wt% loading (10mg of rapamycin) PLLA microspheres had a higher encapsulation efficiency of 67.26% compared to the 62.37% of P(3HB) microspheres. The amount of Rapamycin encapsulated in P(3HB) microspheres with 5 and 10 wt% drug loadings are 3.16mg and 6.68 mg respectively and the amount of Rapamycin encapsulated in PLLA microspheres with 5 and 10 wt% drug loadings are 2.92 mg and 6.7 mg respectively. In both the cases, encapsulation efficiency was found to increase with increase in drug/polymer ratio.

#### 4.2.4.2. In vitro Release kinetics

*In vitro* release profiles of rapamycin encapsulated P(3HB) and PLLA microspheres were carried out for a period of 30 days, after which the drug was detected using HPLC was found to be inaccurate, possibly due to degradation of the drug. Samples were drawn periodically from PBS immersed with 5 wt% and 10 wt% rapamycin loaded P(3HB) and PLLA microspheres and these were analysed for their drug content using HPLC (**Figure 4.12**).

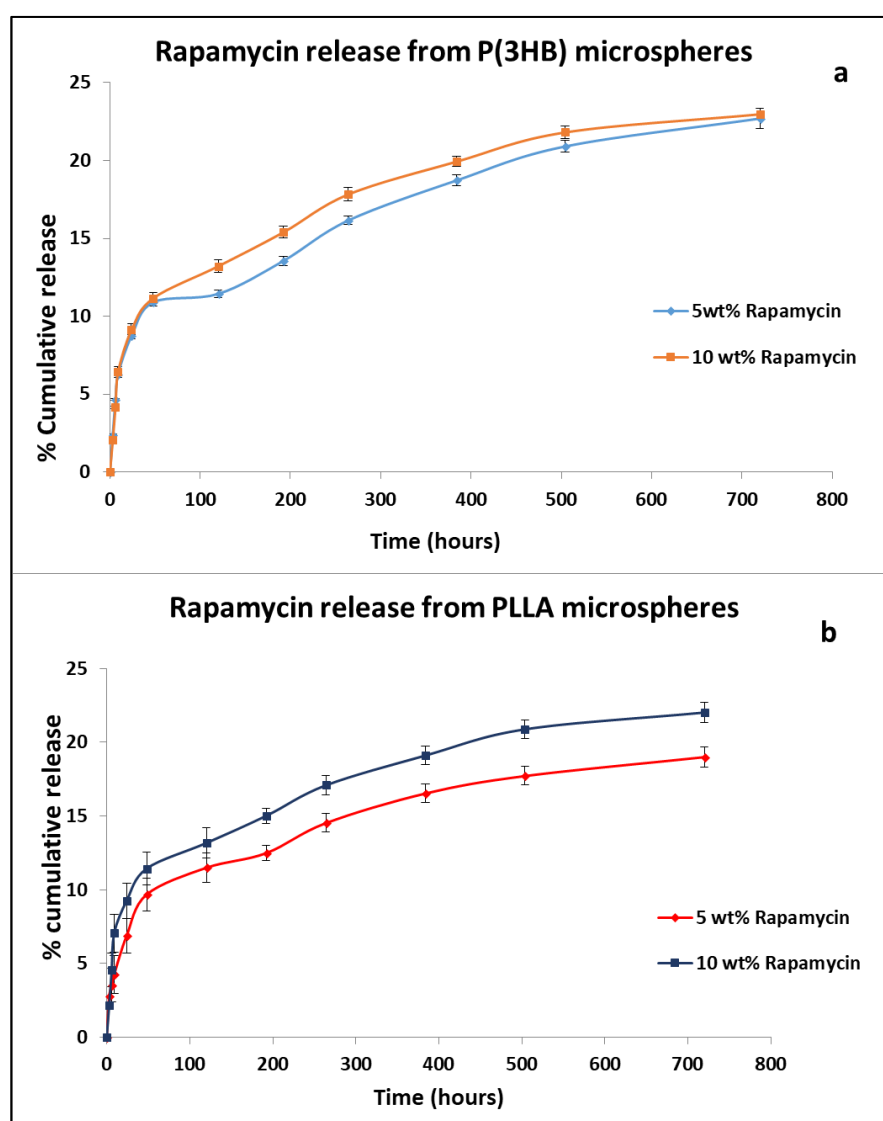


**Figure 4.12:** Rapamycin release profile from a) P(3HB) microspheres, b) PLLA microspheres (n=3; error bars = SD).

The release data was fitted in models as described in section 2.2.11.  $R^2$  value of each of the linear regression was compared (Table 4.4).

		P(3HB) microspheres with Rapamycin loading of		PLLA microspheres with Rapamycin loading of	
Model	Parameters	5 wt%	10 wt%	5 wt%	10 wt%
Zero-order	$R^2$	0.827	0.786	0.790	0.766
	$Adj-R^2$	0.909	0.764	0.769	0.742
	<i>Slope</i>	0.028	0.029	0.0241	0.0277
	<i>SSR</i>	102.13	143.89	94.48	139.01
First-order	$R^2$	0.853	0.813	0.811	0.793
	$Adj-R^2$	0.838	0.794	0.792	0.773
	<i>Slope</i>	-0.0001	-0.0001	-0.0001	-0.0001
	<i>SSR</i>	0.002	0.003	0.002	0.003
Higuchi	$R^2$	0.956	0.947	0.952	0.932
	$Adj-R^2$	0.952	0.941	0.947	0.926
	<i>Slope</i>	0.796	0.846	0.693	0.789
	<i>SSR</i>	25.78	35.79	21.68	40.08
Hixson-Crowell	$R^2$	0.804	0.804	0.804	0.784
	$Adj-R^2$	0.784	0.784	0.784	0.763
	<i>Slope</i>	-0.0005	-0.0005	-0.0004	-0.0005
	<i>SSR</i>	0.026	0.037	0.024	0.036
Korsmeyer-Peppas	$R^2$	0.943	0.933	0.985	0.917
	$Adj-R^2$	0.936	0.925	0.983	0.908
	<i>Slope</i>	0.351	0.384	0.353	0.357
	<i>SSR</i>	0.052	0.074	0.014	0.080

Table 4.4: Summary of model fitting for Rapamycin release from P(3HB) and PLLA microspheres.

In all the 4 preparations, the release data was found to be more fitting to Higuchi model.

In the case of both PLLA and P(3HB), microspheres with 5% rapamycin loading was

observed to have a higher correlation in comparison with 10% loading. This indicates diffusion mode of drug release. To assess the nature of drug release, the slope (which corresponds to 'n', the release exponent) for Korsmeyer- Peppas regression was analysed, and since all the values were less than 0.43, it was confirmed that in all the 4 cases, diffusion follows Fickian mode.

## **Part II: Comparison of P(3HB) nano and microspheres with encapsulated tacrolimus**

### **4.2.5. Production of micro/nanospheres with encapsulated tacrolimus using solid-in-oil-in-water emulsion technique**

P(3HB) microspheres and nanospheres with encapsulated tacrolimus were prepared using solid-in-oil-in-water emulsion technique by the solvent evaporation method. Unloaded microspheres and nanospheres are used as controls throughout this chapter. After an initial set of pilot experiments for optimization, 1, 5 and 10 wt% of tacrolimus was dissolved in 20 mL solution of 6.5 mg/ mL solution of P(3HB) to produce nanospheres and in an 8 mL solution of 12.5 mg/ mL solution of P(3HB) to produce microspheres. 0.5 w/v% of PVA was used as the surfactant in both cases. The processing conditions are as represented in the **Table 4.5**. These were centrifuged, washed, and lyophilized and subjected to thermal and physical characterization and finally drug release kinetics was compared.

Sample	P(3HB) concentration (mg/ mL)	Organic phase volume (mL)	Amount of Tacrolimus loaded (mg)	Stirrer speed (rpm)
P(3HB) (n)	6.5	20	-	800
1 wt% Tac (n)		20	0.0013	800
5 wt% Tac (n)		20	0.0065	800
10 wt% Tac (n)		20	0.013	1000
P(3HB) (m)	12.5	8	-	1000
1 wt% Tac (m)		8	0.01	1000
5 wt% Tac (m)		8	0.05	1000
10 wt% Tac (m)		8	0.1	1000

**Table 4.5:** Processing conditions for the production of P(3HB) microspheres and nanospheres with encapsulated Tacrolimus

## 4.2.6. Characterization of P(3HB) microspheres and nanospheres with encapsulated tacrolimus

### 4.2.6.1. Surface morphology analysis using SEM

The nanospheres and microspheres compared had very distinct differences in surface morphology (**Figure 4.13**).

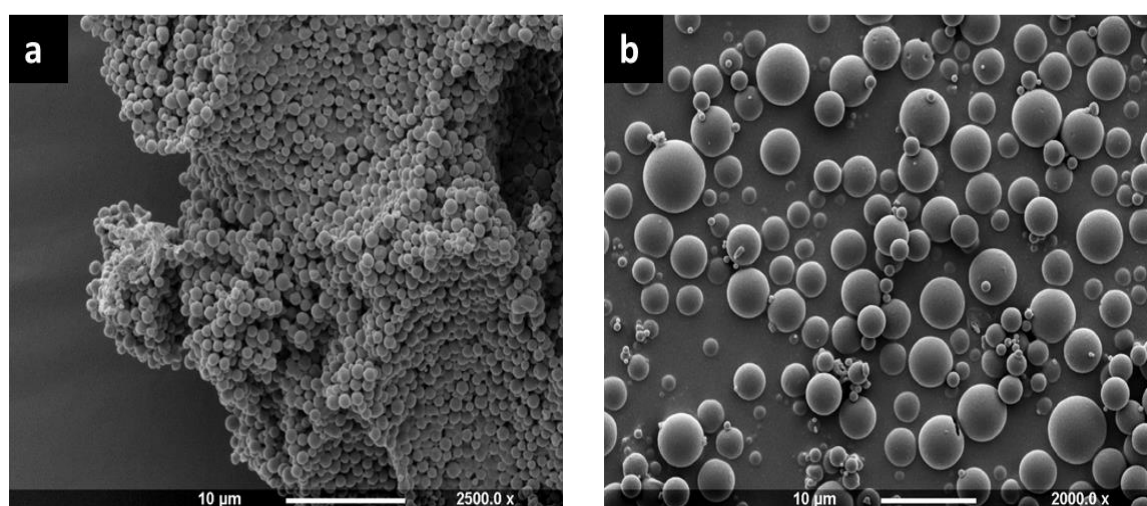


**Figure 4.13:** SEM images of a) unloaded P(3HB) nanospheres, b) unloaded P(3HB) microspheres (size bar= 10  $\mu$ m)

While the microspheres had more pronounced sphericity, tacrolimus encapsulated nanospheres in comparison with the unloaded ones had slight occurrence of intermittent disc shaped particles. However, their size distribution was observed to be sufficiently monodisperse. Both microspheres and nanospheres had smooth surfaces with minimal agglomeration. In the case of microspheres, with increasing drug loading, particle size and was observed to increase markedly with drug loading and smoothness of the surface was observed to decrease. With increased drug loading, the microspheres seemed to have the presence of some thread like features and residual particulates on the surface of spheres (Figure 4.14)

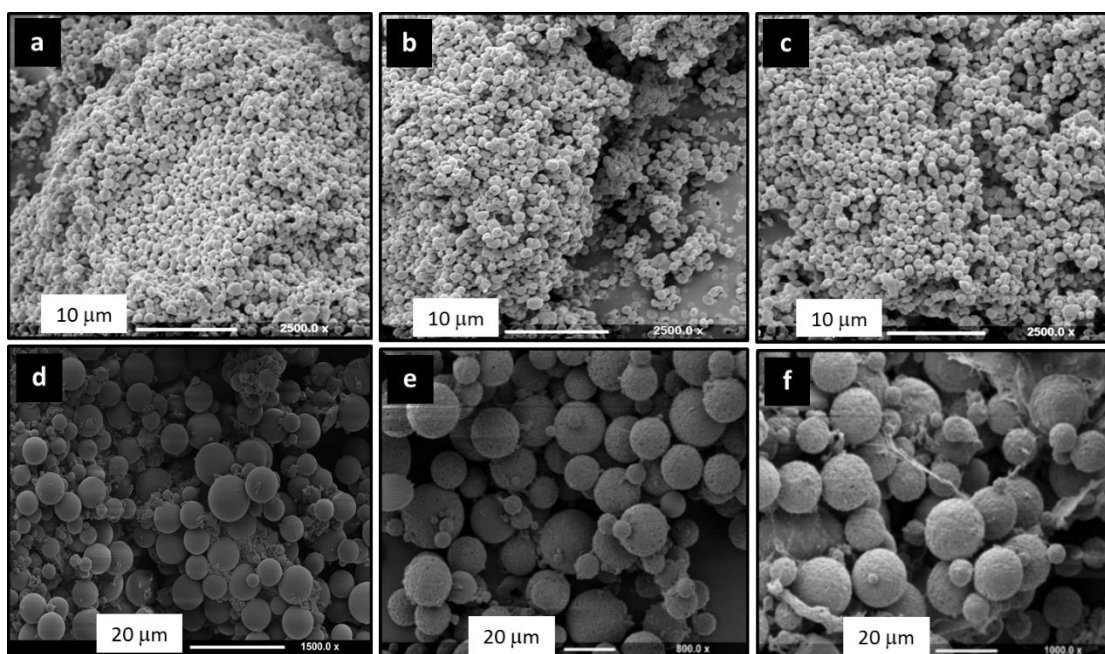


**Figure 4.14:** SEM images of a-c) 1 wt%, 5 wt% and 10 wt% Tacrolimus encapsulated nanospheres, d-e) 1 wt%, 5 wt% and 10 wt% Tacrolimus encapsulated microspheres

#### 4.2.6.2. Particle size analysis

Particle sizes of the micro and nanospheres produced with and without Tacrolimus were analysed using the software imageJ, with appropriate threshold adjustments. It was found

that in the case of both nanospheres and microspheres, the average size of microspheres increased with drug loading and the differences were statistically significant (**Figure 4.15**).

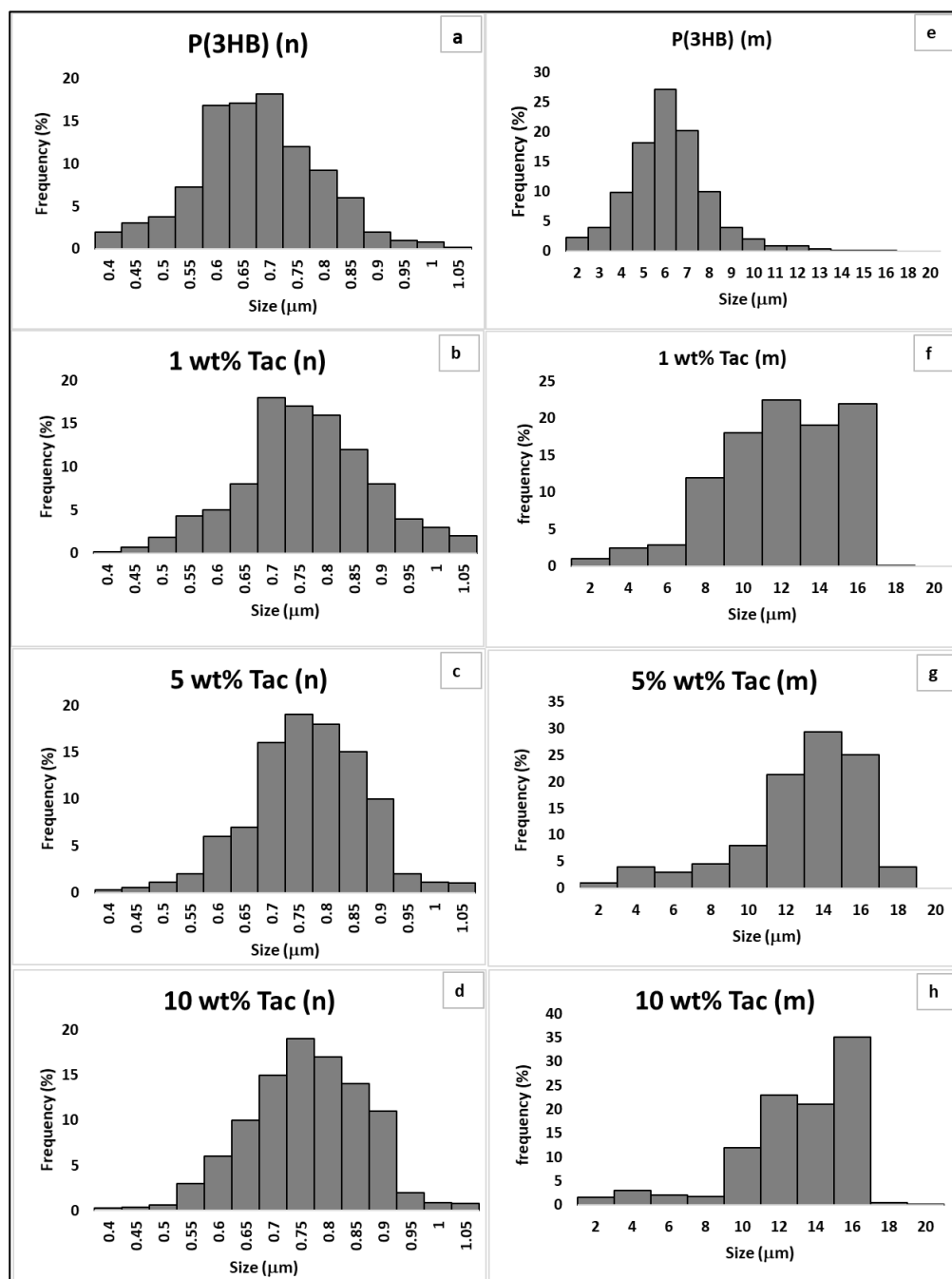


**Figure 4.15:** Particle size distribution of a-d) unloaded nanospheres and 1 wt%, 5 wt% and 10 wt% Tacrolimus and e-h) unloaded microspheres and wt%, 5 wt% and 10 wt% Tacrolimus respectively

In the case of nanospheres, there was no pronounced differences in size between the three different drug loadings of Tacrolimus tested. While the unloaded nanospheres had an average diameter size of  $672.2 \pm 12.89$  nm, 1, 5 and 10 wt% Tacrolimus loaded nanospheres were found to be  $763.1 \pm 19.87$ ,  $765.6 \pm 27.9$  and  $761.4 \pm 18.21$  nm respectively. In the case of microspheres, there was a gradual increase in microsphere size after drug loading. While the unloaded microspheres had an average diameter size of  $6.15 \pm 0.32$   $\mu$ m, 1, 5 and 10 wt% Tacrolimus loaded microspheres were found to have diameter size of  $11.75 \pm 0.58$ ,  $13.12 \pm 0.93$  and  $14.62 \pm 0.82$   $\mu$ m respectively.

#### 4.2.6.3. Porosity

Porosity was quantified using liquid displacement method as explained in section 2.2.8.3. In comparison with unloaded nanospheres, unloaded microspheres were found to be more porous with a porosity of  $77.09 \pm 3.83\%$ , as opposed to  $67.90 \pm 2.12\%$  for the nanospheres (Figure 4.16).

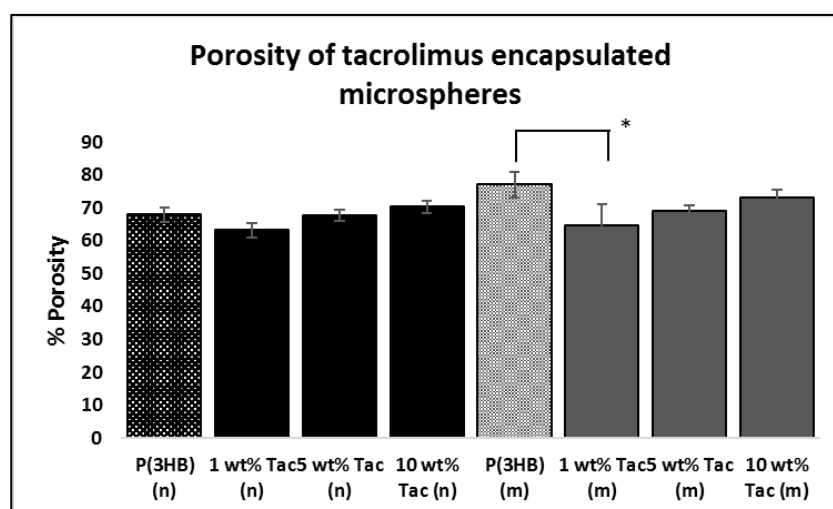


**Figure 4.16:** Porosity measurements of microspheres and nanospheres prepared with and without encapsulated tacrolimus (n=3; error bars=  $\pm$ SD) [n=nanospheres, m=microspheres]

Porosity was found to increase with drug loading, in the case of both microspheres and nanospheres. However, comparing between unloaded and Tacrolimus loaded spheres in both micro and nano size range, spheres with encapsulated tacrolimus were found to be more porous. In the case of nanospheres, porosity was found to have increased from 63% to 70% between 1 wt% and 10 wt% tacrolimus loading and in the case of microspheres, porosity was found to have increased from 64% to 73%.

#### 4.2.6.4. Residual PVA

Residual PVA was estimated to be the highest in the case of unloaded nanospheres and was found to be  $0.499 \pm 0.09$  %w/w of unit mass of spheres (**Figure 4.17**).

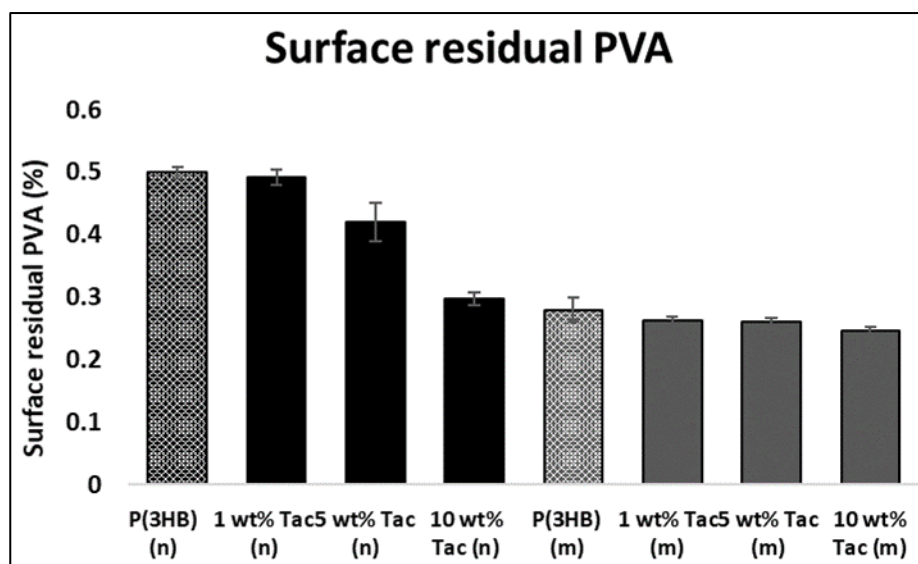


**Figure 4.17:** Surface residual PVA of microspheres and nanospheres prepared with and without encapsulated tacrolimus (n=3; error bars=  $\pm$ SD) [n=nanospheres, m=microspheres].

A slight decrease of 0.009% was observed with 1 wt% Tacrolimus loading, but the decrease was much more pronounced with 10 wt% loading of the drug, to,  $0.298 \pm 0.01$  %. Although

the trend was followed in the case of microspheres, the difference in residual PVA with drug loading was not as significant. Residual PVA was found to have reduced from  $0.263 \pm 0.004$  to  $0.245 \pm 0.007$  between 1 wt% and 10 wt% drug loading in microspheres. To summarize, there was a 40% reduction in residual PVA between unloaded nanospheres and nanospheres loaded with 10 wt% Tacrolimus, while there was only a reduction of 12% in the case of microspheres.

#### 4.2.6.5. Hydrophobicity

Surface hydrophobicity of microspheres and nanospheres prepared were expressed as a function of the amount of Rose Bengal dye bound on the surface of the spheres at dye saturation (**Figure 4.18**)

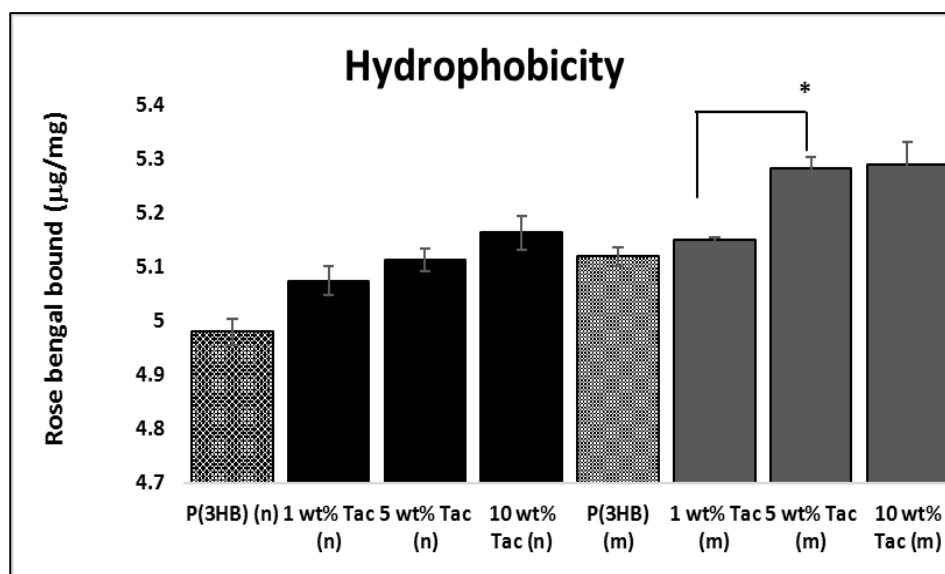


**Figure 4.18:** Hydrophobicity expressed as a function of surface bound Rose Bengal dye on micro/nanospheres with and without encapsulated tacrolimus ( $n=3$ ; error bars= $\pm$ SD) [ $n$ =nanospheres,  $m$ =microspheres].

Unloaded nanospheres had a smaller amount of Rose Bengal dye bound on their surface ( $4.98 \pm 0.098$  µg/mg), indicating that they are relatively less hydrophobic than the

microspheres ( $5.11 \pm 0.07 \mu\text{g}/\text{mg}$ ). The amount of Rose Bengal dye bound on the surface of the spheres were found to increase with drug loading in the case of both microspheres and nanospheres, suggesting that hydrophobicity of the particles increased with drug loading. In the case of nanospheres, the amount of surface bound Rose Bengal dye increased from  $5.074 \pm 0.11 \mu\text{g}/\text{mg}$  to  $5.162 \pm 0.123 \mu\text{g}/\text{mg}$  between 1 wt% and 10 wt% drug loading. The difference was found to be higher in the case of microspheres, with an increase of  $5.149 \pm 0.198 \mu\text{g}/\text{mg}$  to  $5.288 \pm 0.170 \mu\text{g}/\text{mg}$  between 1 wt% and 10 wt% drug loading. The differences were found to be statistically insignificant.

#### 4.2.6.6. Protein adsorption

Protein adsorption on the surface of microspheres and nanospheres was estimated by immersing samples in BSA solution for 24 hours and subjecting the supernatant to Bradford assay. The nanospheres in general were found to adsorb an increased amount of proteins in comparison with the microspheres (**Figure 4.19**).

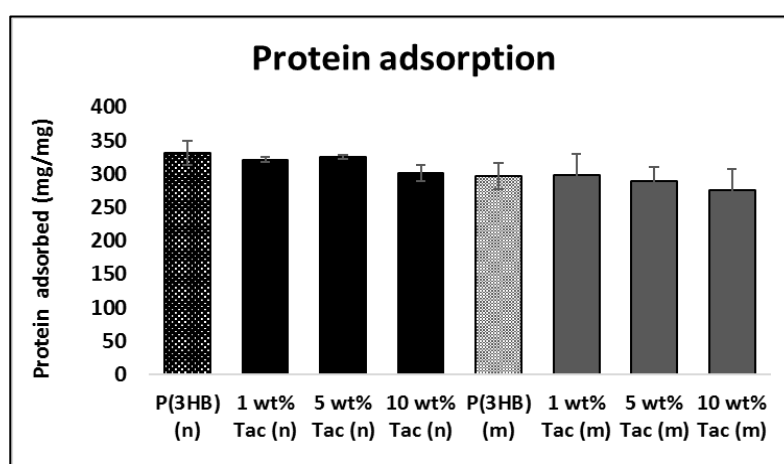


**Figure 4.19:** Protein adsorption on the surface of unloaded and 1 wt%, 5 wt% and 10 wt% tacrolimus loaded nanospheres and microspheres ( $n=3$ ; error bars=  $\pm$  SD) [ $n$ =nanospheres,  $m$ =microspheres].

Unloaded nanospheres adsorbed  $332.12 \pm 17.78 \mu\text{g}/\text{mg}$ , compared to a  $297 \pm 19.313 \mu\text{g}/\text{mg}$  for the unloaded microspheres. While in the case of microspheres, the amount of protein adsorbed was observed to decrease with drug loading, nanospheres did not follow this trend. The amount of protein adsorbed on nanospheres with 5 wt% Tacrolimus ( $325 \pm 2.9 \mu\text{g}/\text{mg}$ ) was slightly higher than the amount on nanospheres with 1 wt% ( $321 \pm 3.2 \mu\text{g}/\text{mg}$ ) and less than nanospheres with 10 wt% tacrolimus ( $308 \pm 11.9 \mu\text{g}/\text{mg}$ ). The differences in the amount of absorbed protein between each preparation were not statistically significant.

#### 4.2.6.7. In vitro degradation

##### I. Water uptake and weight loss

Water uptake and weight loss was estimated with samples immersed in PBS for a duration of 36 days (**Figure 4.20**). Compared to unloaded and Tacrolimus encapsulated microspheres, unloaded and tacrolimus encapsulated nanospheres exhibited higher extent of water uptake. The estimated water loss estimated was also found to follow the same trend. Unloaded nanospheres absorbed a maximum of 459% water and experienced a weight loss of 16.6% over 36 days. In the case of unloaded microspheres maximum water uptake was 409% and weight loss was 11.9%. In the case of nanospheres, water uptake was found to decrease with drug loading, with nanospheres with, 1 wt% tacrolimus absorbing a maximum of 402%, 5 wt% tacrolimus absorbing a maximum of 392% and 10 wt% tacrolimus absorbing a maximum of 361%. Weight loss followed a similar trend with a decrease from 11.3 to 10.9% between 1 wt% tacrolimus loading and 10 wt% tacrolimus loading. In the case of microspheres, maximum water uptake was found to be 442%, 420%

and 361% for 1 wt% tacrolimus loading, 5 wt% tacrolimus loading and 10 wt% tacrolimus loading respectively.

But in the case of weight loss, although weight loss was found to have decelerated in the beginning, towards the end of 36 days, the weight loss experienced by all the three drug loaded microspheres were similar.

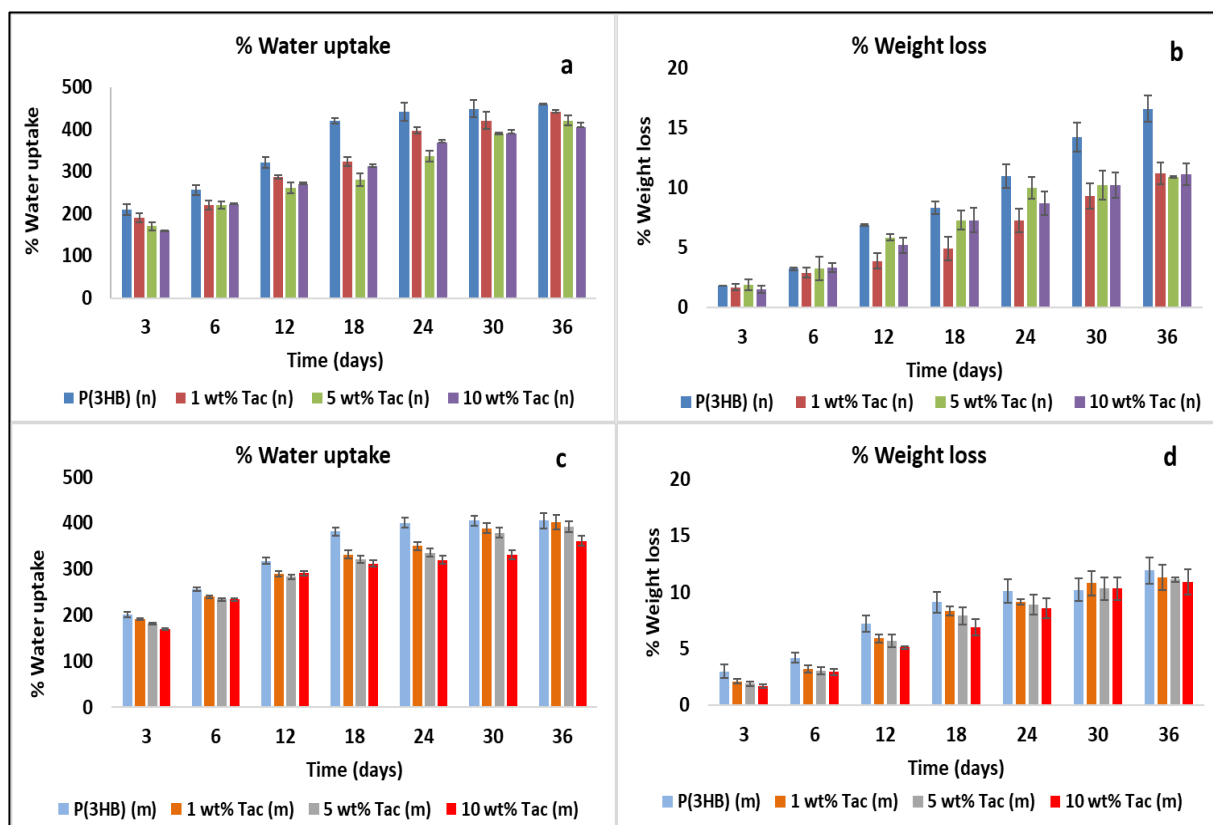


**Figure 4.20:** Water uptake measurements and weight loss measurements in a) & b) unloaded P(3HB) nanospheres and nanospheres with 1 wt%, 5 wt% and 10 wt% tacrolimus, weight loss measurements in c) & d) unloaded P(3HB) microspheres and microspheres with 1 wt%, 5 wt% and 10 wt% tacrolimus (n=3; error bars= ±SD). [n=nanospheres, m=microspheres].

### I. pH changes

P(3HB) nanospheres and microspheres with and without encapsulated tacrolimus were immersed in PBS at pH 7.4 and pH changes over time was recorded. A gradual decrease in pH was observed in all 8 cases and the decrease was found to be more in the case of nanospheres, in general. Unloaded nanospheres reached a final pH of 6.1 while unloaded microspheres reached a final pH of 6.2 (Figure 4.21).

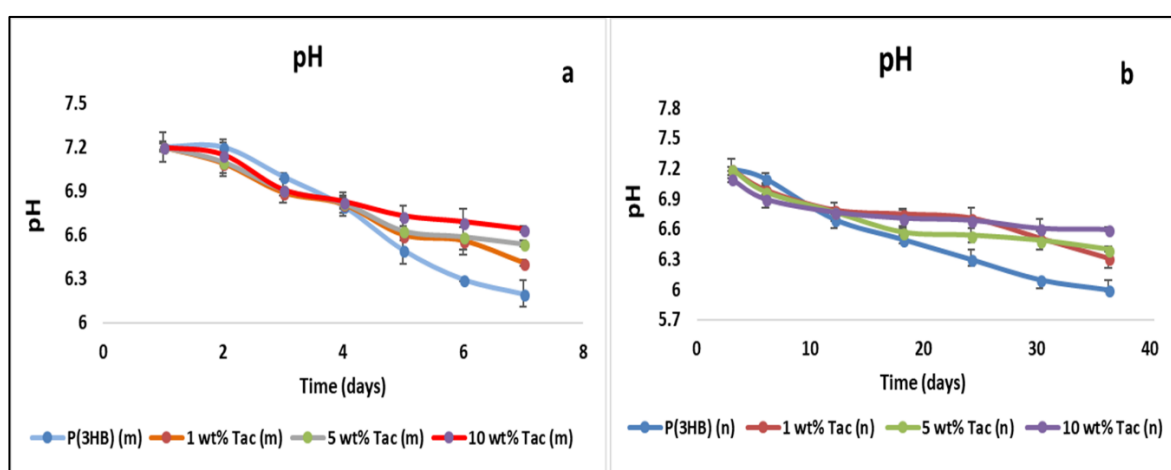


**Figure 4.21:** pH changes observed in the PBS solution containing a) unloaded and 1 wt%, 5 wt% and 10 wt% tacrolimus encapsulated nanospheres, b) unloaded and 1 wt%, 5 wt% and 10 wt% tacrolimus encapsulated microspheres, (n=3; error bars =  $\pm$ SD). [n=nanospheres, m=microspheres].

#### 4.2.7. Tacrolimus encapsulation and release kinetics

1 wt%, 5 wt and 10 wt% tacrolimus was encapsulated in P(3HB) nanospheres and microspheres and the experimental drug loading was quantified using HPLC method (Figure 4.22). Experimental drug loading and hence encapsulation efficiency was found to be higher in microspheres, in comparison with nanospheres. Encapsulation efficiency increased with increasing drug/ polymer ratio, or in other words drug loading. In the case of microspheres, encapsulation efficiency increased from  $61.2 \pm 4.18\%$  to  $69.8 \pm 1.9\%$  and

72.3 ± 2.21% between 1 wt%, 5 wt% and 10 wt% tacrolimus loading respectively. In the case of nanospheres, this was 59.8 ± 2.1%, 62.3 ± 2.01% and 65.8 ± 1.54% respectively.

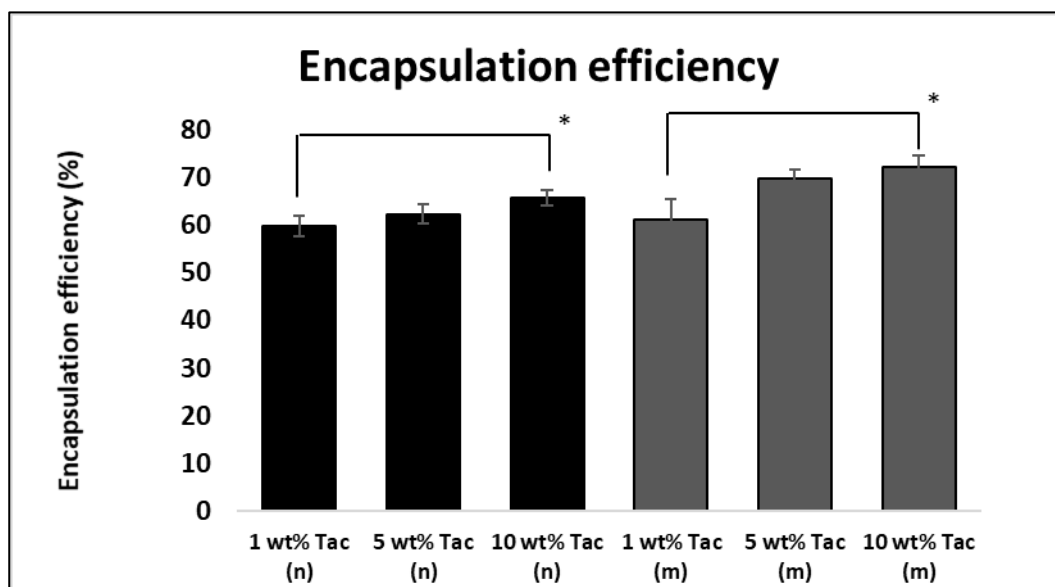


**Figure 4.22:** Representation of percentage of Tacrolimus encapsulated in P(3HB) nanospheres and microspheres at 1 wt%, 5 wt% and 10 wt% drug loading (n=3; error bars = SD). [n=nanospheres, m=microspheres].

#### 4.2.8. Release kinetics

Release kinetics of tacrolimus from both P(3HB) nanospheres and microspheres was identical in all the 6 cases, with a burst release up to 48 hours (Figure 4.23). Release from nanospheres were comparatively faster than microspheres, with a cumulative release of 71.2%, 73.1% and 76.2% from nanospheres encapsulated with 1 wt%, 5 wt% and 10 wt% tacrolimus. In the case of microspheres, this was 68.12, 70.37 and 72.3% respectively. Beyond 1440 hours, tacrolimus traces were not detectable as distinct peaks using HPLC, in all the cases. Maximum release was obtained from P(3HB) nanospheres with 10 wt% tacrolimus loading.

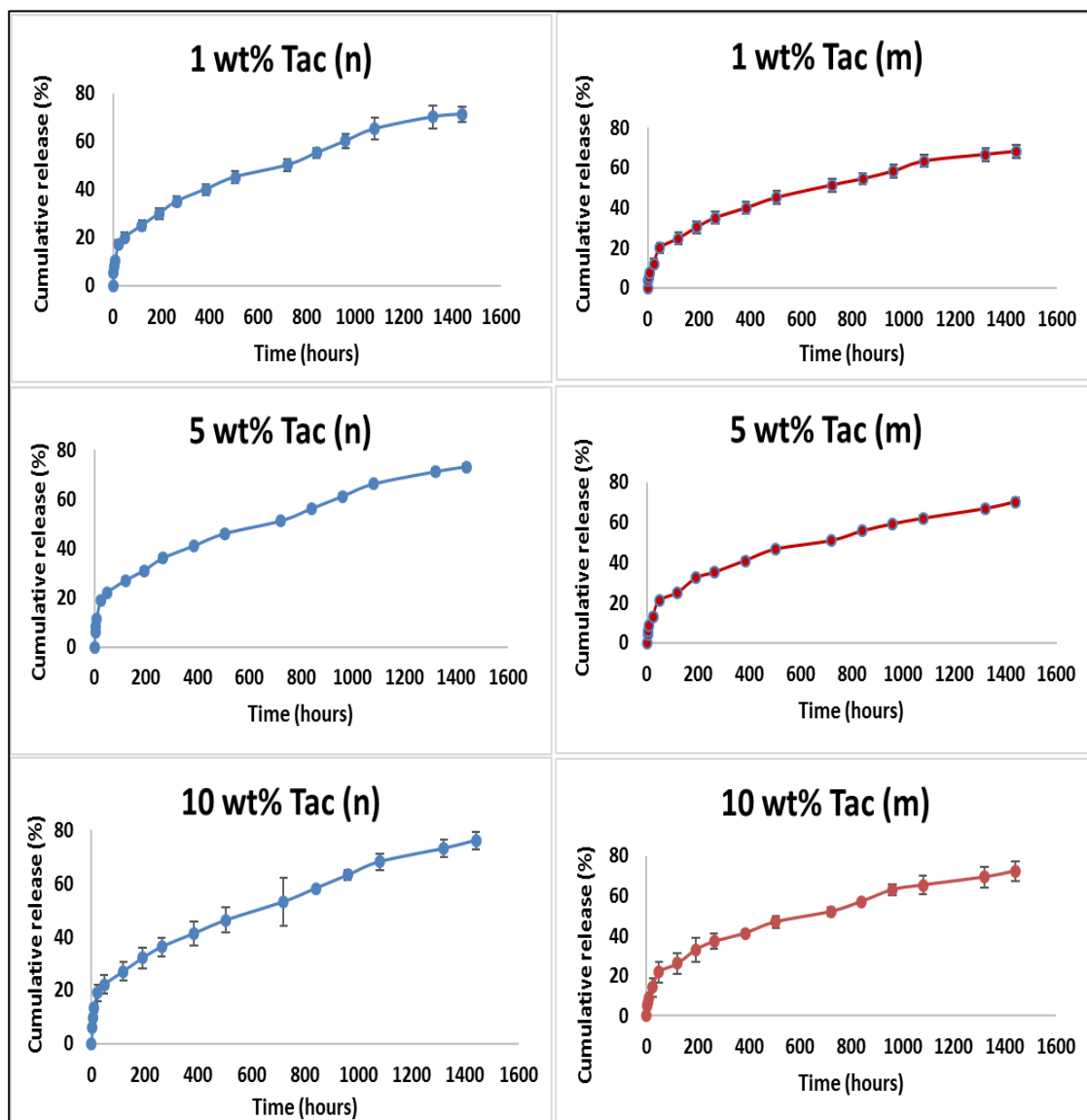


**Figure 4.23:** Tacrolimus release from P(3HB) nanospheres and microspheres with 1 wt%, 5 wt% and 10 wt% drug loading (n=3; error bars = SD).

The release data was fitted in models as described in section 2.2.11.  $R^2$  value of each of the linear regression was compared (**Table 4.6**). In all the 4 preparations, the release data was found to be more fitting to Higuchi model. All preparations showed 99% correlation in Higuchi model, suggesting a diffusion mode of release mechanism.

		P(3HB) nanospheres with tacrolimus loading of			P(3HB) microspheres with tacrolimus loading of		
Model	Parameters	1 wt%	5 wt%	10 wt%	1 wt%	5 wt%	10 wt%
Zero-order	$R^2$	0.914	0.911	0.920	0.894	0.890	0.895
	$Adj-R^2$	0.908	0.905	0.915	0.887	0.883	0.888
	<i>Slope</i>	0.0454	0.0456	0.0471	0.0447	0.0448	0.046
	<i>SSR</i>	769.43	808.96	767.55	938.45	985.46	995.75
First-order	$R^2$	0.977	0.977	0.983	0.965	0.965	0.970
	$Adj-R^2$	0.976	0.976	0.982	0.962	0.963	0.968
	<i>Slope</i>	-0.0004	-0.0004	-0.0004	-0.0003	-0.0003	-0.0004
	<i>SSR</i>	0.012	0.012	0.010	0.016	0.017	0.016
Higuchi	$R^2$	0.992	0.990	0.991	0.992	0.990	0.990
	$Adj-R^2$	0.992	0.989	0.990	0.991	0.989	0.990
	<i>Slope</i>	1.7391	1.803	1.856	1.7855	1.793	1.843
	<i>SSR</i>	69.98	93.60	88.14	72.64	89.22	90.28
Hixson-Crowell	$R^2$	0.962	0.962	0.970	0.945	0.944	0.950
	$Adj-R^2$	0.959	0.959	0.968	0.942	0.941	0.947
	<i>Slope</i>	-0.001	-0.001	-0.001	-0.001	-0.001	-0.001
	<i>SSR</i>	0.166	0.174	0.152	0.222	0.231	0.230
Korsmeyer-Peppas	$R^2$	0.990	0.988	0.984	0.992	0.990	0.993
	$Adj-R^2$	0.989	0.987	0.983	0.991	0.990	0.993
	<i>Slope</i>	0.393	0.377	0.365	0.448	0.437	0.417
	<i>SSR</i>	0.001	0.002	0.002	0.020	0.023	0.014

**Table 4.6:** Summary of model fitting for Rapamycin release from P(3HB) and PLLA microspheres.

All preparations were found to fit with Korsmeyer- Peppas model as well, suggesting a non-linearity between release and time, when approximated to 60%. The release exponents determined from the slope of the linear regression are represented in **table 4.7**. In all three cases of nanospheres, the release exponent was found to be less than 0.43, suggesting a Fickian case of diffusion. In the case of microspheres, the preparations with 1 wt% and 10 wt% tacrolimus loading had a release exponent between 0.43 and 0.85 (0.45 and 0.47

respectively). This suggests anomalous, non-Fickian mode of diffusion where heterogeneous factors are involved. Microspheres with 10 wt% tacrolimus loading was again found to release following Fickian mode, with a release exponent value of 0.41.

### **Part III P(3HB) microspheres as VEGF delivery systems in Collagen scaffolds for Cardiac regeneration**

#### **4.2.9. Process optimisation of spheres of different size ranges with encapsulated VEGF**

Process parameters obtained from initial optimisations (refer chapter 3) were used for the synthesis of microspheres and nanospheres with encapsulated VEGF. Initially process parameters corresponding to 3 different sizes of 500-1000nm, 5-15  $\mu\text{m}$  and 20-30  $\mu\text{m}$ , were tested with VEGF incorporation in the aqueous phase. Particle size and surface morphology of production was recorded (**Table 4.7**). The process parameters corresponding to size range 20-30  $\mu\text{m}$  gave microspheres with smooth surface morphology and sphericity, whereas the process parameters corresponding to the smaller sizes were not found to be suitable for VEGF incorporation as they were found to form agglomerates of smaller spheres. Therefore, new set of parameters had to be optimised. The parameters employed are as represented in **table 4.7**. 6.5 mg/mL of P(3HB) with a PVA concentration of 0.25 w/v% at stirrer speed of 800 rpm gave nanospheres with a mean diameter of 0.71  $\mu\text{m}$ . 9 mg/mL of P(3HB) with a PVA concentration of 0.5 w/v% at stirrer speed of 1000 rpm gave nanospheres with a mean diameter of 0.83  $\mu\text{m}$ . Microspheres prepared under the same conditions, but with a polymer concentration of 37.5 mg/mL gave microspheres with a mean diameter of 28  $\mu\text{m}$ .

Experiment. Number	P(3HB) concentration (mg/mL)	PVA concentration (%)	Stirrer Speed (RPM)	Morphology	Diameter ( $\mu\text{m}$ ) $\pm$ S. D
1	5	0.5	800	Irregular	-
2	6.5	0.5	800	Irregular	-
3	5	0.25	1200	Clustered, Porous	-
4	5	5	1200	Clustered, Porous	-
5	10	1	800	Clustered	-
6	10	0.5	1200	irregular	-
7	6.5	0.25	800	Smooth spheres	0.71 $\pm$ .018
8	9	0.5	1000	Smooth spheres	9.83 $\pm$ 1.1
9	37.5	0.5	1000	Smooth spheres	28 $\pm$ 5.3

**Table 4.7:** Process parameters employed for the synthesis of VEGF encapsulated microspheres and nanospheres.

#### 4.2.10. Surface morphology under SEM

Surface morphology of VEGF encapsulate microspheres and nanospheres were observed using SEM (**Figure 4.24**). It was found that the process parameters as established in chapter 3 for the synthesis of nanospheres in the range of 500-900 nm and microspheres in the size range of 5-15  $\mu\text{m}$  needed altering, when VEGF was incorporated in using the water in-oil-in- water emulsion technique. Particles of suitable morphology were achieved by reducing the concentration of PVA in the aqueous phase and reducing the concentration of P(3HB) and increasing stirrer speed in the second case. The process parameters corresponding to the highlighted images were chosen for incorporation in collagen 3D-scaffolds.

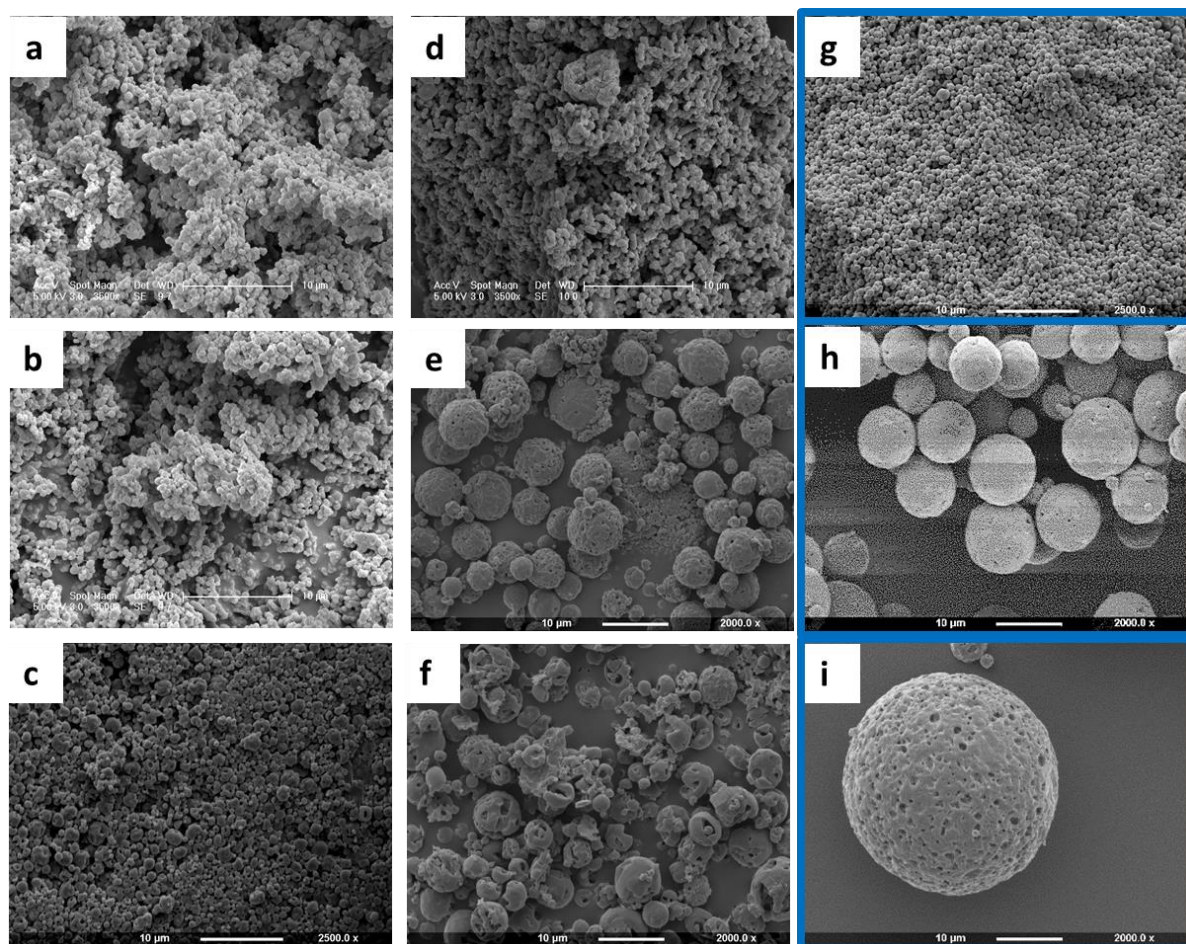


**Figure 4.24 a-i:** SEM images of spheres corresponding to experiment number 1-9 in table 4.7.

#### **4.2.11. Characterization of VEGF encapsulated particles chosen for incorporation in 3D-collagen scaffolds**

##### **4.2.11.1. Particle size analysis**

VEGF encapsulated microspheres and nanospheres were imaged using SEM and different magnifications of images were used to analyse particle size distribution using the ImageJ software (**Figure 4.27**).

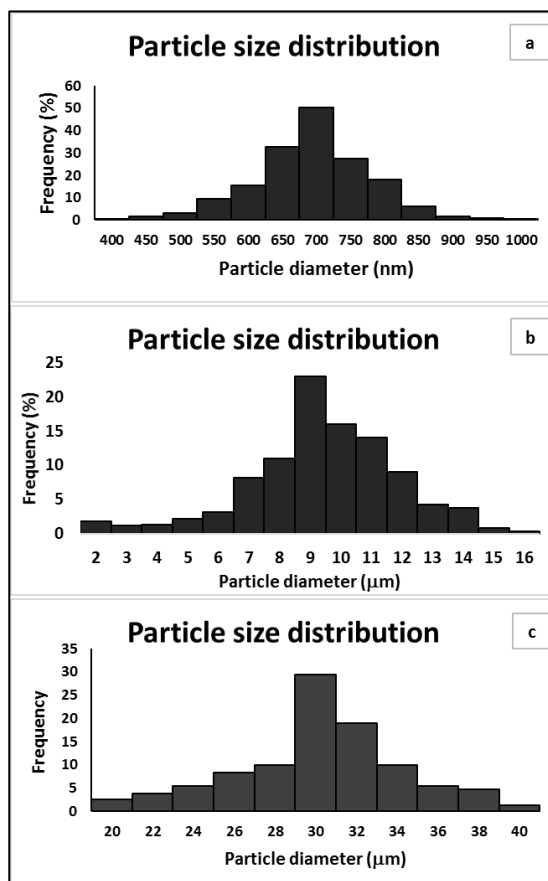


**Figure 4.25:** Particle size distribution of VEGF encapsulated a) nanospheres b) microspheres in the size range of 5-15  $\mu\text{m}$  and c) microspheres in the size range of 20-30  $\mu\text{m}$

The nanospheres had an average size of  $710 \pm 10.11$  nm, and the microspheres in the 5-15  $\mu\text{m}$  range had an average size of  $9.83 \pm 1.1$   $\mu\text{m}$  and microspheres in the size range of 20-30  $\mu\text{m}$  had an average size of  $28 \pm 5.3$   $\mu\text{m}$ .

#### 4.2.11.2. Porosity

Porosity of the VEGF encapsulated microspheres and nanospheres were calculated using the liquid displacement method and was compared with unloaded controls. Porosity of both unloaded and VEGF loaded particles were in the range of 60-80%. However, there was no correlation between porosity and VEGF encapsulation. While porosity increased very

slightly, from 67.9% to 69 % in the case of nanospheres with VEGF encapsulation, it decreased from 77% to 75% in the case of microspheres in the size range of 5-10  $\mu\text{m}$ . The microspheres in the size range of 20-30  $\mu\text{m}$  showed an increase of 0.9% in porosity with VEGF encapsulation. None of the differences observed were found to be statistically significant (**Figure 4.26**). It can be concluded that in all the preparations, the differences in porosity were considerably small and negligible.

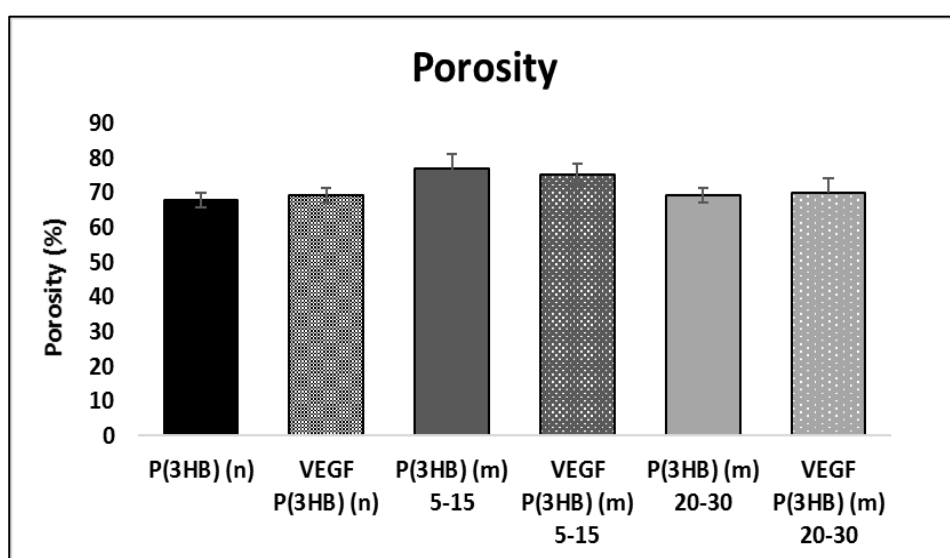


**Figure 4.26:** Porosity measurements of microspheres prepared with and without encapsulated VEGF ((n=3; error bars=  $\pm$ SD).

#### 4.2.11.3. Surface residual PVA

Surface residual PVA bound on microspheres and nanospheres prepared with and without encapsulated VEGF was estimated and expressed as percentage PVA per unite mass of nanosphere/ microsphere sample. It was found that in all the samples, the amount of surface residual PVA increased with VEGF loading. The amount of surface residual PVA was also found to be inversely proportional to the size of the particles. The unloaded nanospheres had 0.50 w/w% residual PVA on them which increased to 0.51 w/w% with

VEGF encapsulation. In the case of smaller microspheres, surface residual PVA increased from 0.30 w/w% to 0.31 w/w% and in the case of larger microspheres, surface residual PVA increased from 0.28 w/w% to 0.29 w/w% with VEGF encapsulation (**Figure 4.27**).

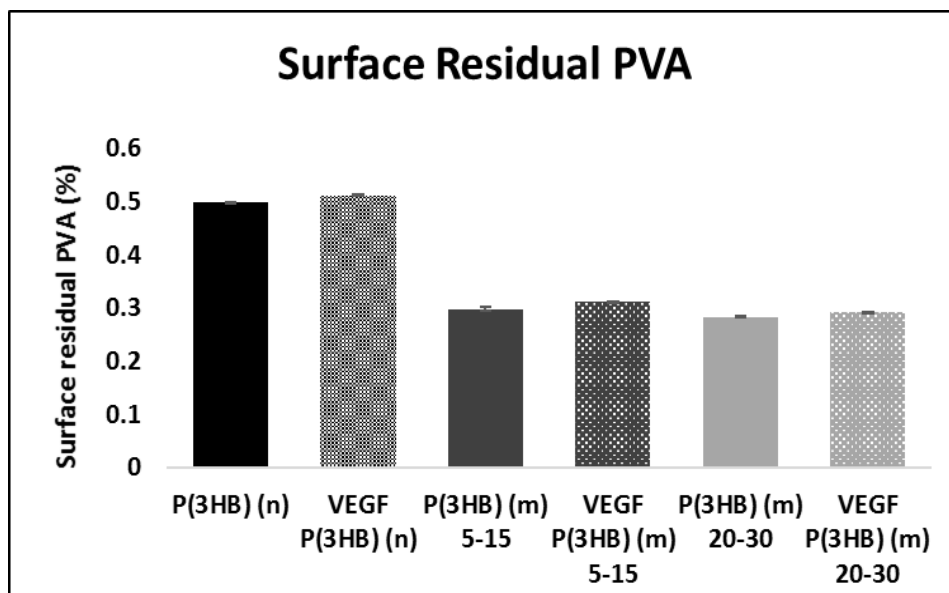


**Figure 4.27:** Surface residual PVA of unloaded and VEGF encapsulated P(3HB) microspheres and nanospheres (n=3; error bars=  $\pm$ SD).

#### 4.2.11.4. Hydrophobicity

Hydrophobicity, expressed as a function of the amount of Rose Bengal dye bound on the particles at saturation, was found to decrease with VEGF encapsulation, when compared to unloaded particles (**Figure 4.28**). When compared with unloaded preparations, VEGF loaded preparations were found to have a reduced amount of Rose Bengal dye bound on their surfaces. The differences in each case were statistically significant. Unloaded microspheres in the size range of 20-30  $\mu$ m was found to have 5.12  $\mu$ g/mg of Rose Bengal dye bound on their surface.

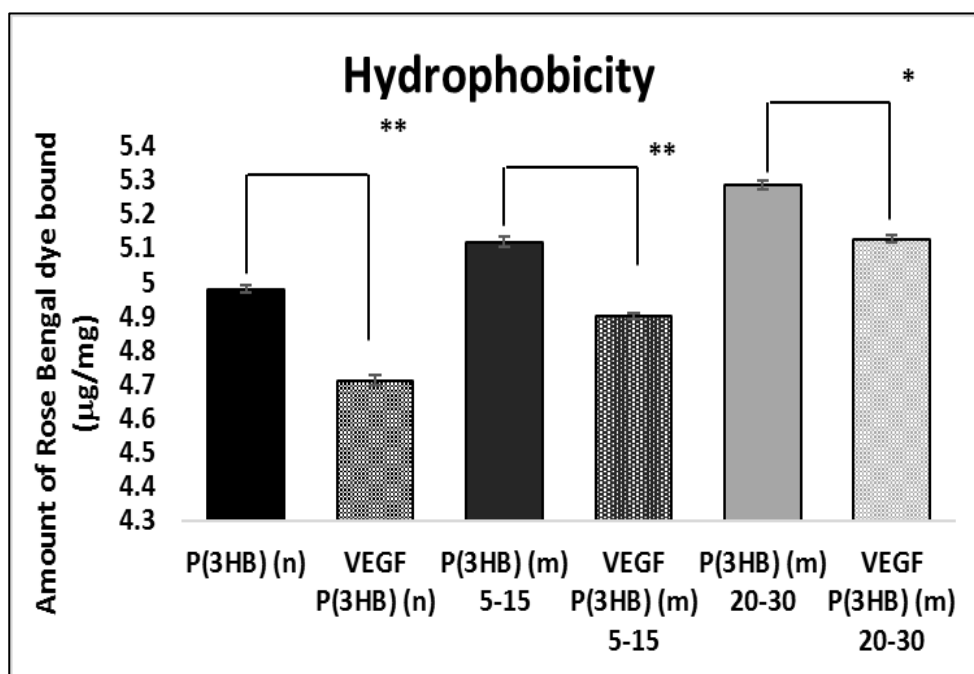


**Figure 4.28:** Hydrophobicity expressed as a function of amount of Rose Bengal dye bound at saturation, for unloaded and VEGF encapsulated microspheres and nanospheres (n=3, error bars=  $\pm$ SD).

#### 4.2.11.5. Protein adsorption

The amount of protein bound on the surface of VEGF encapsulated nanospheres and microspheres were found to be lower than the unloaded controls in all the three cases (**Figure 4.29**).

In the case of nanospheres, amount of protein adsorbed decreased from  $332.12 \pm 8.123$   $\mu$ g/mg to  $32.67 \pm 2.89$   $\mu$ g/mg. In the case of smaller microspheres, the change was from  $299.31 \pm 5.313$   $\mu$ g/mg to  $272.00 \pm 21.37$   $\mu$ g/mg and in the case of larger microspheres, the change was from  $291.34 \pm 13.91$   $\mu$ g/mg to  $269.13 \pm 2.12$   $\mu$ g/mg.

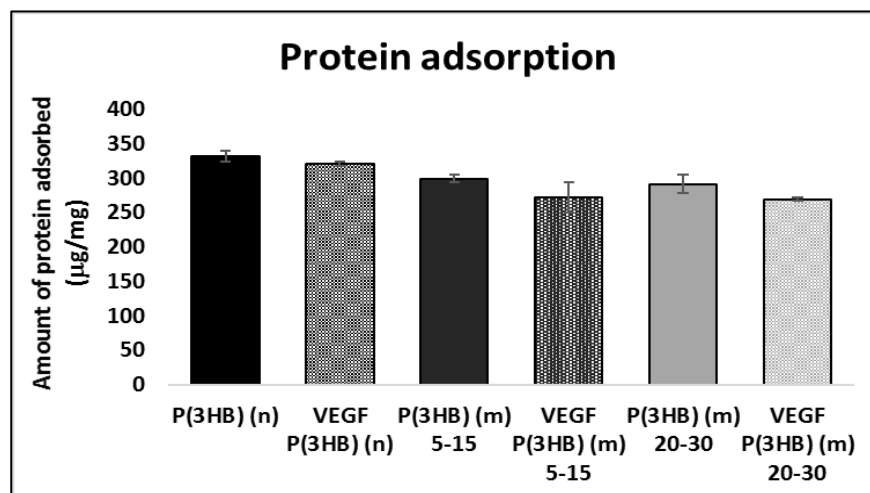


**Figure 4.29:** Protein adsorption on the surface of unloaded and VEGF encapsulated nanospheres and microspheres (n=3; error bars=  $\pm$  SD).

#### 4.2.11.6. In vitro degradation studies

##### I. Water uptake and weight loss

Changes in water uptake and weight loss with VEGF encapsulation was observed to be the same in all three cases (**Figure 4.30**). Water uptake and weight loss over the period of 36 days was found to have been increased in all the cases. Amongst the unloaded particles, the nanospheres were found to experience the highest water uptake and weight loss, of 459% and 16.6% respectively. These increased to 472% and 17.17% respectively, with VEGF incorporation. In the case of smaller microspheres, the water uptake increased from 444% to 469% and weight loss increased from 16.4% to 16.9%. In the case of larger microspheres, the water uptake increased from 405% to 457% and weight loss increased from 11.1% to 15.9%.

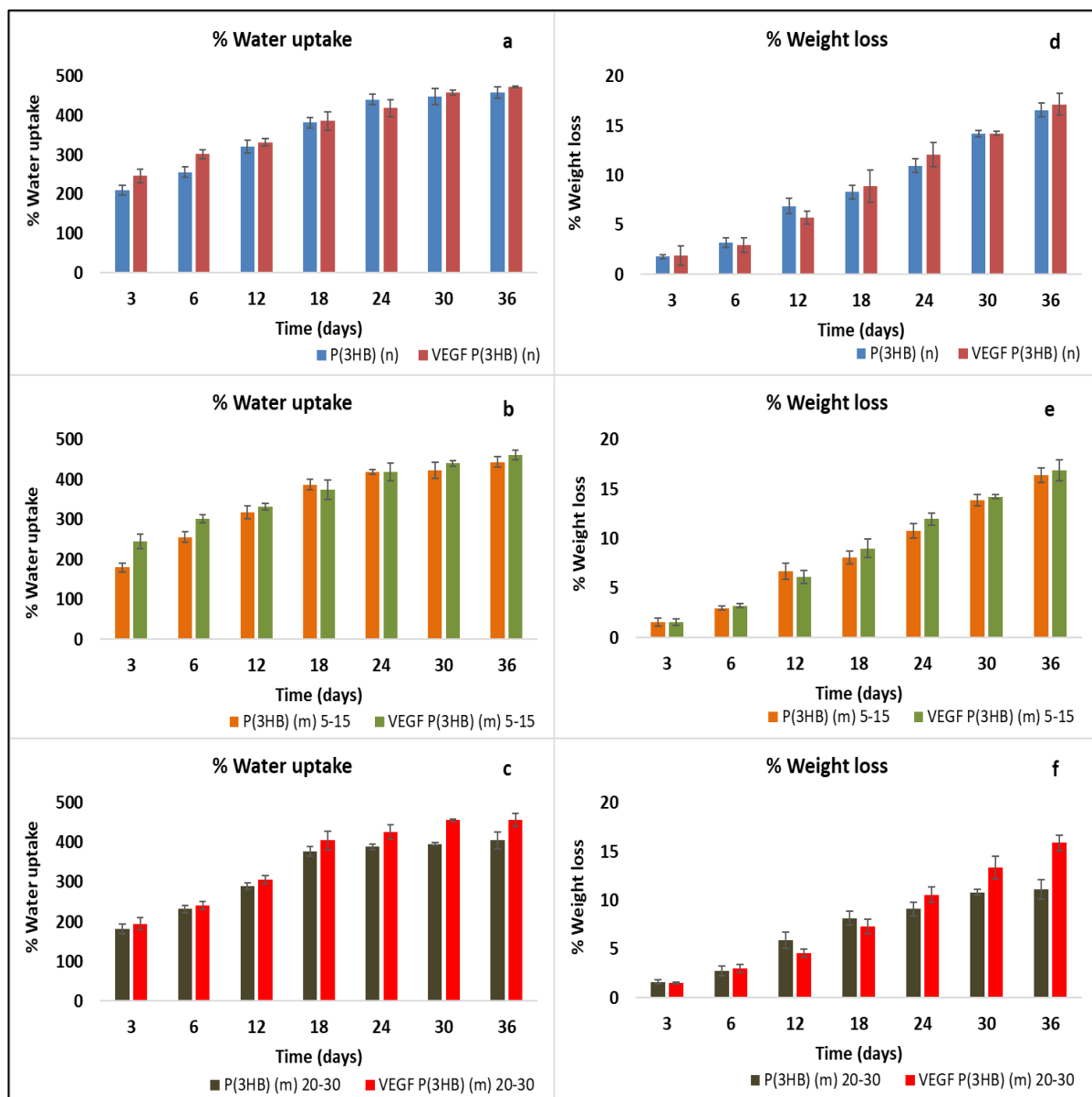


**Figure 4.30:** Water uptake measurements and weight loss measurements over 36 days in a & b) nanospheres with and without encapsulated VEGF, c & d) microspheres of 20-30  $\mu\text{m}$  with and without encapsulated VEGF and e & f) microspheres of 5-15  $\mu\text{m}$  with and without encapsulated VEGF (n=3; error bars=  $\pm$  SD).

### I. pH changes

pH changes for unloaded and VEGF loaded particles over the period of 36 days compared with their unloaded counterparts (Figure 4.31).

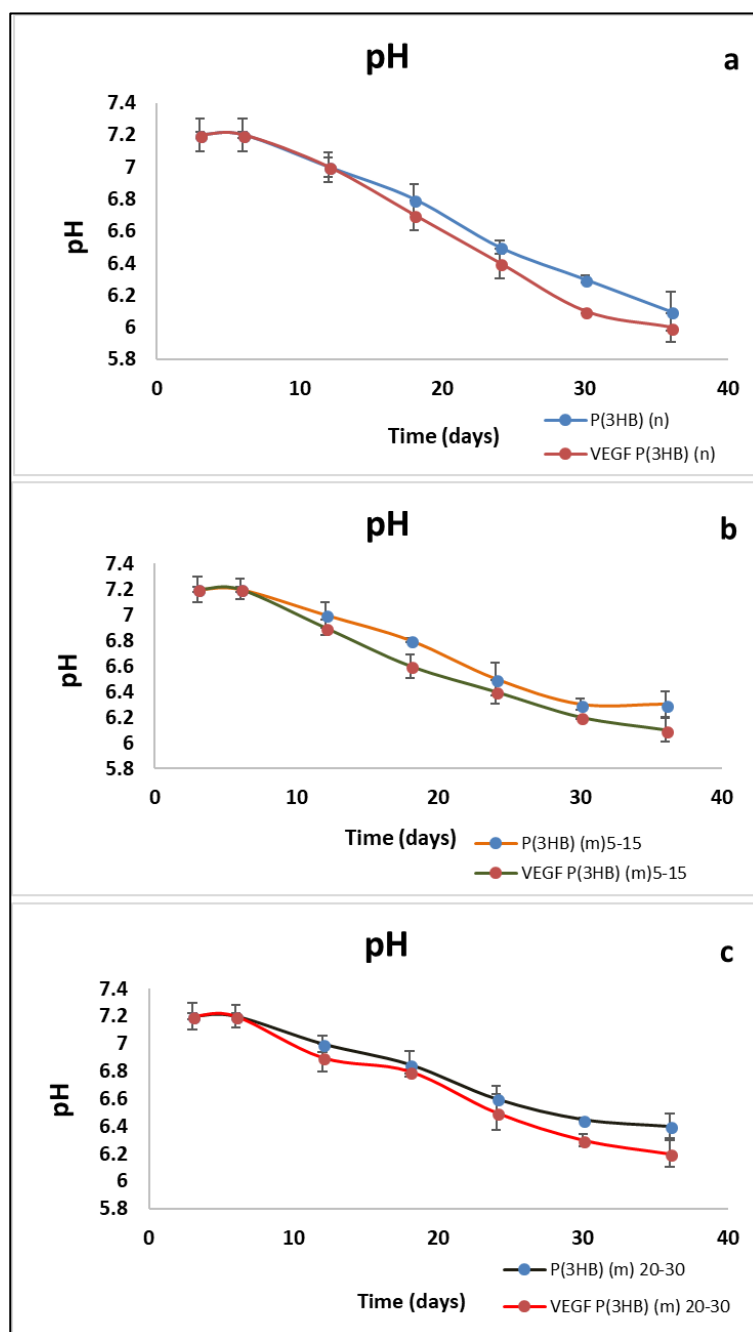


**Figure 4.31:** Comparison of pH changes with and without encapsulated VEGF in a) nanospheres, b) microspheres of 5-15  $\mu\text{m}$  and c) microspheres of 20-30  $\mu\text{m}$  ( $n=3$ ; error bars=  $\pm$  SD).

pH changes for unloaded and VEGF loaded particles over the period of 36 days were between 7.4 to 6. Decrease in pH was found to be inversely proportional with particle size. Compared to their unloaded controls, VEGF loaded particles were found to result in higher

reduction in pH values of the surrounding medium. The pH of the surrounding medium containing the unloaded nanospheres reduced from 7.4 to 6.1 over 36 days while the pH of medium containing VEGF encapsulated nanospheres reduced to 6. In the case of smaller microspheres, the pH of the medium dropped to 6.3 for unloaded microspheres and 6.1 for VEGF loaded microspheres. In the cases of larger microspheres, the pH of the medium containing unloaded microspheres dropped to 6.4 and that of the VEGF loaded microspheres dropped to 6.2.

#### **4.2.12. Incorporation of VEGF encapsulated microspheres and nanospheres in Collagen scaffolds**

##### **4.2.12.1. Characterization**

###### **I. Surface morphology analysis under SEM**

The microspheres and nanospheres thus produced were incorporated into collagen scaffolds by Ms. Rabia Nazir at Oxford University. They were loaded into a 28 wt% collagen slurry and press moulded into scaffolds of 12mm diameter and 2-3 mm thickness. Nanospheres of a size range 500-900 nm were well incorporated in the scaffold with a uniform distribution. Microspheres of the size range 5-15  $\mu\text{m}$  were also satisfactorily incorporated in the scaffolds whereas microspheres of the size range 20- 30  $\mu\text{m}$  formed clumped structures in the scaffold (**Figure 4.32**). Therefore, collagen scaffolds incorporated with the 20-30  $\mu\text{m}$  sized microspheres were excluded from the study.

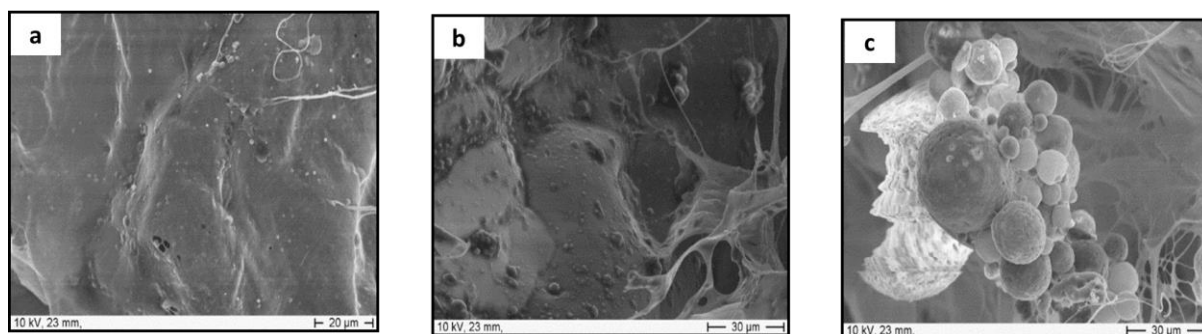


**Figure 4.32:** SEM images of collagen scaffolds embedded with a) nanospheres, b) microspheres of size range 5-15  $\mu\text{m}$  and c) microspheres of size range 20-30  $\mu\text{m}$ .

### I. Swelling studies

Swelling studies were conducted by immersing empty and particle embedded collagen scaffolds in PBS over a period of 36 days (**Figure 4.33**).

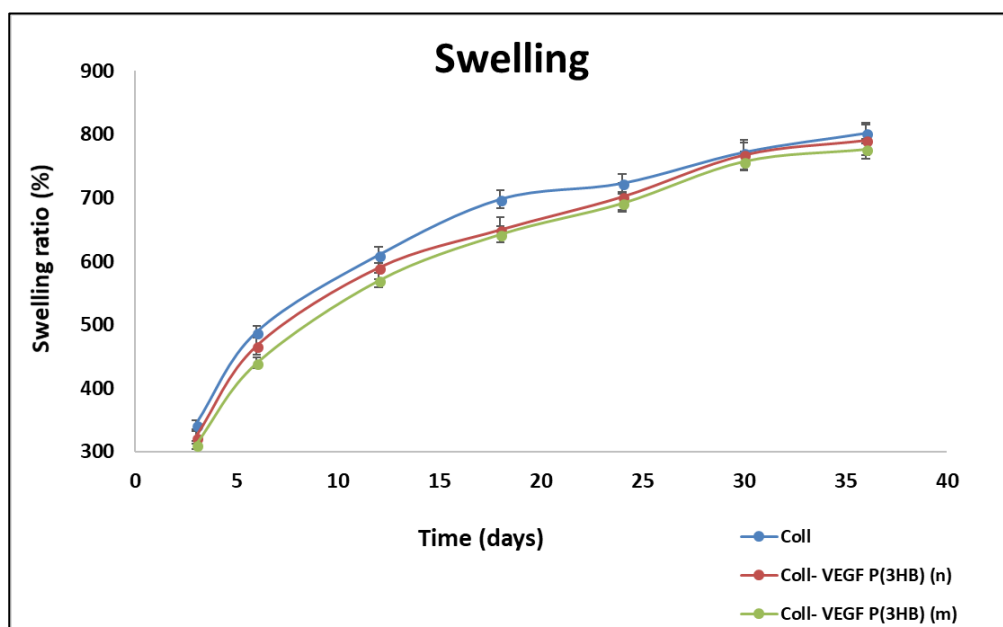


**Figure 4.33:** Comparison of swelling ratio of collagen scaffolds with particle embedded collagen scaffolds ( $n=3$ , error bars= $\pm$  SD)

The collagen scaffolds were found to uptake as much as 800% of their volume of water over this period. Compared to particle embedded scaffolds, empty scaffolds were found to have

a higher swelling ratio. In first three days, empty collagen scaffolds absorbed  $343 \pm 3.12\%$  and this increased to a maximum of  $802 \pm 7.9\%$  in 36 days. Compared to the empty controls, particle embedded scaffold absorbed a lesser amount of water. The nanospheres embedded scaffolds absorbed  $323 \pm 4.12\%$  in first three days and  $791 \pm 6.8\%$  water by the end of 36 days. The microsphere embedded scaffolds absorbed and  $311 \pm 4.12\%$  water in the first 3 days and  $777 \pm 8.72\%$  water in 36 days.

#### 4.2.13. Encapsulation efficiency

Encapsulation efficiency of the microspheres and nanospheres were quantified using VEGF ELISA tests. This was done before and after they were incorporated in the collagen scaffold as the processing conditions may have influenced the amount of drug remaining in the particles after they were embedded in the scaffolds (**Figure 4.34**).

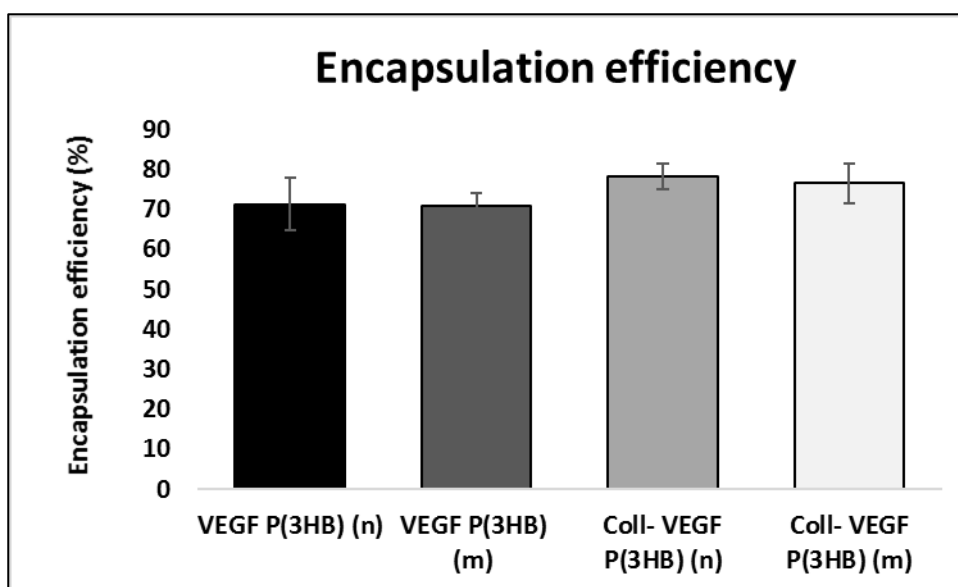


**Figure 4.34:** Encapsulation efficiency of VEGF in nanospheres and microspheres before and after being embedded in collagen scaffolds ( $n=3$ , error bars  $\pm$  SD).

The amount of drug encapsulated was found to reduce once the particles were embedded in the scaffolds, probably due to processing. The encapsulation efficiency of P(3HB) microspheres was found to be  $78.32 \pm 3.21\%$  and on being embedded in the scaffolds, the encapsulation efficiency was found to have reduced by 7%, to  $71.32 \pm 6.6\%$ . In the case of nanospheres, encapsulation efficiency was found to be  $76.52 \pm 5\%$  and it was found to reduce to  $70.70 \pm 3.5\%$ .

#### **4.2.14. Release kinetics**

To assess release kinetics, VEGF encapsulated nanospheres, microspheres, and collagen scaffolds embedded with VEGF encapsulated nanospheres and microspheres were immersed in PBS at 37 °C and amount of VEGF in periodically drawn samples were quantified using the VEGF ELISA assay (**Figure 4.35**). The release from VEGF encapsulated nanospheres were found to be faster than the release from VEGF encapsulated microspheres. VEGF release from nanospheres lasted up to 40 days and VEGF release from microspheres lasted up to 48 days, beyond which traces of VEGF were not detectable using the ELISA assay. A cumulative release of  $98.23 \pm 1.98\%$  was achieved from VEGF encapsulated nanospheres whereas a cumulative release of  $94.12 \pm 1.21\%$  was achieved from VEGF encapsulated microspheres. Release from microspheres were found to have a burst release in the first 48 hours.

However, VEGF release from microspheres embedded in collagen scaffolds did not exhibit a burst release. VEGF release from the collagen scaffolds embedded with nanospheres lasted up to 44 days and VEGF release from microsphere encapsulated collagen scaffolds lasted up to 48 days. The maximum cumulative release from VEGF encapsulated nanospheres, collagen scaffolds embedded with the same, VEGF encapsulated

microspheres, and collagen scaffolds embedded with the same were found to be 96.21, 98.23, 93.4 and 99.27% respectively.

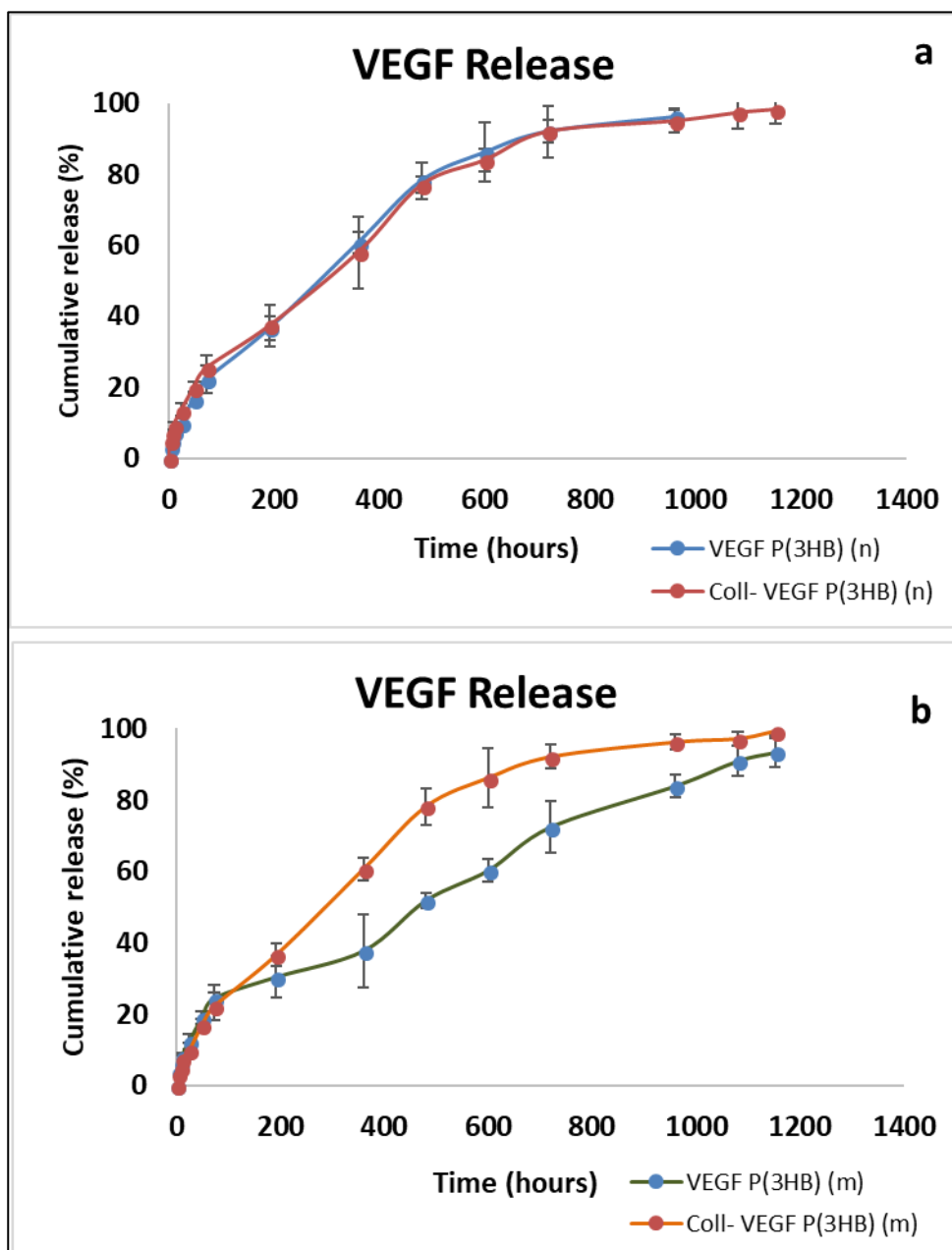


**Figure 4.35:** Comparison of VEGF release profile from a) VEGF encapsulated P(3HB) nanospheres and collagen scaffold embedded with the same, b) VEGF encapsulated P(3HB) microspheres and collagen scaffold embedded with the same (n=3, error bars=  $\pm$  SD)

The release from VEGF encapsulated nanospheres were found to be faster than the release from VEGF encapsulated microspheres. VEGF release from nanospheres lasted up to 40 days and VEGF release from microspheres lasted up to 48 days, beyond which traces of VEGF were not detectable using the ELISA assay. A cumulative release of  $98.23 \pm 1.98\%$  was achieved from VEGF encapsulated nanospheres whereas a cumulative release of  $94.12 \pm 1.21\%$  was achieved from VEGF encapsulated microspheres. Release from microspheres were found to have a burst release in the first 48 hours.

However, VEGF release from microspheres embedded in collagen scaffolds did not exhibit a burst release. VEGF release from the collagen scaffolds embedded with nanospheres lasted up to 44 days and VEGF release from microsphere encapsulated collagen scaffolds lasted up to 48 days. The maximum cumulative release from VEGF encapsulated nanospheres, collagen scaffolds embedded with the same, VEGF encapsulated microspheres, and collagen scaffolds embedded with the same were found to be 96.21, 98.23, 93.4 and 99.27% respectively.

The release data was fitted in models as described in section 2.2.11.  $R^2$  value of each of the linear regression was compared (**Table 4.8**). The release data was found to be most fitting with first- order release for all the four preparations with 99% correlation, except free microspheres with encapsulated VEGF ( $R^2= 0.956$  for first- order). This means, the drug release was dependent on the concentration of drug. The data for free microspheres was found to fit better with the Hixson- Crowell model, with 98.3 % correlation. However, considering Hixson- Crowell model assumes dissolution and reduction in surface area of the particles, whether this model can be considered in this scenario is questionable (VEGF release was carried out for a maximum of 48 days and this period is too short for P(3HB) to

have undergone any substantial erosion). The release data was found to fit with Higuchi and First-order as well, (98.3% and 95.6% correlation).

		P(3HB)nanospheres with VEGF		P(3HB)microspheres with VEGF	
Model	Parameters	Free	Embedded in Collagen	Free	Embedded in Collagen
Zero-order	$R^2$	0.935	0.907	0.973	0.902
	$Adj-R^2$	0.929	0.900	0.971	0.895
	Slope	0.1113	0.0874	0.0775	0.0904
	SSR	1103.79	1983.39	424.02	2239.31
First-order	$R^2$	0.991	0.990	0.956	0.994
	$Adj-R^2$	0.990	0.989	0.953	0.993
	Slope	-0.0015	-0.0014	-0.0009	-0.0015
	SSR	0.026	0.055	0.092	0.026
Higuchi	$R^2$	0.986	0.984	0.983	0.981
	$Adj-R^2$	0.985	0.983	0.981	0.980
	Slope	3.4645	3.131	2.679	3.241
	SSR	231.56	332.78	270.30	429.45
Hixson-Crowell	$R^2$	0.991	0.987	0.985	0.989
	$Adj-R^2$	0.990	0.986	0.984	0.988
	Slope	-0.0034	-0.003	-0.0022	-0.0032
	SSR	0.138	0.289	0.184	0.293
Korsmeyer-Peppas	$R^2$	0.871	0.897	0.841	0.895
	$Adj-R^2$	0.858	0.889	0.827	0.886
	Slope	39.45	39.87	33.18	41.53
	SSR	1964.138	1936.385	2220.728	2150.454

**Table 4.8:** Summary of model fitting for VEGF release from free P(3HB) nanospheres and microspheres and P(3HB) nanospheres and microspheres embedded in collagen.

### 4.3. Discussion

#### 4.3.1. Comparison of rapamycin encapsulated P(3HB) and PLLA microspheres

##### 4.3.1.1. The effect of process parameters on characteristics of microspheres

PLLA and P(3HB) are two widely researched polymers in drug delivery. Although P(3HB) is a recent successor to PLLA in active drug delivery research, the manipulability of it due to the availability of a multitude of monomer units make it an interesting biopolymer. This study investigated into the process parameters influencing microsphere formation using P(3HB) and PLLA. The microspheres fabricated were characterised for their morphology, size distribution, porosity, hydrophobicity and protein adsorption. P(3HB) microspheres of the size range 1-8  $\mu\text{m}$  and PLLA microspheres of the size range 1-5.5  $\mu\text{m}$  were obtained. In the case of PLLA, the polymer with the least molecular weight was found to produce the smallest spheres, corroborating the argument regarding molecular weight and viscosity on the size distribution of particles (Honary *et al.*, 2009; Ansary *et al.*, 2014).

Microspheres of a smaller size ensure high surface area-to-volume ratio (Freiberg and Zhu, 2004). Microspheres were successfully synthesized using PLLA of molecular weight 30-50 kDa and non-hydrolysed P(3HB) (~280 kDa). Molecular weight although cannot be stated as the single contributing parameter in microsphere fabrication, has a significant effect on the formation of spheres (O'Donnell and McGinity, 1997; Freitas, Merkle and Gander, 2005; Li, Rouaud and Poncelet, 2008). Hydrolysis of P(3HB) was carried out to obtain P(3HB) of lower molecular weight. However, the microspheres formed of hydrolysed polymer were widely polydispersed with lumps of polymer intermittently adorned with well-formed

microspheres. P(3HB) hydrolysed to 8 and 12 hours had high polydispersity index (3.71 and 4.18 respectively). This could have been the reason for obtaining highly polydispersed microspheres in this case. This indicated that further optimisation of the hydrolysis process was imperative.

However, both PLLA and P(3HB) at a concentration of 5mg/mL of chloroform presented excellently formed spheres, the latter being slightly larger than the former. This can be interpreted as a correlation between molecular weight and particle size, since all the other processing conditions were same for both P(3HB) and PLLA. The molecular weight range of PLLA is 30-50 kDa which is smaller than P(3HB) (~280 kDa). Hence, the independent variable here is the molecular weight of the polymers which effectively contributes to the viscosity and rheology of the emulsion, and subsequently, size of emulsion droplets.

In the case of polymers that undergo bulk erosion as opposed to surface erosion, molecular weight is a key determinant of drug release. This is because, the diffusivity of the drug in this case depends on the formation of water channels, which result from the 'loosening' of oligomers and monomers from the particles, as a result of bulk degradation (Kim and Pack, 2006). An increase in molecular weight therefore will suggest a decrease in diffusivity. However, in the case of surface eroding polymers, their inherent hydrophobicity makes the inner layers resistant to water penetration, while only the particle/ water interphase undergoes degradation. This mode of delivery is more controlled and independent of molecular weight, which is a great advantage when processing natural polymers (Freitas, Merkle and Gander, 2005; Kim and Pack, 2006; Hossain, Patel and Ahmed, 2014). PLLA, is a bulk eroding polymer, while P(3HB) is a surface eroding polymer.

Porosity of the microspheres can impact the release kinetics of the encapsulated drug. Controlled drug release can be achieved by optimising these contributing factors during the processing stage. Porosity of controlled drug delivery system is a key determinant of sustained delivery. P(3HB) based drug delivery system enable drug release by surface erosion under the influence of physiological changes in the immediate biological milieu, controlled by pH. However, release via means of only surface or bulk erosion may not suffice for the required dosage. Under these circumstances, porosity of the microspheres become important in allowing the drug molecules to seep through and be released out. The optimization studies revealed that PLLA microspheres were about 15% porous whereas P(3HB) microspheres amounted to a significant 35% porosity. However, the rapamycin encapsulated microspheres of both the polymers exhibited much higher porosity. Rapamycin encapsulated PLLA microspheres exhibited porosity in the range of ~50- 56% with a direct correlation between porosity and drug loading. Rapamycin encapsulated P(3HB) microspheres exhibited similar trend, however with a very high porosity range of ~64-71% porosity. The microspheres without rapamycin had uniformly arranged polymer matrices, thus resulting in a closely packed structure which may have reduced porosity. But the presence of rapamycin may have presented oddities in the matrix, thus resulting in comparatively less packed matrices leading to increased porosity. This well explains the increase in porosity with drug loading. Porous systems increase the diffusivity of drug molecules from microspheres matrices, as with porosity, 'diffusion pathway length' for the drug decrease. This effect of exemplified in a study by Klose *et al.*, 2006, who compared the drug release kinetics of Lidocaine from PLGA microspheres of varying porosity. This

study concluded that, the presence of pores increases mobility and diffusivity of the drug (Klose *et al.*, 2006).

#### **4.3.1.2. Encapsulation efficiency and drug release**

Encapsulation efficiency of rapamycin in both P(3HB) and PLLA microspheres was found to increase with drug loading. In the case of 5 wt% drug loading, P(3HB) had an increased encapsulation efficiency (62.37%), in comparison with PLLA (58.58%). Without statistical optimisation of all the contributing parameters, it is impossible to establish the effect of molecular weight and concentration of the oil phase on encapsulation efficiency. In general, increasing the viscosity of the oil phase will produce viscous emulsion droplets, which resists the partition of drug molecules into the aqueous phase (Sharma *et al.*, 2016). This explains the liner relationship of drug loading with encapsulation efficiency. Along the same lines, an increase in molecular weight results in an emulsion with increased viscosity, which explains the higher encapsulation efficiency of P(3HB) microspheres in comparison with PLLA microspheres. Another reason for this phenomenon is the availability of more polymer for the drug molecules to bind with, per unit volume, when concentration is increased. Sharma *et al.*, in their study on process parameters in formulating PLGA: PLA nanospheres observed a similar trend, wherein, on increasing the polymer concentration from 10 to 20 w/v%, the encapsulation efficiency of paclitaxel in these nanospheres were increased from 77.5 to 94.3% (Sharma *et al.*, 2015).

Drug release kinetics in the case of both P(3HB) and PLLA was found to be have a burst release of about 11%, by 48 hours. This can be considered a reasonable amount of burst release, especially in the case of PLLA, as bulk eroding polymers are expected to have a burst release up to 50% (Kim and Pack, 2006). After first 48 hours, both P(3HB) and PLLA

microspheres exhibited a steady release of Rapamycin. P(3HB) microspheres exhibited a slightly faster release when compared to PLLA microspheres, with 5 wt% Rapamycin loaded PLLA microspheres releasing up to 22.70% and 10 wt% rapamycin loaded PLLA microspheres releasing up to 22.97% in 30 days. This was found to be 19.01% and 22.02% respectively, in the case of 5 wt% and 10 wt% loaded PLLA microspheres. P(3HB) microspheres produced were found to have increased porosity in comparison with PLLA microspheres, which would have resulted in the faster release of rapamycin. However, PLLA microspheres were smaller than P(3HB) microspheres, which would mean their diffusion pathway length for rapamycin to elute out was smaller. This might have resulted in the release rate in both the cases not being significantly different.

The drug release data was fitted to 5 different models frequently published in literature namely, zero- order, first- order, Higuchi, Hixson-Crowell and Korsmeyer- Peppas. The release data was found to fit best with Higuchi model, as is expected of polymeric matrix systems with poorly soluble drug such as rapamycin (Costa and Sousa Lobo, 2001). This is explained well considering both PLLA and P(3HB) microspheres were of considerable porosity, which is a contributing parameter in Higuchi diffusion model. Higuchi model implies diffusion as the release mechanism and fitting 60% of release data to Korsmeyer- Peppas gave insights into the type of diffusion. In all the 4 cases, the release exponent was found to be less than 0.43, which suggests the diffusion to follow Fickian mode. The release data also gave good correlation with Korsmeyer- Peppas for all the formulations tested, and this indicates a non- linearity of release with time (Parhizkar *et al.*, 2016). However, this model assumes the reduction of surface area of the DDS with time and considering the drug release profiles analysed here were only up to a maximum of 36 days, whether the

effects of change in surface area here can be considered is questionable. However, the *in vitro* degradation studies indicate up to 14.3% weight loss in the case of PLLA and 13.8% weight loss in the case of P(3HB) within 36 days. Therefore, surface erosion as a contributing release mechanism cannot be neglected.

#### **4.3.2. Comparison of tacrolimus encapsulated P(3HB) microspheres and nanospheres**

P(3HB) nanospheres and microspheres were successfully synthesised with 1, 5 and 10 wt% drug loading of tacrolimus. The particle size increased with drug loading.

An interesting observation made with respect to tacrolimus encapsulated P(3HB) spheres of two different sizes were their differences in *in vitro* degradation. As indicated by weight loss, and pH changes in the surrounding media. Nanospheres were found to undergo slower degradation than microspheres. This is similar to the degradation behaviour of PLGA microspheres of different sizes, as studied by Kok et al., in determining the effect of particle size on drug loading and Release Kinetics of Gefitinib-Loaded PLGA Microspheres (Kok et al., 2016). PLGA is a bulk eroding polymer and once the degradation is initiated, it undergoes autocatalysis, from within the microsphere core (Kocbek et al., 2007; Ahmed et al., 2016). Larger microspheres with reduced crystallinity are more prone to initiation of degradation and hence their faster rate of degradation is expected in bulk eroding polymers. In the case of P(3HB), this effect is thought to have resulted from the decreased crystallinity, as well as increased porosity of the microspheres, which would have enhanced hydrolytic degradation.

Experimental drug loading and hence encapsulation efficiency was found to be higher in microspheres, in comparison with nanospheres. This could be due to the reduced diffusivity of drug to the aqueous phase from emulsion droplets, with increasing viscosity. Encapsulation efficiency increased with increasing drug/ polymer ratio, or in other words drug loading. Increasing drug polymer ratio would indicate an increased content of drug molecules per unit of polymer in given volume. In the case of microspheres, encapsulation efficiency increased from  $61.2 \pm 4.18\%$  to  $69.8 \pm 1.9\%$  and  $72.3 \pm 2.21\%$  between 1 wt%, 5 wt% and 10 wt% tacrolimus loading respectively. In the case of nanospheres, this was  $59.8 \pm 2.1\%$ ,  $62.3 \pm 2.01\%$  and  $65.8 \pm 1.54\%$  respectively.

Release kinetics of tacrolimus from both P(3HB) nanospheres and microspheres was identical in all the 6 cases, with a burst release up to 48 hours. Release from nanospheres were comparatively faster than microspheres, with a cumulative release of 71.2%, 73.1% and 76.2% from nanospheres encapsulated with 1 wt%, 5 wt% and 10 wt% tacrolimus. In the case of microspheres, this was 68.12, 70.37 and 72.3% respectively. Beyond 1440 hours, tacrolimus traces were not detectable as distinct peaks using HPLC, in all the cases. Maximum release was obtained from P(3HB) nanospheres with 10 wt% tacrolimus loading. Solubilised form of tacrolimus is only capable of extending release up to 5-14 days and therefore, the sustained release extending up to a month (Tajdaran *et al.*, 2015), from P(3HB) spheres is quite promising.

With regards to drug release kinetics, two antagonistic effects can be observed. Since the surface to volume ratio of particles is higher in the case of nanospheres, this would mean that, for a given mass, there is more efflux of drug into the surrounding media from nanospheres than microspheres. This is especially relevant in the case of surface eroding

polymers such as P(3HB), where drug release is primarily dependant on a degradation behaviour that is analogous to 'peeling' off surface layers. The second phenomenon is degradation, which is influenced by crystallinity of the spheres. Since larger spheres have lower thermal properties, they can be expected to degrade faster, resulting in faster release of drug molecules. Drug release rate is a combinatorial effect of these two factors.

The release data when fitted to zero- order, first- order, Higuchi, Hixson-Crowell and Korsmeyer- Peppas models, was found to have the best fit with Higuchi model, as in the case of rapamycin release. All the 6 formulations tested had 99% correlation in Higuchi model, suggesting diffusion as the mechanism of mass transfer. This is typical of porous polymeric matrices containing poorly soluble drug such as tacrolimus. The release exponent calculated from Korsmeyer- Peppas model indicated two different modes of diffusion in the case of nanospheres and microspheres. All the three formulations of nanospheres (1 wt%, 5 wt% and 10 wt% tacrolimus loading) had release exponents less than 0.43, suggesting a Fickian mode of diffusion. However, although microspheres with 10 wt% tacrolimus was found to follow Fickian mode of diffusion, microspheres with 1 and 5 wt% tacrolimus exhibited anomalous case, indicating the influence of multiple factors for mass transfer such as diffusion and degradation. The reason for anomalous diffusion in the case of 1 wt% and 5 wt% is not well understood, but perhaps can be assumed as result for non- uniform distribution of the drug through the bulk of the matrix, or the increased polydispersity of the microspheres.

The results of this particular study can confirm that P(3HB) has the potential in developing DDSs for antiproliferative drugs, ensuring minimal burst release and sustained release up to a month. 10 wt% drug loading of tacrolimus in P(3HB) nanospheres eluted out about

76.2% of encapsulated drug. It is clearly illustrated that by fine tuning particle size and drug polymer ratio, distinctive drug release profiles can be obtained. This is favourable, especially when research in controlled drug delivery is moving closer to achieving personalised solutions.

### **4.3.3. P(3HB) microspheres as VEGF delivery systems in Collagen scaffolds for Cardiac regeneration**

The most popular strategy for cardiac regeneration post myocardial infarction is reperfusion either by pharmacological means or mechanical means, where the percutaneously administered agents or coronary grafts initiate the expression of chemotactic factors. These chemotactic factors enable remodelling of the infarcted tissue by inducing fibrosis and repair. Various biopolymers have been exploited for the purpose of generating mechanically viable grafts with incorporated growth factors, especially vascular endothelial growth factor (VEGF) (Ruiz-Esparza *et al.*, 2013).

Chronic myocardial ischemia after myocardial infarction and associated remodelling can be effectively treated by growth factor treatment. However, the initial stages of research concerning direct delivery of the growth factor demonstrated insufficient clinical success, mainly due to their short half- life span (Hao, 2007). Many of the disappointing initial results were found to be less effective than placebos, as when injected as intravenous infusion or intercoronary delivery in the form of a bolus, VEGF was rendered inactive by the time it reached the site of action.

Although there have been alternate approaches using gene delivery and combine factor delivery, these methods rendered the systems overly complicated and resulted in poor

success. The latest approach towards this objective is the use of biopolymers as drug delivery systems for growth factors, with controllable release rate. Various modes of drug delivery systems such as protein delivery, polymeric scaffolds, polymeric micro/nanoparticles have been explored. In this study, VEGF was encapsulated P(3HB) nanospheres and microspheres were embedded in collagen scaffolds for their use as cardiac regeneration patches. Release kinetics of VEGF from neat spheres and spheres embedded in collagen scaffolds were compared. A reduction in burst release was observed when the spheres were embedded in collagen scaffolds. This is similar to the results obtained by Tajdaran *et al.*, by immobilizing PLGA microspheres in fibrin network, for the release of tacrolimus (Tajdaran *et al.*, 2015). With this system, sustained release was observed up to 30 days, in comparison with PLGA particulate system that released only up to 15 days. There are several strategies of such immobilizations reported in literature, where particulate systems are immobilized on fibrin network (Baumann *et al.*, 2009; Garbayo *et al.*, 20010). However, the analysis of collagen in this context, as studied in this chapter is the first one of its kind.

Swelling studies conducted by immersing empty and particle embedded collagen scaffolds in PBS over a period of 36 days revealed collagen to uptake as much as 800% of their volume of water over this period. Compared to particle embedded scaffolds, empty scaffolds were found to have a higher swelling ratio. This can be hypothesised due to the presence of highly hydrophobic P(3HB) microspheres in the patch by 28 w/w%. In first three days, empty collagen scaffolds absorbed  $343 \pm 3.12\%$  and this increased to a maximum of  $802 \pm 7.9\%$  in 36 days. Compared to the empty controls, particle embedded scaffold absorbed a lesser amount of water. The nanospheres embedded scaffolds absorbed  $323 \pm$

4.12% in first three days and  $791 \pm 6.8\%$  water by the end of 36 days. The microsphere embedded scaffolds absorbed and  $311 \pm 4.12\%$  water in the first 3 days and  $777 \pm 8.72\%$  water in 36 days.

This water uptake, however, did not result in an increase in burst release. Immobilization of the microspheres on collagen scaffolds was found to increase the duration of release for 48 hours more, in comparison with the neat spheres. More than 90% of VEGF was released in a span of 30 days, in all the 4 cases. This is far more superior to several VEGF encapsulation methods describe in literature (Gu, Amsden and Neufeld, 2004; De *et al.*, 2009; Jay and Saltzman, 2009).

Contrary to release profiles observed in the case of rapamycin and tacrolimus, VEGF release was found to follow first- order release kinetics, except in the case of free microspheres. suggesting concentration of the drug to be the most contributing factor of release. First-order release kinetics is observed in DDS that are formulated as porous matrices containing water soluble drugs (Dash *et al.*, 2010). Since VEGF is a fairly water- soluble drug, its release profile to fit well with first- order model is expected. In the case of free microspheres with encapsulated VEGF, the release data was found to fit better with Hixson- Crowell and Higuchi model (98.5 and 98.3% correlation respectively). From the release data it can also be seen that the release from free microspheres follow a slower rate when compared to the other three formulations. However, considering the good fit of all the release data to Higuchi model as well, it can be concluded that diffusion is a major contributing factor of mass transport. Embedding the microspheres and nanospheres did not change the release profiles effectively, as VEGF was contained only in the bulk of spheres and not in the collagen matrix.

Apart from the benefits of controlled delivery of VEGF, immobilization of the spheres on collagen scaffold is hypothesized to support cell viability. This is because cells have been reported to have increased affinity for surfaces with 'artefacts' that provide a better surface topography, and the presence of crystalline microspheres in collagen matrix can render this. Therefore, these scaffolds, currently in small animal trials can be considered to have immense potential in cardiac regeneration.

# **Chapter 5**

## **P(3HB) Microspheres as novel target specific delivery systems for Anticancer Photodynamic Therapy**

## 5.1. Introduction

Controlled drug delivery is the sustained release of therapeutic agents, as a response to time or stimuli, allowing for the maintenance of drug concentrations in the biological milieu within the therapeutic window (Yun, Lee and Park, 2014). This is achieved by the incorporation of therapeutic agents into specialised drug delivery systems, a majority of which are made of synthetic and natural polymers. These polymers are primarily designated to protect the therapeutic agents from biomolecules of the blood stream and ensure delivery at the site of action by virtue of their suitable functionalities (Liechty *et al.*, 2010). Cancer therapy is a field that can benefit greatly from controlled drug delivery as many existing therapeutic agents are found to be of poor water solubility, lack of targeting capability, nonspecific distribution, systemic toxicity, and low therapeutic index (Sun *et al.*, 2014). According to World Health Organisation estimates, cancer is the most prominent reason of mortality, having overtaken coronary diseases and strokes (Ferlay *et al.*, 2015). In the next 10 years, about 20 million new cancer cases are predicted to be reported. Female breast cancer continues to be the most prevalent and most frequently diagnosed neoplasm with over 5.2 million breast cancer cases worldwide, and the need for a long-term and effective care for breast cancer is indisputable (Ferlay *et al.*, 2015).

Conventional chemotherapy has serious impediments in the form of many side effects such as gastro-intestinal damage, peripheral neuropathy, neurological or psychiatric disorders and infections (Nordlinger *et al.*, 2008). Hence, novel anticancer therapeutic avenues are being explored, an emerging one is the highly promising photodynamic therapy (PDT). Photodynamic therapy involves the topical or systemic application of photosensitizers, followed by illumination with light of a suitable wavelength and dosage. This elicits a

photodynamic reaction (PDR), which in turn results in the release of cytotoxic species, specifically reactive oxygen species (ROS), ultimately leading to programmed cell death.

The exact mechanism of PDR has yet to be revealed, but the ROS have a radius of destruction in the nanometre range and elicit a cascade of immunological and necrotic events leading to effective tumour control (Dolmans, Fukumara and Jain., 2003). Porphyrins are an effective class of photosensitizers with a chemical structure including the porphyrin ring formed from tetrapyrrole molecules connected using methine bridges, and they are known to produce ROS efficiently through illumination. A few derivatives of porphyrins have been synthesised by modifying lateral substituents of the ring, which have been explored within the scope of PDT. Here we compare three different porphyrin derivatives, namely protoporphyrin IX (PP), hematoporphyrin ether (HP) and tetraphenylporphyrin (TPP) (Figure 5.1).

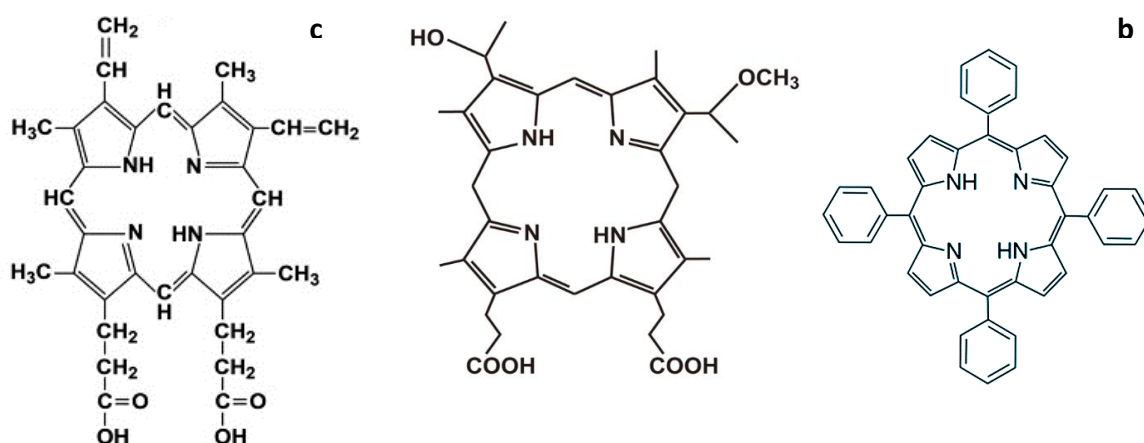


**Figure 5.1:** Porphyrin derivatives: a) Protoporphyrin IX, b) Hematoporphyrin ether c) Tetraphenylporphyrin (Kadish, 1999, Wintrobe and Greer, 2009)

Both PP and HP are naturally occurring porphyrins, being the precursor to biologically essential prosthetic groups such as heme, cytochrome c, and chlorophylls, or being formed

by the acid hydrolysis of haemoglobin, respectively. A derivative of HP is also in clinical use as a PDT agent under the trade name Photophrin (HPD, an oligomer of HP), and HP itself is an effective PDT agent and is a first-generation PDT agent. Thus, the use of naturally occurring agents would have clear advantages. TPP was chosen as a readily available synthetic alternative to PP and HP to compare their efficiencies; water soluble TPP derivatives have been studied for PDT, but TPP as such has not been used due to its low solubility in aqueous solutions, which is a general obstacle in using porphyrins for PDT (Ding, 2004).

After cellular uptake of porphyrins, they are irradiated with light of a suitable wavelength (600-800nm), yielding a high energy excited state. This energy is transferred to molecular oxygen to produce highly reactive singlet oxygen, leading to cell membrane damage (Dolmans, Fukumara and Jain., 2003, Agostinis *et al.*, 2011). The photosensitizers can also be oxidised, producing superoxide radicals, leading to more cell damage (Dolmans, Fukumara and Jain., 2003). The useful range of wavelength typically applied for PDT is 600-800nm, which rules out endogenous chromophores of the body, yet provides energy suitable for PDT. High-intensity light of this order results in rapid tumour necrosis that releases intracellular chemicals and cytokines, contributing to the bystander effect (SharmanAllen and Lier, 1999). Here, intercellular necrotic substances are released by microcolonies of cells directly exposed to photosensitizers, to alert neighbouring cells to undergo apoptosis (Oleinick, Morris, and Belichenko, 2002). PDT mediated tumour lysis also causes the release of tumour specific neo-antigens that are phagocytosed by dendritic cells thus resulting in a long-lasting immune response.

In addition to choosing efficient PDT agents, controlled delivery of these photosensitizers is one of the key aspects, which needs to be improved, as most of the photosensitizers are insoluble in an aqueous environment. The drug delivery system should ideally be biodegradable, biocompatible, and non-immunogenic and should protect the drug from the biological milieu. However, a carrier system can considerably reduce the photodynamic effect because of the tendency of photosensitizers to aggregate within the hydrophilic carrier. Also, the use of drug delivery systems can result in considerable light quenching (Debele, Peng and Tsai, 2015). In addition, the drug delivery vehicle needs to be sufficiently porous to result in continuous but controlled release of the drug.

This chapter describes the optimisation of the production of P(3HB) microspheres based on process parameters such as polymer concentration, surfactant concentration and stirring speed of the emulsion, for targeted delivery of the porphyrins. The microspheres thus produced were characterised for size distribution, porosity, and hydrophobicity. The best-optimised conditions were repeated to encapsulate porphyrin derivatives that presented possible drug-polymer interactions, leading to a further step of optimisation with a different set of boundary conditions. Targeted drug delivery effectively reduces bio distribution of the drug delivery system in tissue spaces that aren't affected, hence increasing efficiency of therapy. Targeting was achieved by the introduction of specific neoplastic antigens on the surface of breast cancer cells, specifically anti-HER-2 antibodies. The cell line used was a SK-BR-3 breast carcinoma cell, which overexpress HER-2 markers. Markiv *et al.*, 2011 designed a recombinant antibody-fluorophore conjugate of Red Fluorescent Protein (RFP) in-between the variable regions of anti-p185HER2-ECD antibody 4D5-8, resulting in optimal VH/VL interface interaction to create soluble coloured

antibodies (Markiv *et al.*, 2011). Since the anti-HER-2 antibody was coupled with RFP, it was used as an imaging strategy to observe the homing effect of the antibody to cancer cells. An in-depth analysis of the targeted and non-targeted anticancer photodynamic therapy using the three different porphyrins PP, HP and TPP, encapsulated within P(3HB) microspheres, was carried out confirming the high potential of this system to be used in cancer therapy.

## 5.2. Results

### 5.2.1. Encapsulation of Porphyrin derivatives

Based on the optimisation experiments from Chapter 3, experimental conditions 1 and 9 (Chapter 3, section 3.2.3.2) were chosen for encapsulation of the porphyrins, which however led to microspheres with extremely uneven and collapsed surfaces (**Figure 5.2**).

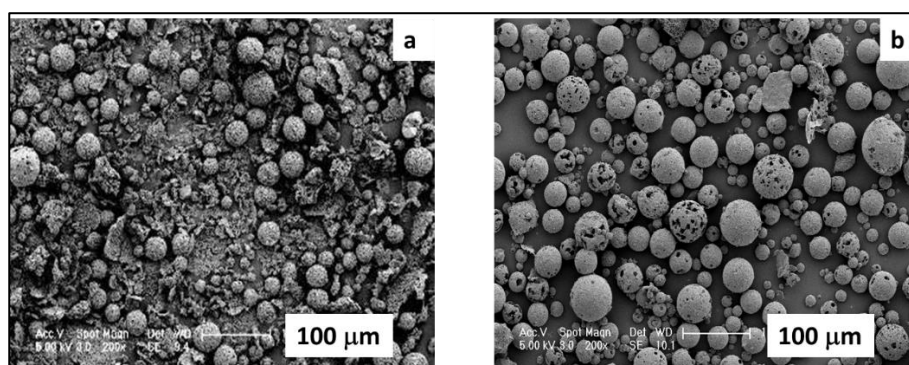


**Figure 5.2:** SEM images of Porphyrin encapsulated microspheres corresponding to experiment number a) 1 (0.0625 g/mL Polymer concentration, 1 % w/v PVA concentration and 500 rpm stirrer speed) and b) 9 (0.1 g/mL Polymer concentration, 1 % w/v PVA concentration and 800 rpm stirrer speed).

All the microspheres formed were exceedingly porous and non-uniform and therefore, did not promise successful encapsulation or controlled delivery. Following this, a different set

of experimental design was generated using the same software, Design Expert, with lower boundary conditions for all parameters- concentration of polymer solution, PVA concentration and stirrer speed in rpm (**Table 5.1**).

Expt. number	Amount of P(3HB) in chloroform (g/mL)	PVA concentration (%)	Stirrer speed (RPM)
1	0.0125	0.3	300
2	0.0625	0.3	800
3	0.0125	0.8	300
4	0.0625	0.8	800
5	0.0125	0.3	800
6	0.0125	0.8	800
7	0.0625	0.8	300
8	0.0625	0.3	300
9	0.0375	0.5	500
10	0.0125	0.5	500
11	0.0375	0.3	500
12	0.0375	0.5	300
13	0.0625	0.5	500
14	0.0375	0.8	500
15	0.0375	0.5	800

**Table 5.1:** Experimental design for optimization of porphyrin encapsulated microspheres production.

Polymer concentration was lowered to compensate for the increased hydrophobicity resulting from the addition of porphyrins. PVA concentration was lowered to attain an optimum interphase mechanics of the oil-water emulsion. As the porphyrin encapsulated

microspheres corresponding to the initial set of experiments were highly porous, the boundary conditions for the stirring speed of the emulsion was lowered, because faster stirring can cause quicker evaporation of chloroform resulting in uneven and extensive pore formation.

The resulting microspheres were further optimised, and the best conditions were chosen to encapsulate 2.5 wt%, 5 wt% and 10 wt% drug loading of the porphyrin derivatives. The microspheres prepared under the conditions of 0.0375g/mL polymer concentration, 0.5 % PVA concentration and 800 rpm were chosen for encapsulation of porphyrin derivatives. Only this condition, corresponding to experiment number 15 (**Table 5.1**) yielded well-formed microspheres when encapsulated with all three porphyrin derivatives.

## 5.2.2. Characterization of porphyrin encapsulated microspheres

### 5.2.2.1. Surface morphology and particle size analysis of Porphyrin encapsulated microspheres

The surface morphology of microspheres produced with encapsulated porphyrins was observed under SEM (**Figure 5.3**).

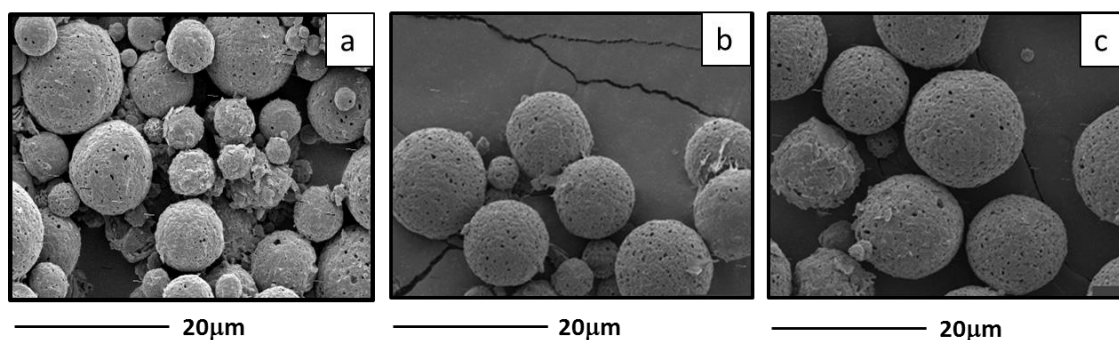


**Figure 5.3:** Microspheres encapsulated with 10 wt% drug loading of a) PP b) HP c) TPP

The microspheres appeared to be more porous than the ones without porphyrins. These were also visibly slightly more polydispersed than the empty control microspheres (as described in Chapter 3). The microspheres were found to be well separated from one another and had appreciable spherical appearance.

The size distributions of microspheres encapsulated with porphyrins were estimated from the SEM images, using the ImageJ software (**Figure 5.4**). The PP encapsulated microspheres were found to be slightly smaller in size compared to HP encapsulated and TPP encapsulated ones. In each case, particle size was found to increase with drug loading, as represented in **Table 5.2**.

<b>Drug loading</b>	<b>Average particle diameter (<math>\mu\text{m}</math>)</b>
<b>2.5 wt% PP</b>	$12.51 \pm 2.21$
<b>5 wt% PP</b>	$12.66 \pm 1.29$
<b>10 wt% PP</b>	$12.78 \pm 1.09$
<b>2.5 wt% HP</b>	$13.08 \pm 0.8$
<b>5 wt% HP</b>	$13.44 \pm 1.53$
<b>10 wt% HP</b>	$13.68 \pm 2.09$
<b>2.5 wt% TPP</b>	$13.82 \pm 1.98$
<b>5 wt% TPP</b>	$14.18 \pm 1.29$
<b>10 wt% TPP</b>	$14.67 \pm 1.37$

**Table 5.2:** Average particle diameter of porphyrin encapsulated microspheres (n=3, error=  $\pm$  s.d).

The average diameter of PP encapsulated microspheres was found to be  $12.5 \pm 2.21\mu\text{m}$ , in the case of 2.5 wt% drug loading and  $12.7 \pm 1.29 \mu\text{m}$  and  $12.7 \pm 1.09 \mu\text{m}$  respectively in the case of 5 wt% and 10 wt% drug loading. The average diameter of HP encapsulated microspheres was found to be higher than PP encapsulated microspheres. With 2.5 wt% drug loading, the average diameter was found to be  $13.08 \pm 0.8 \mu\text{m}$  and this was found to

increase to  $13.44 \pm 1.53 \mu\text{m}$  with 5 wt% and  $13.68 \pm 2.09 \mu\text{m}$  with 10 wt% drug loading. TPP encapsulated microspheres were found to be the largest, with an average diameter of  $13.82 \pm 1.98 \mu\text{m}$ ,  $14.18 \pm 1.29 \mu\text{m}$ , and  $14.67 \pm 1.37 \mu\text{m}$ , with 2.5, 5 and 10 wt% drug loading, respectively.

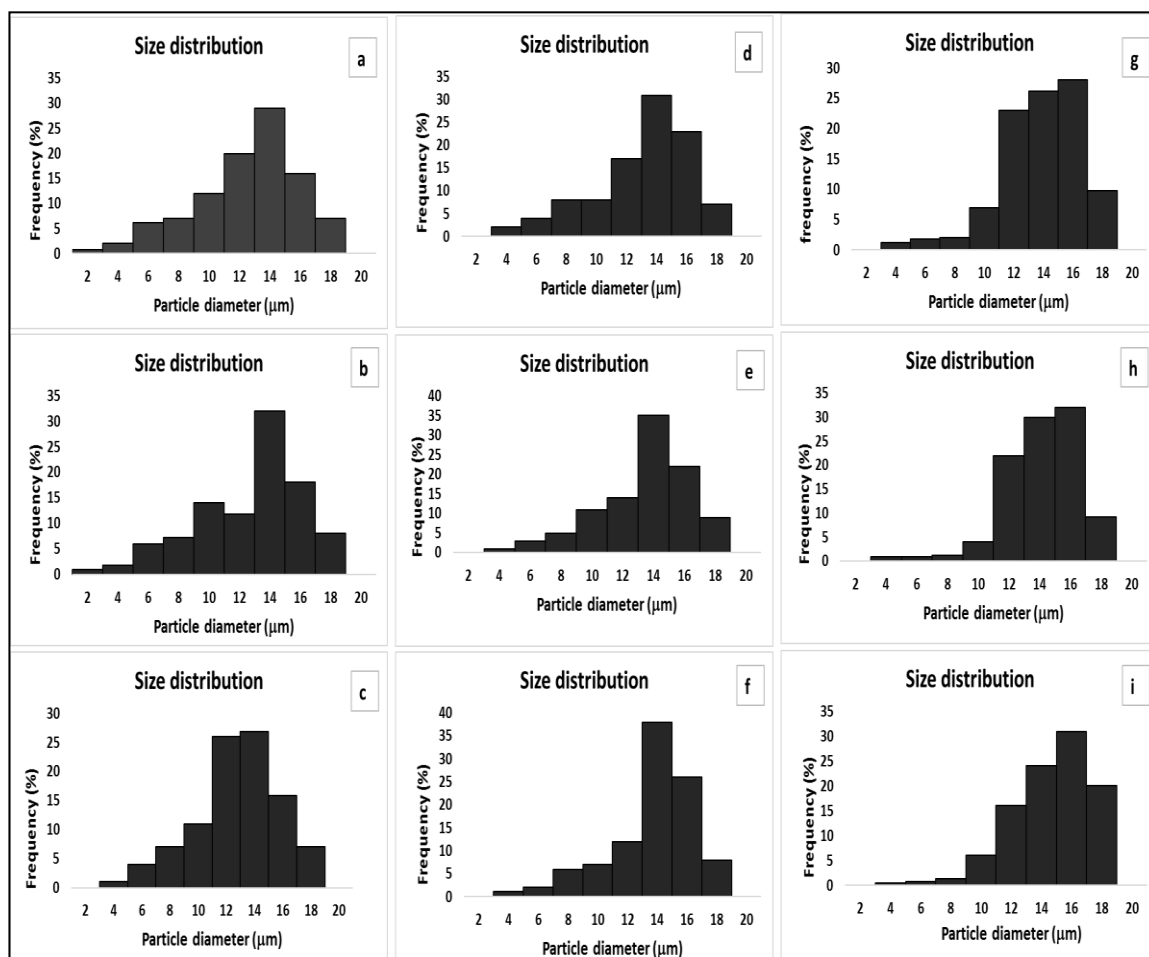


**Figure 5.4:** Particle size distribution of microspheres with a) 2.5 wt% PP, b) 5 wt% PP, c) 10 wt% PP, d) 2.5 wt% HP, e) 5 wt% HP, f) 10 wt% HP, g) 2.5 wt% TPP, h) 5 wt% TPP and i) 10 wt% TPP.

### 5.2.2.2. Porosity

Porosity of microspheres encapsulated with porphyrins was calculated using the liquid displacement method. Porosity was found to be higher than control microspheres

prepared under similar conditions, without drug encapsulation ( $51.82 \pm 2.17\%$ ). Porosity was found to increase with drug loading in each case, and in general TPP encapsulated microspheres were found to be more porous than the rest (**Figure 5.5**). Porosity of 10 wt% TPP loaded microspheres ( $73.21 \pm 4.3\%$ ) were found to be significantly higher than 10 wt% HP loaded ( $65.29 \pm 1.2\%$ ) and 10 wt% PP loaded ( $63.92 \pm 1.92\%$ ).

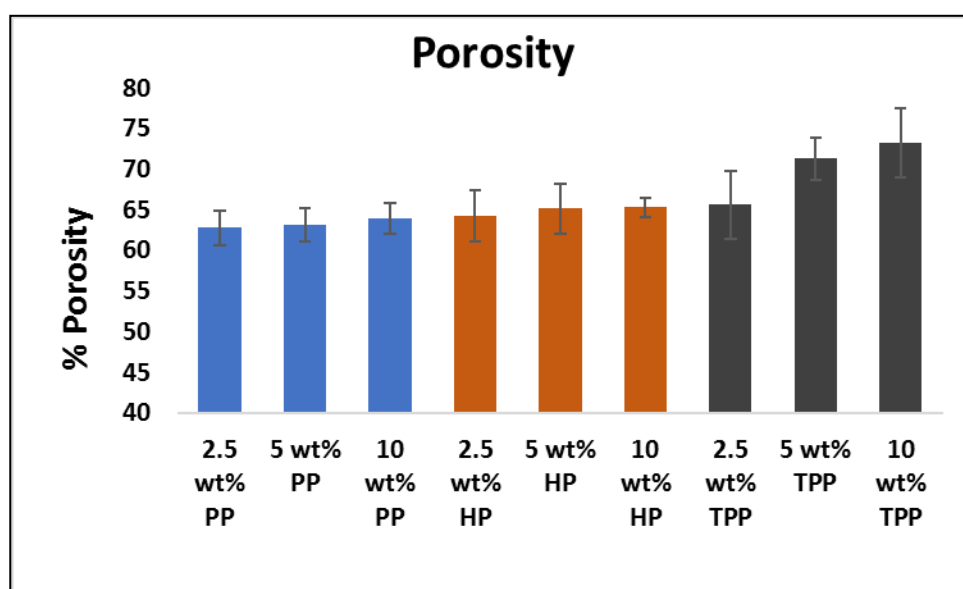


**Figure 5.5:** Porosity of porphyrin encapsulated microspheres ( $n=3$ , error=  $\pm$  s.d).

Porosity of PP encapsulated microspheres was found to be the least of the 3 derivatives, however, a trend of increased porosity was observed with increased drug loading, with  $62.8 \pm 2.12\%$ ,  $63.12 \pm 2.0\%$  and  $63.92 \pm 1.92\%$  for 2.5 wt%, 5 wt% and 10 wt% drug loading respectively. This trend was maintained in the case of HP, with  $64.29 \pm 3.12\%$ ,  $65.18 \pm 3.07\%$ , and  $65.29 \pm 1.2$ , and in the case of TPP, with  $65.6 \pm 4.12$ ,  $71.29 \pm 2.61$  and  $73.21 \pm 4.3$  for 2.5 wt%, 5 wt% and 10 wt% drug loading respectively.

### 5.2.2.3. Residual PVA and hydrophobicity

Surface residual PVA of the microspheres prepared were measured by the method described in Chapter 2. These were represented as percentage mass if PVA residual per unit mass of microspheres. There appeared to be an inverse correlation between surface residual PVA and hydrophobicity. Surface residual PVA of porphyrin encapsulated microspheres ranged from  $0.17 \pm .002\%$  (for microspheres loaded with 10 wt% TPP) to  $0.83 \pm 0.014\%$  (for microspheres loaded with 2.5 wt% PP). Amount of PVA residue on the surface was found to decrease with drug loading (**Figure 5.6.a**). In the case of PP encapsulated microspheres, surface residual PVA varied from  $0.83 \pm .014\%$ ,  $0.77 \pm 0.018\%$  and  $0.72 \pm 0.011\%$  for 2.5 wt%, 5 wt% and 10 wt% drug loading respectively. In the case of HP, this was found to be  $0.62 \pm 0.03$ ,  $0.47 \pm 0.027$  and  $0.36 \pm 0.027$  for 2.5 wt%, 5 wt% and 10 wt% drug loading and in the case of TPP, this was found to be  $0.37 \pm 0.001$ ,  $0.21 \pm 0.01$  and  $0.17 \pm 0.001$  for 2.5 wt%, 5 wt% and 10 wt% drug loading, respectively.

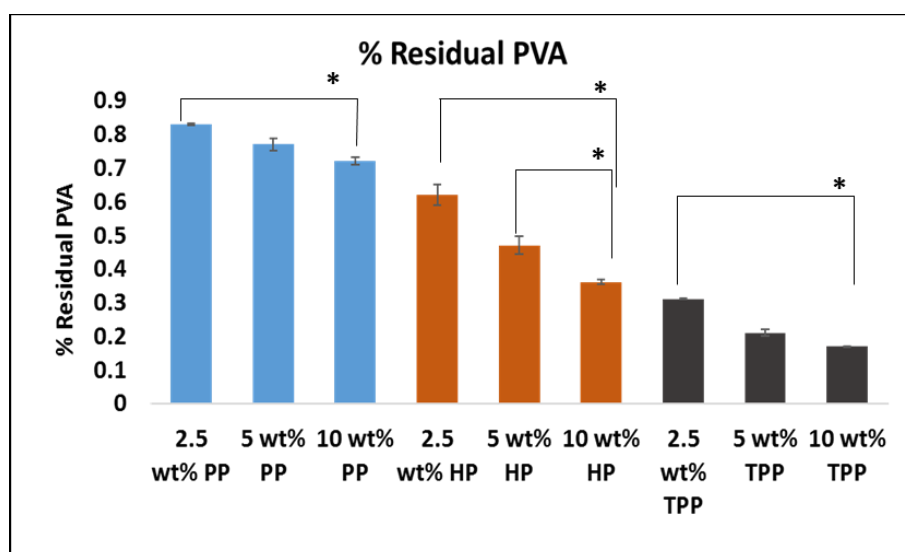


**Figure 5.6.a):** Surface residual PVA of porphyrin encapsulated microspheres (n=3, error=  $\pm$  s.d). (\* p< 0.05)

Porphyrin encapsulated microspheres were found to be extremely hydrophobic in comparison with microspheres encapsulated with various other molecules as described in previous chapters. Hydrophobicity was found to increase with increased drug loading and was found to be significantly higher in the case of 10 wt% TPP encapsulated microspheres ( $9.1 \pm 0.28 \mu\text{g}/\text{mg}$ ), when compared to 10 wt% HP ( $5.3 \pm 0.31 \mu\text{g}/\text{mg}$ ) and PP encapsulated microspheres ( $3.1 \pm 0.47 \mu\text{g}/\text{mg}$ ) (**Figure 5.6.b**).

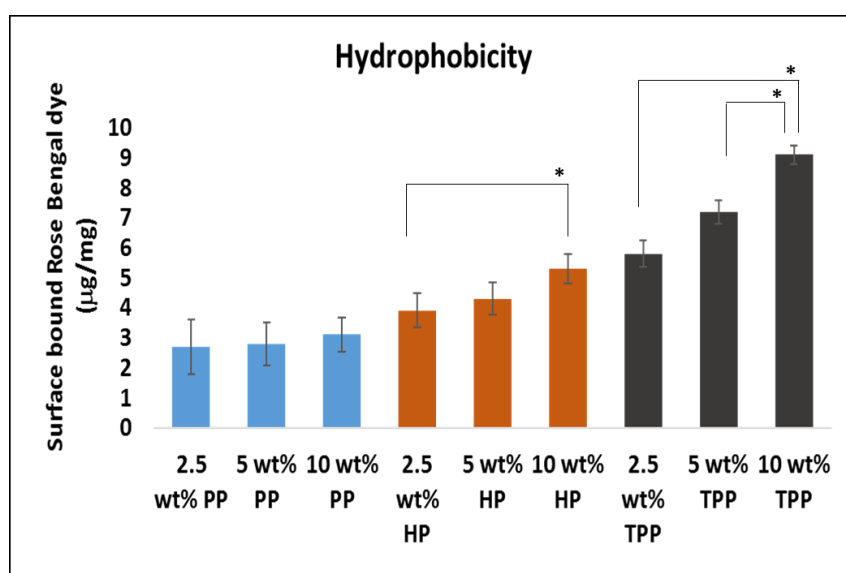


**Figure 5.6.b):** Hydrophobicity represented as a function of the amount of Rose Bengal dye adsorbed at  $50 \mu\text{g}/\text{mL}$  on porphyrin encapsulated microspheres ( $n=3$ , error =  $\pm$  s.d). (\*  $p < 0.05$ )

#### 5.2.2.4. Protein adsorption

Protein adsorption on the surface of microspheres was estimated by immersing samples in BSA solution for 24 hours and subjecting the supernatant to Bradford assay. Protein adsorbed on the surface of microspheres were found to have a positive correlation with the hydrophobicity, with 10 wt% TPP encapsulated microspheres having the maximum amount of surface adsorbed protein ( $929.9 \pm 62.8 \mu\text{g}/\text{mg}$ ). An exception to this case was

microspheres encapsulated with 2.5 wt% of HP (with  $443.3 \pm 1.9$   $\mu\text{g}/\text{mg}$  surface adsorbed BSA), which although were more hydrophobic than 10 wt% PP encapsulated microspheres (with  $514.7 \pm 9.8$   $\mu\text{g}/\text{mg}$  surface adsorbed BSA), had a lower amount of proteins adsorbed on their surface (**Figure 5.7**). In general, protein adsorption was found to increase with drug loading, and hydrophobicity.

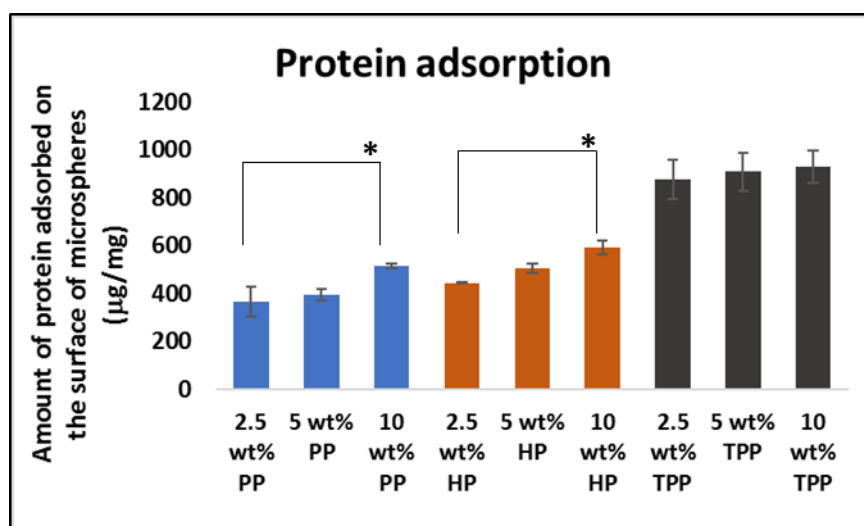


**Figure 5.7:** Amount of protein adsorbed on the surface of porphyrin encapsulated microspheres ( $n=3$ , error =  $\pm$  s.d) (\*  $p < 0.05$ ).

### 5.2.3. Encapsulation efficiency

Encapsulation efficiency as quantified by fluorescence spectrometry, was found to increase with increased drug loading, in each case. TPP, which exhibited the highest solubility in chloroform, had the highest amount (87.8%, with 10 wt% drug loading) of encapsulation, while PP exhibited the least amount of encapsulation. A few preparations of PP exhibited large particles of surface adsorbed drug, indicating low solubility of PP in chloroform as compared to the other two derivatives.

The graph below (**Figure 5.8**) compares encapsulation efficiencies of increasing drug loadings of PP, TPP and HP.

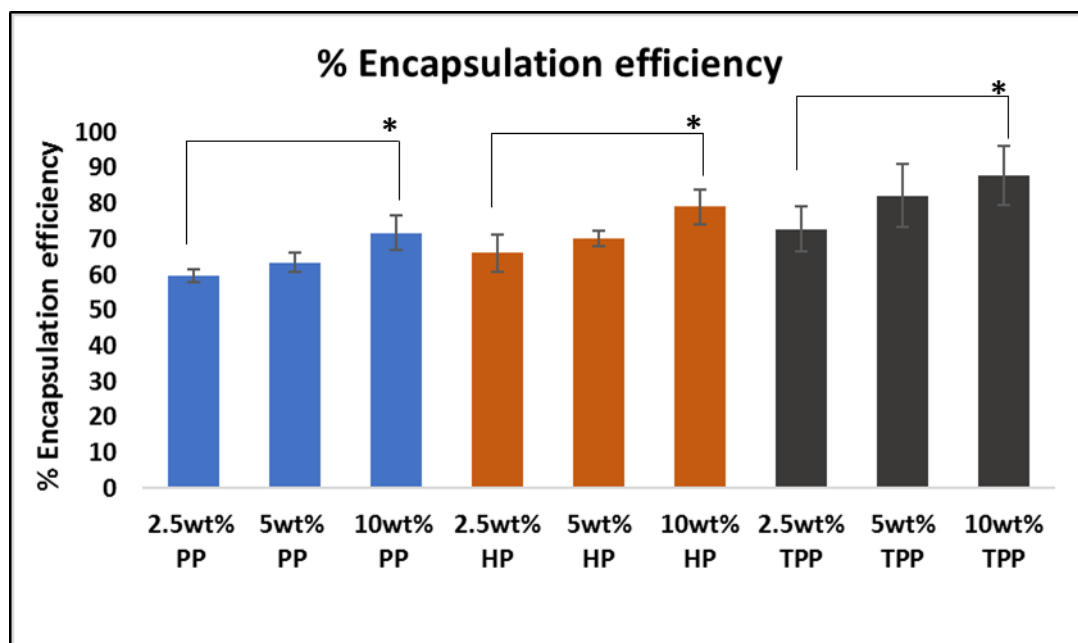


**Figure 5.8:** Encapsulation efficiencies of microspheres with increasing loadings of porphyrin derivatives (n=3, error= ±sd) (\* p< 0.05).

Encapsulation efficiency increased from  $59.7 \pm 1.8\%$  of 2.5 wt% drug loading of PP, to  $63.4 \pm 2.6\%$  with 5 wt% drug loading of PP and  $71.7 \pm 5\%$  with 10 wt% drug loading of PP. This was found to be  $66 \pm 5.3\%$ ,  $70.2 \pm 2.1\%$  and  $79.1 \pm 4.9\%$ , in the case of 2.5 wt%, 5 wt% and 10 wt% HP loading. In the case of TPP, encapsulation efficiency was found to be  $72.8 \pm 6.2\%$ ,  $82.1 \pm 8.9\%$  and  $87.8 \pm 8.3\%$  for 2.5 wt%, 5 wt% and 10 wt% drug loading respectively.

#### 5.2.4. Expression and purification of RFP linked Anti -HER2 antibody

To achieve target specific drug delivery, the photosensitizer encapsulated microspheres with the highest encapsulation efficiency of each porphyrin derivative were used to adsorb Anti-HER2 antibody on the surface of the microspheres so as to allow selective binding to

the overexpressed cancer marker HER-2 on SK-BR-3 cells. 4D5-8 is an anti-HER-2 antibody conventionally used as a therapeutic antibody, also known as Trastuzumab. Markiv *et al.*, 2011 designed a recombinant antibody-fluorophore conjugate of Red Fluorescent Protein (RFP) in-between the variable regions of the anti-HER-2 antibody 4D5-8, to create soluble coloured antibodies. This resulting coloured antibody, called 4D5-8RFP12, has an isoelectric point of 6.0-6.5, as opposed to the conventional 4D5-8 single chain antibody that precipitated at physiological pH (Markiv *et al.*, 2011).

This recombinant antibody can be used as a homing agent for target specific drug delivery of breast cancer as they overexpress HER2. This 52kDa antibody was expressed and purified as described in section 2.2.12 and analysed using SDS-PAGE (**Figure 5.9**).

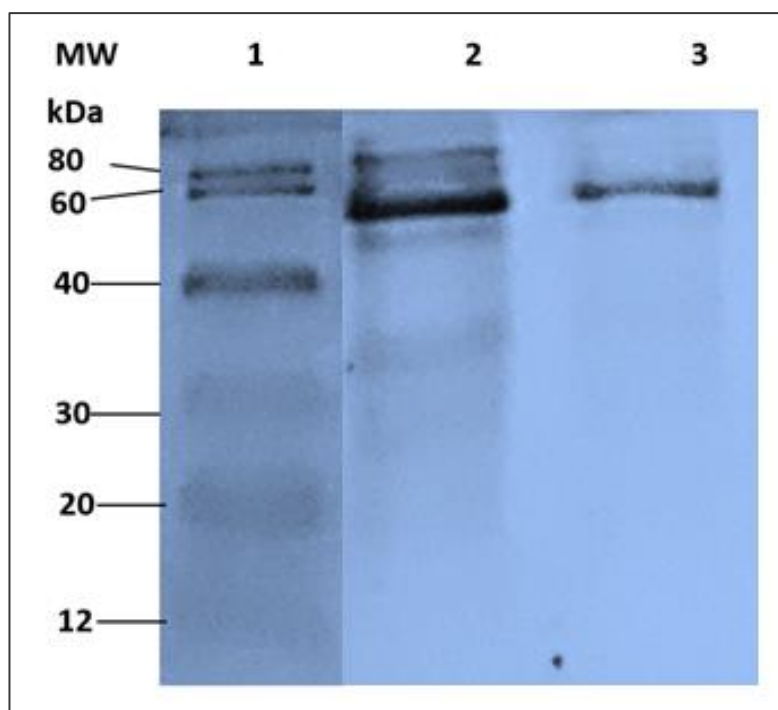


**Figure 5.9:** SDS-PAGE and Coomassie stained gel of anti-HER-2 antibody 4D5-8 with RFP, 4D5-8RFP12. Lane 1: Protein ladder, Lane 2: Elution fraction of 4D5-8RFP12.

SDS-PAGE confirmed the presence of the intact protein in the upper molecular weight range (52 kDa). The purified protein had a concentration of  $3.63 \pm 0.18$  mg/mL as opposed to the uninduced sample filtrate that had a concentration of  $0.081 \pm 0.08$  mg/mL.

### 5.2.5. Antibody adsorption on the microspheres

Antibody purified as described above was adsorbed on porphyrin encapsulated microspheres (10% drug loading of PP, HP and TPP) using the method described in section 2.2.13. Unbound antibodies in the supernatant after centrifugation were quantified using Bradford's assay and were subtracted from the amount initially used. The amounts of antibody bound on microspheres were found to be  $430 \pm 26$   $\mu\text{g}/\text{mg}$ ,  $490 \pm 18$   $\mu\text{g}/\text{mg}$  and  $580 \pm 46$   $\mu\text{g}/\text{mg}$  for PP, HP and TPP, respectively, as represented in **figure 5.10**.

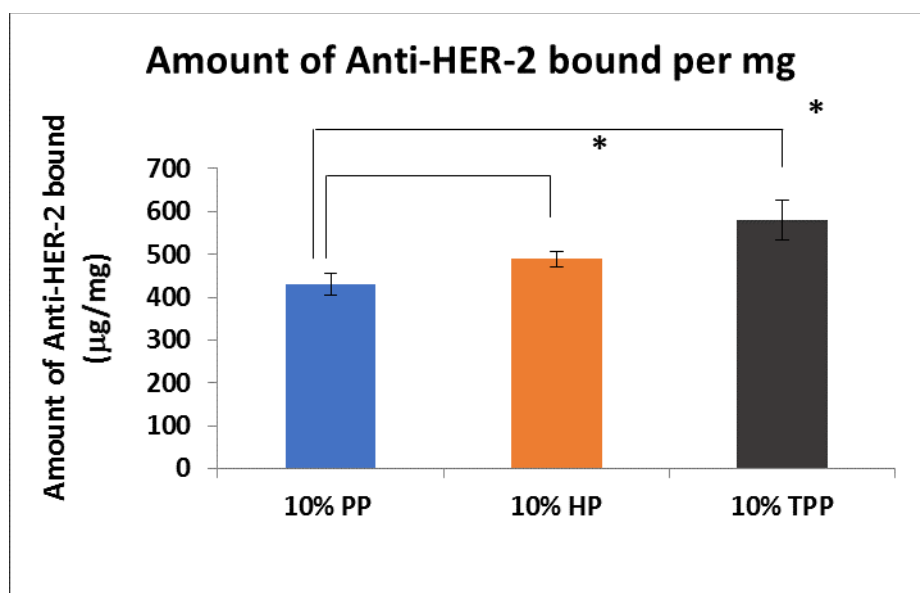


**Figure 5.10:** Amount of Anti-HER-2 adsorbed on P(3HB) microspheres encapsulated with 10 wt% drug loading of PP, HP and TPP ( $n=3$ , error =  $\pm$ sd) (\*  $p < 0.05$ ).

### 5.2.6. Cell viability studies

Cell viability studies were conducted on SK-BR-3 treated with microspheres alone, microspheres encapsulated with 2.5 wt%, 5 wt% and 10 wt% drug loading of each porphyrin derivative, and anti-HER-2 adsorbed microspheres of 10 wt% drug loading of each porphyrin derivative (**Figure 5.11**).

Cells were cultured at a density of  $1 \times 10^4$  in 96 well plates for 24 hours. These were incubated with each of the microsphere constructs for 48 hours, followed by exposure to white light for 30 minutes. Metabolic activity was quantified using the MTT assay. Cell toxicity was calculated as the reduction in cell viability, in comparison with the positive control. Of the three types of porphyrin, TPP was shown to have the best ability to induce photodynamic reaction (PDR), followed by HP, whereas PP was the least efficient of the three.

Percentage cell viability decreased with increasing drug loading of all the photosensitizers. Anti-HER-2 adsorption seemed to cause a decrease in cell viability in the case of all porphyrin derivatives, although not very pronounced in the case of PP. In the case of PP, cell cytotoxicity increased from  $52.20 \pm 1.14\%$  to  $58.01 \pm 0.53\%$  with 5 wt% drug loading and to a further  $59.9 \pm 0.8\%$  with 10 wt% drug loading. There was only an increase of  $0.8 \pm 0.08\%$  cell cytotoxicity with antibody incorporation.

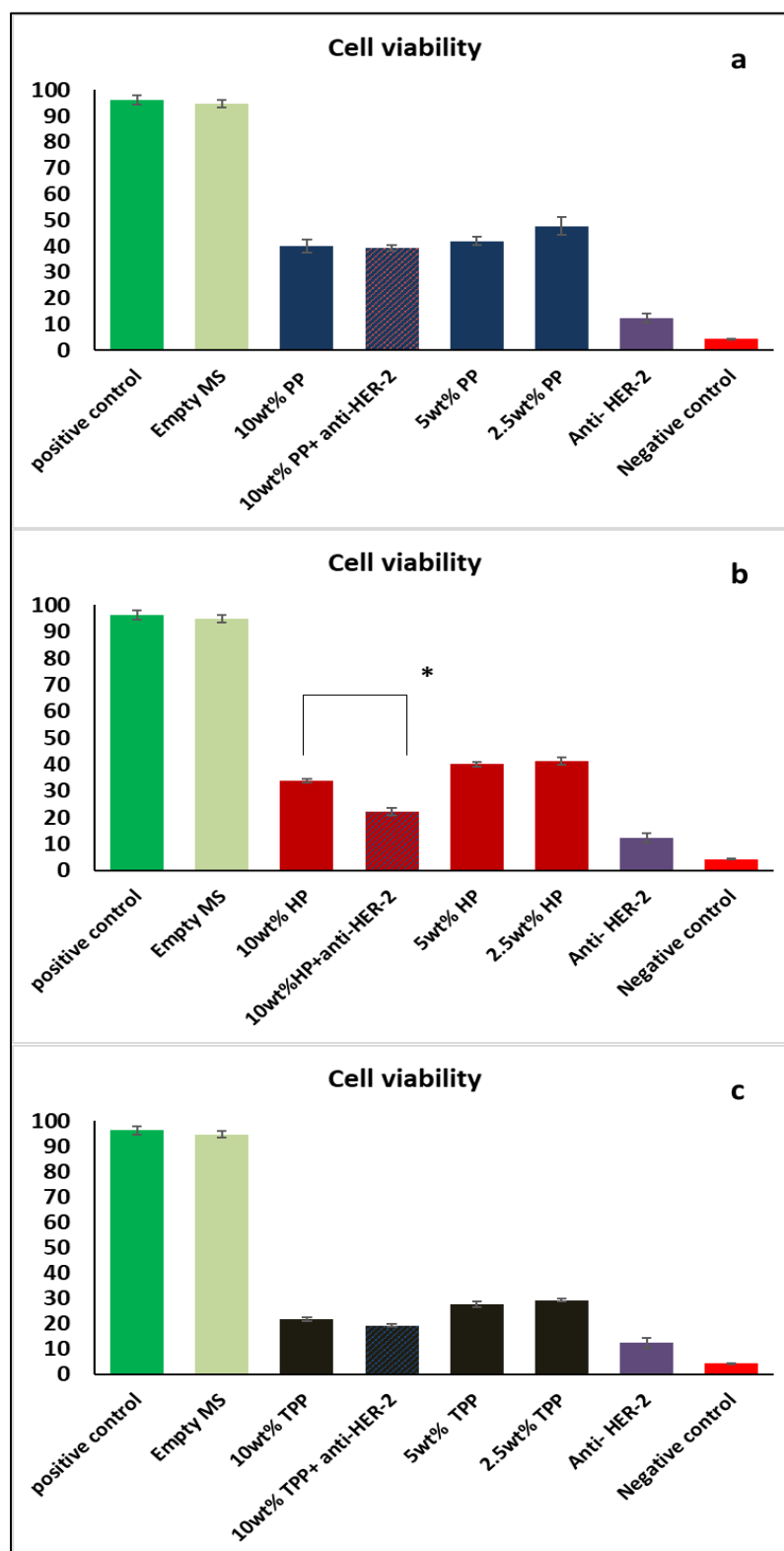


**Figure 5.11:** Percentage cell viability of SK-BR-3 cells after treatment with microspheres encapsulated with varying drug loadings of a) PP, b) HP and c) TPP. Tissue culture plate (TCP) was used as the positive control whereas the 4% hydrogen peroxide was used as the negative control (\* $p < 0.05$ ) ( $n = 3$ , error =  $\pm$  s.d).

HP encapsulated microspheres exhibited a higher cytotoxicity in comparison with PP, and this was found to increase with drug loading. The cytotoxicity of 10 wt% HP encapsulated microspheres in conjugation with anti-HER-2 was found to be significantly higher ( $77.8 \pm 3.3\%$ ) than the ones without the antibodies ( $66.2 \pm 0.62\%$ ). A similar trend, although not statistically significant, was observed in the case of TPP encapsulated microspheres, with 10 wt% drug loaded microspheres without antibody conjugation exhibiting a cytotoxicity of  $78.4 \pm 2.6\%$  and with antibody,  $80.7 \pm 1.4\%$ .

### 5.2.7. Confocal imaging

Confocal imaging of the SK-BR-3 cells treated with microspheres alone, microspheres encapsulated with 5 wt% and 10 wt% drug loading of each porphyrin derivative, and anti-HER-2 adsorbed microspheres of 10 wt% drug loading of each of the porphyrin derivatives was carried out. Live/Dead analysis was done using Calcein-AM and Ethidium homodimer III (EthD-III). The live cells stained green and the dead cells stained red as described in section 2.2.15

Confocal imaging thus confirmed the high tumour cell toxicity of the porphyrin loaded P(3HB) microspheres with a further increase of the cytotoxicity in the case of the targeted anti-HER-2 adsorbed microspheres. Almost all the cells were found to be dead by the end of imaging (2 hours after photoexcitation), in the case of cells cultured with anti-HER-2 adsorbed microspheres, thus confirming the effectiveness of these modified microspheres (**Figure 5.12**).

The cells treated with anti-HER-2 adsorbed P(3HB) microspheres containing porphyrin were enlarged ( $\sim 60\mu\text{m}$ ) as opposed to those treated with P(3HB) microspheres containing

porphyrins but without the antibodies. There was a clear difference in morphology and size of the resulting dead cells. However, whether this is due to any cellular phenomena or as a result of the presence of RFP and porphyrins, both of which fluoresce in the same wavelength range as (EthD-III) is yet to be understood.

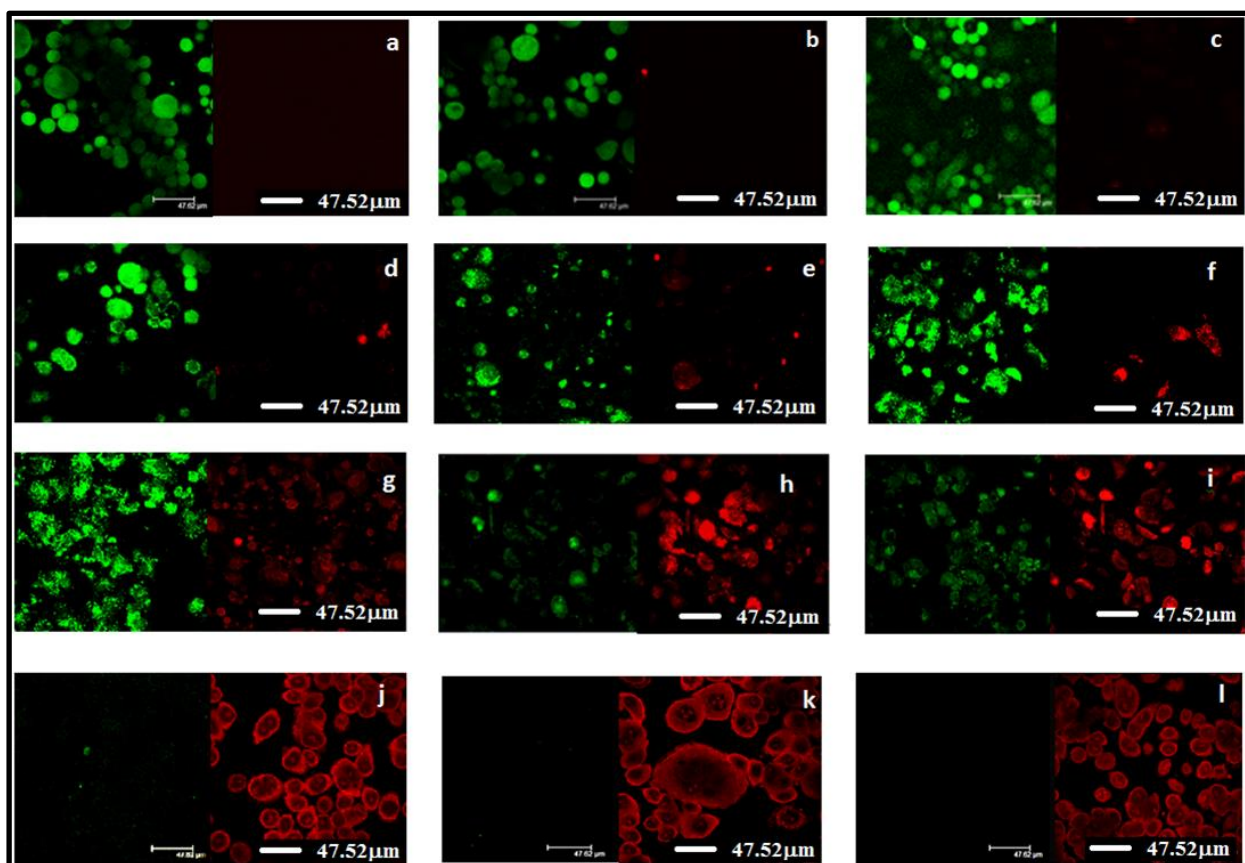


**Figure 5.12:** Confocal images of live/dead assay conducted on SK-BR-3 grown a) on tissue culture plastic, b) with empty microspheres c) with 10wt% drug loading of TPP, but non-photo activated, d-f) 5wt% drug loadings of PP, HP and TPP, photo activated, g-i) 10wt% drug loadings of PP, HP and TPP, photo activated, j-l) anti-HER-2 adsorbed 10wt% drug loadings of PP, HP and TPP

Although EthD-III nucleic acid stain, in the case of cells treated with anti-HER-2 adsorbed P(3HB) microspheres containing porphyrin, the periphery as well as the nuclei of the cells appeared to fluoresce. The exact reason of this phenomenon is yet to be understood, but

it can be hypothesised that, since the antibody is conjugated with a red fluorescent protein, this is indicative of the presence of the antibody around the cell membrane.

### 5.2.8. Calculation of IC<sub>50</sub> for 10 wt% TPP encapsulated P(3HB) microspheres with and without anti-HER-2 conjugation.

Based on the cell viability, TPP encapsulated microspheres were established to be the most potent of the 3 porphyrin derivatives. Therefore, these were chosen to be further characterised for establishing IC<sub>50</sub> values. Dose response of SK-BR-3 cells treated with microspheres encapsulated with 10 wt% drug loading of TPP, with and without antibody conjugation was calculated. A plot depicting natural logarithms of microsphere concentrations in  $\mu\text{g}/\text{mL}$  against cell viability of microspheres, with and without antibody conjugation was generated and from the regression equation, concentration corresponding to 50% viability inhibition was calculated (**Figure 5.13**).

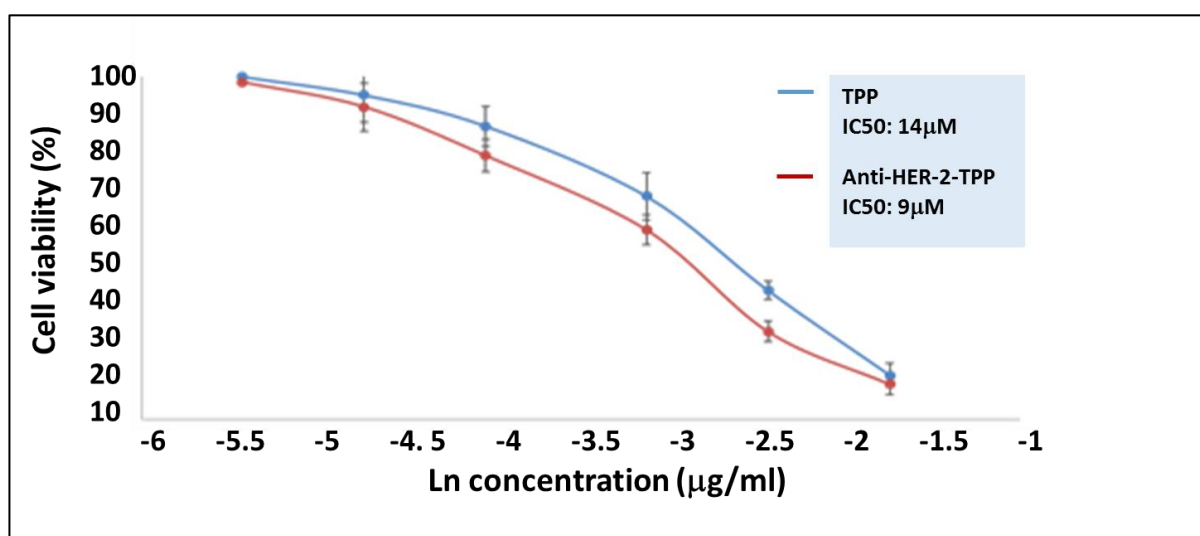


**Figure 5.13:** IC<sub>50</sub> calculations for 10 wt% TPP encapsulated microspheres (n=3, error=± s.d).

The values 50% growth inhibitory values of antibody conjugated microspheres were found to be slightly lower (9  $\mu\text{M}$ ) than the non-conjugated microspheres (14  $\mu\text{M}$ ), establishing the increased cytotoxicity of the former. The differences were not found to be statistically significant. Given the complexity of the formulations, it can be concluded that more trials are required to establish a correlation.

### 5.3. Discussion

P(3HB) production was successfully carried out using *B. cereus* SPV. Well-formed P(3HB) microspheres were produced using optimisation experiments based on process parameters such as polymer concentration, surfactant concentration and stirring speed of the emulsion, as described in chapter 3. Based on the optimisation experiments, experimental conditions 1 and 9 were chosen for encapsulation of the porphyrins, which however led to microspheres with extremely uneven and collapsed surfaces. This can be attributed to the highly hydrophobic nature of the porphyrins. This increased hydrophobicity of the organic phase could have resulted in a drastic change in the interphase mechanics of the oil-water emulsion, resulting in unevenly formed microspheres. Increase in the amount of drug encapsulated increases viscosity of the dispersed phase, leading to larger particles (Allison *et al.*, 2004, Allison *et al.*, 2005). Lee *et al.*, 1999, describe viscosity of the organic phase, volume fraction of the organic phase to the aqueous phase, quantity of drug in the organic phase and concentration of surfactant as critical parameters in microencapsulation (Lee *et al.*, 1999). Witschi *et al.*, 1998 reported that addition of drug in the organic phase resulted in more porous and irregular shaped microspheres (Witschi *et al.*, 1998).

Following this, lower boundary conditions so as to enable a reduced viscosity of the dispersed phase were applied. Polymer concentration was lowered to compensate for the increased hydrophobicity resulting from the addition of porphyrins. PVA concentration was lowered to attain an optimum interphase mechanics of the oil- water emulsion. As the porphyrin encapsulated microspheres corresponding to the initial set of experiments were highly porous, the boundary conditions for the stirring speed of the emulsion was lowered, because faster stirring can cause quicker evaporation of chloroform resulting in uneven and extensive pore formation. The microspheres generated were porous enough to expose encapsulated porphyrin derivatives to light. The optimised process followed by photosensitizer encapsulation showed that polymer-drug interaction is one of the main parameters to be considered in drug encapsulation.

2.5 wt%, 5 wt% and 10 wt% drug loadings of PP, HP and TPP were successfully encapsulated in microspheres, with an average diameter in the range of size 12.5 to 14.7 $\mu$ m. Particle size was found to increase with drug loading in each case. This is due to the increased viscosity of the dispersed phase, in the presence of increased amount of drug. These results are consistent with various microsphere formulations reported in literature, such as in the case of Paclitaxel loaded PLGA microspheres as described by Sharma, Madan and Lin 2015, that exhibited an increase in diameter from 440 nm to 600 nm when the drug loading was increased from 2mg to 4mg (Sharma, Madan and Lin, 2015).

It is generally known that hydrophobic drug molecules entrap better in hydrophobic polymer matrices. Encapsulation efficiency increased with increased drug loading in each case and was found to be the highest for 10 wt% drug loading. TPP encapsulated microspheres had the highest encapsulation efficiency (87.8%), followed by HP (79.1%) and

PP (71.7%). This was reflected in their ability to induce photodynamic damage, quantified by reduction in cell viability. 10 wt% drug loading of each porphyrin derivative was chosen to be complexed with anti-HER-2 antibody, to aid in target specific delivery. An increase in the cytotoxic effect was observed in microspheres with adsorbed antibodies in the case of HP, the differences being statistically significant ( $p < 0.05$ ). In the case of cells treated with antibody adsorbed porphyrin encapsulated microspheres, a phenomenon resembling autophagy associated with non-apoptotic breast cancer cells was observed, wherein the cells were massively enlarged and were multinucleate (Belaid *et al.*, 2013). Autophagy is described as a mechanism, wherein a cell generates an autophagosome to engulf and lyse cellular proteins and organelles. Autophagy is also suggested as the cell death mechanism in anti-apoptotic cancer cells, a category to which SK-BR-3 belongs (Yang *et al.*, 2011). Autophagy results in an increased surface to volume-ratio of cells, providing a plausible explanation for the increased size of dead cells (Belaid *et al.*, 2013). These cells also appear to be multinucleated which is a common phenomenon in autophagy. However, whether this is indeed a change in morphology of the cells or a misrepresentation due to the complexity of the factors involved, needs further elucidation. Both porphyrins and RFP fluoresce in the same wavelength as EthD-III and therefore, the use of a different stain can perhaps make the analysis better and conclusive.

Successful localisation of the photosensitizer in the target tissue is a key factor in determining the extent of PDT. A PDT carrier system has dual selectivity for tumour cells attributed by the affinity of lipophilic tumour lesions to both the polymer and photosensitizer that are hydrophobic in nature. It is also to be noted that, unlike chemotherapeutic moieties that must be released from carrier particles, release is not a

prerequisite of PDT (Solban *et al.*, 2006). The life span of singlet oxygen species generated is only  $\sim 3.5 \mu\text{s}$  and apoptotic factors generated by these have a diffusion range of only 0.01-0.02  $\mu\text{m}$  (Stuchinskaya *et al.*, 2011). Therefore, absolute localisation of the photosensitizers is necessary, which was achievable by the combined hydrophobicity of P(3HB) and porphyrin derivatives. As described in section 5.2.2.3, the porphyrin derivative encapsulated microspheres were found to be extremely hydrophobic, an attractive feature in this case. A further addition of a target specific monoclonal antibody (mAb) such as anti-HER2 recognizing the antigens presented by neoplastic transformation was designed to result in a more efficient Photoimmunotargeting (PIT), as we have demonstrated above.

In summary, both porphyrin encapsulated microspheres with and without antibody adsorption were found to cause effective cell death. The phenomenon resembling autophagy was only observed in the case of cells treated with porphyrin encapsulated microspheres with anti-HER-2 adsorbed on the surface.

All these findings promise the development of a novel immunotargeting drug delivery system based on the biodegradable polymer P(3HB). Investigations using the breast cancer cell line SK-BR-3 have shown the effectiveness of the system. Hence, this work confirms that targeted PDT can be used successfully to treat breast cancer, decreasing, or eliminating the related cytotoxicity to chemotherapy, a great step forward.

---

# **Chapter 6**

## **Process optimisation and synthesis of amphiphilic P(3HB)-HA microspheres and their application in drug delivery**

## 6.1. Introduction

PHAs, although extremely useful in various biomedical applications intended for long-term implantation, often fall short in applications that specifically require a shorter period of degradation. In addition, PHAs are quite hydrophobic and in applications requiring hydrophilicity, this can prove to be a disadvantage. Further, development of amphiphilic PHAs that can solubilize in water, while maintaining the presence of hydrophobic domains would be useful for drug delivery applications since such amphiphilic structures are known to self-assemble in to micelle like structures with the suitable active factors entrapped within. Several strategies have been reported, most prominent of which are functionalization and grafting. Functionalization involves processes such as transesterification, carboxylation, and sulphonation (Hazer, 2010). Melts or solutions of PHAs when treated with alcohols exchange ester groups to result in diols. Catalysed transesterifications can produce telechelic P(3HB) with insignificant amphiphilic properties such as the diol moieties are too short in comparison with the long hydrophobic chains. However, these can be used in the synthesis of polyurethanes via diisocyanate chain extension reaction, with any chosen aliphatic polyesters as soft segments (Hazer, 2010). Unsaturated PHAs such as Poly(3-hydroxy octanoate-co-10-undecenoate), PHOU, have been reported to be oxidized to diols and carboxylic acids due to the presence of unsaturated pendant groups. The resulting diols were found to be soluble in polar solvents (Hazer, 2010). Saturated PHAs such as P(3HB) were also reported to have been made water wettable by subjecting to carboxyl ion incorporation. Graft polymerisation with hydrophilic molecules such as chitosan, cellulose and PEG are gaining momentum, but the prospects of these are limited by their exogeneity to the human body, particularly within the context of biomedical applications.

Hyaluronic acid is a ubiquitous polysaccharide, naturally occurring in various species. It is a polymer of D-glucuronic acid and N-acetyl-D-glucosamine disaccharide with molecular mass as high as 10 MDa, which helps in the polymer's various functions such as maintaining the viscoelasticity of liquid connective tissue, control of tissue hydration, water transport, proteoglycan organization in the extracellular matrix (ECM), tissue repair and various receptor-mediated functions in cell detachment, tumour development and inflammation (Mero and Campisi 2014). These reasons render hyaluronic acids excellent building blocks for a variety of biodegradable and biocompatible structures such as hydrogels, self-assembly micelles, *in-situ* injections, in biomedical applications, especially drug delivery. HAylation is a common strategy adopted in many delivery systems such as protein delivery, anticancer drug delivery and anti-inflammatory drug delivery. Hyaluron binding protein vis-à-vis, CD-44, RHAMM, LYVE-1, IVd4 and LEC receptors have been investigated within the context of HA mediated anticancer drug delivery. HA's biodegradability, biocompatibility, increased drug loading capacity, water solubility and receptor mediated endocytosis makes it an ideal candidate as carriers. Synthesis of amphiphilic HA have been previously attempted and reported in several investigations, however, the process is not straightforward from a synthetic point of view. This is mainly due to the lack of availability of common working solvents. Most of the research focused on the synthesis of amphiphilic HA conjugates have exploited the carboxylic group of HA, which unfortunately is the CD44 receptor binding site. This has serious implications in hampering the ability of the molecule's inherent binding with tumour cells, which otherwise can exploit the increased permeability and retention property presented by cancer tissues. Furthermore, the strategy of grafting at the hydroxyl moiety, which has been reported with the use of aliphatic polyesters such as PCL, PLGA and PEG, although provided slower clearance from

biological systems, still did not manage to achieve desired biocompatibility due to their exogenous origin (Mero and Campisi 2014).

In this study, hydrophilic HA and hydrophobic P(3HB), both of which are of natural origin, were used to produce an amphiphilic graft polymer. Hydrolysed P(3HB) was used to conjugate with HA, in a DMSO solution. A variety of lengths of the hydrolysed polymer were used to obtain the best optimised conjugate and these were well characterised at Contipro a.s. and University of Westminster. The polymer thus produced was used to optimise the production of amphiphilic microspheres with encapsulated drugs (hydrophilic drugs Aspirin and gentamicin and hydrophobic drug curcumin). The degradation profile, and release kinetics of the drugs were studied.

Curcumin is a natural derivative from turmeric and has been implied to have several anticancer, anti-inflammatory and antibacterial properties. To date, a wide range of researches advertising antibacterial properties of curcumin against various spectra of bacteria such as *Staphylococcus aureus*, *Trichophyton gypseum*, *Salmonella paratyphi*, and *Mycobacterium tuberculosis* have been published (Teow *et al.*, 2016). However, native curcumin has low solubility and requires much higher doses of administration. This section describes the study of P(3HB)-HA conjugate microspheres with encapsulated curcumin and their antibacterial activity against (MRSA).

## 6.2. Results

P(3HB) was subjected to hydrolytic depolymerisation to varying lengths of time in concentrated acetic acid to produce hydrolysed polymers of low molecular weight (carried out by Dr. Rinat Nigmatullin). The conjugate was synthesised using a 93:7% molar ratio of HA to OligoHB (Carried out by Contipro a.s.).

### 6.2.1. Optimisation of microsphere production

The amphiphilic polymer this produced was used for the production of microspheres. Microsphere production using an inverse emulsion crosslinking method in water-in-oil (w/o) dispersion was optimised as described in section 2.2.7.2. The conditions employed in the optimisation are given in **Table 6.1**.

Experiment No.	Polymer concentration (g/mL)	Oil - Phase	Surfactant	Crosslinking Agent	Post-Lyophilisation Results
1	0.01	Ethyl acetate	Nil	Nil	Did not yield spheres
2	0.05	Ethyl acetate	Nil	Nil	Did not yield spheres
3	0.01	Ethyl acetate	Nil	GST	Did not yield spheres
4	0.01	Ethyl acetate	Span 80	GST	Did not yield spheres
5	0.01	Paraffin oil / Petroleum ether	Tween 80	GST	Spheres visibility dispersed, but on drying became too clumped to a jelly consistency
6	0.01	Paraffin oil/ Petroleum ether	Span 80 (1% v/v)	GST	Spheres visibly dispersed, but on drying attained a jelly consistency
7	0.01	Paraffin oil	Tween 80	1% Glutaraldehyde	Spheres visibly dispersed, but on drying attained a jelly consistency
8	0.01	Paraffin oil	1% Span 80	1% Glutaraldehyde	Could not separate oil from microspheres
9	0.01	Paraffin oil	Span 80 (0.1% v/v)	Heat	Formed spheres
10	0.01	Paraffin oil	Span 80 (0.1% v/v)	GST	Formed spheres

**Table 6.1:** Optimization of microspheres using P(3HB)- HA conjugate

### 6.2.2. Analysis of surface morphology and particle size distribution

The surface morphology of the microspheres was observed under scanning electron microscopy. It was found that, an increased concentration of the surfactant (1% v/v) as per experiment number 8, yielded in microspheres of smaller size range (1-5  $\mu\text{m}$ ). However, these were too clumped together and were not responsive to washing, to remove excessive oil, with any of the three solvents (**Figure 6.1**).

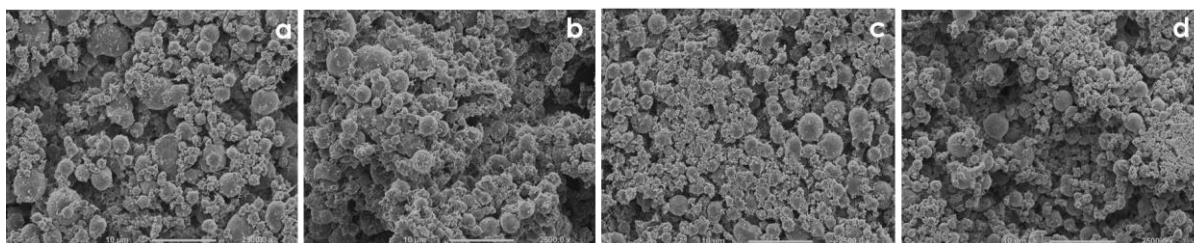


**Figure 6.1:** P(3HB)-HA microspheres prepared under conditions corresponding to experiment number 8, washed with a) water only, b) hexane, c) petroleum ether and d) isopropanol (size bar= 10  $\mu\text{m}$ )

Experiment number 9 and 10 resulted in larger microspheres of the range 15- 30  $\mu\text{m}$ . However, the heat crosslinked microspheres were found to be unstable at room temperature, after 6 hours. The GST crosslinked microspheres had smooth surface sphericity and was found to be present with surface residual paraffin oil (**Figure 6.2**).

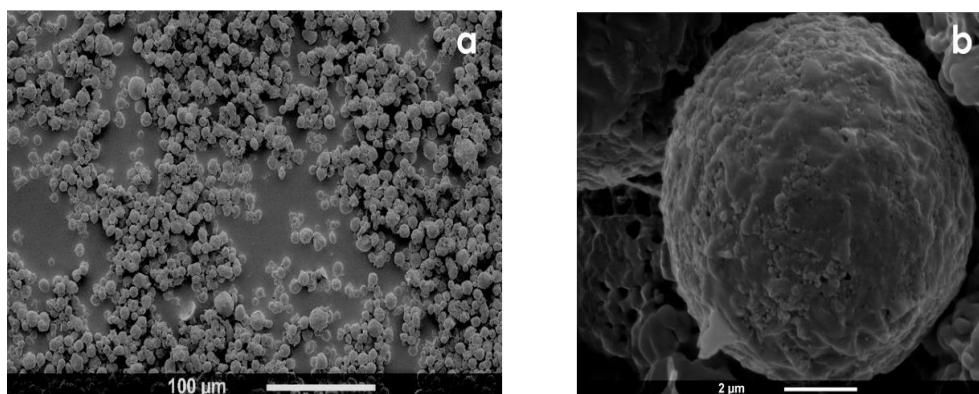


**Figure 6.2:** SEM images of P(3HB)-HA microspheres prepared under conditions corresponding to experiment number 10

These were washed with hexane, petroleum ether and isopropanol respectively. It was observed that, without washing the microspheres formed were lumpy and lacked sphericity (Figure 4). Washing with hexane and petroleum ether did not result in appreciable results and continuous washing resulted in the disintegration of microspheres. The microspheres washed with isopropanol, which was found to be effectively devoid of the oil, without compromising the structure of the microspheres. 4 washes with isopropanol, was found to completely remove the appearance of oil on the surface of microspheres (Figure 6.3). The spheres were smooth and porous.

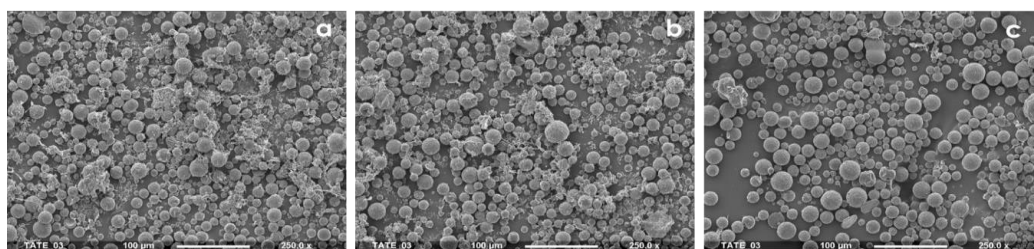


**Figure 6.3:** P(3HB)-HA microspheres a) not washed with isopropanol b) washed twice with isopropanol and c) washed 4 times with isopropanol (size bar= 100 µm).

The microspheres produced were within the size range of 15-30 µm and exhibited increased polydispersity compared to P(3HB) microspheres (Figure 6.4).

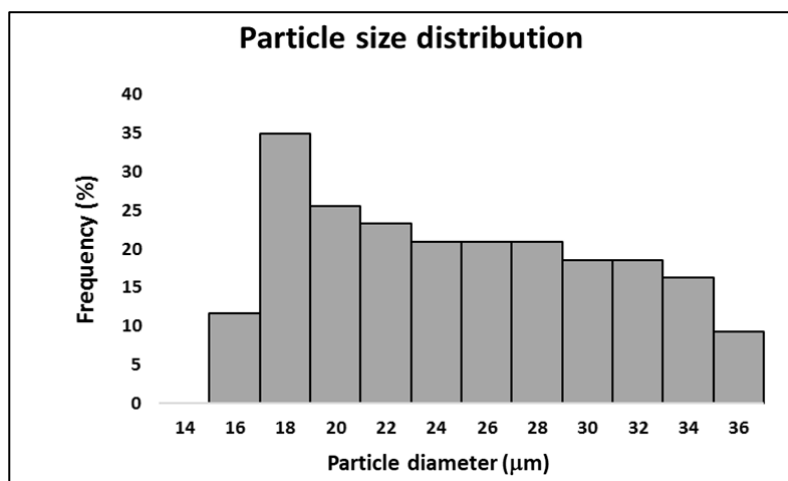


**Figure 6.4:** Particle size distribution of P(3HB)-HA microspheres

The average size of microspheres was found to be  $22.9 \pm 3.2 \mu\text{m}$ .

### 6.2.3. Characterisation of P(3HB)- HA microspheres

#### 6.2.3.1. FTIR

FTIR spectra of P(3HB)-HA microspheres showed peaks characteristic to HA published in literature (Figure 6.5).

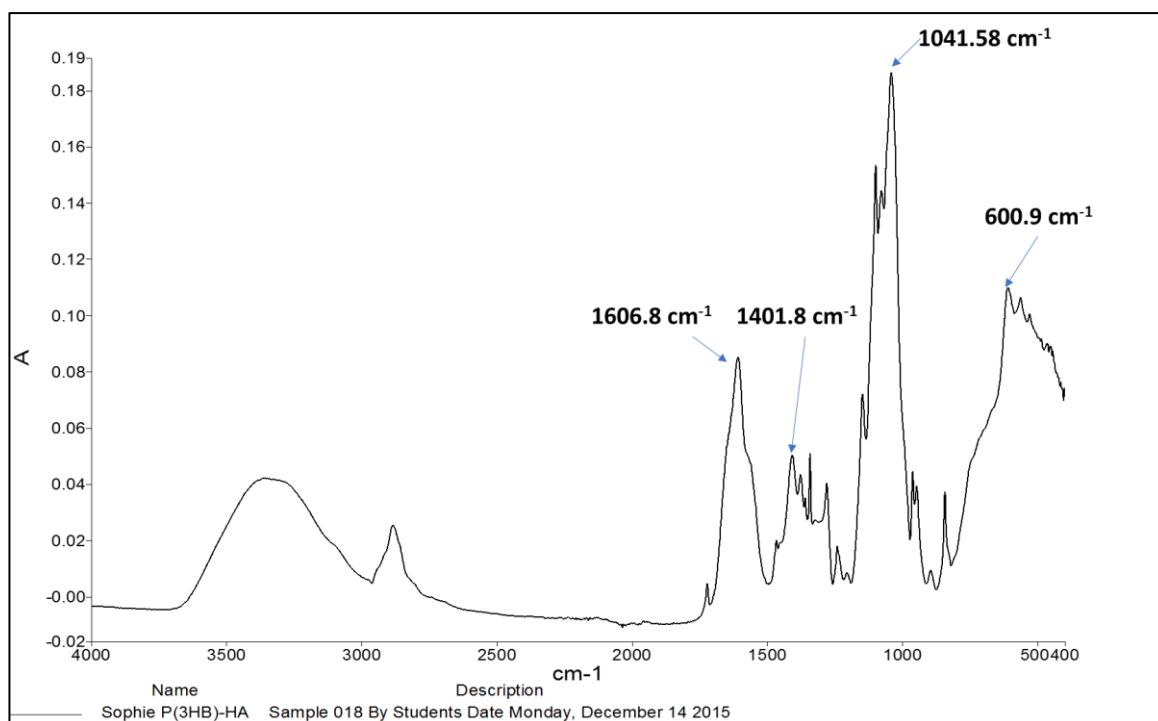


**Figure 6.5:** FTIR spectra of P(3HB)- HA microspheres

The spectra showed several sharp peaks ( $\text{cm}^{-1}$ ) such as at 600.37 and at 1041.3 that could be due to the C-O-C stretching, at 1407.86 that corresponds to the presence of C-O group with C=O combination, at 1606.06 that indicates the presence of amide II group, at 2885.26 due to the C-H stretching and at 3306.6 that confirms the presence of OH stretching (Reddy and Karunakaran 2013).

#### 6.2.3.2. Swelling studies at different pH

Swelling studies were conducted by immersing P(3HB)-HA microspheres in phosphate

buffer saline of pH 6, 6.8, 7.4 and 10 for a period of 9 days. The degree of swelling was found to increase corresponding to increase in pH (**Figure 6.6**). It was found that with an increase in pH from 6 to 10, the maximum swelling ratio increased from 198 to 216%. In all the cases, there was an exponential increase in swelling up to day 3, and the swelling was found to plateau from that point onwards. The PBS solution containing the microspheres had seemed to appear cloudy by this point, with the appearance of structural disintegration in the microspheres.

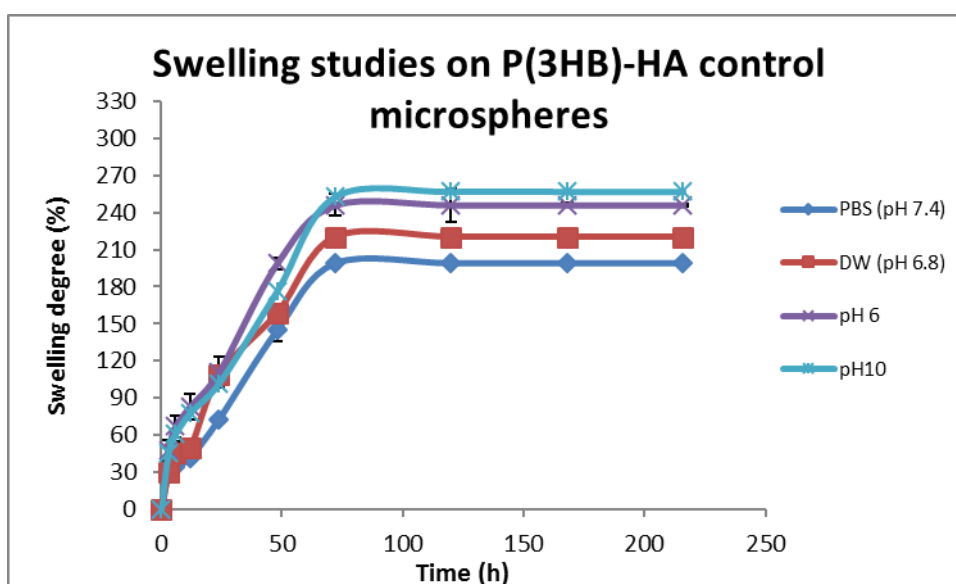


**Figure 6.6:** Swelling studies of P(3HB)-HA microspheres at different pH values

#### 6.2.4. Hydrophilic drug encapsulation

2 hydrophilic agents namely aspirin and gentamycin were encapsulated in P(3HB)-HA microspheres. These were dispersed in the water phase and homogenised, before being emulsified in paraffin oil. The microspheres thus produced were characterised for surface morphology, particle size distribution, and microsphere yield and encapsulation efficiency. The microspheres produced were of good sphericity, smooth surfaced and porous (**Figure 6.7**).

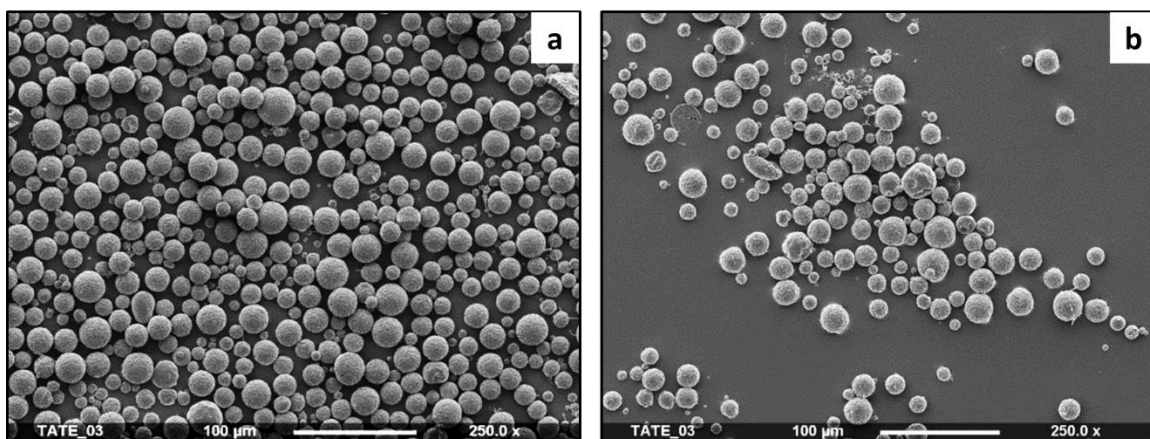


**Figure 6.7:** P(3HB)-HA microspheres encapsulated with a) Aspirin, b) Gentamycin (Size bar=100 µm)

The FTIR spectra of all the drug encapsulated microspheres resembled that of the controls and did not exhibit any significant peaks indicative of the presence of the drug. A comparison of these results is tabulated (**Table 6.2**).

Drug	Yield (%)	particle diameter (µm)	Encapsulation efficiency (%)
Aspirin	70.36	19.01	71.34
Gentamycin	79.38	20.61	82.4

**Table 6.2:** Comparison of P(3HB)-HA microspheres encapsulated with Aspirin and Gentamycin.

Gentamycin encapsulated microspheres had the highest yield (79.38%), in comparison with the other two. The particle size was not found to vary significantly amongst the three samples, however, gentamycin encapsulated microspheres were found to be the largest. Encapsulation efficiency of Gentamycin in the microspheres were found to be significantly higher, in comparison with Aspirin (71.34%).

### 6.2.5. Drug release kinetics

P(3HB)- HA microspheres encapsulated with the two drugs were immersed in PBS solution and incubated at 37°C. Samples were drawn periodically, and cumulative release was analysed according to methods described in Chapter 2.

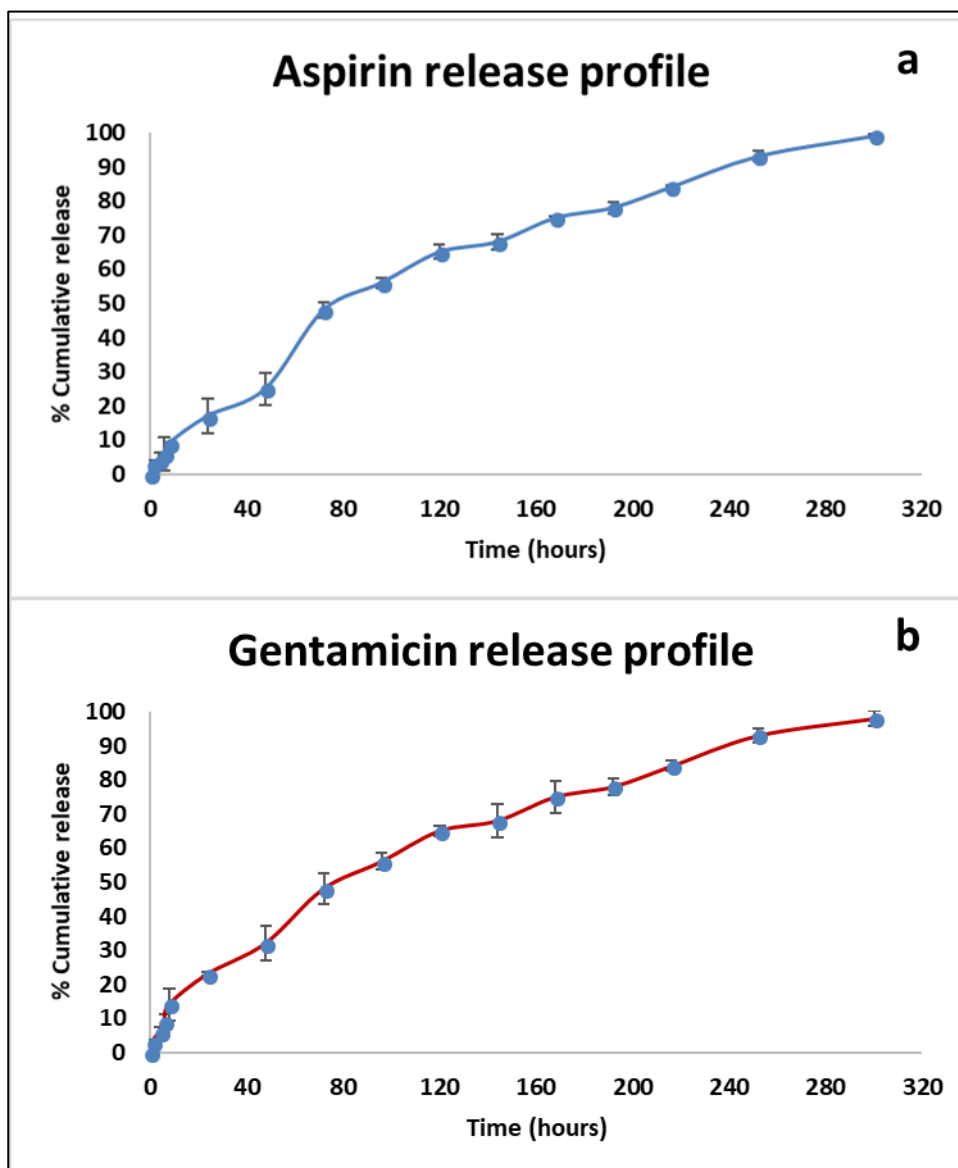


**Figure 6.8:** Drug release profile of a) Aspirin and b) Gentamycin encapsulated in P(3HB)- HA microspheres

Both the microsphere samples exhibited an initial burst release (Figure 6.8). Aspirin and gentamycin encapsulated microspheres exhibited a burst release up to 48 hours and

followed by a slower rate up to day 11. 46.36% Aspirin and 48.37% gentamycin were released by 48 hours. The microspheres underwent complete disintegration by day 11 in both the cases.

### 6.2.6. Hydrophobic drug encapsulation

Curcumin was added to the oil phase- paraffin oil containing span 80, and the P(3HB)- HA solution was added to this. The microspheres thus produced were characterised for surface morphology, particle size distribution, yield and encapsulation efficiency. The microspheres produced were of good sphericity, smooth surfaced and porous (**Figure 6.9**).

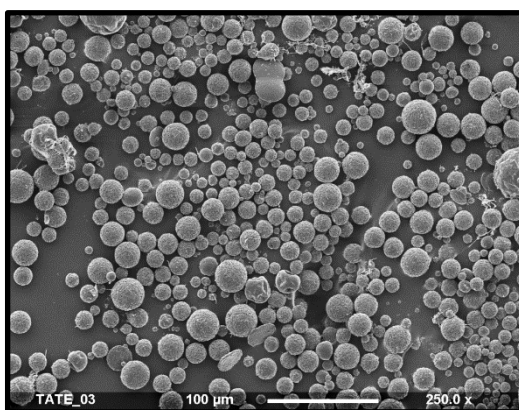


**Figure 6.9:** P(3HB)- HA microspheres encapsulated with curcumin

The FTIR spectra of all the drug encapsulated microspheres resembled as that of the controls and did not exhibit any significant peaks indicative of drug conjugation. Curcumin encapsulated microspheres were of the size range 17.91  $\mu\text{m}$ , and thus were found to be smaller than the microspheres encapsulated with hydrophilic drugs. Microsphere yield was 74.38%. In comparison with hydrophilic drugs, curcumin was encapsulated to a lesser amount within P(3HB)- HA microspheres (67.37%).

### 6.2.7. Drug release kinetics

P(3HB)- HA microspheres encapsulated with the curcumin were immersed in PBS solution

and incubated at 37°C. Samples were drawn periodically, and cumulative release was analysed according to methods described in Chapter 2. Curcumin had a sharp burst release within 12 hours, amounting to 44.27%. Curcumin release proceeded up to 13 days, after an initial period of rapid release after which the rate fell and thereafter continued to slowly decay. (Figure 6.10).

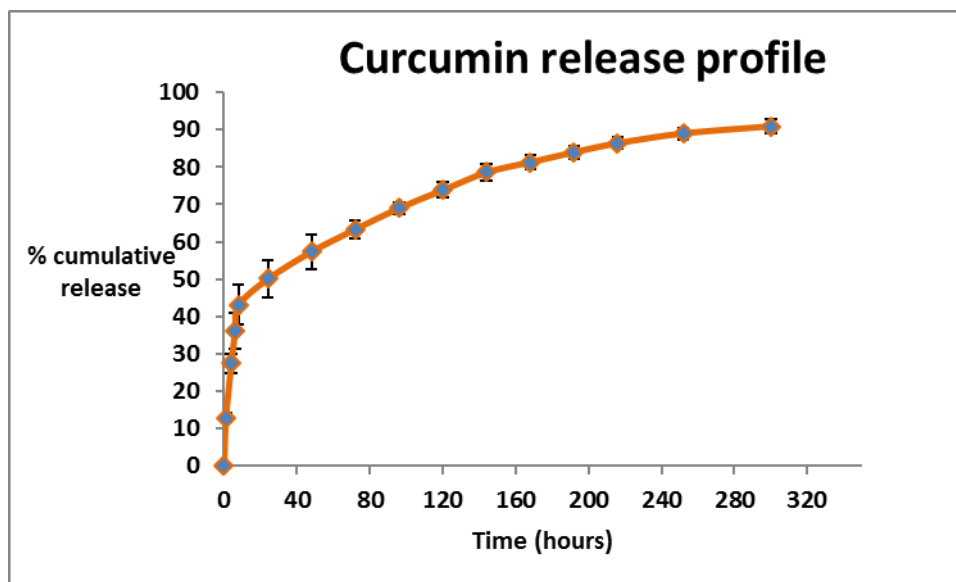


**Figure 6.10:** Release profile of curcumin from P(3HB)-HA microspheres

### 6.2.8. Comparison of drug release profiles

The release data was fitted in models as described in section 2.2.11.  $R^2$  value of each of the linear regression was compared. A clear difference in release profile was observed between the hydrophilic drugs (aspirin and gentamicin). The release profile of aspirin and gentamicin was found to fit well with Higuchi model with 98.6 and 99.5% correlation. Curcumin release on the other hand was found to follow first-order kinetics, indicating the release was dependent on the initial concentration. The release exponent of both aspirin and gentamicin was found to correspond to anomalous non-Fickian diffusion, indicating matrix degradation and diffusion as contributing parameters. The microspheres underwent

complete degradation in 11 days and this corroborates the fit of the release data to Korsmeyer- Peppas.

		P(3HB)- HA microspheres with encapsulated		
Model	Parameters	Aspirin	Gentamicin	Curcumin
Zero- order	R <sup>2</sup>	0.941	0.938	0.767
	Adj- R <sup>2</sup>	0.937	0.934	0.751
	Slope	0.943	0.938	0.767
	SSR	1130.76	1106.63	2789.34
First- order	R <sup>2</sup>	0.880	0.927	0.960
	Adj- R <sup>2</sup>	0.872	0.922	0.958
	Slope	-0.0051	-0.0046	-0.0032
	SSR	0.514	0.244	0.064
Higuchi	R <sup>2</sup>	0.986	0.995	0.925
	Adj- R <sup>2</sup>	0.985	0.995	0.920
	Slope	6.20	5.99	4.74
	SSR	268.79	84.65	898.77
Hixson- Crowell	R <sup>2</sup>	0.982	0.989	0.911
	Adj- R <sup>2</sup>	0.981	0.988	0.904
	Slope	-0.0109	-0.0103	-0.0077
	SSR	0.319	0.174	0.867
Korsmeyer- Peppas	R <sup>2</sup>	0.982	0.993	0.946
	Adj- R <sup>2</sup>	0.980	0.992	0.942
	Slope	0.689	0.624	0.300
	SSR	0.073	0.023	0.042

**Table 6.3:** Summary of model fitting for drug release from free P(3HB)- HA microspheres.

## 6.2.9. Antibacterial activity of Curcumin

### 6.2.9.1. Growth inhibition

Growth inhibition of MRSA was compared using 1mg/mL, 0.5 mg/ml and 0.25 mg/mL of free curcumin and encapsulated curcumin for 18 and 36 hours (**Figure 6.11**). Encapsulation was found to increase the antibacterial effect of curcumin in all the cases. While at 18

hours, 0.25 and 0.5 mg/mL of free curcumin inhibited 33.2% and 42.39% of bacterial growth, 1 mg/mL inhibited 56.71%. at 18 hours, 0.25mg/mL, 0.5mg/mL and 1mg/mL curcumin encapsulated in P(3HB)-HA microspheres inhibited 42.39%, 42.39% and 57.28% respectively in comparison with bacteria grown in culture media. A similar trend was observed at 36 hours, with 1 mg/mL of encapsulated curcumin inhibiting 96.21% of bacterial growth while the same concentration of free curcumin inhibiting 91.2% bacterial growth.

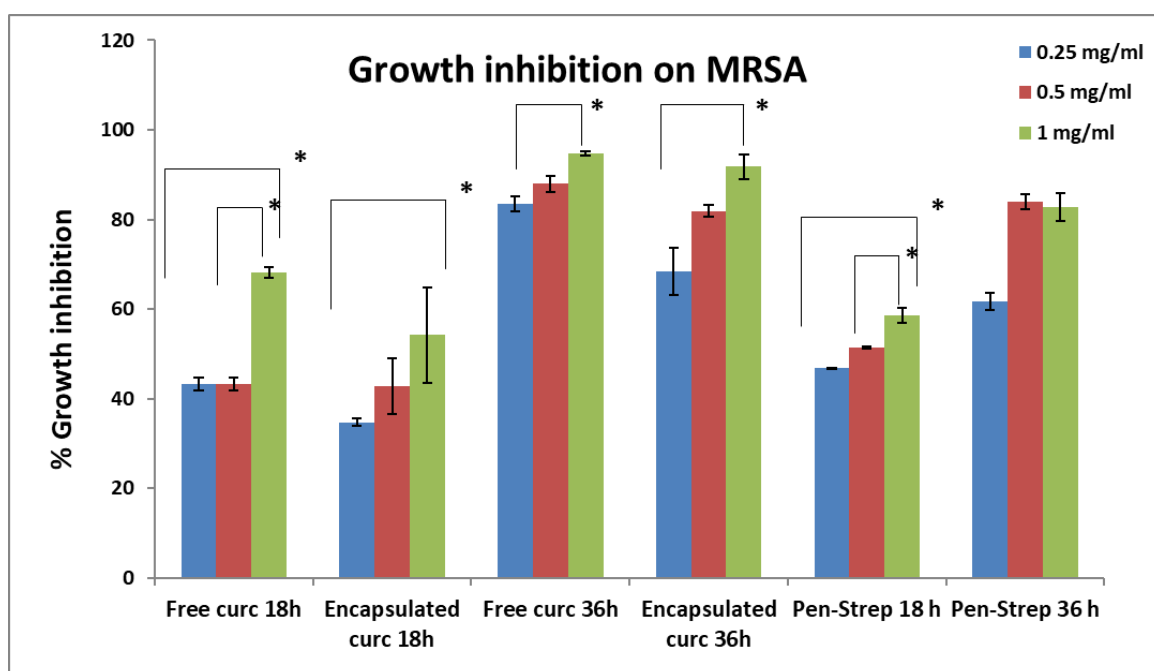


**Figure 6.11:** MRSA inhibition of free and encapsulated curcumin (\*\* $p < 0.05$ ) ( $n=3$ , error= $\pm$  s.d).

#### 6.2.9.2. Quantification of Minimum inhibitory concentration (MIC)

An overnight culture of MRSA of equal dilution was used to carry out MIC analysis. Empty P(3HB)-HA microspheres were used as controls. From the encapsulation efficiency of curcumin in P(3HB)-HA microspheres, 100  $\mu$ L of various dilutions of the microspheres (500, 250, 125, 62.5, 31.25, 16, 8, 4, 2, 1  $\mu$ g /mL of curcumin respectively) were prepared. These were incubated with 100 ml of overnight culture of MRSA. The tubes were incubated at 37

°C for 24 hours. After the incubation period, the OD of each of the wells were recorded and compared with controls. MIC of curcumin encapsulated microspheres were found to be 93.75 µg/mL.

### 6.3. Discussion

HA is a naturally occurring glycosaminoglycan with high biocompatibility, as it is inherently present in ECM, cartilage matter and synovial fluid of most animals (Yun *et al.*, 2004). A water in oil emulsion was used for the preparation of P(3HB)-HA microspheres, with glutaraldehyde as the cross-linking agent. The surface morphology of the microspheres prepared using this optimised technique was found to be smooth surfaced, spherical with low polydispersity. These appeared to be morphologically superior than some formulations that were prepared using spray drying (Fatnassi *et al.*, 2014). The process optimisation of P(3HB)-HA microsphere production was successfully achieved with Paraffin as the oil phase and in the presence of Span 80 surfactant. It was found that a surfactant concentration of (1% v/v) resulted in microspheres of smaller size (less than 5 µm), where as a surfactant concentration of 0.1% v/v resulted in microspheres of average size (22.9 µm). This is similar to the observation made in the case of P(3HB) microspheres. An increased concentration of surfactant resulted in an increased proximity of water and oil interphase, which results in smaller micelles (Maia *et al.*, 2004). However, the viscosity of the emulsion was found to be too high in the case of an emulsion with higher concentration of surfactants and resulted in microspheres that had an excessive deposition of paraffin oil on the surface. Due to this reason, a lower surfactant concentration was used in the preparation of microspheres in this work. Span 80 is reported to be the most commonly used surfactant in DDS formulations involving HA (Qiu *et al.*, 2016; Ma *et al.*, 2015).

Three different solvents namely hexane, petroleum ether and isopropanol were used to wash the excessive amount of paraffin oil present on the surface. Of these, isopropanol was found to be the most effective in washing off the paraffin oil and span 80 from the surface of microspheres, while not compromising the structural integrity of the microspheres. Isopropanol is commonly used as surgical spirit and is a good solvent for paraffin oil.

HA microspheres synthesised with 1 v/v% of Span 80 were found to be in the size range of 6-20  $\mu\text{m}$  in a study intended for sustained gene delivery and targeting (Yun *et al.*, 2004). Here, the preparation strategy involved the use of adipic dihydrazide as a cross linking agent, for 24 hours during the last stage of preparation. Comparing these with the preparation strategy employed in the case of P(3HB)-HA microspheres in this work, it can be concluded that the latter produced microspheres of a smaller size distribution. Yun *et al.*, reported that these microspheres were washed three times with isopropanol and were found to appear well separated from one another with no occurrence of residual paraffin oil on the surface, corroborating the results obtained in this work (Yun *et al.*, 2004). Ma *et al.*, in a similar study describe the synthesis of HA- chitosan microspheres in the context of controlled-release of cytokine response modifier A for osteoarthritis (Ma *et al.*, 2015). Sodium tripolyphosphate, a commonly used crosslinker was used here, as the mass ratio of chitosan dominated in the preparation (2g chitosan and 0.1g HA). With the addition of 10 w/v% of the cross- linking agent, microspheres of 8-15  $\mu\text{m}$  diameter were obtained. However, these were washed with acetone to remove residual oil and this method was not found to be entirely successful as the SEM images revealed the presence of surface deposition of oil residues (Ma *et al.*, 2015).

Chemical characterisation of the microspheres carried out by FTIR revealed spectra

resembling that of standard HA, with no significant peak corresponding to P(3HB). This may have been due to the comparatively lower molar proportion (93:7) of P(3HB) in the conjugate. The case remained the same in all encapsulated microspheres, indicating that the drug encapsulation did not bring about any chemical changes in the structure of the conjugate. The FTIR spectra analysed in this study is comparable to standard HA spectra published in literature (Reddy and Karunakaran 2013).

With drug encapsulation, it was found that hydrophilic drug containing microspheres were larger (~20  $\mu\text{m}$ ) than those containing a hydrophobic drug (~17  $\mu\text{m}$ ). This is probably due to the fact that, hydrophilic drug moieties have better affinity for HA, and the a more concentrated and viscous emulsion interphase was formed in this case. This increased affinity was found to influence drug encapsulation efficiency as well, since the hydrophilic drugs were found to have higher encapsulation interphase (aspirin: 71.34%, and gentamycin 82.4%) as opposed to the hydrophobic drug (curcumin 67.37%).

Encapsulation efficiency of the hydrophilic drugs appeared to be influenced by their solubility in water, as gentamycin with a higher solubility (50 mg/mL) had significantly higher encapsulation efficiency in comparison with aspirin with a lower solubility (3 mg/mL). An aspect to be improved in the case of P(3HB)- HA microspheres examined here would be the extent of burst release. Although comparable with published literature on controlled release from HA microspheres (Yun *et al.*, 2004; Mero and Campisi, 2014; Qiu *et al.*, 2016), a strategy to minimise burst release would be desirable here. In the case of hydrophilic drugs, all the three microsphere samples exhibited a burst release. Microspheres with encapsulated aspirin and gentamycin exhibited a burst release of up to 48 hours and followed a steady release up to day 11. 46.36% aspirin and 48.37% gentamycin were released within 48 hours. The microspheres underwent complete

disintegration by day 11 in both the cases. In spite of the burst release, there appeared to be a linear and controlled release of these drugs after the burst release. This is possibly due to the swelling behaviour of these microspheres, as they absorbed about 200% more water than their weight, in 3 days. This influx of water may have resulted in the dissolution of a large amount of drug, resulting in burst release. This study has demonstrated the controllability of swelling behaviour at different pH. The varied behaviour exhibits a potential to further fine tune the swelling behaviour with different stimuli and thereby control release. In all the cases, the drug release profile from the point of burst release was found to be of zero order, with an  $R^2$  value close to 1. This suggests the plausibility of fine tuning these microspheres for better control, with interventions to avoid burst release. Aspirin and gentamycin being antimicrobial, P(3HB)-HA microspheres containing these agents have potential application in wound healing and post-operative care.

Finally, encapsulation of curcumin in P(3HB)-HA microspheres was examined. In comparison with the hydrophilic drugs, curcumin exhibited a lower encapsulation efficiency in P(3HB)-HA microspheres (67.37%). An interesting observation made with reference to the release kinetics was the reduced window of burst release period. Here, burst release was limited to 12 hours, suggesting that the release of curcumin is dependent on the disintegration of the microspheres and increased solubility of curcumin rendered by the presence of HA. Just water influx does not have a direct correlation to curcumin release since curcumin is hydrophobic in nature and would interact relatively strongly with the P(3HB), a hydrophobic polymer. Hence, the burst release was not extended to 48 hours or more. There are very few reported studies on encapsulation of hydrophobic moieties in HA, due to the inherent hydrophilic nature of HA. However, there are instances of coating hydrophobic pulmonary drugs with HA for enhanced mucosal adhesion (Byron and Patton,

2007). The encapsulation efficiency of curcumin achieved here is reasonable and this is due to the presence of hydrophobic P(3HB) pockets in the conjugate, with increased affinity to hydrophobic curcumin, a great advantage. Hence, this is the first ever report of encapsulation of a hydrophobic drug in a HA based drug delivery system. Curcumin is an interesting molecule in various therapeutic contexts such as anti-inflammatory, anticancerous, and antimicrobial (Teow *et al.* 2016; Bansal *et al.*, 2011). Here, the antimicrobial effects of curcumin against MRSA were examined. MRSA is a widespread infective agent, and post-operative MRSA infections are increasing at an alarming rate. As new resistant strains of potent pathogens arise under antibiotic selection pressure, curcumin, that has been reported to be obliterating methicillin resistance in *S. aureus* has tremendous potential (Mun *et al.*, 2013). In this study, the curcumin encapsulated P(3HB)-HA microspheres were found to be more efficient in killing MRSA in comparison with free curcumin and this increase was statistically significant. All these results indicate the huge potential of P(3HB)-HA microspheres in drug delivery, especially in the context of antimicrobials.

The drug release of aspirin, gentamicin, and curcumin from P(3HB)-HA microspheres were compared and fitted to the five models as mentioned before. The release of hydrophilic drugs was found to fit better with Higuchi model, whereas that of the hydrophobic drug was found to fit better with first-order kinetics. The release exponents in the case of hydrophilic drugs were found to indicate anomalous non-Fickian mode of mass transfer where both diffusion and degradation of the polymer matrix influence mass transfer. This can be true considering the entire sample disintegrated within 11 days. However, in the case of curcumin, the slower release must have been a result of the poor solubility of the drug. Good fit of all the three-release data gives insight into the swellable nature of the

polymer, as indicated in section 6.2.3.2.

# Chapter 7

## Conclusion

## 7.1. Conclusions

P(3HB) particulate drug delivery systems established and characterised in this research have the potential in the controlled and sustained delivery of various therapeutic agents. There is a growing need for reproducible and controllable drug delivery systems, considering the lengthy and costly process of drug development. P(3HB) is a short chain length variety of PHA which has specifically been recognised for its potential to form DDS. In the first part of this study the solid-in-oil-in-water technique was used to optimise production of P(3HB) microspheres a response surface methodology based on the Box Behnken design. Through statistical optimisation, it has been possible to develop a mathematical model for the synthesis of P(3HB) microspheres. The model was validated within 95% confidential interval. Along with other contributing parameters such as PVA concentration and stirrer speed, polymer concentration was found to be the most important variable in determining particles size. Microspheres in a size range of 25-45  $\mu\text{m}$  were produced with experiments run under a set of 15 randomized trials. The results of these optimisation experiments were used to tailor micro and nanospheres of different size ranges and these were characterised for their size distribution, porosity, amount of surface residual surfactant and hydrophobicity. Spheres of 5 distinct average diameters ( $118 \pm 12.3$  nm,  $728 \pm 32.96$  nm,  $1.6 \pm 0.13$   $\mu\text{m}$ ,  $9.8 \pm 2.18$   $\mu\text{m}$  and  $22.83 \pm 1.21$   $\mu\text{m}$ ) were produced under varying process parameters. P(3HB) produced from different producer organisms (*B. cereus* SPV and *B. subtilis* OK2) were found to be of different molecular weight (~150 and 850 kDa respectively) and therefore, when processed under the same conditions resulted in nanospheres of varying morphology and diameter.

P(3HB) micro and nanospheres with encapsulated therapeutic agents relevant in cardiovascular diseases were developed, for potential incorporation in drug eluting biodegradable stents. P(3HB) and PLLA microspheres with encapsulated rapamycin was compared with respect to their characteristics such as size distribution, porosity, hydrophobicity, encapsulation efficiency and drug release kinetics. PLLA microspheres formed were smaller than (average diameter 2.98  $\mu\text{m}$ ) P(3HB) microspheres (average diameter 4.82  $\mu\text{m}$ ). In both the cases, encapsulation efficiency was found to increase with drug loading. P(3HB) microspheres were more suitable for applications as their degradation products were found to be less acidic than that of PLLA microspheres. Drug release rate from P(3HB) microspheres were found to be slightly faster than PLLA microspheres. In both the cases, an initial burst release for 48 hours was observed. In all the 4 preparations, the release data was found to be more fitting to Higuchi model, indicating diffusion as the mode of mass transfer. The release exponent indicated that the release followed Fickian mode of diffusion.

Tacrolimus encapsulated micro and nanospheres of P(3HB) were compared, to analyse drug encapsulation and release kinetics with respect to size of the spheres. P(3HB) microspheres were found to have increased encapsulation efficiency in comparison with P(3HB) nanospheres. In the case of microspheres, encapsulation efficiency increased from  $61.2 \pm 4.18\%$  to  $69.8 \pm 1.9\%$  and  $72.3 \pm 2.21\%$  between 1 wt%, 5 wt% and 10 wt% tacrolimus loading respectively. In the case of nanospheres, this was  $59.8 \pm 2.1\%$ ,  $62.3 \pm 2.01\%$  and  $65.8 \pm 1.54\%$  respectively. Nanospheres were found to exhibit a faster release rate, in comparison with microspheres. Both P(3HB) nanospheres and microspheres maintained a sustained release of tacrolimus for 30 days, with a cumulative release of 71.2%, 73.1% and

76.2% from nanospheres encapsulated with 1 wt%, 5 wt% and 10 wt% tacrolimus. In the case of microspheres, this was 68.12, 70.37 and 72.3% respectively. Here again, drug release was found to fit well with Higuchi model, suggesting diffusion as the reason for mass transfer.

Vascular Endothelial Growth Factor (VEGF), commonly used in the context of cardiovascular regeneration, was encapsulated within P(3HB) micro and nanospheres and were embedded in collagen scaffolds. P(3HB) spheres of 3 different size ranges were considered for immobilization on collagen scaffolds. Nanospheres of a size range 500-900 nm were well incorporated in the scaffold with a uniform distribution. Microspheres of the size range 5-15  $\mu\text{m}$  were also satisfactorily incorporated in the scaffolds whereas microspheres of the size range 20- 30  $\mu\text{m}$  formed clumped structures in the scaffold, and therefore were not considered for further studies. A cumulative release of  $98.23 \pm 1.98\%$  was achieved from VEGF encapsulated microspheres whereas a cumulative release of  $94.12 \pm 1.21\%$  was achieved from VEGF encapsulated nanospheres. The differences in release of VEGF from spheres embedded and not embedded in the collagen scaffold were quantified and it was established that embedding in the scaffolds reduced burst release. In all these cases mentioned above an initial burst release up to 48 hours was observed. All the four formulations were able to sustain release of VEGF for more than 30 days, implying the potential of these in controlled delivery, with relevance in cardiac regeneration. The release data was found to be most fitting with first- order release for all the four preparations with 99% correlation, except free microspheres with encapsulated VEGF ( $R^2=0.956$  for first- order). This means, the drug release was dependent on the concentration

of drug. The data for free microspheres was found to fit better with the Hixson- Crowell model, with 98.3 % correlation.

P(3HB) microspheres were developed as novel anti- cancer target specific photodynamic drug delivery systems. 3 different derivatives of porphyrin, a well- studied photosensitizer molecule in the context of photodynamic therapy, was encapsulated in P(3HB) microspheres. The optimization process followed by photosensitizer encapsulation showed that polymer-drug interaction is one of the main parameters to be taken into account in drug encapsulation. 2.5 wt%, 5wt% and 10wt% drug loadings of PP, HP and TPP were successfully encapsulated in microspheres of size  $\sim 10\text{-}20\mu\text{m}$ . The encapsulation efficiency of 10wt% TPP was found to be the highest (87.8%). The encapsulation efficiencies were found to be desirably high, within a range of  $\sim 60\text{-}90\%$ . It is generally agreed that hydrophobic drug molecules better entrap in hydrophobic polymer matrices. Encapsulation efficiency increased with increased drug loading in each case and was found to be the highest for 10wt% drug loading, in each case. TPP encapsulated microspheres had the highest encapsulation efficiency, followed by HP and PP. This pattern was reflected in their ability to induce photodynamic damage, quantified by cytotoxicity estimations. 10 wt% drug loading of each porphyrin derivative was chosen to be incorporated with anti-HER-2 antibody, to aid in target specific delivery. An increase in cytotoxic effects was observed in antibody linked microspheres in the case of TPP. P(3HB) microspheres with 10 wt% loading of TPP, in conjugation with anti-HER-2 was found to be the most potent in inducing cytotoxicity.  $IC_{50}$  of this formulation was quantified  $9\mu\text{M}$ . The results obtained from this study affirms the ability of P(3HB) microspheres encapsulated with porphyrin derivatives in conjugation with target specific antibody to evoke cellular stress. All these

findings promise the development of a novel Photoimmunotargeting drug delivery system based on the biodegradable polymer P(3HB).

P(3HB) is a crystalline, hydrophobic polymer and degrades through surface erosion. There are applications that necessitate drug delivery systems that can retain moisture (especially in the context of wound healing) and a quicker release of drug moieties. Bearing this requirement in mind, a conjugate of P(3HB) with hyaluronic acid (HA) was synthesised by Contipro a.s. and the final part of this study examined the optimisation of microsphere synthesis using these conjugates. As this conjugate was amphiphilic, a water in oil emulsion, coupled with crosslinking was employed for the synthesis process. Microspheres of  $\sim 20 \mu\text{m}$  diameter were synthesised, and hydrophilic and hydrophobic drugs were encapsulated within them. The microspheres were found to be fast degrading, maintaining their structure up to a maximum of 11 days. The drug release kinetics from these showed an increased burst release compared to P(3HB) microspheres. The hydrophilic drugs (aspirin and gentamicin) were release from these conjugate microspheres following Higuchi model, whereas the hydrophobic drug (curcumin) followed first-order.

# Chapter 8: Future work

## **8.1. Future work**

The results obtained in this study with regards to the potential of P(3HB) in formulating DDS have been promising. However, there are areas that need further exploration and improvement.

### **8.1.1. Statistical optimisation of preparation of nanospheres using P(3HB) from different producer organisms**

The metabolic pool of each microorganism varies and hence the polymer produced by each of them differ in molecular weight. This particular study successfully optimised preparation of P(3HB) microspheres using different molecular weight polymers. In the future, a similar study can be extended to the statistical optimisation of the synthesis of nanospheres, incorporating molecular weight as an independent variable.

### **8.1.2. Characterization of microspheres and nanospheres**

Throughout this study, there are parameters and effects that can be better understood in the light of zeta potential analysis of the microspheres and nanospheres. This can elucidate behaviours of spheres such as aggregation, protein adsorption and drug interactions. Also, drug polymer interactions could be better studied to be able to explain encapsulation efficiency and release kinetics.

### **8.1.3. Cardiovascular drugs**

To test the efficacy of micro and nanospheres encapsulated with antiproliferative drugs on a cardiac cell line such as C2C12 is another direction that could be undertaken in the future.

P(3HB) spheres encapsulated with VEGF are currently being implanted in small animal models. The VEGF incorporated in this study was VEGF-A and it has been suggested that

AdVEGF-B186 produces a better response than VEGF-A. Encapsulation and release kinetics of this form in P(3HB) microspheres have been attempted and, in the future, its release kinetics will be compared with release from microspheres embedded in collagen scaffolds. To test whether sterilization procedures compromise the stability of the VEGF and release kinetics will also be investigated both before and after sterilization.

#### **8.1.4. Photodynamic therapy**

To understand the mechanism of drug delivery, it is important to be able to identify the distribution DDS. Although this study was able to observe the effect of P(3HB) microspheres encapsulated with porphyrin derivatives on SK-BR-3, the location of microspheres (whether they have penetrated the cells or not) is yet to be elucidated. To achieve this SK-BR-3 cells treated with microspheres prepared under the same conditions, encapsulated with Rhodamine will be observed using confocal microscopy.

#### **8.1.5. P(3HB)- HA microspheres in wound healing**

A 3D printed wound healing patch incorporated with P(3HB)-HA microspheres can be achieved in the future. P(3HB) can be used to form a mesh like, layered structures, especially when blended with a more elastomeric PHA, in between which P(3HB)- HA microspheres with curcumin can be incorporated. This way, P(3HB) will provide the necessary mechanical strength and the amphiphilic microspheres can provide the moisture needed at the wound site and release the antibiotics.

---

## References:

- Abdelwahed, W., Degobert, G., Stainmesse, S., Fessi, H. (2006). Freeze-drying of nanoparticles: formulation, process and storage considerations. *Advanced Drug Delivery Reviews*. 58 (15), 1688-1713.
- Abrego, G., Alvarado, H., Souto, E.B., Guevara, B., Bellowa, L.H., Parra, A., Calpena, A., Garcia, M.L. (2015). Biopharmaceutical profile of pranoprofen-loaded PLGA nanoparticles containing hydrogels for ocular administration. *European Journal of Pharmaceutics and Biopharmaceutics*. 95, 261-270.
- Agostinis, P., Berg, K., Cengel, K.A., Foster, T.H., Girotti, A.W., Gollnick, S.O., Hahn, S.M., Hamblin, M.R., Juzeniene, A., Kessel, D. (2011). Photodynamic therapy of cancer: an update. *CA: A Cancer Journal for Clinicians*. 61 (4), 250-281.
- Ahmed, T.A., Alharby, Y.A., El-Helw, A.R., Hosny, K.M., El-Say, K.M. (2016). Depot injectable atorvastatin biodegradable in situ gel: development, optimization, in vitro, and in vivo evaluation. *Drug Design, Development and Therapy*. 10, 405-415.
- Allen, T.M. and Cullis, P.R. (2004). Drug delivery systems: entering the mainstream. *Science (New York, N.Y.)*. 303 (5665), 1818-1822.
- Ansary, R.H., Awang, M.B., Rahman, M.M. (2014). Biodegradable poly (D, L-lactic-co-glycolic acid)-based micro/nanoparticles for sustained release of protein drugs-A review. *Tropical Journal of Pharmaceutical Research*. 13 (7), 1179-1190.
- Bansal, S.S., Goel, M., Aqil, F., Vadhanam, M.V., Gupta, R.C. (2011). Advanced drug delivery systems of curcumin for cancer chemoprevention. *Cancer Prevention Research (Philadelphia, Pa.)*. 4 (8), 1158-1171.
- Baumann, M.D., Kang, C.E., Stanwick, J.C., Wang, Y., Kim, H., Lapitsky, Y., Shoichet, M.S. (2009). An injectable drug delivery platform for sustained combination therapy. *Journal of Controlled Release*. 138 (3), 205-213.
- Belaid, A., Cerezo, M., Chargui, A., Corcelle-Termeau, E., Pedeutour, F., Giuliano, S., Ilie, M., Rubera, I., Tauc, M., Barale, S., Bertolotto, C., Brest, P., Vouret-Craviari, V.,

- Klionsky, D.J., Carle, G.F., Hofman, P., Mograbi, B. (2013). Autophagy plays a critical role in the degradation of active RHOA, the control of cell cytokinesis, and genomic stability. *Cancer Research*. 73 (14), 4311-4322.
- Bidone, J., Melo, A.P.P., Bazzo, G.C., Carmignan, F., Soldi, M.S., Pires, A.T., Lemos-Senna, E. (2009). Preparation and characterization of ibuprofen-loaded microspheres consisting of poly (3-hydroxybutyrate) and methoxy poly (ethylene glycol)-b-poly (D, L-lactide) blends or poly (3-hydroxybutyrate) and gelatin composites for controlled drug release. *Materials Science and Engineering: C*. 29 (2), 588-593.
- Brigham, C.J. and Sinskey, A.J. (2012). Applications of polyhydroxyalkanoates in the medical industry. *International Journal of Biotechnology for Wellness Industries*. 1 (1), 52-60.
- Bruschi, M.L. (2015). *Strategies to modify the drug release from pharmaceutical systems*. Amsterdam: Woodhead Publishing.
- Bugnicourt, E., Cinelli, P., Lazzeri, A., Alvarez, V.A. (2014). Polyhydroxyalkanoate (PHA): Review of synthesis, characteristics, processing and potential applications in packaging. *Express Polymer Letters*. 8 (2014), 791-808
- Byron, P.R. and PATTON, J.S. (1994). Drug delivery via the respiratory tract. *Journal of Aerosol Medicine*. 7 (1), 49-75.
- Caetano, L.A., Almeida, A.J., Gonçalves, L. (2016). Effect of experimental parameters on alginate/chitosan microparticles for BCG encapsulation. *Marine Drugs*. 14 (5), 90.
- Carbinatto, F.M., de Castro, A.D., Evangelista, R.C., Cury, B.S. (2014). Insights into the swelling process and drug release mechanisms from cross-linked pectin/high amylose starch matrices. *Asian Journal of Pharmaceutical Sciences*. 9 (1), 27-34.
- Charpentier, E., Barna, A., Guillevin, L., Juliard, J. (2015). Fully bioresorbable drug-eluting coronary scaffolds: a review. *Archives of Cardiovascular Diseases*. 108 (6-7), 385-397.

- Chen, W., Palazzo, A., Hennink, W.E., Kok, R.J. (2016). Effect of particle size on drug loading and release kinetics of gefitinib-loaded PLGA microspheres. *Molecular Pharmaceutics*. 14 (2), 459-467.
- Cheng, S., Chen, G., Leski, M., Zou, B., Wang, Y., Wu, Q. (2006). The effect of D, L- $\beta$ -hydroxybutyric acid on cell death and proliferation in L929 cells. *Biomaterials*. 27 (20), 3758-3765.
- Chew, S., Hinojosa, V. Arriaga, M. (2017). Bioresorbable polymer microparticles in the medical and pharmaceutical fields. *Bioresorbable Polymers for Biomedical Applications*. Elsevier, 229-264.
- Costa, P. and Lobo, J.M.S. (2001). Modeling and comparison of dissolution profiles. *European Journal of Pharmaceutical Sciences*. 13 (2), 123-133.
- Cuenca, R.E., Allison, R.R., Sibata, C., Downie, G.H. (2004). Breast cancer with chest wall progression: treatment with photodynamic therapy. *Annals of Surgical Oncology*. 11 (3), 322-327.
- Daemen, J. and Serruys, P.W. (2007). Drug-eluting stent update 2007: part I. A survey of current and future generation drug-eluting stents: meaningful advances or more of the same? *Circulation*. 116 (3), 316-328.
- Dash, S., Murthy, P.N., Nath, L., Chowdhury, P. (2010). Kinetic modeling on drug release from controlled drug delivery systems. *Acta Poloniae Pharmaceutica*. 67 (3), 217-223.
- De la Riva, B., Nowak, C., Sánchez, E., Hernández, A., Schulz-Siegmund, M., Pec, M.K., Delgado, A., Évora, C. (2009). VEGF-controlled release within a bone defect from alginate/chitosan/PLA-H scaffolds. *European Journal of Pharmaceutics and Biopharmaceutics*. 73 (1), 50-58.
- Debeaufort, F., Voilley, A., Luu, D. (2009). Biopolymer interactions affect the functional properties of edible films based on agar, cassava starch and arabinoxylan blends. *Journal of Food Engineering*. 90 (4), 548-558.

- Debele, T.A., Peng, S., Tsai, H. (2015). Drug carrier for photodynamic cancer therapy. *International Journal of Molecular Sciences*. 16 (9), 22094-22136.
- Deveza, L., Choi, J., Yang, F. (2012). Therapeutic angiogenesis for treating cardiovascular diseases. *Theranostics*. 2 (8), 801-814.
- Ding, X., Xu, Q., Liu, F., Zhou, P., Gu, Y., Zeng, J., An, J., Dai, W., Li, X. (2004). Hematoporphyrin monomethyl ether photodynamic damage on HeLa cells by means of reactive oxygen species production and cytosolic free calcium concentration elevation. *Cancer Letters*. 216 (1), 43-54.
- Dolmans, D.E., Fukumura, D., Jain, R.K. (2003). Photodynamic therapy for cancer. *Nature Reviews Cancer*. 3 (5), 380.
- Doyle, C., Tanner, E., Bonfield, W. (1991). In vitro and in vivo evaluation of polyhydroxybutyrate and of polyhydroxybutyrate reinforced with hydroxyapatite. *Biomaterials*. 12 (9), 841-847.
- Eke, G., Kuzmina, A., Goreva, A., Shishatskaya, E., Hasirci, N., Hasirci, V. (2014). In vitro and transdermal penetration of PHBV micro/nanoparticles. *Journal of Materials Science: Materials in Medicine*. 25 (6), 1471-1481.
- Elzoghby, A.O., Samy, W.M., Elgindy, N.A. (2012). Protein-based nanocarriers as promising drug and gene delivery systems. *Journal of Controlled Release*. 161 (1), 38-49.
- Errico, C., Bartoli, C., Chiellini, F., Chiellini, E. (2009). Poly(hydroxyalkanoates)-based polymeric nanoparticles for drug delivery. *Journal of Biomedicine & Biotechnology*. 2009, 571702.
- Faisant, N., Siepmann, J., Benoit, J. (2002). PLGA-based microparticles: elucidation of mechanisms and a new, simple mathematical model quantifying drug release. *European Journal of Pharmaceutical Sciences*. 15 (4), 355-366.

- Farhangi, M., Dadashzadeh, S., Bolourchian, N. (2017). Biodegradable gelatin microspheres as controlled release intraarticular delivery system: The effect of formulation variables. *Indian Journal of Pharmaceutical Sciences*. 79 (1), 105-112.
- Fatnassi, M., Jacquart, S., Brouillet, F., Rey, C., Combes, C., Fullana, S.G. (2014). Optimization of spray-dried hyaluronic acid microspheres to formulate drug-loaded bone substitute materials. *Powder Technology*. 255, 44-51.
- Ferlay, J., Soerjomataram, I., Dikshit, R., Eser, S., Mathers, C., Rebelo, M., Parkin, D.M., Forman, D., Bray, F. (2015). Cancer incidence and mortality worldwide: sources, methods and major patterns in GLOBOCAN 2012. *International Journal of Cancer*. 136 (5), E359-E386.
- Ferrara, N., Winer, J., Henzel, W.J. (1992). Pituitary follicular cells secrete an inhibitor of aortic endothelial cell growth: identification as leukemia inhibitory factor. *Proceedings of the National Academy of Sciences of the United States of America*. 89 (2), 698-702.
- Fogh, J., Wright, W.C., Loveless, J.D. (1977). Absence of HeLa cell contamination in 169 cell lines derived from human tumors. *Journal of the National Cancer Institute*. 58 (2), 209-214.
- Formiga, F.R., Pelacho, B., Garbayo, E., Abizanda, G., Gavira, J.J., Simon-Yarza, T., Mazo, M., Tamayo, E., Jauquicoa, C., Ortiz-de-Solorzano, C. (2010). Sustained release of VEGF through PLGA microparticles improves vasculogenesis and tissue remodeling in an acute myocardial ischemia–reperfusion model. *Journal of Controlled Release*. 147 (1), 30-37.
- Francis, L., Meng, D., Knowles, J.C., Roy, I., Boccaccini, A.R. (2010). Multi-functional P (3HB) microsphere/45S5 Bioglass®-based composite scaffolds for bone tissue engineering. *Acta Biomaterialia*. 6 (7), 2773-2786.
- Francis, L., Meng, D., Knowles, J., Keshavarz, T., Boccaccini, A., Roy, I. (2011). Controlled delivery of gentamicin using poly (3-hydroxybutyrate) microspheres. *International Journal of Molecular Sciences*. 12 (7), 4294-4314.

- Freiberg, S. and Zhu, X. (2004). Polymer microspheres for controlled drug release. *International Journal of Pharmaceutics*. 282 (1-2), 1-18.
- Freitas, S., Merkle, H.P., Gander, B. (2005). Microencapsulation by solvent extraction/evaporation: reviewing the state of the art of microsphere preparation process technology. *Journal of Controlled Release*. 102 (2), 313-332.
- Gangrade, N. and Price, J.C. (1992). Properties of implantable pellets prepared from a biodegradable polyester. *Drug Development and Industrial Pharmacy*. 18 (15), 1633-1648.
- Garcia-Bennett, A., Nees, M., Fadeel, B. (2011). In search of the holy grail: folate-targeted nanoparticles for cancer therapy. *Biochemical Pharmacology*. 81 (8), 976-984.
- Gelperina, S., Kisich, K., Iseman, M.D., Heifets, L. (2005). The potential advantages of nanoparticle drug delivery systems in chemotherapy of tuberculosis. *American Journal of Respiratory and Critical Care Medicine*. 172 (12), 1487-1490.
- Granum, P.E. and Lund, T. (1997). *Bacillus cereus* and its food poisoning toxins. *FEMS Microbiology Letters*. 157 (2), 223-228.
- Gu, F., Amsden, B., Neufeld, R. (2004). Sustained delivery of vascular endothelial growth factor with alginate beads. *Journal of Controlled Release*. 96 (3), 463-472.
- Hao, X., Silva, E.A., Månsson-Broberg, A., Grinnemo, K., Siddiqui, A.J., Dellgren, G., Wårdell, E., Brodin, L.Å., Mooney, D.J., Sylvén, C. (2007). Angiogenic effects of sequential release of VEGF-A165 and PDGF-BB with alginate hydrogels after myocardial infarction. *Cardiovascular Research*. 75 (1), 178-185.
- Hazer, B. (2010). Amphiphilic poly (3-hydroxy alkanoate) s: potential candidates for medical applications. *International Journal of Polymer Science*. 2010
- Hoare, T.R. and Kohane, D.S. (2008). Hydrogels in drug delivery: Progress and challenges. *Polymer*. 49 (8), 1993-2007.

- Honary, S., Maleki, M., Karami, M. (2009). The effect of chitosan molecular weight on the properties of alginate/chitosan microparticles containing prednisolone. *Tropical Journal of Pharmaceutical Research*. 8 (1), 53-61.
- Hossain, K.M.Z., Patel, U., Ahmed, I. (2015). Development of microspheres for biomedical applications: a review. *Progress in Biomaterials*. 4 (1), 1-19.
- Hu, X., Feng, Y., Lu, J.Q., Allison, R.R., Cuenca, R.E., Downie, G.H., Sibata, C.H. (2005). Modeling of a type II photofrin-mediated photodynamic therapy process in a heterogeneous tissue phantom. *Photochemistry and Photobiology*. 81 (6), 1460-1468.
- Huang, X. and Brazel, C.S. (2001). On the importance and mechanisms of burst release in matrix-controlled drug delivery systems. *Journal of Controlled Release*. 73 (2-3), 121-136.
- Ismail, A.F.H., Mohamed, F., Rosli, L.M.M., Shafri, M.A.M., Haris, M.S., Adina, A.B. (2016). Spectrophotometric determination of gentamicin loaded PLGA microparticles and method validation via ninhydrin-gentamicin complex as a rapid quantification approach. *Journal of Applied Pharmaceutical Science Vol. 6* (01), 007-014.
- Jay, S.M. and Saltzman, W.M. (2009). Controlled delivery of VEGF via modulation of alginate microparticle ionic crosslinking. *Journal of Controlled Release*. 134 (1), 26-34.
- Kadish, K.M., Smith, K.M., Guillard, R. (2000). *The Porphyrin Handbook: Inorganic, organometallic and coordination chemistry*. Vol 3. New York: The academic press.
- Kassab, A.C., Xu, K., Denkbaz, E., Dou, Y., Zhao, S., Piskin, E. (1997). Rifampicin carrying polyhydroxybutyrate microspheres as a potential chemoembolization agent. *Journal of Biomaterials Science, Polymer Edition*. 8 (12), 947-961.
- Kazuhiko, J., Masahiro, N., Miho, K. (1986). Controlled release of aclarubicin, an anticancer antibiotic, from poly- $\beta$ -hydroxybutyric acid microspheres. *Journal of Controlled Release*. 4 (1), 25-32.

- Keraliya, R.A., Patel, C., Patel, P., Keraliya, V., Soni, T.G., Patel, R.C., Patel, M. (2012). Osmotic drug delivery system as a part of modified release dosage form. *ISRN Pharmaceutics*. 2012
- Khang, G., Kim, S.W., Cho, J.C., Rhee, J.M., Yoon, S.C., Lee, H.B. (2001). Preparation and characterization of poly (3-hydroxybutyrate-co-3-hydroxyvalerate) microspheres for the sustained release of 5-fluorouracil. *Bio-Medical Materials and Engineering*. 11 (2), 89-103.
- Kılıçay, E., Demirbilek, M., Türk, M., Güven, E., Hazer, B., Denkbaz, E.B. (2011). Preparation and characterization of poly (3-hydroxybutyrate-co-3-hydroxyhexanoate) (PHBHHX) based nanoparticles for targeted cancer therapy. *European Journal of Pharmaceutical Sciences*. 44 (3), 310-320.
- Kim, K.K. and Pack, D.W. (2006). Microspheres for drug delivery. In *BioMEMS and biomedical nanotechnology*. New York: Springer, 19-50.
- Kim, S., Shi, Y., Kim, J.Y., Park, K., Cheng, J. (2010). Overcoming the barriers in micellar drug delivery: loading efficiency, in vivo stability, and micelle–cell interaction. *Expert Opinion on Drug Delivery*. 7 (1), 49-62.
- Klose, D., Siepmann, F., Elkharraz, K., Siepmann, J. (2008). PLGA-based drug delivery systems: importance of the type of drug and device geometry. *International Journal of Pharmaceutics*. 354 (1-2), 95-103.
- Kocbek, P., Obermajer, N., Cegnar, M., Kos, J., Kristl, J. (2007). Targeting cancer cells using PLGA nanoparticles surface modified with monoclonal antibody. *Journal of Controlled Release*. 120 (1-2), 18-26.
- Kunze, C., Bernd, H.E., Androsch, R., Nischan, C., Freier, T., Kramer, S., Kramp, B., Schmitz, K. (2006). In vitro and in vivo studies on blends of isotactic and atactic poly (3-hydroxybutyrate) for development of a dura substitute material. *Biomaterials*. 27 (2), 192-201.

- Kutz, M. (2003). *Standard handbook of biomedical engineering and design* McGraw-Hill New York.
- Kwon, H., Jung, S., Kim, H., Parker, S.A., Batt, C.A., Kim, Y. (2014). A multi-functional polyhydroxybutyrate nanoparticle for theranostic applications. *Journal of Materials Chemistry B*. 2 (25), 3965-3971.
- Lageveen, R.G., Huisman, G.W., Preusting, H., Ketelaar, P., Eggink, G., Witholt, B. (1988). Formation of Polyesters by *Pseudomonas oleovorans*: Effect of Substrates on Formation and Composition of Poly-(R)-3-Hydroxyalkanoates and Poly-(R)-3-Hydroxyalkenoates. *Applied and Environmental Microbiology*. 54 (12), 2924-2932.
- Lao, L.L., Venkatraman, S.S., Peppas, N.A. (2008). Modeling of drug release from biodegradable polymer blends. *European Journal of Pharmaceutics and Biopharmaceutics*. 70 (3), 796-803.
- Le Meur, S., Zinn, M., Egli, T., Thöny-Meyer, L., Ren, Q. (2012). Production of medium-chain-length polyhydroxyalkanoates by sequential feeding of xylose and octanoic acid in engineered *Pseudomonas putida* KT2440. *BMC Biotechnology*. 12 (1), 53.
- Lee, J., Jung, S., Park, C., Kim, H., Batt, C.A., Kim, Y. (2011). Tumor-specific hybrid polyhydroxybutyrate nanoparticle: surface modification of nanoparticle by enzymatically synthesized functional block copolymer. *Bioorganic & Medicinal Chemistry Letters*. 21 (10), 2941-2944.
- Lee, S.C., Oh, J.T., Jang, M.H., Chung, S.I. (1999). Quantitative analysis of polyvinyl alcohol on the surface of poly (D, L-lactide-co-glycolide) microparticles prepared by solvent evaporation method: effect of particle size and PVA concentration. *Journal of Controlled Release*. 59 (2), 123-132.
- Li, B., Li, Q., Mo, J., Dai, H. (2017). Drug-loaded polymeric nanoparticles for cancer stem cell targeting. *Frontiers in Pharmacology*. 8, 51.

- Li, M., Rouaud, O., Poncelet, D. (2008). Microencapsulation by solvent evaporation: State of the art for process engineering approaches. *International Journal of Pharmaceutics*. 363 (1-2), 26-39.
- Liechty, W.B., Kryscio, D.R., Slaughter, B.V., Peppas, N.A. (2010). Polymers for drug delivery systems. *Annual Review of Chemical and Biomolecular Engineering*. 1 149-173.
- Lu, D., Xiao, C., Xu, S. (2009). Starch-based completely biodegradable polymer materials. *Express Polymer Letters*. 3 (6), 366-375.
- Lutolf, M. and Hubbell, J. (2005). Synthetic biomaterials as instructive extracellular microenvironments for morphogenesis in tissue engineering. *Nature Biotechnology*. 23 (1), 47.
- Lyu, S. and Untereker, D. (2009). Degradability of polymers for implantable biomedical devices. *International Journal of Molecular Sciences*. 10 (9), 4033-4065.
- Ma, B., Zhou, P., Xie, T., Shi, L., Qiu, B., Wang, Q. (2015). Inhibition of interleukin-1beta-stimulated dedifferentiation of chondrocytes via controlled release of CrmA from hyaluronic acid-chitosan microspheres. *BMC Musculoskeletal Disorders*. 16 (1), 61.
- Maia, J., Santana, M., Ré, M. (2004). The effect of some processing conditions on the characteristics of biodegradable microspheres obtained by an emulsion solvent evaporation process. *Brazilian Journal of Chemical Engineering*. 21 (1), 01-12.
- Mallakpour, S. and Zadehnazari, A. (2011). Advances in synthetic optically active condensation polymers--A review. *Express Polymer Letters*. 5 (2).
- Manavitehrani, I., Fathi, A., Badr, H., Daly, S., Negahi Shirazi, A., Dehghani, F. (2016). Biomedical applications of biodegradable polyesters. *Polymers*. 8 (1), 20.
- Manohar, M., Joseph, J., Selvaraj, T., Sivakumar, D. (2013). Application of Box Behnken design to optimize the parameters for turning Inconel 718 using coated carbide tools. *International Journal of Scientific & Engineering Research*. 4 (4), 620-644.

- Mansour, H.M., Sohn, M., Al-Ghananeem, A., DeLuca, P.P. (2010). Materials for pharmaceutical dosage forms: molecular pharmaceuticals and controlled release drug delivery aspects. *International Journal of Molecular Sciences*. 11 (9), 3298-3322.
- Markiv, A., Beatson, R., Burchell, J., Durvasula, R.V., Kang, A.S. (2011). Expression of recombinant multi-coloured fluorescent antibodies in *gor-/trxB-E. coli* cytoplasm. *BMC Biotechnology*. 11 (1), 117.
- Mero, A. and Campisi, M. (2014). Hyaluronic acid bioconjugates for the delivery of bioactive molecules. *Polymers*. 6 (2), 346-369.
- Mishra, P., Nayak, B., Dey, R. (2016). PEGylation in anti-cancer therapy: An overview. *Asian Journal of Pharmaceutical Sciences*. 11 (3), 337-348.
- Misra, S.K., Valappil, S.P., Roy, I., Boccaccini, A.R. (2006). Polyhydroxyalkanoate (PHA)/inorganic phase composites for tissue engineering applications. *Biomacromolecules*. 7 (8), 2249-2258.
- Mitra, A.K. and Agrawal, D.K. (2006). In stent restenosis: bane of the stent era. *Journal of Clinical Pathology*. 59 (3), 232-239.
- Mun, S., Joung, D., Kim, Y., Kang, O., Kim, S., Seo, Y., Kim, Y., Lee, D., Shin, D., Kweon, K. (2013). Synergistic antibacterial effect of curcumin against methicillin-resistant *Staphylococcus aureus*. *Phytomedicine*. 20 (8-9), 714-718.
- Narasimhan, B. and Peppas, N.A. (1997). Molecular analysis of drug delivery systems controlled by dissolution of the polymer carrier. *Journal of Pharmaceutical Sciences*. 86 (3), 297-304.
- Nigmatullin, R., Thomas, P., Lukasiewicz, B., Puthussery, H., Roy, I. (2015). Polyhydroxyalkanoates, a family of natural polymers, and their applications in drug delivery. *Journal of Chemical Technology & Biotechnology*. 90 (7), 1209-1221.
- Nordlinger, B., Sorbye, H., Glimelius, B., Poston, G.J., Schlag, P.M., Rougier, P., Bechstein, W.O., Primrose, J.N., Walpole, E.T., Finch-Jones, M. (2008). Perioperative

- chemotherapy with FOLFOX4 and surgery versus surgery alone for resectable liver metastases from colorectal cancer (EORTC Intergroup trial 40983): a randomised controlled trial. *The Lancet*. 371 (9617), 1007-1016.
- Numata, K., Abe, H., Iwata, T. (2009). Biodegradability of poly (hydroxyalkanoate) materials. *Materials*. 2 (3), 1104-1126.
- O'Donnell, P.B. and McGinity, J.W. (1997). Preparation of microspheres by the solvent evaporation technique. *Advanced Drug Delivery Reviews*. 28 (1), 25-42.
- Oenbrink, G., Jurgenlimke, P., Gabel, D. (1988). Accumulation of porphyrins in cells: influence of hydrophobicity aggregation and protein binding. *Photochemistry and Photobiology*. 48 (4), 451-456.
- Oleinick, N.L., Morris, R.L., Belichenko, I. (2002). The role of apoptosis in response to photodynamic therapy: what, where, why, and how. *Photochemical & Photobiological Sciences*. 1 (1), 1-21.
- Pachekoski, W.M., Dalmolin, C., Agnelli, J.A.M. (2013). The influence of the industrial processing on the degradation of poly (hidroxybutyrate)-PHB. *Materials Research*. 16 (2), 237-332.
- Pandian, S.R.K., Deepak, V., Nellaiah, H., Sundar, K. (2015). PEG–PHB-glutaminase nanoparticle inhibits cancer cell proliferation in vitro through glutamine deprivation. *In Vitro Cellular & Developmental Biology-Animal*. 51 (4), 372-380.
- Parhizkar, M., Reardon, P.J., Knowles, J.C., Browning, R.J., Stride, E., Barbara, P.R., Harker, A.H., Edirisinghe, M. (2016). Electrohydrodynamic encapsulation of cisplatin in poly (lactic-co-glycolic acid) nanoparticles for controlled drug delivery. *Nanomedicine: Nanotechnology, Biology and Medicine*. 12 (7), 1919-1929.
- Park, J., Ye, M., Park, K. (2005). Biodegradable polymers for microencapsulation of drugs. *Molecules*. 10 (1), 146-161.

- Peña, C., Castillo, T., García, A., Millán, M., Segura, D. (2014). Biotechnological strategies to improve production of microbial poly-(3-hydroxybutyrate): a review of recent research work. *Microbial Biotechnology*. 7 (4), 278-293.
- Puranik, A.S., Dawson, E.R., Peppas, N.A. (2013). Recent advances in drug eluting stents. *International Journal of Pharmaceutics*. 441 (1-2), 665-679.
- Qiu, B., Gong, M., He, Q., Zhou, P. (2016). Controlled release of interleukin-1 receptor antagonist from hyaluronic acid-chitosan microspheres attenuates interleukin-1 $\beta$ -induced inflammation and apoptosis in chondrocytes. *BioMed Research International*. 2016
- Rai, R., Keshavarz, T., Roether, J., Boccaccini, A.R., Roy, I. (2011). Medium chain length polyhydroxyalkanoates, promising new biomedical materials for the future. *Materials Science and Engineering: R: Reports*. 72 (3), 29-47.
- Rajput, M.S. and Agrawal, P. (2010). Microspheres in cancer therapy. *Indian Journal of Cancer*. 47 (4), 458-468.
- Ramteke, K., Dighe, P., Kharat, A., Patil, S. (2014). Mathematical models of drug dissolution: a review. *Scholars Academic Journal of Pharmacy*. 3 (5), 388-396.
- Rashid, M., Kaur, V., Hallan, S.S., Sharma, S., Mishra, N. (2016). Microparticles as controlled drug delivery carrier for the treatment of ulcerative colitis: A brief review. *Saudi Pharmaceutical Journal*. 24 (4), 458-472.
- Reddy, K.J. and Karunakaran, K. (2013). Purification and characterization of hyaluronic acid produced by *Streptococcus zooepidemicus* strain 3523-7. *Journal of BioScience & Biotechnology*. 2 (3), 173-179.
- Reis, A.V., Guilherme, M.R., Rubira, A.F., Muniz, E.C. (2007). Mathematical model for the prediction of the overall profile of in vitro solute release from polymer networks. *Journal of Colloid and Interface Science*. 310 (1), 128-135.
- Rodríguez-Contreras, A., García, Y., Manero, J.M., Rupérez, E. (2017). Antibacterial PHAs coating for titanium implants. *European Polymer Journal*. 90, 66-78.

- Ruiz-Esparza, G.U., Flores-Arredondo, J.H., Segura-Ibarra, V., Torre-Amione, G., Ferrari, M., Blanco, E., Serda, R.E. (2013). The physiology of cardiovascular disease and innovative liposomal platforms for therapy. *International Journal of Nanomedicine*. 8, 629-640.
- Safari, J. and Zarnegar, Z. (2014). Advanced drug delivery systems: Nanotechnology of health design A review. *Journal of Saudi Chemical Society*. 18 (2), 85-99.
- Sahoo, S.K., Panyam, J., Prabha, S., Labhasetwar, V. (2002). Residual polyvinyl alcohol associated with poly (D, L-lactide-co-glycolide) nanoparticles affects their physical properties and cellular uptake. *Journal of Controlled Release*. 82 (1), 105-114.
- Sampath, U.G., Ching, Y.C., Chuah, C.H., Sabariah, J.J., Lin, P. (2016). Fabrication of porous materials from natural/synthetic biopolymers and their composites. *Materials*. 9 (12), 991.
- Sánchez, R.J., Schripsema, J., da Silva, L.F., Taciro, M.K., Pradella, J.G., Gomez, J.G.C. (2003). Medium-chain-length polyhydroxyalkanoic acids (PHAmcl) produced by *Pseudomonas putida* IPT 046 from renewable sources. *European Polymer Journal*. 39 (7), 1385-1394.
- Sato, H., Hoshino, M., Aoi, H., Seino, T., Ishida, Y., Aoi, K., Ohtani, H. (2005). Compositional analysis of poly (3-hydroxybutyrate-co-3-hydroxyvalerate) by pyrolysis-gas chromatography in the presence of organic alkali. *Journal of Analytical and Applied Pyrolysis*. 74 (1-2), 193-199.
- Schatton, T., Frank, N.Y., Frank, M.H. (2009). Identification and targeting of cancer stem cells. *Bioessays*. 31 (10), 1038-1049.
- Sell, S.A., Wolfe, P.S., Garg, K., McCool, J.M., Rodriguez, I.A., Bowlin, G.L. (2010). The use of natural polymers in tissue engineering: a focus on electrospun extracellular matrix analogues. *Polymers*. 2 (4), 522-553.
- Sharma, N., Madan, P., Lin, S. (2016). Effect of process and formulation variables on the preparation of parenteral paclitaxel-loaded biodegradable polymeric

- nanoparticles: A co-surfactant study. *Asian Journal of Pharmaceutical Sciences*. 11 (3), 404-416.
- Sharman, W.M., Allen, C.M., Van Lier, J.E. (1999). Photodynamic therapeutics: basic principles and clinical applications. *Drug Discovery Today*. 4 (11), 507-517.
- Shi, L., Chen, J., Yang, J., Pan, T., Zhang, S., Wang, Z. (2010). MiR-21 protected human glioblastoma U87MG cells from chemotherapeutic drug temozolomide induced apoptosis by decreasing Bax/Bcl-2 ratio and caspase-3 activity. *Brain Research*. 1352 (2010), 255-264.
- Shishatskaya, E.I., Nikolaeva, E.D., Vinogradova, O.N., Volova, T.G. (2016). Experimental wound dressings of degradable PHA for skin defect repair. *Journal of Materials Science: Materials in Medicine*. 27 (11), 165.
- Shoji, T., Ii, M., Mifune, Y., Matsumoto, T., Kawamoto, A., Kwon, S., Kuroda, T., Kuroda, R., Kurosaka, M., Asahara, T. (2010). Local transplantation of human multipotent adipose-derived stem cells accelerates fracture healing via enhanced osteogenesis and angiogenesis. *Laboratory Investigation*. 90 (4), 637.
- Shrivastav, A., Kim, H.Y., Kim, Y.R. (2013). Advances in the applications of polyhydroxyalkanoate nanoparticles for novel drug delivery system. *BioMed Research International*. 2013, 581684.
- Siepmann, J. and Siepmann, F. (2008). Mathematical modeling of drug delivery. *International Journal of Pharmaceutics*. 364 (2), 328-343.
- Singh, R. and Lillard Jr, J.W. (2009). Nanoparticle-based targeted drug delivery. *Experimental and Molecular Pathology*. 86 (3), 215-223.
- Siqueira, G., Bras, J., Dufresne, A. (2010). Cellulosic bionanocomposites: a review of preparation, properties and applications. *Polymers*. 2 (4), 728-765.
- Solban, N., Rizvi, I., Hasan, T. (2006). Targeted photodynamic therapy. *Lasers in Surgery and Medicine: The Official Journal of the American Society for Laser Medicine and Surgery*. 38 (5), 522-531.

- Sosnik, A. and Seremeta, K.P. (2017). Polymeric hydrogels as technology platform for drug delivery applications. *Gels*. 3 (3), 25.
- Srivastava, A., Yadav, T., Sharma, S., Nayak, A., Kumari, A.A., Mishra, N. (2015). Polymers in drug delivery. *Journal of Biosciences and Medicines*. 4 (01), 69.
- Subedi, G., Shrestha, A.K., Shakya, S. (2016). Study of Effect of Different Factors in Formulation of Micro and Nanospheres with Solvent Evaporation Technique. *Open Pharmaceutical Sciences Journal*. 3 (1).
- Sun, T., Zhang, Y.S., Pang, B., Hyun, D.C., Yang, M., Xia, Y. (2014). Engineered nanoparticles for drug delivery in cancer therapy. *Angewandte Chemie International Edition*. 53 (46), 12320-12364.
- Tajdaran, K., Shoichet, M.S., Gordon, T., Borschel, G.H. (2015). A novel polymeric drug delivery system for localized and sustained release of tacrolimus (FK506). *Biotechnology and Bioengineering*. 112 (9), 1948-1953.
- Tejashree, A., Sagar, D., Chavare, D., Ajit, K., Shruti, K. (2014). A review on parenteral implants. *International Journal of Research and Reviews in Pharmacy and Applied Science*. 4 (2), 1056-1072.
- Teow, S., Liew, K., Ali, S.A., Khoo, A.S., Peh, S. (2016). Antibacterial action of curcumin against *Staphylococcus aureus*: a brief review. *Journal of Tropical Medicine*. 2016
- Thakkar, F.M.V., Soni, T., Gohel, M., Gandhi, T. (2009). Supercritical fluid technology: a promising approach to enhance the drug solubility. *Journal of Pharmaceutical Sciences and Research*. 1 (4), 1-14.
- Tsung, J. and Burgess, D. (2012). Fundamentals and applications of controlled release drug delivery. *Fundamentals and Applications of Controlled Release Drug Delivery*. 107-123.
- Valappil, S.P., Peiris, D., Langley, G., Herniman, J., Boccaccini, A.R., Bucke, C., Roy, I. (2007). Polyhydroxyalkanoate (PHA) biosynthesis from structurally unrelated

- carbon sources by a newly characterized *Bacillus* spp. *Journal of Biotechnology*. 127 (3), 475-487.
- Vasapollo, G., Sole, R.D., Mergola, L., Lazzoi, M.R., Scardino, A., Scorrano, S., Mele, G. (2011). Molecularly imprinted polymers: present and future prospective. *International Journal of Molecular Sciences*. 12 (9), 5908-5945.
- Verlinden, R.A., Hill, D.J., Kenward, M., Williams, C.D., Radecka, I. (2007). Bacterial synthesis of biodegradable polyhydroxyalkanoates. *Journal of Applied Microbiology*. 102 (6), 1437-1449.
- Vilos, C. and Velasquez, L. (2012). Therapeutic strategies based on polymeric microparticles. *BioMed Research International*. 2012
- Vroman, I. and Tighzert, L. (2009). Biodegradable polymers. *Materials*. 2 (2), 307-344.
- Warren, M. and Smith, A. (2009). *Tetrapyrroles: birth, life and death*. New York: Springer Science & Business Media.
- Williams, S.F. and Martin, D.P. (2005). Applications of polyhydroxyalkanoates (PHA) in medicine and pharmacy. *Biopolymers Online: Biology • Chemistry • Biotechnology • Applications*. 4
- Wintrobe, M.M. (2009). *Wintrobe's clinical hematology*. 10th Ed. Philadelphia: Lippincott Williams & Wilkins.
- Witschi, C. and Doelker, E. (1998). Influence of the microencapsulation method and peptide loading on poly (lactic acid) and poly (lactic-co-glycolic acid) degradation during in vitro testing. *Journal of Controlled Release*. 51 (2-3), 327-341.
- Wu, X., Liu, H., Liu, J., Haley, K.N., Treadway, J.A., Larson, J.P., Ge, N., Peale, F., Bruchez, M.P. (2003). Immunofluorescent labeling of cancer marker Her2 and other cellular targets with semiconductor quantum dots. *Nature Biotechnology*. 21 (1), 41.

- Xie, J., Shen, Z., Li, K.C., Danthi, N. (2007). Tumor angiogenic endothelial cell targeting by a novel integrin-targeted nanoparticle. *International Journal of Nanomedicine*. 2 (3), 479-485.
- Xing, L., Xu, Y., Sun, K., Wang, H., Zhang, F., Zhou, Z., Zhang, J., Zhang, F., Caliskan, B., Qiu, Z. (2018). Identification of a peptide for folate receptor alpha by phage display and its tumor targeting activity in ovary cancer xenograft. *Scientific Reports*. 8 (1), 8426.
- Xiong, Y., Yao, Y., Zhan, X., Chen, G. (2010). Application of polyhydroxyalkanoates nanoparticles as intracellular sustained drug-release vectors. *Journal of Biomaterials Science, Polymer Edition*. 21 (1), 127-140.
- Yan, H. and Row, K.H. (2006). Characteristic and synthetic approach of molecularly imprinted polymer. *International Journal of Molecular Sciences*. 7 (5), 155-178.
- Yang, Y., Chung, T., Ng, N.P. (2001). Morphology, drug distribution, and in vitro release profiles of biodegradable polymeric microspheres containing protein fabricated by double-emulsion solvent extraction/evaporation method. *Biomaterials*. 22 (3), 231-241.
- Yao, Y., Zhan, X., Zhang, J., Zou, X., Wang, Z., Xiong, Y., Chen, J., Chen, G. (2008). A specific drug targeting system based on polyhydroxyalkanoate granule binding protein PhaP fused with targeted cell ligands. *Biomaterials*. 29 (36), 4823-4830.
- Yun, Y.H., Goetz, D.J., Yellen, P., Chen, W. (2004). Hyaluronan microspheres for sustained gene delivery and site-specific targeting. *Biomaterials*. 25 (1), 147-157.
- Yun, Y., Lee, B.K., Park, K. (2014). Controlled drug delivery systems: the next 30 years. *Frontiers of Chemical Science and Engineering*. 8 (3), 276-279.
- Zeukeng, M., Seoane-Vazquez, E., Bonnabry, P. (2018). A comparison of new drugs approved by the FDA, the EMA, and Swissmedic: an assessment of the international harmonization of drugs. *European Journal of Clinical Pharmacology*. 74 (6), 811-818.

- Zhai, P., Chen, X., Schreyer, D.J. (2013). Preparation and characterization of alginate microspheres for sustained protein delivery within tissue scaffolds. *Biofabrication*. 5 (1), 015009.
- Zhang, C., Zhao, L., Dong, Y., Zhang, X., Lin, J., Chen, Z. (2010). Folate-mediated poly (3-hydroxybutyrate-co-3-hydroxyoctanoate) nanoparticles for targeting drug delivery. *European Journal of Pharmaceutics and Biopharmaceutics*. 76 (1), 10-16.
- Zhang, D., Tian, A., Xue, X., Wang, M., Qiu, B., Wu, A. (2012). The effect of temozolomide/poly (lactide-co-glycolide) (PLGA)/nano-hydroxyapatite microspheres on glioma U87 cells behavior. *International Journal of Molecular Sciences*. 13 (1), 1109-1125.
- Zielhuis, S., Nijsen, J., Figueiredo, R., Feddes, B., Vredenberg, A., Van het Schip, A., Hennink, W. (2005). Surface characteristics of holmium-loaded poly (L-lactic acid) microspheres. *Biomaterials*. 26 (8), 925-932.